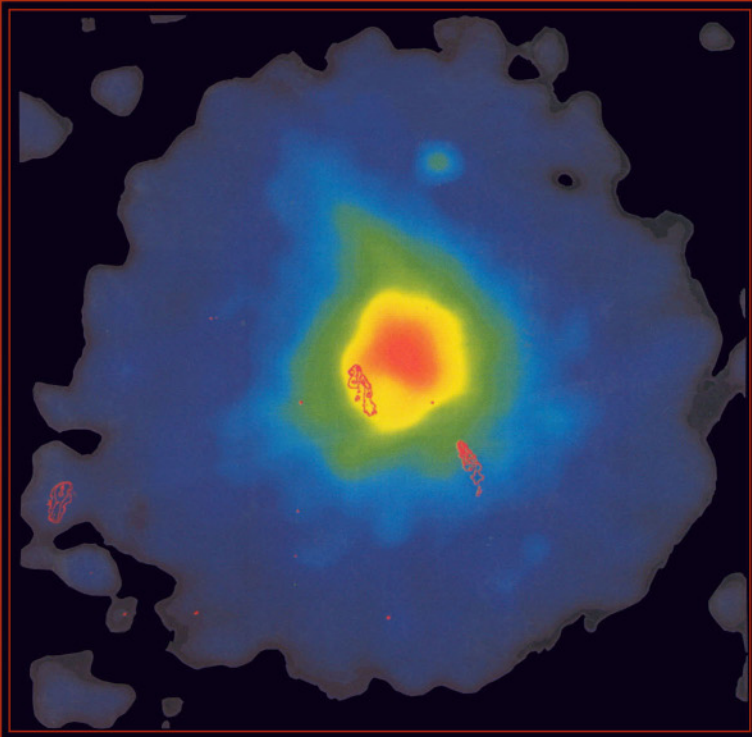


AS
SL

ASTROPHYSICS AND
SPACE SCIENCE LIBRARY

MERGING PROCESSES IN GALAXY CLUSTERS

L. FERETTI
I.M. GIOIA
G. GIOVANNINI
Editors



KLUWER ACADEMIC PUBLISHERS

MERGING PROCESSES IN GALAXY CLUSTERS

ASTROPHYSICS AND SPACE SCIENCE LIBRARY

VOLUME 272

EDITORIAL BOARD

Chairman

W.B. BURTON, National Radio Astronomy Observatory, Charlottesville, Virginia, U.S.A.
(burton@starband.net); University of Leiden, The Netherlands (burton@strw.leidenuniv.nl)

Executive Committee

- J. M. E. KUIJPERS, *Faculty of Science, Nijmegen, The Netherlands*
E. P. J. VAN DEN HEUVEL, *Astronomical Institute, University of Amsterdam,
The Netherlands*
H. VAN DER LAAN, *Astronomical Institute, University of Utrecht,
The Netherlands*

MEMBERS

- I. APPENZELLER, *Landessternwarte Heidelberg-Königstuhl, Germany*
J. N. BAHCALL, *The Institute for Advanced Study, Princeton, U.S.A.*
F. BERTOLA, *Università di Padova, Italy*
J. P. CASSINELLI, *University of Wisconsin, Madison, U.S.A.*
C. J. CESARSKY, *Centre d'Etudes de Saclay, Gif-sur-Yvette Cedex, France*
O. ENGVOLD, *Institute of Theoretical Astrophysics, University of Oslo, Norway*
R. McCRAY, *University of Colorado, JILA, Boulder, U.S.A.*
P. G. MURDIN, *Institute of Astronomy, Cambridge, U.K.*
F. PACINI, *Istituto Astronomia Arcetri, Firenze, Italy*
V. RADHAKRISHNAN, *Raman Research Institute, Bangalore, India*
K. SATO, *School of Science, The University of Tokyo, Japan*
F. H. SHU, *University of California, Berkeley, U.S.A.*
B. V. SOMOV, *Astronomical Institute, Moscow State University, Russia*
R. A. SUNYAEV, *Space Research Institute, Moscow, Russia*
Y. TANAKA, *Institute of Space & Astronautical Science, Kanagawa, Japan*
S. TREMAINE, *CITA, Princeton University, U.S.A.*
N. O. WEISS, *University of Cambridge, U.K.*

MERGING PROCESSES IN GALAXY CLUSTERS

edited by

L. FERETTI

*Istituto di Radioastronomia CNR,
Bologna, Italy*

I.M. GIOIA

*Istituto di Radioastronomia CNR,
Bologna, Italy*

and

G. GIOVANNINI

*Physics Department,
University of Bologna, Italy*

KLUWER ACADEMIC PUBLISHERS

NEW YORK, BOSTON, DORDRECHT, LONDON, MOSCOW

eBook ISBN: 0-306-48096-4
Print ISBN: 1-4020-0531-8

©2004 Kluwer Academic Publishers
New York, Boston, Dordrecht, London, Moscow

Print ©2002 Kluwer Academic Publishers
Dordrecht

All rights reserved

No part of this eBook may be reproduced or transmitted in any form or by any means, electronic, mechanical, recording, or otherwise, without written consent from the Publisher

Created in the United States of America

Visit Kluwer Online at: <http://kluweronline.com>
and Kluwer's eBookstore at: <http://ebooks.kluweronline.com>

Contents

Preface	xi
Contributing Authors	xiii
1	
The Physics of Cluster Mergers	1
<i>Craig L. Sarazin</i>	
1 Basic Merger Rates and Kinematics	2
1.1 Estimates of Merger Rates	2
1.2 Estimates of Merger Kinematics	5
1.2.1 Turn-Around Distances	6
1.2.2 Merger Velocities	7
1.2.3 Angular Momenta, Impact Parameters, and Transverse Velocities	8
2 Thermal Physics of Merger Shocks	10
2.1 Shock Kinematics	11
2.2 Nonequilibrium Effects	14
3 Mergers and Cool Cluster Cores	15
3.1 Cooling Flows vs. Mergers	15
3.2 Cold Fronts	18
3.2.1 Kinematics of Cold Fronts	18
3.2.2 Width of Cold Fronts	21
4 Nonthermal Physics of Merger Shocks	21
4.1 Particle Lifetimes and Losses	22
4.2 Sources of Relativistic Particles	25
4.2.1 Particle Acceleration in Shocks	25
4.2.2 Reacceleration by Merger Shocks	26
4.2.3 Turbulent Acceleration Following a Merger	27
4.2.4 Secondary Electron Production	27
4.3 Models for Merger Shocks and Primary Electrons	28
4.4 Nonthermal Emission and Mergers	29
4.4.1 Radio Halos and Relics	29
4.4.2 EUV/Soft X-ray Emission	29
4.4.3 Hard X-ray Tails	31
4.4.4 Predicted Gamma-Ray and Neutrino Emission	33
4.4.5 Ultra High Energy Cosmic Rays	33
5 Summary	34

Optical Analysis of Cluster Mergers	39
<i>Marisa Girardi and Andrea Biviano</i>	
1 Detecting and Quantifying Substructure	41
1.1 Spatial Substructure	42
1.2 Velocity Substructure	44
1.3 Spatial–Velocity Substructure	45
1.4 Different Methods Compared	48
2 Frequency and Nature of Subclusters	50
3 Dynamical Effects of Cluster Mergers	52
4 Substructure and Cosmology	57
4.1 Accretion from the LSS	57
4.2 Estimating Ω	61
5 Cluster Mergers and Galaxy Properties	64
5.1 Brightest Cluster Members	64
5.2 Galaxy Star–Formation	67

X-Ray Observations of Cluster Mergers	79
<i>David A. Buote</i>	
1 Quantitative Analysis of Individual Substructures	82
2 Quantitative Classification of Global Morphology	85
2.1 Methods	86
2.2 Merger Frequency of ROSAT Clusters	90
3 High-Redshift Clusters	91
4 Morphology and Cosmology	92
4.1 Semi-Analytical Models	92
4.2 N-Body Simulations	95
5 Morphology and Radio Halos	96
6 Temperature Substructure	98
6.1 X-Ray Temperature Maps	98
6.2 Quantitative Classification of Temperature Morphology	101
7 Conclusions	103

High Angular Resolution Cluster Observations with Chandra	109
<i>W. Forman, C. Jones, M. Markevitch, A. Vikhlinin, E. Churazov</i>	
1 Cluster Mergers	110
1.1 Multiple Cold Fronts in A2142	112
1.2 Cluster Physics and Cold Fronts	115
1.3 Cold Fronts in Other Clusters	118
1.3.1 RX J1720.1+2638	118
1.3.2 ZW3146 – A Cluster with Three Edges	118
1.4 Merger shocks and Cluster Radio Halo Sources	121
2 The Radio—X-ray Connection	122
2.1 A First Look at Radio Emitting Plasma Bubbles in Cluster Atmospheres	123
2.2 Bubbles in A Galaxy Atmosphere – M84	124
2.3 Evolution of Buoyant Plasma Bubbles in Hot Gaseous Atmospheres	125
3 Conclusions	129

5	Observational signatures and statistics of galaxy cluster mergers	133
	<i>Hans Böhringer and Peter Schuecker</i>	
1	X-ray diagnostics for cluster mergers	135
2	The Virgo Cluster as a Laboratory for Detailed Merger Studies	142
3	Observational Consequences of Cluster Mergers	145
4	Merger statistics	148
4.1	Robust substructure tests to measure substructure occurrence rates	149
4.2	Observed substructure occurrence rates	151
4.3	Theoretical aspects	154
4.4	Substructure density relation	156
4.5	Substructures in halo, relic, and cooling flow clusters	157
6	Radio Galaxies and their Environment	163
	<i>Luigina Feretti and Tiziana Venturi</i>	
1	Cluster X-ray emitting gas	166
2	Radio Structures	168
2.1	Narrow-angle tailed radio galaxies	169
2.2	Wide-Angle tailed radio galaxies	172
2.3	Radio galaxies in cooling flows	175
3	Confinement	177
4	Statistics of Radio Sources:Radio luminosity functions	179
4.1	Local RLF for field galaxies	180
4.2	Local RLF for cluster galaxies	181
4.3	Radio emission and large scale environment	183
5	Radio power-size correlation	184
6	Environment and starburst radio emission	184
6.1	Radio sources and the Butcher-Oemler effect	185
6.2	FIR/Radio correlation for spirals in clusters	187
7	Gas stripping and HI deficiency in cluster spirals	189
7	Diffuse Radio Sources and Cluster Mergers	197
	<i>Gabriele Giovannini and Luigina Feretti</i>	
1	A Working Definition	200
2	Observations and Results	202
2.1	The Radio Halo Coma C	203
2.2	Diffuse emission in the Coma Cluster Periphery	204
2.3	Clusters with well known Diffuse Sources	205
2.4	New Halo and Relic Sources	206
3	Statistical properties of radio halos and relics	208
3.1	Radio properties	209
3.2	Occurrence	210
3.3	Correlations with cluster properties	210
4	Relevance of Cluster Merger Events	212
5	Models	215
5.1	Magneticfield	215
5.1.1	Observational results	215
5.1.2	Interpretation	216

5.2	Relativistic particles in halos	217
5.2.1	Primary electron models	218
5.2.2	Primary electron reacceleration models	218
5.2.3	Origin of the primary relativistic electrons	219
5.2.4	Secondary electron model	219
5.2.5	The Two Phase model	221
5.3	Relativistic particles in Relics	222
6	Summary	223
8		
Mergers of Galaxy Clusters in		229
Numerical Simulations		
<i>Sabine Schindler</i>		
1	Simulation Methods	230
2	Cluster Models	232
3	Effects of mergers	232
3.1	Shocks	235
3.2	Observable Effects of Mergers	237
4	Physical Processes	239
4.1	Simulations of Mergers with Magnetic Fields	239
4.2	Cooling and Star Formation	241
5	Metallicity-Merger Connection	242
6	Mass Determination in Merging Clusters	246
7	Summary and Prospects	248
9		
Clusters, Cosmology and Mergers		253
<i>August E. Evrard and Isabella M. Gioia</i>		
1	Gravitational Instability: Theory and Computation	256
1.1	The late universe	256
1.2	Isolated, spherical clusters	257
1.3	3-D hierarchical clustering	259
2	The Discrete Cluster Population	267
2.1	From cluster surveys to cosmology	267
2.2	The mass function	268
2.2.1	Frequency of Mergers	272
2.3	Cluster internal structure	274
2.3.1	Dark matter density profiles	274
2.3.2	The dark matter virial theorem	276
2.3.3	The ICM virial relation	278
2.4	Cluster observables	282
3	Constraints on Cosmological parameters	283
3.1	Cluster surveys	284
3.2	Ω_m from the cluster baryon fraction	286
3.3	σ_8 from the local temperature function	288
3.4	Ω_m from distant cluster counts	290
3.4.1	SZ survey yields	293
3.4.2	X-ray flux limited samples from ROSAT	295
4	Summary	296

<i>Contents</i>	ix
Topic Index	305
Object Index	309
Copyright Credits	311

This page intentionally left blank

Preface

The idea for this book originated from the Joint Discussion 10 of the XXIV IAU General Assembly held in Manchester (England) in the summer of 2000. The extremely successful session on mergers in clusters of galaxies persuaded the publisher of this book to have a volume on such a topic.

Clusters of galaxies are by now recognized to be not simple relaxed structures, but rather they are evolving via merging processes in a hierarchical fashion from poor groups to rich clusters. Much progress has been made in recent years in the observations of the signatures of merging processes at many wavelengths. Substructures have been detected in optical and in X-rays, temperature gradients have been found in X-ray spectroscopic data and evidence of non-thermal processes in clusters have been provided by studies in the radio, EUV and hard X-ray bands. A new aspect of these investigations is the comparison of the results at different wavelengths which gives us overall insight on cluster formation and evolution. At the same time, theoretical progress has been made in the modeling of clusters, supported by numerical simulations, which are more and more sophisticated due to the growing power of modern computers.

We have asked several colleagues, working observationally and theoretically on clusters of galaxies, to write the reviews which are presented here. We do not mean to cover all the cluster phenomenology, but mainly those aspects related to the merger processes: the physics of cluster mergers, the observational situation of mergers from optical, radio and X-ray points of view, the simulations and theoretical aspects, and, the cosmological implications. There are nine chapters, each authored by one or more researchers who are expert in the chosen topic. The present set of chapters puts the emphasis on the type of data available to us today, on their interpretation and on theoretical issues of cluster merging processes. We want to stress that the chapters are not necessarily expected to be comprehensive reviews of any of the fields covered, but rather overall outlines which the individual authors felt would be suit-

able for graduate students and workers in the field alike. Each chapter is self-contained and it is not intended to be the continuation of the previous chapter. This implies that the same topic can be presented and discussed in more than one review but from a slightly different point of view, reflecting the knowledge and expertise of the reviewer.

We believe such a book is particularly timely given the wealth of data that we are receiving from ground telescopes (extremely large and sensitive radio and optical telescopes) and from space telescopes (Hubble, Chandra and XMM-Newton). Data from ROSAT, ASCA and BeppoSAX are reviewed as well. The flow of the new and high quality data is continuous. Thus some of the most recent results will be inevitably missing from this book when it goes to press. However we feel that this is unavoidable and that it actually reflects a very dynamic and positive trend in our knowledge of cluster mergers. We note, in particular, that during the preparation of this book the standard cooling flow scenario has been the object of much debate since the XMM-Newton spectral results suggest the absence of large amounts of cooling and condensing gas in the centers of cooling flow clusters. Here we do not go into the details of this issue which is still in dispute, and we retain the standard scenario.

Some figures have been reprinted from the Journals where they were originally published. We thank all the authors who have allowed us to reproduce their material, and we acknowledge all the publishers for granting copyright permissions.

Bologna, 13 November 2001

Luigina Feretti
Isabella M. Gioia
Gabriele Giovannini

Contributing Authors

Dr. Andrea Biviano is a Scientific Staff Member of the INAF, Trieste (Italy). After earning his PhD at the Trieste University in 1992, he worked at IAP, Paris, at the Leiden Observatory, and at ESA, Madrid. He works on galaxy clusters and galaxy evolution.

Dr. Hans Böhringer is a Scientific Staff Member of the Max-Planck-Institut für extraterrestrische Physik in Garching (Germany) where he is leading a research group for theoretical astrophysics and X-ray astronomy of clusters of galaxies. Since 1999 he is also a lecturer at the Ludwig-Maximilians-Universität of Munich.

Dr. David Buote is an Assistant Professor in the Department of Physics and Astronomy at the University of California at Irvine (USA) where he has taught since January, 2000. He earned his PhD from the Massachusetts Institute of Technology and studies the dynamical and chemical properties of galaxies and clusters using X-ray observations.

Dr. Eugene Churazov is a Scientific Staff Member at Max-Planck Institute for Astrophysics in Garching (Germany). He earned his PhD from the Space Research Institute in Moscow in 1989. He works on X-ray emission from clusters of galaxies and compact binary sources.

Dr. August E. Evrard is a Professor in the Departments of Physics and Astronomy at the University of Michigan (USA). He joined the faculty in Ann Arbor in 1990, after obtaining a doctoral degree in physics from State University of New York at Stony Brook in 1986. His main research area of computational cosmology includes modeling the formation of galaxies and clusters of galaxies.

Dr. Luigina Feretti joined the Istituto di Radioastronomia del CNR in Bologna (Italy) as Scientific Staff Member in 1996, after being an Assistant Professor at the Astronomy Department of the University of Bologna. She obtained her PhD in physics from the University of Bologna. She works mainly on the non-thermal emission processes in radiogalaxies and galaxy clusters.

Dr. William Forman is a Senior Astrophysicist at the Smithsonian Astrophysical Observatory in Cambridge (USA). He received his undergraduate degree at Haverford College and his PhD from Harvard University. He joined the staff of the Smithsonian in 1973 where he has participated in X-ray astronomy missions including Einstein, ROSAT, and Chandra. His interests include the study of hot gas in galaxies and galaxy clusters and the evolution and formation of large scale structure.

Dr. Isabella M. Gioia is a Senior Astrophysicist at the Istituto di Radioastronomia del CNR in Bologna (Italy). She obtained her PhD in physics from the University of Bologna and worked at the Smithsonian Astrophysical Observatory in Cambridge (USA) and at the Institute for Astronomy of the University of Hawaii in Honolulu (USA). She studies the evolutionary properties of clusters of galaxies using optical and X-ray telescopes.

Dr. Gabriele Giovannini is a Professor of Astrophysics in the Physics Department of the Bologna University and obtained his PhD in physics from the University of Bologna (Italy). He is a Scientific Collaborator of the Istituto di Radioastronomia del CNR and studies radio emission from active galactic nuclei and clusters of galaxies.

Dr. Marisa Girardi is an Assistant Professor at the Department of Astronomy of the University of Trieste (Italy). She earned her PhD from the SISSA in 1992. She works on galaxy clusters, their optical properties and internal dynamics.

Dr. Christine Jones is a Senior Astrophysicist at the Smithsonian Astrophysical Observatory in Cambridge (USA). She received her undergraduate and graduate degrees from Harvard University. She studies the X-ray emission from binary X-ray sources, elliptical galaxies, clusters, and gravitational lenses.

Dr. Maxim Markevitch is an Astrophysicist at the Smithsonian Astrophysical Observatory in Cambridge (USA) where he works on X-ray studies of galaxy clusters. He earned his PhD in 1993 from Moscow (Russia) Institute of Physics and Technology.

Dr. Craig L. Sarazin is the W. H. Vanderbilt Professor of Astronomy at the University of Virginia (USA), where he has taught since 1977. He earned his PhD in physics from Princeton University in 1975, and works on X-ray emission, clusters of galaxies, and elliptical galaxies.

Dr. Sabine Schindler is a Senior Research Fellow at the Astrophysics Research Institute of the Liverpool John Moores University (UK). She earned her PhD from the Ludwig-Maximilians-Universität of Munich, (Germany). She works on various aspects of clusters of galaxies combining numerical simulations with observations at several wavelengths.

Dr. Peter Schuecker is a Scientific Staff Member at the Max-Planck Institut für Extraterrestrische Physik in Garching (Germany) since 1998. He is also a lecturer at the Physics Department of the University of Muenster where he obtained his PhD. He works on galaxy clusters and their large-scale distribution.

Dr. Tiziana Venturi is an Astronomer at the Istituto di Radioastronomia del CNR in Bologna (Italy). She obtained her PhD in Astronomy at the University of Bologna and works on active galactic nuclei and clusters of galaxies under an observational perspective.

Dr. Alexey Vikhlinin is an Astrophysicist at the Smithsonian Astrophysical Observatory in Cambridge (USA). He earned his PhD from the Space Research Institute in Moscow (Russia). His research is concentrated on using X-ray cluster observations to understand the physical state of the intracluster medium, and also on the relation between clusters and cosmology.

This page intentionally left blank

Chapter 1

THE PHYSICS OF CLUSTER MERGERS

Craig L. Sarazin

Department of Astronomy

University of Virginia

P. O. Box 3818

Charlottesville, VA 22903-0818, USA

sarazin@virginia.edu

Abstract Clusters of galaxies generally form by the gravitational merger of smaller clusters and groups. Major cluster mergers are the most energetic events in the Universe since the Big Bang. Some of the basic physical properties of mergers will be discussed, with an emphasis on simple analytic arguments rather than numerical simulations. Semi-analytic estimates of merger rates are reviewed, and a simple treatment of the kinematics of binary mergers is given. Mergers drive shocks into the intracluster medium, and these shocks heat the gas and should also accelerate non-thermal relativistic particles. X-ray observations of shocks can be used to determine the geometry and kinematics of the merger. Many clusters contain cooling flow cores; the hydrodynamical interactions of these cores with the hotter, less dense gas during mergers are discussed. As a result of particle acceleration in shocks, clusters of galaxies should contain very large populations of relativistic electrons and ions. Electrons with Lorentz factors $\gamma \sim 300$ (energies $E = \gamma m_e c^2 \sim 150$ MeV) are expected to be particularly common. Observations and models for the radio, extreme ultraviolet, hard X-ray, and gamma-ray emission from nonthermal particles accelerated in these mergers are described.

Introduction

Major cluster mergers are the most energetic events in the Universe since the Big Bang. Cluster mergers are the mechanism by which clusters are assembled. In these mergers, the subclusters collide at velocities of ~ 2000 km/s, releasing gravitational binding energies of as much as $\gtrsim 10^{64}$ ergs. During mergers, shocks are driven into the intracluster medium. In major mergers, these hydrodynamical shocks dissipate en-

ergies of $\sim 3 \times 10^{63}$ ergs; such shocks are the major heating source for the X-ray emitting intracluster medium. The shock velocities in merger shocks are similar to those in supernova remnants in our Galaxy, and we expect them to produce similar effects. Mergers shocks should heat and compress the X-ray emitting intracluster gas, and increase its entropy. We also expect that particle acceleration by these shocks will produce relativistic electrons and ions, and these can produce synchrotron radio, inverse Compton (IC) extreme ultraviolet (EUV) and hard X-ray, and gamma-ray emission.

In this chapter, I will review some of the basic physics of cluster mergers. As later chapters discuss the optical, X-ray, and radio observations of mergers, I will concentrate of theoretical issues. Also, because later chapters discuss simulations of cluster mergers and of large scale structure, I will mainly discuss analytical or semi-analytical aspects of cluster mergers. In § 1.1, semi-analytic estimates of merger rates based on Press-Schechter theory are reviewed. Some simple estimates of the kinematics of binary cluster mergers are given in § 1.2. The thermal effects of merger shocks are discussed in § 2, with an emphasis on determining the physical conditions in mergers from X-ray observations of temperatures and densities. Many clusters and groups contain cooling flow cores. During a merger, these cool cores will interact hydrodynamically with the hotter, more diffuse intracluster gas (§ 3). This can lead to the disruption of the cooling flow core, as discussed in § 3.1. Recently, the Chandra X-ray Observatory has detected a number of “cold fronts” in merging clusters, which apparently are cool cores moving through hot, shock heated, diffuse cluster gas (§ 3.2). Relativistic particles may be accelerated or reaccelerated in merger shocks or turbulence generated by mergers. The nonthermal effects of mergers are discussed in § 4. The resulting radio, extreme ultraviolet, hard X-ray, and gamma-ray emission is described.

1. BASIC MERGER RATES AND KINEMATICS

1.1. ESTIMATES OF MERGER RATES

The rates of cluster mergers as a function of the cluster masses and redshift can be estimated using a simple formalism originally proposed by Press & Schechter (1974, hereafter PS), and developed in more detail by Bond et al. (1991) and Lacey & Cole (1993), among others. Comparisons to observations of clusters and to numerical simulations show that PS provides a good representation of the statistical properties of clusters, if the PS parameters are carefully selected (e.g., Lacey & Cole

1993; Bryan & Norman 1998). This formalism assumes that galaxies and clusters grow by the gravitational instability of initially small amplitude gaussian density fluctuations generated by some process in the early Universe. The fluctuation spectrum is assumed to have larger amplitudes on smaller scales. Thus, galaxies and clusters form hierarchically, with lower mass objects (galaxies and groups of galaxies) forming before larger clusters. These smaller objects then merge to form clusters.

In the extended PS formalism, the density fluctuations in the Universe are smoothed on a variety of mass scales. Regions are assumed to collapse when their density exceeds a critical value, which is usually taken to be the density for the collapse for an isolated, spherical mass concentration of the same mass. If one smooths the density fluctuations in some region on a variety of mass scales, the average density may exceed the critical density for collapse on a variety of different mass scales. The assumption of the extended PS formalism is that material is associated with the largest mass scale for which collapse has occurred, and that smaller mass scales have merged into the larger object. With these assumptions, the PS formalism allows one to estimate the abundance of clusters as a function of their mass, and the rates at which clusters merge.

Let $n(M, z)dM$ be the comoving number density of clusters with masses in the range M to $M + dM$ in the Universe at a redshift of z . According to PS, the differential number density is given by

$$n(M, z) dM = \sqrt{\frac{2}{\pi}} \frac{\bar{\rho}}{M^2} \frac{\delta_c(z)}{\sigma(M)} \left| \frac{d \ln \sigma(M)}{d \ln M} \right| \exp \left[-\frac{\delta_c^2(z)}{2\sigma^2(M)} \right] dM, \quad (1)$$

where $\bar{\rho}$ is the current mean density of the Universe, $\sigma(M)$ is the current rms density fluctuation within a sphere of mean mass M , and $\delta_c(z)$ is the critical linear overdensity for a region to collapse at a redshift z .

In Cold Dark Matter models, the initial spectrum of fluctuations can be calculated for various cosmologies (Bardeen et al. 1986). Over the range of scales covered by clusters, it is generally sufficient to consider a power-law spectrum of density perturbations, which is consistent with these CDM models:

$$\sigma(M) = \sigma_8 \left(\frac{M}{M_8} \right)^{-\alpha}, \quad (2)$$

where σ_8 is the present day rms density fluctuation on a scale of $8 h^{-1}$ Mpc, $M_8 = (4\pi/3)(8 h^{-1} \text{ Mpc})^3 \bar{\rho}$ is the mass contained in a sphere of radius $8 h^{-1}$ Mpc, and the scaling with the Hubble constant is $h = H_0/100$. When the scaling with the Hubble constant is not given explicitly, we assume $H_0 = 50 \text{ km s}^{-1} \text{ Mpc}^{-1}$, i.e. $h = 0.5$. The exponent α is given

by $\alpha = (n + 3)/6$, where the power spectrum of fluctuations varies with wavenumber k as k^n . The observations are generally reproduced with values of $-2 \lesssim n \lesssim -1$, leading to $1/6 \lesssim \alpha \lesssim 1/3$. The normalization of the power spectrum and overall present-day abundance of clusters is set by σ_8 . The observed present-day abundance of clusters leads to $\sigma_8 \approx 0.6\Omega_m^{-1/2}$, where $\Omega_m \equiv \bar{\rho}/\rho_c$ is the ratio of the current mass density to the critical mass density, $\rho_c = 3H_0^2/(8\pi G)$ (e.g., Bahcall & Fan 1998).

The evolution of the density of clusters is encapsulated in the critical over-density $\delta_c(z)$ in equation (1). In general, $\delta_c(z) \propto 1/D(t)$, where $D(t)$ is the growth factor of linear perturbations as a function of cosmic time t (see Peebles 1980, § 11 for details). Expressions for the $\delta_c(z)$ in different cosmological models are:

$$\delta_c(z) = \begin{cases} \frac{3}{2}D(t_0) \left[1 + \left(\frac{t_\Omega}{t} \right)^{\frac{2}{3}} \right] & (\Omega_m < 1, \Omega_\Lambda = 0) \\ \frac{3(12\pi)^{\frac{2}{3}}}{20} \left(\frac{t_\Omega}{t} \right)^{\frac{2}{3}} & (\Omega_m = 1, \Omega_\Lambda = 0) \\ \frac{D(t_0)}{D(t)} \left(\frac{3(12\pi)^{\frac{2}{3}}}{20} \right) (1 + 0.0123 \log \Omega_z) & (\Omega_m + \Omega_\Lambda = 1) \end{cases} \quad (3)$$

Here, Ω_Λ gives the contribution due to a cosmological constant Λ , where $\Omega_\Lambda \equiv \Lambda/(3H_0^2)$. For the open model ($\Omega_m < 1, \Omega_\Lambda = 0$), $t_\Omega \equiv \pi H_0^{-1} \Omega_m (1 - \Omega_m)^{-\frac{3}{2}}$ represents the epoch at which a nearly constant expansion takes over and no new clustering can occur. The growth factor can be expressed as

$$D(t) = \frac{3 \sinh \eta (\sinh \eta - \eta)}{(\cosh \eta - 1)^2} - 2 \quad (4)$$

where η is the standard parameter in the cosmic expansion equations (Peebles 1980, eqn. 13.10)

$$\begin{aligned} \frac{1}{1+z} &= \frac{\Omega_m}{2(1-\Omega_m)} (\cosh \eta - 1) , \\ H_0 t &= \frac{\Omega_m}{2(1-\Omega_m)^{\frac{3}{2}}} (\sinh \eta - \eta) . \end{aligned} \quad (5)$$

The solution for δ_c in the Einstein-de Sitter model ($\Omega_m = 1, \Omega_\Lambda = 0$) can be obtained from the open model solution by the limit $t_\Omega/t \rightarrow \infty$. The expression for δ_c in the flat model ($\Omega_m + \Omega_\Lambda = 1$) is an approximation given by Kitayama & Suto (1996). Here Ω_z is the value of the mass density ratio Ω_m at the redshift z ,

$$\Omega_z = \frac{\Omega_m (1+z)^3}{\Omega_m (1+z)^3 + \Omega_\Lambda} . \quad (6)$$

In this model the growth factor can be written as

$$D(x) = \frac{(x^3 + 2)^{1/2}}{x^{3/2}} \int_0^x x^{3/2} (x^3 + 2)^{-3/2} dx \quad (7)$$

(Peebles 1980, eqn. 13.6) where $x_0 \equiv (2\Omega_\Lambda/\Omega_m)^{1/3}$ and $x = x_0/(1+z)$.

The PS formalism also provides estimates of the merger history, rates, and probabilities for clusters. For example, the probability that a cluster with a mass M_0 at the present time t_0 had a progenitor with a mass of M at an earlier time $t < t_0$ is given by

$$\frac{dp}{dM}(M, t|M_0, t_0) = \frac{\delta_c(t) - \delta_c(t_0)}{\sqrt{2\pi} [\sigma^2(M) - \sigma^2(M_0)]^{3/2}} \left(\frac{M_0}{M}\right) \left| \frac{d\sigma^2(M)}{dM} \right| \exp \left\{ -\frac{[\delta_c(t) - \delta_c(t_0)]^2}{2[\sigma^2(M) - \sigma^2(M_0)]} \right\}. \quad (8)$$

Similarly, the probability that a cluster of mass M undergoes a merger with cluster of mass ΔM per unit time is given by

$$\frac{d^2p}{d\Delta M dt} = \sqrt{\frac{2}{\pi}} \frac{\delta_c(z)}{\sigma(M')} \left| \frac{d \ln \delta_c(z)}{dt} \right| \left| \frac{d \ln \sigma(M')}{dM'} \right| \left[1 - \frac{\sigma^2(M')}{\sigma^2(M)} \right]^{-3/2} \times \exp \left\{ -\frac{\delta_c^2(z)}{2} \left[\frac{1}{\sigma^2(M')} - \frac{1}{\sigma^2(M)} \right] \right\}, \quad (9)$$

where $M' = M + \Delta M$.

These probability distributions can be used to make Monte Carlo simulations of the merger histories which produced clusters of a various masses at present. Figure 1.1 shows one such ‘‘merger tree’’ for a cluster with a mass of $10^{15} h^{-1} M_\odot$ at the present time (Randall et al. 2001). At least to the extent that the development of a cluster can be treated as a series of separate, discrete merger events separated by periods of approximate equilibrium (the ‘‘punctuated equilibrium’’ model; Cavaliere et al. 1999), these merger histories can be used to determine the effects of mergers on clusters.

1.2. ESTIMATES OF MERGER KINEMATICS

I now give some simple analytic arguments to estimate the kinematics of an individual binary merger collision. The kinematic quantities describing the merger are defined in Figure 1.2, which is taken from Ricker & Sarazin (2001). The two subclusters have masses M_1 and M_2 . Let d be the separation of the centers of the two subclusters, let v be the relative velocity of the centers, and let b be the impact parameter of the collision.

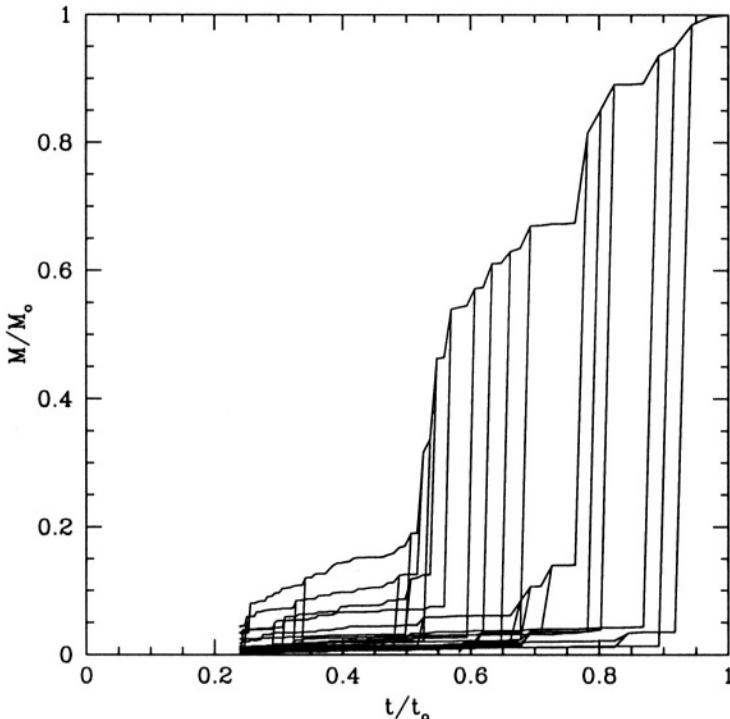


Figure 1.1. An example of a PS merger tree for a cluster of galaxies with a final mass of $M_0 = 10^{15} h^{-1} M_\odot$ (Randall et al. 2001). The mass is shown as a function of the age of the Universe t ; the present age is t_0 . This model was for an open Universe with $\Omega_m = 0.3$ and $\Omega_\Lambda = 0$.

1.2.1 Turn-Around Distances. Assume that the two subclusters of mass M_1 and M_2 merge at some time t_{merge} (the age of the Universe at the time of the merger). It is assumed that the two subclusters have fallen together from a large distance d_0 with (possibly) nonzero angular momentum. (The exact value of d_0 does not affect the collision velocity very strongly as long as it is large and the infall velocity approaches free-fall from infinity.) For the purpose of computing the initial relative velocity, we approximate the two clusters as point masses. We assume that the two subclusters were initially expanding away from one another in the Hubble flow, and that their radial velocity was zero at their greatest separation d_0 . If we assume that the two subclusters dominate the mass in the region of the Universe they occupy, we can treat their initial expansion and recollapse as the orbit of two point masses, and Kepler's Third Law gives the greatest separation as

$$d_0 \approx [2G(M_1 + M_2)]^{1/3} \left(\frac{t_{\text{merge}}}{\pi} \right)^{2/3}$$

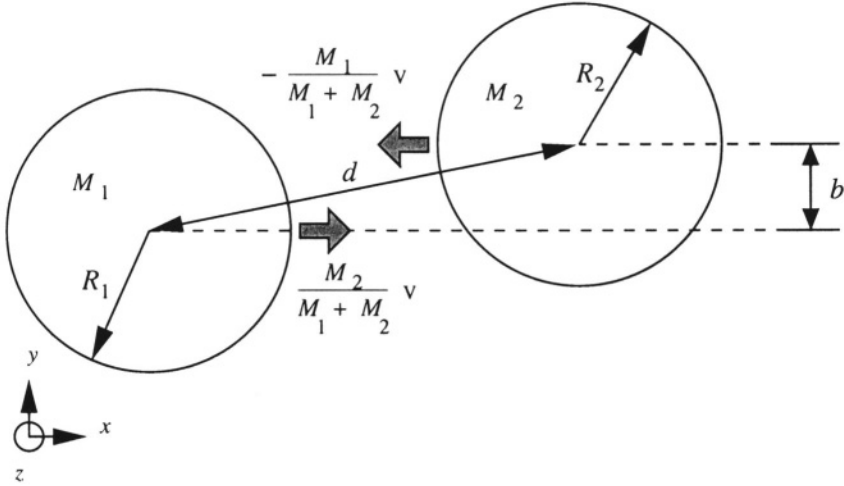


Figure 1.2. A schematic diagram of the kinematics for a merger between two sub-clusters of masses M_1 and M_2 and radii R_1 and R_2 . The separation of the cluster centers is d , and the impact parameter is b , and the initial relative velocity is v .

$$\approx 4.5 \left(\frac{M_1 + M_2}{10^{15} M_\odot} \right)^{1/3} \left(\frac{t_{\text{merge}}}{10^{10} \text{ yr}} \right)^{2/3} \text{ Mpc}. \quad (10)$$

1.2.2 Merger Velocities. At the separation d_0 , the clusters are assumed to have zero relative radial velocity; hence their orbital angular momentum and energy are

$$\begin{aligned} J_{\text{orb}} &\approx m v_0 d_0 \\ E_{\text{orb}} &\approx \frac{1}{2} m v_0^2 - \frac{G M_1 M_2}{d_0}, \end{aligned} \quad (11)$$

where their reduced mass is

$$m \equiv \frac{M_1 M_2}{M_1 + M_2}, \quad (12)$$

and v_0 is their initial relative transverse velocity. At the separation d , the relative velocity v is perpendicular to the direction of b , so we can write

$$\begin{aligned} J_{\text{orb}} &\approx m v b \\ E_{\text{orb}} &\approx \frac{1}{2} m v^2 - \frac{G M_1 M_2}{d}. \end{aligned} \quad (13)$$

Conserving angular momentum and energy, we eliminate v_0 and find

$$v^2 \approx 2G(M_1 + M_2) \left(\frac{1}{d} - \frac{1}{d_0} \right) \left[1 - \left(\frac{b}{d_0} \right)^2 \right]^{-1}, \quad (14)$$

or

$$v \approx 2930 \left(\frac{M_1 + M_2}{10^{15} M_\odot} \right)^{1/2} \left(\frac{d}{1 \text{ Mpc}} \right)^{-1/2} \left[\frac{1 - \frac{d}{d_0}}{1 - \left(\frac{b}{d_0} \right)^2} \right]^{1/2} \text{ km s}^{-1}. \quad (15)$$

1.2.3 Angular Momenta, Impact Parameters, and Transverse Velocities.

The remaining kinematic parameter for the merger is the impact parameter b , or equivalently the orbital angular momentum J_{orb} or the initial tangential velocity v_0 . In principal, a range of values are possible for mergers of subclusters with similar masses and similar merger epochs t_{merge} . The angular momentum will be determined by tidal torques from surrounding material. Thus, I give an estimate of the range of possible values based on the linear-theory result for the dimensionless spin of dark-matter halos; this argument is given in Ricker & Sarazin (2001). The spin parameter λ is defined as (Peebles 1969)

$$\lambda \equiv \frac{J|E|^{1/2}}{GM^{5/2}}. \quad (16)$$

Here J is the total angular momentum of the halo, E is its total energy, and M is its mass. In linear theory, the average value of λ is expected to be approximately constant, independent of the mass of the halo. Recently, Sugerman et al. (2000) have performed a detailed comparison of linear-theory predictions to actual angular momenta of galaxies formed in cosmological N -body/hydro calculations. These simulations did not include cooling or star formation, so at the upper end of the mass range they studied their results should carry over to clusters. They find, in agreement with White (1984), that linear theory overpredicts the final angular momentum of galaxies by roughly a factor of three, with a large ($\sim 50\%$) dispersion in the ratio of the linear-theory prediction to the actual value. However, given the uncertainties, the angular momenta agree with the results in equation (16) for a value of $\lambda \approx 0.05$. Thus, we will assume that the average total angular momenta of clusters of galaxies are given by

$$J \approx \frac{\lambda GM^{5/2}}{|E|^{1/2}}, \quad (17)$$

with $\lambda \approx 0.05$. The normal virial relations for clusters imply that the energies of clusters scale with their mass as $|E| \propto M^{5/3}$, which implies that the angular momenta scale as $J \propto M^{5/3}$ as well.

Let us take the halo to be the final merged cluster. Its final total angular momentum is the sum of the angular momenta of the two subclusters plus the orbital angular momentum J_{orb} . Applying equation (17) to the initial masses M_1 and M_2 and the final mass $M_1 + M_2$ and taking the difference gives the orbital angular momentum J_{orb} . We assume that the angular momenta are correlated (i.e., that they lie along the same direction), since they are all produced by approximately the same local tidal field. The final energy of the merged cluster is the sum of the energies of the initial subclusters plus the orbital energy E_{orb} . The rotational kinetic energies can be ignored as they are only a fraction $\sim 2\lambda^2 \lesssim 1\%$ of the total energies.

Using these relations, the average orbital angular momentum of the merger is found to be

$$J_{\text{orb}} \approx \frac{\lambda G M_1 M_2}{\left[\frac{G(M_1 + M_2)}{d_0} - \frac{1}{2} v_0^2 \right]^{1/2}} f(M_1, M_2). \quad (18)$$

Here, the function $f(M_1, M_2)$ corrects for the internal angular momenta and energy of the subclusters. This correction can be written as

$$f(M_1, M_2) \equiv \frac{(M_1 + M_2)^3}{M_1^{3/2} M_2^{3/2}} \left[1 - \frac{(M_1^{5/3} + M_2^{5/3})}{(M_1 + M_2)^{5/3}} \right]^{3/2}, \quad (19)$$

but it only depends on the ratio ($M_{<}/M_{>}$) of the smaller to larger mass of the two subclusters. It varies between $4(2^{2/3} - 1)^{3/2} \approx 1.80 \leq f(M_1, M_2) \leq (5/3)^{3/2} \approx 2.15$, so that $f(M_1, M_2) \approx 2$. The kinetic energy term $v_0^2/2$ in the denominator of equation (18) can be shown to be approximately $2\lambda^2 \approx 1\%$ of the potential energy term. Thus, this term can be dropped to yield

$$J_{\text{orb}} \approx \lambda M_1 M_2 \sqrt{\frac{G d_0}{M_1 + M_2}} f(M_1, M_2). \quad (20)$$

The corresponding initial transverse velocity is

$$\begin{aligned} v_0 &\approx \lambda \sqrt{\frac{G(M_1 + M_2)}{d_0}} f(M_1, M_2) \\ &\approx 93 \left(\frac{\lambda}{0.05} \right) \left(\frac{M_1 + M_2}{10^{15} M_\odot} \right)^{1/2} \left(\frac{d_0}{5 \text{ Mpc}} \right)^{-1/2} \left(\frac{f}{2} \right) \text{ km s}^{-1}. \end{aligned} \quad (21)$$

After the clusters have fallen towards one another to a separation d , the impact parameter for the collision is (Figure 1.2)

$$b \approx \left(\frac{v_0}{v} \right) d_0, \quad (22)$$

where the infall velocity is given by equation (15). Note that equation (22) implies that $b \ll d_0$, so that one can drop the (b/d_0) term in equation (15). Substituting equations (15) & (21) into equation (22) gives

$$\begin{aligned} b &\approx \lambda \sqrt{\frac{d_0 d}{2}} \left(1 - \frac{d}{d_0}\right)^{-1/2} f(M_1, M_2) \\ &\approx 160 \left(\frac{\lambda}{0.05}\right) \left(\frac{d}{1 \text{ Mpc}}\right)^{1/2} \left(\frac{d_0}{5 \text{ Mpc}}\right)^{1/2} \left(1 - \frac{d}{d_0}\right)^{-1/2} \left(\frac{f}{2}\right) \text{ kpc}. \end{aligned} \quad (23)$$

Thus, most mergers are expected to involve fairly small impact parameters, comparable to the sizes of the gas cores in clusters. Many examples are known of mergers where the X-ray morphology suggests a small offset; an example is the merger in the cluster surrounding Cygnus-A (Markevitch et al. 1999). However, the preceding arguments are approximate and statistical, and mergers with larger impact parameters are also expected to occur; based on the X-ray image and temperature map, it is likely that Abell 3395 is an example of such a merger (Markevitch et al. 1998). Larger impact parameters may occur in mergers involving more than two subclusters. On the other hand, the distribution of impact parameters may be biased to lower values if most mergers occur along large scale structure filaments (e.g., Evrard & Gioia, this volume).

2. THERMAL PHYSICS OF MERGER SHOCKS

The intracluster medium (ICM) is generally close to hydrostatic equilibrium in clusters which are not undergoing strong mergers. The virial theorem then implies that the square of the thermal velocity (sound speed) of the ICM is comparable to the gravitational potential. During a merger, the infall velocities of the subclusters (equation 15) are comparable to the escape velocity, which implies that the square of the infall velocity is larger (by roughly a factor of two) than the gravitational potential. Thus, the motions in cluster mergers are expected to be supersonic, but only moderately so. As a result, one expects that cluster mergers will drive shock waves into the intracluster gas of the two subclusters. Let v_s be the velocity of such a shock wave relative to the preshock intracluster gas. The sound speed in the preshock gas is $c_s = \sqrt{(5/3)P/\rho}$, where P is the gas pressure and ρ is the density. Then,

the Mach number of the shock is $\mathcal{M} \equiv v_s/c_s$. Based on the simple argument given above and confirmed by merger simulations (Schindler & Müller 1993; Roettiger et al. 1999; Ricker & Sarazin 2001; Schindler, this volume), one expects shocks with Mach numbers of $\mathcal{M} \lesssim 3$. Stronger shocks may occur under some circumstances, such as in the outer parts of clusters, or in low mass subclusters merging with more massive clusters. However, in the latter case, the shocks in the less massive subcluster may also be weak if the intergalactic gas in the smaller subcluster is denser than that in the more massive subclusters (§ 3).

Shocks are irreversible changes to the gas in clusters, and thus increase the entropy S in the gas. A useful quantity to consider is the specific entropy per particle in the gas, $s \equiv S/N$, where N is the total number of particles. To within additive constants, the specific entropy of an ideal gas is

$$\begin{aligned} s &= \frac{3}{2} k \ln \left(\frac{P}{\rho^{5/3}} \right), \\ &= \frac{3}{2} k \ln \left(\frac{T}{\rho^{2/3}} \right), \end{aligned} \quad (24)$$

where T is the gas temperature. Observations of X-ray spectra can be used to determine T , while the X-ray surface brightness depends on ρ^2 . Thus, one can use X-ray observations to determine the specific entropy in the gas just before and just after apparent merger shocks seen in the X-ray images. Since merger shocks should produce compression, heating, pressure increases, and entropy increases, the corresponding increase in all of these quantities (particularly the entropy) can be used to check that discontinuities are really shocks (e.g., not “cold fronts” or other contact discontinuities, § 3.2).

Markevitch et al. (1999) applied this test to ASCA temperature maps and ROSAT images of Cygnus-A and Abell 3667, two clusters which appeared to show strong merger shocks. (Recent Chandra images have cast doubt on the interpretation of Abell 3667, Vikhlinin et al. 2001b.) In Cygnus-A, the increase in specific entropy in the shocked regions is roughly $\Delta s \approx (3/2)k$. The specific heat per particle q which must be dissipated to produce this change in entropy is $q \approx T\Delta s \approx (3/2)kT$, or about the present specific heat content in the shocked gas. Thus, these observations provide a direct confirmation that merger shocks contribute significantly to the heating of the intracluster gas.

2.1. SHOCK KINEMATICS

The variation in the hydrodynamical variables in the intracluster medium across a merger shock are determined by the standard Rankine–

Hugoniot jump conditions (e.g., Landau & Lifshitz 1959, § 85), if one assumes that all of the dissipated shock energy is thermalized. Consider a small element of the surface of a shock (much smaller than the radius of curvature of the shock, for example). The tangential component of the velocity is continuous at the shock, so it is useful to go to a frame which is moving with that element of the shock surface, and which has a tangential velocity which is equal to that of the gas on either side of the shock. In this frame, the element of the shock surface is stationary, and the gas has no tangential motion. Let the subscripts 1 and 2 denote the preshock and postshock gas; thus, $v_1 = v_s$ is the longitudinal velocity of material into the shock (or alternative, the speed with which the shock is advancing into the preshock gas). Conservation of mass, momentum, and energy then implies the following jump conditions

$$\begin{aligned} \rho_1 v_1 &= \rho_2 v_2, \\ P_1 + \rho_1 v_1^2 &= P_2 + \rho_2 v_2^2, \\ w_1 + \frac{1}{2} v_1^2 &= w_2 + \frac{1}{2} v_2^2. \end{aligned} \quad (25)$$

Here, $w = P/\rho + \epsilon$ is the enthalpy per unit mass in the gas, and ϵ is the internal energy per unit mass. If the gas behaves as a perfect fluid on each side of the shock, the internal energy per unit mass is given by

$$\epsilon = \frac{1}{\gamma_{\text{ad}} - 1} \frac{P}{\rho}, \quad (26)$$

where γ_{ad} is the ratio of specific heats (the adiabatic index) and is $\gamma_{\text{ad}} = 5/3$ for fully ionized plasma. The jump conditions can be rewritten as:

$$\begin{aligned} \frac{P_2}{P_1} &= \frac{2\gamma_{\text{ad}}}{\gamma_{\text{ad}} + 1} \mathcal{M}^2 - \frac{\gamma_{\text{ad}} - 1}{\gamma_{\text{ad}} + 1} \\ \frac{v_2}{v_1} = \frac{\rho_1}{\rho_2} \equiv \frac{1}{C} &= \frac{2}{\gamma_{\text{ad}} + 1} \frac{1}{\mathcal{M}^2} + \frac{\gamma_{\text{ad}} - 1}{\gamma_{\text{ad}} + 1}, \end{aligned} \quad (27)$$

where $C \equiv \rho_2/\rho_1$ is the shock compression.

If one knew the velocity structure of the gas in a merging cluster, one could use these jump condition to derive the temperature, pressure, and density jumps in the gas. At present, the best X-ray spectra for extended regions in clusters of galaxies have come from CCD detectors on ASCA, Chandra, and XMM/Newton. CCDs have a spectral resolution of >100 eV at the Fe K line at 7 keV, which translates into a velocity resolution of >4000 km/s. Thus, this resolution is (at best) marginally insufficient to measure merger gas velocities in clusters. In a few cases with very bright regions and simple geometries, the grating spectrometers on Chandra

and especially XMM/Newton may be useful. However, it is likely that the direct determinations of gas velocities in most clusters will wait for the launch of higher spectral resolution nondispersive spectrometers on Astro-E2 and Constellation-X.

At present, X-ray observations can be used to directly measure the temperature and density jumps in merger shocks. Thus, one needs to invert the jump relations to give the merger shock velocities for a given shock temperature, pressure, and/or density increase. If the temperatures on either side of the merger shock can be measured from X-ray spectra, the shock velocity can be inferred from (Markevitch et al. 1999)

$$\Delta v_s = \left[\frac{kT_1}{\mu m_p} (C - 1) \left(\frac{T_2}{T_1} - \frac{1}{C} \right) \right]^{1/2}, \quad (28)$$

where $\Delta v_s = v_1 - v_2 = [(C - 1)/C]v_s$ is the velocity change across the shock, and μ is the mean mass per particle in units of the proton mass m_p . The shock compression C can be derived from the temperatures as

$$\frac{1}{C} = \left[\frac{1}{4} \left(\frac{\gamma_{\text{ad}} + 1}{\gamma_{\text{ad}} - 1} \right)^2 \left(\frac{T_2}{T_1} - 1 \right)^2 + \frac{T_2}{T_1} \right]^{1/2} - \frac{1}{2} \frac{\gamma_{\text{ad}} + 1}{\gamma_{\text{ad}} - 1} \left(\frac{T_2}{T_1} - 1 \right). \quad (29)$$

Alternatively, the shock compression can be measured directly from the X-ray image. However, it is difficult to use measurements of the shock compression alone to determine the shock velocity, for two reasons. First, a temperature is needed to set the overall scale of the velocities; as is obvious from equation (27), the shock compression allows one to determine the Mach number \mathcal{M} but not the shock velocity. The second problem is that temperature or pressure information is needed to know that a discontinuity in the gas density is a shock, and not a contact interface (e.g., the ‘‘cold fronts’’ discussed in § 3.2 below).

X-ray temperature maps of clusters have been used to derive the merger velocities using these relations. Markevitch et al. (1999) used ASCA observations to determine the kinematics of mergers in three clusters (Cygnus-A, Abell 2065, and Abell 3667). Because of the poor angular resolution of ASCA, these analyses were quite uncertain. More recently, possible shocks have been detected in Chandra images of a number of merging clusters (e.g., Abell 85, Kempner et al. 2001; Abell 665, Markevitch et al. 2001; Abell 3667, Vikhlinin et al. 2001b), and the shock jump conditions have been applied to determine the kinematics in these clusters.

The simplest case is a head-on symmetric merger ($b = 0$ and $M_1 = M_2$) at an early stage when the shocked region lies between the two

cluster centers. Markevitch et al. (1999) suggest that the Cygnus-A cluster is an example. If the gas within the shocked region is nearly stationary, then the merger velocity of the two subclusters is just $v = 2\Delta v_s$. Applying these techniques to the ASCA temperature map for the Cygnus-A cluster, Markevitch et al. found a merger velocity of $v \approx 2200$ km/s. This simple argument is in reasonable agreement with the results of numerical simulations of this merger (Ricker & Sarazin 2001). The radial velocity distribution of the galaxies in this cluster is bimodal (Owen et al. 1997), and consistent with a merger velocity of ~ 2400 km/s.

One can compare the merger velocities derived from the temperature jumps in the merger shocks with the values predicted by free-fall from the turn-around radius (equation 15). In the case of Cygnus-A, Markevitch et al. (1999) found good agreement with the free-fall velocity of ~ 2200 km/s. This consistency suggests that the shock energy is effectively thermalized, and that a major fraction does not go into turbulence, magnetic fields, or cosmic rays. Thus, the temperature jumps in merger shocks can provide an important test of the relative roles of thermal and nonthermal processes in clusters of galaxies. Further tests should be possible by comparing shock heating with velocities determined from optical redshifts, from direct velocity measurements in the gas with Astro-E2 and Constellation-X, and from infall arguments.

2.2. NONEQUILIBRIUM EFFECTS

Cluster mergers are expected to produce collisionless shocks, as occurs in supernova remnants. As such, nonequilibrium effects are expected, including nonequipartition of electrons and ions and nonequilibrium ionization (Markevitch et al. 1999; Takizawa 1999,2000). Collisionless shocks are generally not as effective in heating electrons as ions. Assuming that the postshock electrons are somewhat cooler than the ions, the time scale for electron and protons to approach equipartition as a result of Coulomb collisions in a hot ionized gas is (Spitzer 1962)

$$\begin{aligned}
 t_{\text{eq}} &= \frac{3m_p m_e}{8\sqrt{2\pi} n_e e^4 \ln \Lambda} \left(\frac{kT_e}{m_e} \right)^{3/2} \\
 &\approx 2.1 \times 10^8 \left(\frac{T_e}{10^8 \text{ K}} \right)^{3/2} \left(\frac{n_e}{0.001 \text{ cm}^{-3}} \right)^{-1} \text{ yr}, \quad (30)
 \end{aligned}$$

where n_e and T_e are the electron number density and temperature, respectively, and Λ is the Coulomb factor. The relative velocity between the postshock gas and the shock front is $(1/4)v_s$; thus, one would expect

the electron temperature to reach equipartition at a distance of

$$d_{\text{eq}} \approx 160 \left(\frac{v_s}{3000 \text{ km/s}} \right) \left(\frac{T_e}{10^8 \text{ K}} \right)^{3/2} \left(\frac{n_e}{0.001 \text{ cm}^{-3}} \right)^{-1} \text{ kpc} \quad (31)$$

behind the shock front. Of course, it is the electron temperature (rather than the ion or average temperature) which determines the shape of the X-ray spectrum. This distance is large enough to insure that the lag could be spatially resolved in X-ray observations of low redshift clusters. Similar effects might be expected through non-equilibrium ionization.

On the other hand, it is likely that the nonequilibrium effects in cluster merger shocks are much smaller than those in supernova blast wave shocks because of the low Mach numbers of merger shocks. That is, the preshock gas is already quite hot (both electrons and ions) and highly ionized. Moreover, a significant part of the heating in low Mach number shocks is due to adiabatic compression, and this would still act on the electrons in the postshock gas in merger shocks, even if there were no collisionless heating of electrons. For example, in a $\mathcal{M} = 2$, $\gamma_{\text{ad}} = 5/3$ shock, the total shock increase in temperature is a factor of 2.08 (eq. 27). The shock compression is $C = 2.29$, so adiabatic compression increases the electron temperature by a factor of $C^{2/3} = 1.74$, which is about 83% of the shock heating.

3. MERGERS AND COOL CLUSTER CORES

3.1. COOLING FLOWS VS. MERGERS

The centers of a significant fraction of clusters of galaxies have luminous cusps in their X-ray surface brightness known as “cooling flows” (see Fabian 1994 for an extensive review). In every case, there is a bright (cD) galaxy at the center of the cooling flow region. The intracluster gas densities in these regions are much higher than the average values in the outer portions of clusters. X-ray spectra indicate that there are large amounts of gas at low temperatures (down to $\sim 10^7$ K), which are much cooler than those in the outer parts of clusters. The high densities imply rather short cooling times t_{cool} (the time scale for the gas to cool to low temperature due to its own radiation). The hypothesis is that the gas in these regions is cooling from higher intracluster temperature ($\sim 10^8$ K) down to these lower temperatures as a result of the energy loss due to the X-ray emission we observe. Typical cooling rates are $\sim 100 M_{\odot} \text{ yr}^{-1}$. The cooling times, although much shorter than the Hubble time, are generally much longer than the dynamical time (i.e., sound crossing time) of the gas in these regions. As a result, the gas is believed to remain nearly in hydrostatic equilibrium. Thus, the gas must compress

as it cools to maintain a pressure which can support the weight of the overlying intracluster medium.

The primary observational characteristics of cooling flows are very bright X-ray surface brightnesses which increase rapidly toward the center of the cluster. The high surface brightnesses imply high gas densities which also increase rapidly towards the cluster center. These regions contain cooler cluster gas.

Empirically, there is significant indirect evidence that mergers disrupt cooling flows. There is a strong statistical anticorrelation between cooling flows and/or cooling rates, and irregular structures in clusters as derived by statistical analysis of their X-ray images (Buote & Tsai 1996). The irregular structures are often an indication of an ongoing merger. Looked at individually, very large cooling flows are almost never associated with very irregular or bimodal clusters, which are likely merger candidates (Henriksen 1988; Edge et al. 1992). There are some cases of moderate cooling flows in merging clusters; in most cases, these appear to be early-stage mergers where the merger shocks haven't yet reached the cooling core of the cluster. Examples may include Cygnus-A (Arnaud et al. 1984; Owen et al. 1997; Markevitch et al. 1999) and Abell 85 (Kempner et al. 2001). There also are a large number of merging clusters at a more advanced stage with relatively small cooling cores, both in terms of the cooling rate and the physical radius; Abell 2065 (Markevitch et al. 1999) may be an example. Recently, Chandra Observatory X-ray images have shown a number of merging clusters with rapidly moving cores of cool gas (the "cold fronts" discussed below in § 3.2). In these systems, the cooling flows appear to have survived, at least to the present epoch in the merger.

It is unclear exactly how and under what circumstances mergers disrupt cooling flows. The cooling flows might be disrupted by tidal effects, by shock heating the cooler gas, by removing it dynamically from the center of the cluster due to ram pressure, by mixing it with hotter intracluster gas, or by some other mechanism. Numerical hydrodynamical simulations are needed to study the mechanisms by which cooling flows are disrupted. This is a relatively unexplored area, largely because the small spatial scales and rapid cooling time scales in the inner regions of cooling flows are still a significant challenge to the numerical resolution of hydrodynamical codes. McGlynn & Fabian (1984) argued that mergers disrupted cooling flows, but this was based on purely N-body simulations. Recently, Gómez et al. (2001) have made hydrodynamical simulations of the effects of head-on mergers with relatively small subclusters (1/4 or 1/16 of the mass of the main cluster) on a cooling flow in the main cluster. They find that the mergers disrupt the cooling flow

in some cases, but not in others. Their simulations suggest that the disruption is not due to tidal or other gravitational effects.

Another possibility is that the merger shocks heat up the cooling flow gas and stop the cooling flow. In the simulations, this does not appear to be the main mechanism of cooling flow disruption. There are a number of simple arguments which suggest that merger shocks should be relatively inefficient at disrupting cooling flows. First, it is difficult for these shocks to penetrate the high densities and steep density gradients associated with cooling flows, and the merger shocks would be expected to weaken as they climb these steep density gradients. Even without this weakening, merger shocks have low Mach numbers, and only produce rather modest increases in temperature (\lesssim a factor of 2). These small temperature increases are accompanied by significant compressions. As a result, shock heating actually decreases the cooling time due to thermal bremsstrahlung emission for shocks with Mach numbers $\mathcal{M} \leq (21 + 12\sqrt{3})^{1/2} \approx 6.5$. It is likely that the shocked gas will eventually expand, and adiabatic expansion will lengthen the cooling time. However, even if the gas expands to its preshock pressure, the increase in the cooling time is not very large. For a $\mathcal{M} = 2$ shock, the final cooling time after adiabatic expansion to the original pressure is only about 18% longer than the initial cooling time.

The simulations by Gómez et al. suggest that the main mechanism for disrupting cooling flows is associated with the ram pressure of gas from the merging subcluster. The gas in the cooling flow is displaced, and may eventually mix with the hotter gas (see also Ricker & Sarazin 2001). Earlier, Fabian & Daines (1991) had argued that ram pressure, rather than shock heating, was the main mechanism for disrupting cooling flows. Assuming this is the case, one expects that the merger will remove the cooling flow gas at radii which satisfy

$$\rho_{\text{sc}} v_{\text{rel}}^2 \gtrsim P_{\text{CF}}(r), \quad (32)$$

where $P_{\text{CF}}(r)$ is the pressure profile in the cooling flow, ρ_{sc} is the density of the merging subcluster gas at the location of the cooling flow, and v_{rel} is the relative velocity of the merging subcluster gas and the cooling flow. Gómez et al. (2001) find that this relation provides a reasonable approximation to the disruption in their simulations.

The pressure profile in the cooling flow gas prior to the merger is determined by the condition of hydrostatic equilibrium. If the cluster gravitational potential has a wide core within which the potential is nearly constant (e.g., as in a King model), then the cooling flow pressure will not increase rapidly into the center. In this case, once the merger reaches the central regions of the cluster, if the ram pressure is sufficient

to remove the outer parts of the cooling flow, it should be sufficient to remove nearly all of the cooling flow. On the other hand, if the cluster potential is sharply peaked (as in a NFW profile, Navarro et al. 1997), the merger may remove the outer parts of the cooling flow but not the innermost regions. Thus, the survival and size of cool cores in merging clusters can provide evidence on whether clusters have sharply peaked potentials. Markevitch et al. (1999) applied this argument to the two small cool cores in the merging cluster Abell 2065, and concluded that steep central potentials, consistent with the NFW model, were needed.

3.2. COLD FRONTS

One of the more dramatic early discoveries with the Chandra X-ray Observatory was the presence of very sharp surface brightness discontinuities in merging clusters of galaxies. A pair of such discontinuities were first seen in the public science verification data on the Abell 2142 cluster (Markevitch et al. 2000). Initially, it seemed likely that these were merger shocks. However, temperature measurements showed that this was not the case. The high X-ray surface brightness regions were both dense and *cool*, thus, the gas in these regions had a lower specific entropy than the gas in the less dense regions. The lack of a pressure jump and the incorrect sign of the temperature and entropy variations showed that these features could not be shocks (Markevitch et al. 2000). Instead, they appear to be contact discontinuities between hot, diffuse gas and a cloud of colder, denser gas (Markevitch et al. 2000). The cold cloud is moving rapidly through the hotter gas; Vikhlinin et al. (2001b) refer to this situation as a “cold front.” Markevitch et al. (2000) argue that the source of the cold clouds are the cooling cores of one or both of merging subclusters. As noted above, cooling flows do appear to be able to partially survive in mergers, at least for some period. Subsequently, cold fronts have been observed in a number of other clusters; for an extensive review of the observations of these cold fronts, see Forman et al. (this volume).

3.2.1 Kinematics of Cold Fronts. As discussed extensively in Vikhlinin et al. (2001b), the variation in the density, pressure, and temperature of the gas in a cold front can be used to determine the relative velocity of cold core. This technique is analogous to that for merger shocks discussed above (eqs. 28 & 29). The geometry is illustrated in Figure 1.3, which is drawn in the rest frame of the cold core. We assume that the cold core has a smoothly curved, blunt front edge. The normal component of the flow of hot gas past the surface of the cold core will be zero. There will be at least one point where the flow is perpendicular to

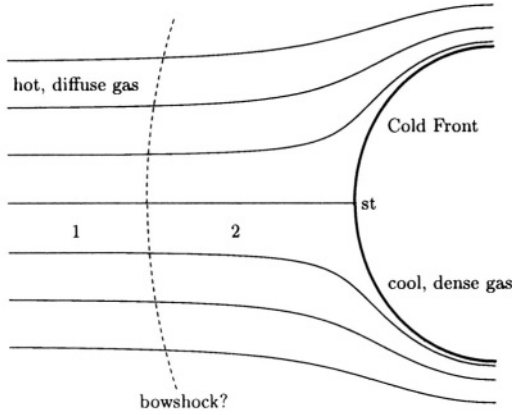


Figure 1.3. A schematic diagram of flow around a “cold front” in a cluster merger. The heavy solid arc at the right represents the contact discontinuity between the cold, dense cold core gas, and the hotter, more diffuse gas from the outer regions of the other cluster. The cold core is moving toward the left relative to the hotter gas. The narrow solid lines are streamlines of the flow of the hotter gas around the cold core. The region labelled “1” represent the upstream, undisturbed hot gas. If the cold front is moving transonically ($\mathcal{M}_1 > 1$), then the cold front will be preceded by a bow shock, which is shown as a dashed arc. The stagnation point, where the relative velocity of the cooler dense gas and hotter diffuse gas is zero, is marked “st”.

the surface of the cold core, and the flow velocity of the hot gas will be zero at this stagnation point (“st” in Fig. 1.3). Far upstream, the flow of the hot gas will be undisturbed at the velocity of the cold core relative to the hotter gas, v_1 . Let c_{s1} be the sound speed in this upstream gas, and $\mathcal{M}_1 \equiv v_1/c_{s1}$ be the Mach number of the motion of the cold core into the upstream gas. If $\mathcal{M}_1 > 1$, a bow shock will be located a head of the cold front.

The ratio of the pressure at the stagnation point to that far upstream is given by (e.g., Landau & Lifshitz 1959, § 114).

$$\frac{P_{\text{st}}}{P_1} = \begin{cases} \left(1 + \frac{\gamma_{\text{ad}} - 1}{2} \mathcal{M}_1^2\right)^{\frac{\gamma_{\text{ad}}}{\gamma_{\text{ad}} - 1}}, & \mathcal{M}_1 \leq 1, \\ \mathcal{M}_1^2 \left(\frac{\gamma_{\text{ad}} + 1}{2}\right)^{\frac{\gamma_{\text{ad}} + 1}{\gamma_{\text{ad}} - 1}} \left(\gamma_{\text{ad}} - \frac{\gamma_{\text{ad}} - 1}{2\mathcal{M}_1^2}\right)^{-\frac{1}{\gamma_{\text{ad}} - 1}}, & \mathcal{M}_1 > 1. \end{cases} \quad (33)$$

The ratio (P_{st}/P_1) increases continuously and monotonically with \mathcal{M}_1 . Thus, in principle, measurements of P_1 and P_{st} in the hot gas could be used to determine \mathcal{M}_1 . The pressures would be determined from X-ray spectra and images. In practice, the emissivity of the hot gas near the stagnation point is likely to be small. However, the pressure is continuous across the cold front, so the stagnation pressure can be determined just inside of the cold core, where the X-ray emissivity is

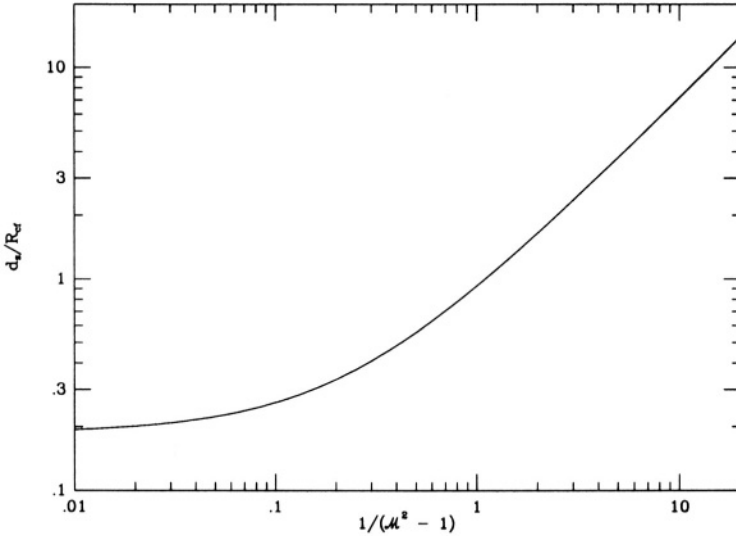


Figure 1.4. The ratio of the stand-off distance of the bow shock d_s to the radius of curvature R_{cf} of the stagnation region of the cold front, as a function of $1/(\mathcal{M}_1^2 - 1)$, where \mathcal{M}_1 is the Mach number. This is for a spherical cold front and $\gamma_{ad} = 5/3$.

likely to be much higher. Once \mathcal{M}_1 has been determined, the velocity of the encounter is given by $v_1 = \mathcal{M}_1 c_{s1}$.

If the motion of the cold core is transonic ($\mathcal{M}_1 > 1$), one can also determine the velocity from the temperature and/or density jump at the bow shock (eqs. 28 & 29). If the bow shock can be traced to a large transverse distance and forms a cone, the opening angle of this Mach cone corresponds to the Mach angle, $\theta_M \equiv \csc^{-1}(\mathcal{M}_1)$. However, variations in the cluster gas temperature may lead to distortions in this shape.

The distance between the stagnation point and the closest point on the bow shock (the shock “stand-off” distance d_s) can also be used to estimate the Mach number of the motion of the cold front (Vikhlinin et al. 2001b). The ratio of d_s to the radius of curvature of the cold front R_{cf} depends on the Mach number \mathcal{M}_1 and on the shape of the cold front. Figure 1.4 shows the values of d_s/R_{cf} as a function of $(\mathcal{M}_1^2 - 1)^{-1}$ for a spherical cold front (Schreier 1982).

Although there is no simple analytic expression for the stand-off distance which applies to all shapes of objects, a fairly general approximate method to calculate d_s has been given by Moekel (1949), and some simple approximate expressions exist for a number of simple geometries (Guy 1974; Radvugin 1974). The stand-off distance increases as the Mach number approaches unity; thus, this method is, in some ways, a very

sensitive diagnostic for the Mach number for the low values expected in cluster mergers. On the other hand, the stand-off distance also depends strongly on the shape of the cold front as the Mach number decreases. The application of this diagnostic to observed clusters is strongly affected by projection effects. Because the radius of curvature of the bow shock is usually greater than that of the cold front (Rusanov 1976), projection effects will generally cause d_s to be overestimated and \mathcal{M}_1 to be underestimated. Projection effects also make the true shape of the cold front uncertain.

These techniques have been used to determine the merger velocities from cold fronts in Abell 3667 (Vikhlinin et al. 2001b), RX J1720.1+2638 (Mazzotta et al. 2001), and Abell 85 (Kempner et al. 2001).

3.2.2 Width of Cold Fronts. One remarkable aspect of the cold fronts observed with the Chandra Observatory in several clusters is their sharpness. In Abell 3667, the temperature changes by about a factor of two across the cold front (Vikhlinin et al. 2001b), and the accompanying change in the X-ray surface brightness occurs in a region which is narrower than 2 kpc (Vikhlinin et al. 2001b). This is less than the mean-free-path of electrons in this region. The existence of this very steep temperature gradient and similar results in other merging clusters with cold fronts requires that thermal conduction be suppressed by a large factor (Ettori & Fabian 2000; Vikhlinin et al. 2001a,b) relative to the classical value in an unmagnetized plasma (e.g., Spitzer 1962). It is likely that this suppression is due to the effects of the intracluster magnetic field. It is uncertain at this point whether this is due to a generally tangled magnetic field (in which case, heat conduction might be suppressed throughout clusters), or due to a tangential magnetic field specific to the tangential flow at the cold front (Vikhlinin et al. 2001a).

Because of the tangential shear flow at the cold front (Fig. 1.3), the front should be disturbed and broadened by the Kelvin-Helmholtz (K-H) instability. Vikhlinin et al. (2001a) argue that the instability is suppressed by a tangential magnetic field, which is itself generated by the tangential flow. This suppression requires that the magnetic pressure P_B be a non-trivial fraction of the gas pressure P in this regions, $P_B \gtrsim 0.1P$. The required magnetic field strength in Abell 3667 is $B \sim 10 \mu\text{G}$.

4. NONTHERMAL PHYSICS OF MERGER SHOCKS

Cluster mergers involve shocks with velocities of ~ 2000 km/s. Radio observations of supernova remnants indicate that shocks with these ve-

locities can accelerate or reaccelerate relativistic electrons and ions (e.g., Blandford & Eichler 1987). In order to explain the general radio emission of supernova remnants, one requires that shocks in these systems generally convert a few percent of the shock energy into relativistic electrons. Even more energy may go into relativistic ions. Thus, one might expect that the intracluster medium would contain relativistic particles or cosmic rays, in addition to the hot thermal gas so evident in X-ray images. Given that all of the thermal energy content of the intracluster gas in clusters is due to shocks with velocities of $\gtrsim 10^3$ km/s, it seems likely that relativistic electrons and ions will have been accelerated with a total energy content of a few percent of the thermal energy in the hot gas. In massive, X-ray luminous clusters, the total thermal energy content in the ICM is $\gtrsim 3 \times 10^{63}$ ergs. Thus, merger or accretion shocks may have accelerated cosmic ray particles with a total energy content of $\gtrsim 10^{62}$ ergs. This would make clusters the largest individual sources of relativistic particles in the Universe; this energy probably exceeds that produced in active galactic nuclei, such as quasars and radio galaxies.

In a major merger, the thermal energy content of a cluster can be significantly increased by the merger shocks (§ 2). Thus, shock acceleration or reacceleration processes in a single merger may produce cosmic ray particles with a total energy of $\sim 10^{62}$ ergs. Thus, one would expect significant nonthermal effects associated with cluster mergers.

4.1. PARTICLE LIFETIMES AND LOSSES

Clusters are also very good storage locations for cosmic rays. These particles gyrate around magnetic field lines in the ICM. The magnetic field is frozen-in to the ionized thermal ICM, which is, in turn, bound by the gravitational field of the cluster. Thus, the relativistic particles cannot simply stream out of a cluster. They can diffuse out along magnetic field lines. Diffusion is limited by scattering off of fluctuations in the magnetic field, and the rate is uncertain. However, under reasonable assumptions, the diffusion coefficient is approximately (Berezinsky et al. 1997; Colafrancesco & Blasi 1998)

$$D(E) \approx 2 \times 10^{29} \left(\frac{E}{1 \text{ GeV}} \right)^{1/3} \left(\frac{B}{1 \mu\text{G}} \right)^{-1/3} \text{ cm}^2 \text{ s}^{-1}, \quad (34)$$

where E is the particle energy and B is the ICM magnetic field. The average time scale to diffuse out to a radius of R is about (Berezinsky

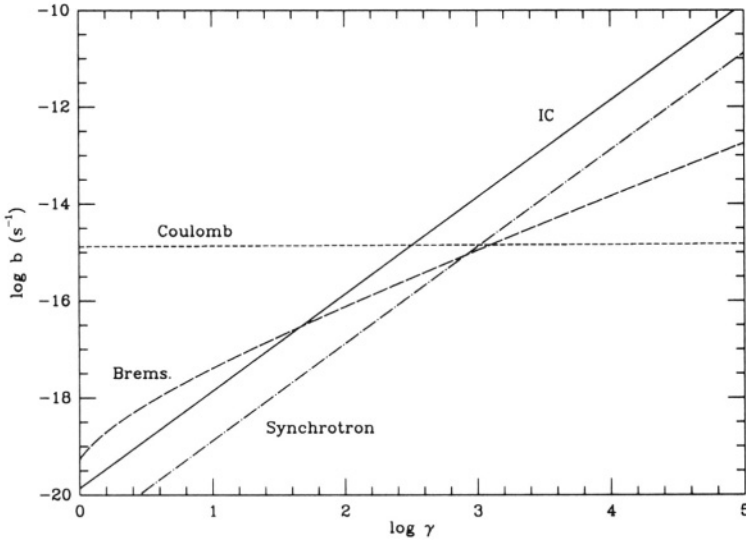


Figure 1.5. Values of the electron loss functions $b(\gamma)$ for inverse Compton (IC) emission, Coulomb losses, synchrotron emission, and bremsstrahlung emission as a function of $\gamma = E/(m_e c^2)$. The values assume $n_e = 10^{-3} \text{ cm}^{-3}$, $B = 1 \mu\text{G}$, and redshift $z = 0$.

et al. 1997; Colafrancesco & Blasi 1998)

$$t_{\text{diff}} \approx \frac{R^2}{6D(E)} \approx 1 \times 10^{12} \left(\frac{R}{2 \text{ Mpc}} \right)^2 \left(\frac{E}{1 \text{ GeV}} \right)^{-1/3} \left(\frac{B}{1 \mu\text{G}} \right)^{1/3} \text{ yr.} \quad (35)$$

Thus, under reasonable assumptions for the diffusion coefficient, particles with energies $\lesssim 10^6 \text{ GeV}$ have diffusion times which are longer than the Hubble time.

Relativistic particles can lose energy, and this can effectively remove them from the cosmic ray population. The time scales for energy loss by ions are generally longer than the Hubble time. Electrons suffer losses due to interactions with ambient radiation fields (via inverse Compton [IC] emission), with the cluster magnetic field (via synchrotron emission), and with the intracluster gas (via Coulomb interactions and bremsstrahlung emission). However, the ICM is an extremely diffuse medium, and these losses are relatively small, at least as compared to the interstellar gas in our Galaxy. The gas density is low ($n_e \sim 10^{-3} \text{ cm}^{-3}$), reducing Coulomb and bremsstrahlung losses. The radiation fields are dilute, with the Cosmic Microwave Background (CMB) radiation providing the majority of the energy density. Magnetic fields are

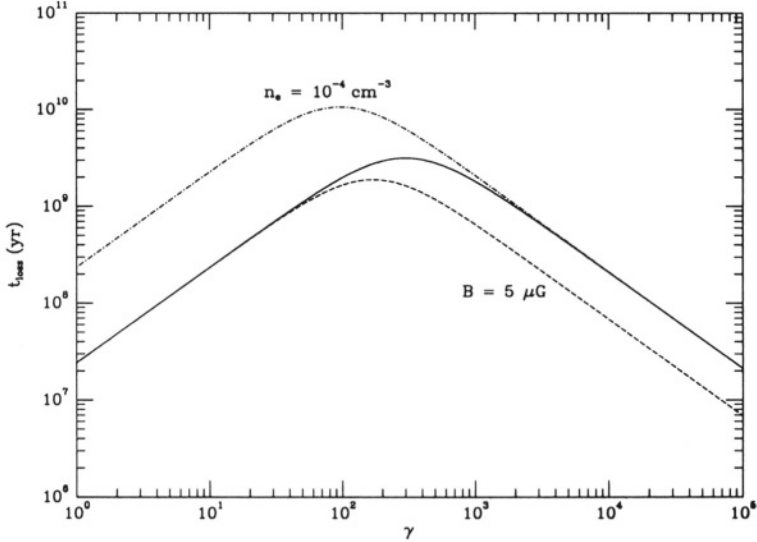


Figure 1.6. The solid curve gives the instantaneous loss time scale t_{loss} for relativistic electrons in a cluster with an electron density of $n_e = 10^{-3} \text{ cm}^{-3}$ and a magnetic field of $B = 1 \text{ } \mu\text{G}$. The short-dash curve is for $B = 5 \text{ } \mu\text{G}$, while the dash-dot curve is for $n_e = 10^{-4} \text{ cm}^{-3}$.

relatively weak; if the cluster fields are mainly smaller than $3 \text{ } \mu\text{G}$, then synchrotron losses are smaller than IC losses.

Let the energy of an electron be $E \equiv \gamma m_e c^2$, where γ is the Lorentz factor. Then, the energy loss of an electron can be written as

$$\frac{d\gamma}{dt} = \frac{1}{m_e c^2} \frac{dE}{dt} = -b(\gamma), \quad (36)$$

assuming the loss is continuous. The values of the loss functions $b(\gamma)$ for various processes are shown in Figure 1.5 (Sarazin 1999a). It is clear that IC and synchrotron losses are dominant at high energies ($\gamma \gtrsim 200$ or $E \gtrsim 100 \text{ MeV}$), while Coulomb losses dominate at low energies ($\gamma \lesssim 200$ or $E \lesssim 100 \text{ MeV}$).

One can define an instantaneous time scale for energy losses as $t_{\text{loss}} \equiv \gamma/b(\gamma) = E/(dE/dt)$. Values for this loss time scale at the present epoch ($z = 0$) are shown in Figure 1.6 (Sarazin 1999a). The solid curve gives values assuming an average electron density of $n_e = 10^{-3} \text{ cm}^{-3}$ and a magnetic field of $B = 1 \text{ } \mu\text{G}$. For values of the magnetic field this small or lower, synchrotron losses are not very significant, and t_{loss} is nearly independent of B . The short dashed curve shows the effect of increasing the magnetic field to $B = 5 \text{ } \mu\text{G}$; the losses at high energies are increased, and the loss time scales shortened. The dash-dot curve shows

the loss time scale if the electron density is lowered to $n_e = 10^{-4} \text{ cm}^{-3}$. This reduces the losses at low energies, and increases the loss times there. Although high energy electrons lose energy rapidly due to IC and synchrotron emission, electrons with Lorentz factors of $\gamma \sim 300$ (energies $\sim 150 \text{ MeV}$) have long lifetimes of $\sim 3 - 10 \text{ Gyr}$, which are comparable to the likely ages of clusters (Sarazin & Lieu 1998; Sarazin 1999a). Thus, clusters of galaxies can retain low energy electrons ($\gamma \sim 300$) and nearly all cosmic ray ions for a significant fraction of a Hubble time.

4.2. SOURCES OF RELATIVISTIC PARTICLES

What are the sources for relativistic particles in clusters? One possibility is that these particles come from active galaxies (quasars, radio galaxies, etc.; e.g., Blasi & Colafrancesco 1999). Because luminous active galaxies were more common in the past, most of the cosmic ray particles would probably have been formed in the past. Another possibility is that these particles were generated as part of star formation in normal galaxies, either at the sites of star formation and supernova, or in galactic winds (e.g., Atoyan & Völk 2000). The galaxies in the inner regions of clusters today are mainly elliptical and S0 galaxies, which have old stellar populations. Thus, most of their star formation, and most of the particle production associated with it, probably occurred in the distant past. In any case, if AGNs or star bursts produced most of particles in clusters directly, then the cosmic ray populations in clusters would have no clear relation to mergers. I concentrate here on models in which the particles were either produced directly in mergers, or are the secondary products of particles produced in mergers, and/or were reaccelerated in mergers.

4.2.1 Particle Acceleration in Shocks. Radio observations of supernova remnants indicate that shocks with $v \gtrsim 10^3 \text{ km/s}$ convert at least a few percent of the shock energy into the acceleration of relativistic electrons (e.g., Blandford & Eichler 1987). Even more energy may go into relativistic ions. Thus, merger shocks seem like a natural acceleration site for relativistic particles. It is worth noting that there are significant differences between merger shocks and those associated with supernova blast waves. The merger shocks have relatively small Mach numbers, and as a result have smaller compressions. The ICM which enters the merger shock is hot. This means that the shocks are subsonic in the electrons; the preshock electrons have thermal velocities which are much greater than the shock velocities. On the other hand,

the Alfvén Mach numbers ($\mathcal{M}_A \equiv v_s/v_A$ where $v_A = B^2/(4\pi\rho)$ is the Alfvén speed) for merger shocks can be quite large, $\mathcal{M}_A \gtrsim 30$. For some aspects of shock acceleration, the Alfvén Mach number is more relevant than the hydrodynamical Mach number.

Assuming that particles scatter repeatedly across the shock, these particles will undergo first-order Fermi shock acceleration. If the accelerating particles are treated as test particles, kinetic theory indicates that the particle spectrum is a power-law in the momentum p (Bell 1978; Blandford & Ostriker 1978):

$$N(p) dp = N_o \left(\frac{p}{mc} \right)^{-\mu} \frac{dp}{mc}, \quad p_l \leq p \leq p_u \quad (37)$$

where m is the particle mass. Here, $N(p) dp$ is the number of particles with momenta between p and $p + dp$, and p_l (p_u) are the lower (upper) limits on the particle spectrum. If the particles are accelerated from nearly thermal energies, then the lower limit may be associated with the production of a nonthermal tail at the high energy end of the ICM thermal particle distribution. The upper limit may correspond to the highest energy for which acceleration is efficient (e.g., § 4.4.5). The particle spectrum expressed in terms of the Lorentz factor is

$$\begin{aligned} N(\gamma) d\gamma &= N_o (\gamma^2 - 1)^{-(\mu+1)/2} \gamma d\gamma, \\ &\approx N_o \gamma^{-\mu} d\gamma, \quad \gamma \gg 1. \end{aligned} \quad (38)$$

The energy spectrum is given by $N(E) dE = N(\gamma) d\gamma$, with $E = \gamma mc^2$. Thus, the energy spectrum for the shock acceleration of relativistic particles is also expected to be a power-law.

For shock acceleration, the exponent is

$$\mu = \frac{C + 2}{C - 1}, \quad (39)$$

where C is the shock compression (eq. 27 & 29). Strong shocks give $C = 4$ and $\mu = 2$, which is in reasonable agreement with the radio observations of supernova remnants. Merger shocks have $C \approx 2 - 3$, which leads to $\mu \approx 4 - 2.5$. Thus, the particle spectra produced by merger shocks are expected to be significantly steeper than those generated by supernova remnant blast waves.

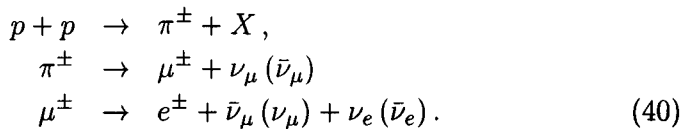
4.2.2 Reacceleration by Merger Shocks. Merger shocks may reaccelerate pre-existing relativistic particles, rather than produce new particles from the thermal ICM. This mechanism has been proposed

as a possible mechanism to explain the radio halo in the Coma cluster and other halos (Brunetti et al. 2001a,b). In this model, the reacceleration occurs gradually over an extended period of time.

Radio relics might also be due to the reacceleration of relativistic particles injected as some time in the past by radio galaxies (Enßlin & Brüggen 2001). In this case, one would only expect to see relics associated with a small fraction of merger shocks; one would require both a merger shock and a pre-existing radio population. If the old radio plasma continues to be separated from the thermal plasma (a radio “ghost”, Enßlin & Gopal-Krishna 2001), then the merger shock will be subsonic in the relativistic radio plasma. Thus, rather than reacceleration, the merger shock might re-energize the radio plasma by adiabatic compression.

4.2.3 Turbulent Acceleration Following a Merger. Cluster mergers may produce a significant level of turbulence in the ICM, and this could lead to turbulent acceleration or reacceleration of relativistic electrons (Eilek & Weatherall 1999). This is second order Fermi acceleration. Turbulent reacceleration has also been suggested as a possible mechanism to explain radio halos in clusters (Brunetti et al. 2001a,b). Radio halos have only been found in merging clusters. However, their smooth distributions and central locations suggest that they are not confined to the region currently passing through a merger shock. Turbulent acceleration following the passage of merger shocks might explain these properties.

4.2.4 Secondary Electron Production. Another source of relativistic electrons is the decay of charged mesons generated in cosmic ray ion collisions (Dennison 1980; Vestrand 1982; Colafrancesco & Blasi 1998). The reactions involved are



Here, X represents some combination of protons, neutrons, and/or other particles. The electrons (and positrons) produced by this mechanism are referred to as secondary electrons. If the primary cosmic ray ions are due to AGNs or star bursts, this process might have no connection with cluster mergers. On the other hand, the ions might have been accelerated or reaccelerated by cluster merger shocks or turbulence associated with cluster mergers.

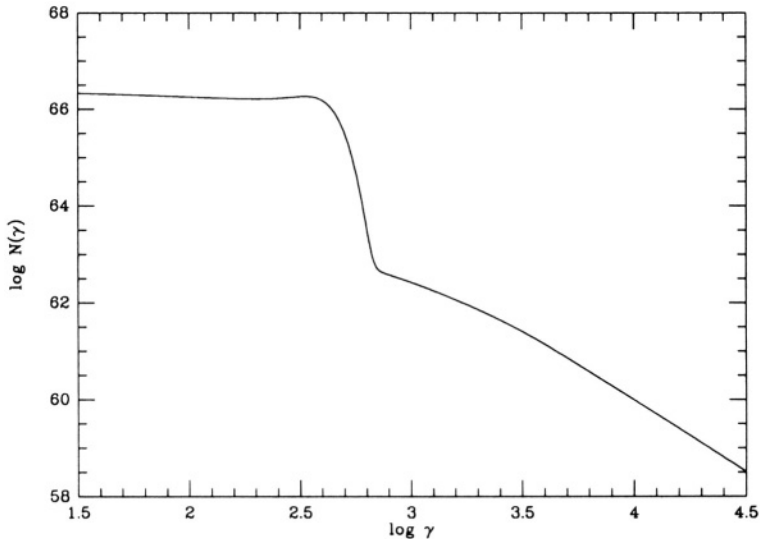


Figure 1.7. A typical model for the relativistic electron population in a cluster of galaxies. The lower energy electrons are due to all of the mergers in the cluster history, while the high energy electrons are due to a small current merger.

4.3. MODELS FOR MERGER SHOCKS AND PRIMARY ELECTRONS

Here, I describe the results of some models for the population of relativistic electrons in clusters, assuming they are primary electrons accelerated in merger shocks (Sarazin 1999a; § 4.2.1). The populations of cosmic ray electrons in clusters depends on their merger histories. Because low energy electrons have long lifetimes, one expects to find a large population of them in most clusters (any cluster which has had a significant merger since $z \sim 1$). On the other hand, higher energy electrons ($E \gtrsim 1$ GeV) have short lifetimes (shorter than the time for a merger shock to cross a cluster). Thus, one only expects to find large numbers of higher energy primary electrons in clusters which are having or have just had a merger. These conclusions follow from a large number of detailed models of the evolution of the integrated electron population in clusters (Sarazin 1999a). Two recent cluster merger simulations have included particle acceleration approximately (Roettiger et al. 1999; Takizawa & Naito 2000), and they reach similar conclusions.

Figure 1.7 shows the electron spectrum in a cluster with a typical history. Most of the electron energy is in electrons with $\gamma \sim 300$, which have the longest lifetimes. These electrons are produced by mergers over the entire history of the cluster. This cluster also has a small ongoing

merger which produces the high energy tail on the electron distribution. In cluster models without a current merger, the high energy tail would be missing.

Most of the emission from these electrons is due to IC, and the resulting spectrum is shown in Figure 1.8. For comparison, thermal bremsstrahlung with a typical rich cluster temperature and luminosity is shown as a dashed curve. Figure 1.8 shows that clusters should be strong sources of extreme ultraviolet (EUV) radiation. Since this emission is due to electrons with $\gamma \sim 300$ which have very long lifetimes, EUV radiation should be a common feature of clusters (Sarazin & Lieu 1998).

In clusters with an ongoing merger, the higher energy electrons will produce a hard X-ray tail via IC scattering of the Cosmic Microwave Background (CMB); the same electrons will produce diffuse radio synchrotron emission.

4.4. NONTHERMAL EMISSION AND MERGERS

4.4.1 Radio Halos and Relics . The oldest and most detailed evidence for nonthermal populations in clusters comes from the radio. A number of clusters of galaxies are known to contain large-scale diffuse radio sources which have no obvious connection to individual galaxies in the cluster (Giovannini et al. 1993). These sources are referred to as radio halos when they appear projected on the center of the cluster, and are called relics when they are found on the cluster periphery (although they have other distinctive properties). In all cases of which I am aware, they have been found in clusters which show significant evidence for an ongoing merger (Giovannini et al. 1993; Feretti 1999, 2001). Since these source are discussed extensively by Giovannini & Feretti in another chapter of this book, I won't discuss them in any more detail here.

4.4.2 EUV/Soft X-ray Emission. Excess EUV emission has apparently been detected with the EUVE satellite in six clusters (Virgo, Coma, Abell 1795, Abell 2199, Abell 4038, & Abell 4059; Lieu et al. 1996a,b; Bowyer & Berghöfer 1998; Mittaz et al. 1998; Bowyer et al. 1999; Kaastra et al. 1999; Lieu et al. 1999a,b; Berghöfer et al. 2000a,b; Bonamente et al. 2001). In fact, the EUVE satellite appears to have detected all of the clusters it observed which are nearby, which have long integration times, and which lie in directions of low Galactic column where detection is possible at these energies. However, the EUV detections and claimed properties of the clusters remain quite contro-

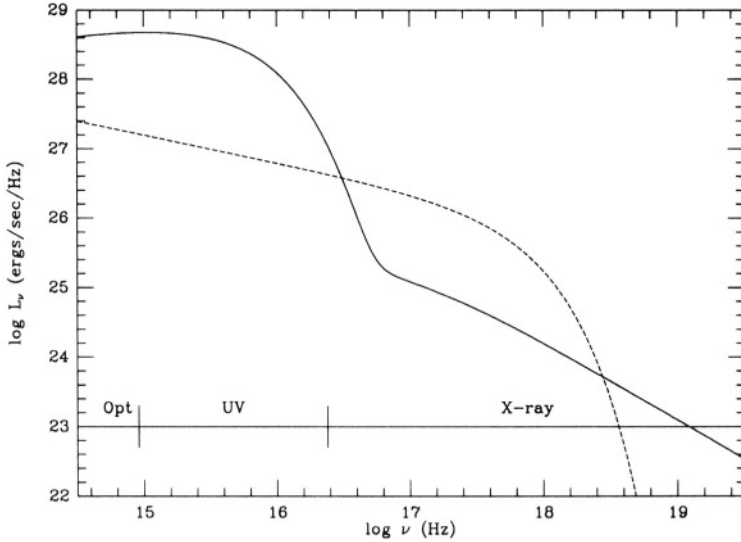


Figure 1.8. The IC spectrum from a typical cluster model (solid curve). This is the same model as shown in Figure 1.7. The dashed curve is a 7 keV thermal bremsstrahlung spectrum.

versial (Bowyer & Berghöfer 1998; Arabadjis & Bregman 1999; Bowyer et al. 1999; Berghöfer et al. 2000a). The EUV observations suggest that rich clusters generally have EUV luminosities of $\sim 10^{44}$ ergs/s, and have spectra which decline rapidly in going from the EUV to the X-ray band.

While it is possible that the EUV emission may be thermal in origin (Fabian 1997; Bonamente et al. 2001), I believe that it is more likely that this emission is due to inverse Compton scattering (IC) of CMB photons by low energy relativistic electrons (Hwang 1997; Bowyer & Berghöfer 1998; Enßlin & Biermann 1998; Sarazin & Lieu 1998). In this model, the EUV would be produced by electrons with energies of ~ 150 MeV ($\gamma \sim 300$; Fig. 1.7). As noted above, these electrons have lifetimes which are comparable to the Hubble time, and should be present in essentially all clusters. In fact, many of the clusters with observed EUV emission do not appear to be undergoing mergers at present. Thus, this emission is not a useful diagnostic for an ongoing merger; instead, it may represent the emission from electrons accelerated in many previous mergers. To produce the EUV luminosities observed, one needs a population of such electrons with a total energy of $\sim 10^{62}$ ergs, which is about 3% of the typical thermal energy content of clusters. This is a reasonable acceleration efficiency for these particles, given that both the thermal energy in the intracluster gas and the relativistic particles result from merger shocks. The steep spectrum in going from EUV to X-ray bands is predicted by

this model (Fig. 1.8); it results from the rapid increase in losses ($\propto \gamma^2$) for particles as the energy increases above $\gamma \sim 300$ (Figs. 1.5 & 1.6).

4.4.3 Hard X-ray Tails. If clusters contain higher energy relativistic electrons with $\gamma \sim 10^4$, these particles will produce hard X-ray emission by IC scattering. These are essentially the same electrons which produce the observed radio halos and relics (§ 4.4.1), although the detailed correspondence depends on the value of the magnetic field. The ratio of hard X-ray IC emission to radio synchrotron emission allows one to determine the magnetic field in clusters (e.g., Rephaeli 1979; Fusco-Femiano et al. 1999). Since these higher energy electrons have short lifetimes, they should only be present in clusters with evidence for a recent or ongoing merger.

Because of the short lifetimes of the electrons producing HXR IC emission, the population of these particles should be close to steady-state. If the accelerated electrons have a power-law distribution (eq. 39), the expected steady-state energy spectral index if IC losses dominated would be $\alpha_{\text{HXR}} = -(\mu + 1)/2$ (Ginzburg & Syrovatskii 1964). For $\mu \approx 2.5 - 4$ (the values expected for typical merger shock compressions), this gives $\alpha_{\text{HXR}} \approx -1.75$ to -2.5 . In the numerical models, the best-fit spectral indices from 20 to 100 keV are flatter than this, $\alpha_{\text{HXR}} \approx -1.1$, mainly because other loss processes are important at the lower energy end of the HXR band (Fig. 1.5).

If the population of high energy electrons is in steady state, the HXR luminosity is just proportional to the energy input from the mergers into high energy electrons. To a good approximation, the present day value of L_{HXR} (20–100 keV) is simply given by

$$L_{\text{HXR}} \approx 0.17 \dot{E}_{\text{CR},e}(\gamma > 5000). \quad (41)$$

where $\dot{E}_{\text{CR},e}(\gamma > 5000)$ is the total present rate of injection of energy in cosmic ray electrons with $\gamma > 5000$. The best-fit coefficient (0.17 in eqn. 41) depends somewhat on the power-law index of the injected electrons; the value of 0.17 applies for $\mu = 2.3$. Assuming a fixed efficiency $\epsilon_{\text{CR},e}(\gamma > 5000)$ of conversion of shock energy into high energy electrons, the rate of particle acceleration is given by

$$\dot{E}_{\text{CR},e}(\gamma > 5000) = \epsilon_{\text{CR},e}(\gamma > 5000) \dot{E}_s, \quad (42)$$

where \dot{E}_s is the total rate of merger shock energy dissipation. This gives $L_{\text{HXR}} \propto \dot{E}_s$.

Hard X-ray emission in excess of the thermal emission and detected as a nonthermal tail at energies $\gtrsim 20$ keV has been seen in at least two

clusters. The Coma cluster, which is undergoing at least one merger and which has a radio halo, was detected with both BeppoSAX and RXTE (Fusco-Femiano et al. 1999; Rephaeli et al. 1999). BeppoSAX has also detected Abell 2256 (Fusco-Femiano et al. 2000), another merger cluster with strong diffuse radio emission. BeppoSAX may have detected Abell 2199 (Kaastra et al. 1999), although I believe the evidence is less compelling for this case. A nonthermal hard X-ray detection of Abell 2199 would be surprising, as this cluster is very relaxed and has no radio halo or relic (Kempner & Sarazin 2000).

An alternative explanation of the hard X-ray tails is that they might be due to nonthermal bremsstrahlung (Blasi 2000; Dogiel 2000; Sarazin & Kempner 2000), which is bremsstrahlung from nonthermal electrons with energies of 10–1000 keV which are being accelerated to higher energies. The nonthermal tail on the particle distribution might also be associated with shock acceleration. On the other hand, these suprathermal electrons have relatively short time scales to relax into the thermal distribution as a result of Coulomb collisions. In fact, this is a general problem of the injection of thermal electrons into the shock acceleration region. IC emission from high energy electrons dominates unless the particle spectrum is very steep (Sarazin & Kempner 2000).

The previous hard X-ray detections of clusters have been done with instruments with very poor angular resolution. Thus, they provide no information on the distribution of the hard X-ray emission. It would be very useful to determine if the hard X-ray emission is localized to the radio emitting regions in clusters. For clusters with radio relics, these might be associated with the positions of merger shocks in the X-ray images. Better angular resolution would also insure that the hard X-ray detections of clusters are not contaminated by emission from other sources. The IBIS instrument on INTEGRAL will provide a hard X-ray capability with better angular resolution, and may allow the hard X-ray emission regions to be imaged (Goldoni et al. 2001).

The predicted IC emission from nonthermal particles is much weaker than the thermal emission in the central portion of the X-ray band from about 0.3 keV to 20 keV (Fig. 1.8). However, if the IC emission is localized to merger shock regions, its local surface brightness might be comparable to the thermal X-ray emission. A possible detection of localized IC emission associated with merger shocks and radio relics has been claimed in Abell 85 (Bagchi et al. 1998). It is possible that Chandra and XMM/Newton will find IC emission associated with other merger shocks and radio relics.

4.4.4 Predicted Gamma-Ray and Neutrino Emission.

Relativistic electrons and ions in clusters are also expected to produce strong gamma-ray emission (Dar & Shaviv 1996; Berezhinsky et al. 1997; Colafrancesco & Blasi 1998; Blasi & Colafrancesco 1999; Blasi 1999; Sarazin 1999b). The region near 100 MeV is particularly interesting, as this region includes bremsstrahlung from the most common electrons with $\gamma \sim 300$, and π^0 decay gamma-rays from ions. The π^0 emission mechanism starts with the essentially the same ion-ion collisions as make secondary electrons (eq. 40)



Both bremsstrahlung and the π^0 decay process involve collisions between relativistic particles (electrons for bremsstrahlung, ions for π^0 emission) and thermal particles, so they should both vary in the same way with density in the cluster. Thus, the ratio of these two spectrally distinguishable emission processes should tell us the ratio of cosmic ray ions to electrons in clusters (Blasi 1999; Sarazin 1999b).

Figure 1.9 shows the predicted gamma-ray spectrum for the Coma cluster, based on a model which reproduces the observed EUV, hard X-ray, and radio emission (Sarazin 1999b). The observed upper limit from CGO/EGRET is $<4 \times 10^{-8}$ cts/cm²/s for $E > 100$ MeV (Sreekumar et al. 1996), while the predicted value for this model is $\sim 2 \times 10^{-8}$ cts/cm²/s. The EGRET upper limit already shows that the ratio of ions to electrons cannot be too large ($\lesssim 30$; Blasi 1999; Sarazin 1999b). The predicted fluxes are such that many nearby clusters should be easily detectable with GLAST.

The same relativistic particles will also produce neutrinos, which might be detectable with future instruments (Dar & Shaviv 1996; Berezhinsky et al. 1997; Colafrancesco & Blasi 1998).

4.4.5 Ultra High Energy Cosmic Rays. The time scale for most relativistic particles to diffuse out of clusters is longer than the Hubble time (eq. 35). However, very high energy cosmic rays ($E \gtrsim 10^{15}$ eV) could escape from clusters on relatively short time scales. In the cosmic ray spectrum seen at the Earth, it is believed that particles with energies up to $\sim 10^{14}$ eV come from supernova explosions in our Galaxy. Other Galactic sources may produce even higher energy cosmic rays. However, it is likely that the highest energy cosmic ray particles ($E \gtrsim 3 \times 10^{18}$ eV) are extragalactic in origin (Cocconi 1956). Merger or accretion shocks in clusters of galaxies are a possible source of such particles (e.g., Kang et al. 1996, 1997; Siemieniec-Oziębło & Ostrowski 2000). The advantages of

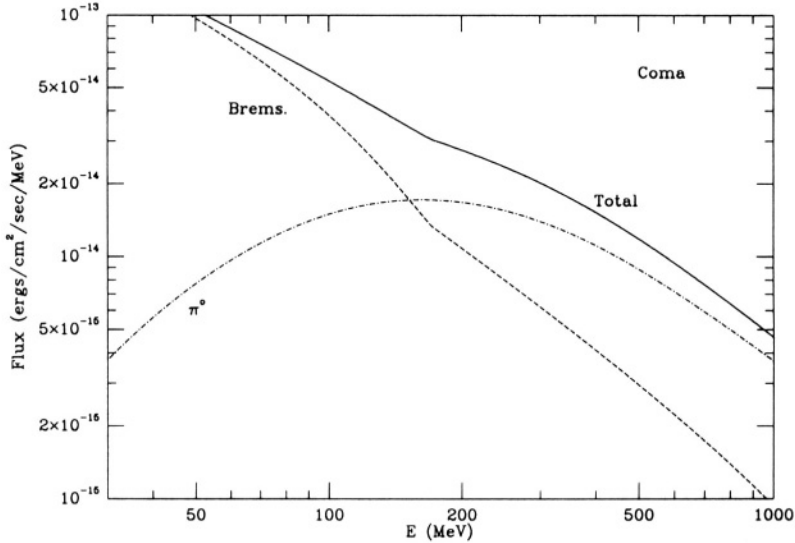


Figure 1.9. The predicted gamma-ray spectrum for the Coma cluster, including electron bremsstrahlung and π^0 decay from ions (Sarazin 1999b).

merger shocks are their high total energies (which helps with the overall flux of cosmic rays), their very large physical sizes (which help with the acceleration of high energy particles with large Larmor radii), their long time scales (which helps to provide enough time for the particles to diffuse to these high energies), and the relatively low losses in the cluster environment (§ 4.1). The Larmor or gyro radius of a high energy particle with a charge Z in the ICM is

$$r_g = \frac{pc}{ZeB} \approx \frac{0.1}{Z} \left(\frac{E}{10^{20} \text{ eV}} \right) \left(\frac{B}{1 \mu\text{G}} \right)^{-1} \text{ Mpc}, \quad (44)$$

and cluster shock regions are likely to be about this size or larger. Assuming Bohm diffusion and a strong shock at a velocity v_s , the acceleration time is about (Kang et al. 1996)

$$t_{\text{acc}} \approx 9 \times 10^9 \left(\frac{E}{10^{20} \text{ eV}} \right) \left(\frac{B}{1 \mu\text{G}} \right)^{-1} \left(\frac{v_s}{3000 \text{ km/s}} \right)^{-2} \text{ yr}. \quad (45)$$

Thus, it might be possible to accelerate protons up to $\lesssim 10^{20}$ eV in cluster shocks.

5. SUMMARY

I've tried to summarize some of the basic aspects of the physics of cluster mergers. Simple estimates for the rates of mergers and for the

infall velocities and impact parameters were given in § 1. The thermal effects of merger shocks are discussed in § 2, with an emphasis on the diagnostics for determining the kinematics of mergers from X-ray observations of temperatures and densities in the ICM. The interaction of cooling flow cores with hotter, more diffuse intracluster gas was considered in (§ 3), including the mechanism for the disruption of the cooling flow cores (§ 3.1), and the hydrodynamics of “cold fronts” (§ 3.2). Relativistic particles may be accelerated or reaccelerated in merger shocks or turbulence generated by mergers. The nonthermal effects of mergers are discussed in § 4, including the resulting radio, extreme ultraviolet, hard X-ray, and gamma-ray emission.

Acknowledgments

I want to thank my collaborators Josh Kempner, Maxim Markevitch, Scott Randall, Paul Ricker, and Alexey Vikhlinin for all their help. I would like to particularly thank Paul Ricker for useful discussions, and Josh Kempner, Scott Randall, and Yutaka Fujita for careful readings of a draft. Scott Randall and Paul Ricker kindly provided figures for this paper. Support for this work was provided by the National Aeronautics and Space Administration through Chandra Award Numbers GO0-1119X, GO0-1173X, GO0-1158X, and GO1-2122X, issued by the Chandra X-ray Observatory Center, which is operated by the Smithsonian Astrophysical Observatory for and on behalf of NASA under contract NAS8-39073. Support also came from NASA XMM grants NAG 5-10074 and NAG 5-10075.

References

- Arabadjis, J.S. & Bregman, J.N. 1999, *ApJ*, 514, 607
Arnaud, K., Fabian, A., Eales, S., Jones, C. & Forman, W. 1984, *MNRAS*, 211, 981
Atoyan, A.M. & Völk, H.J. 2000, *ApJ*, 535, 45
Bagchi, J., Pislar, V. & Lima-Neto, G.B. 1998, *MNRAS*, 296, L23
Bahcall, N.A. & Fan, X. 1998, *ApJ*, 504, 1
Bardeen, J.M., Bond, J.R., Kaiser, N. & Szalay, A.S. 1986, *ApJ*, 304, 15
Bell, A.R. 1978, *MNRAS*, 182, 147
Berezinsky, V.S., Blasi, P. & Ptuskin, V.S. 1997, *ApJ*, 487, 529
Berghöfer, T.W., Bowyer, S. & Korpela, E. 2000a, *ApJ*, 535, 615
Berghöfer, T.W., Bowyer, S. & Korpela, E. 2000b, *ApJ*, 545, 695
Blandford, R.D. & Eichler, D. 1987, *Phys. Rep.*, 154, 1
Blandford, R.D. & Ostriker, J.P. 1978, *ApJL*, 221, L29
Blasi, P. 1999, *ApJ*, 525, 603

- Blasi, P. 2000, ApJL, 532, L9
- Blasi, P. & Colafrancesco, S. 1999, Astropart. Phys, 12, 169
- Bonamente, M., Lieu, R. & Mittaz, J. 2001, ApJL, 547, L7
- Bond, J.R., Cole, S., Efstathiou, G. & Kaiser, N. 1991, ApJ, 379, 440
- Bowyer, S. & Berghöfer, T.W. 1998, ApJ, 506, 502
- Bowyer, S., Berghöfer, T.W. & Korpela, E. 1999, ApJ, 526, 592
- Brunetti, G., Setti, G., Feretti, L. & Giovannini, G. 2001a, MNRAS, 320, 365
- Brunetti, G., Setti, G., Feretti, L. & Giovannini, G. 2001b, New Astron., 6, 1
- Bryan, G.L. & Norman, M.L. 1998, ApJ, 495, 80
- Buote, D.A. & Tsai, J.C. 1996, ApJ, 458, 27
- Cavaliere, A., Menci, N. & Tozzi, P. 1999, MNRAS, 308, 599
- Cocconi, G. 1956, Nuovo Cim., 3, 1433
- Colafrancesco, S. & Blasi, P. 1998, Astropart. Phys., 9, 227
- Dar, A. & Shaviv, N.J. 1996, Astropart. Phys., 4, 343
- Dennison, B. 1980, ApJ, 239, L93
- Dogiel, V.A. 2000, A&A, 357, 66
- Edge, A.C., Stewart, G.C. & Fabian, A.C. 1992, MNRAS, 258, 177
- Eilek, J. & Weatherall, J. 1999, in *Diffuse thermal and relativistic plasma in galaxy clusters*, eds. H. Böhringer, L. Feretti & P. Schuecker, MPE Report 271, 249
- Enßlin, T.A. & Biermann, P.L. 1998, A&A, 330, 90
- Enßlin, T.A. & Brüggen, M. 2001, MNRAS, in press, astro-ph/0104233
- Enßlin, T.A. & Gopal-Krishna 2001, A&A, 366, 26
- Ettori, S. & Fabian, A.C. 2000, MNRAS, 317, L57
- Fabian, A.C. 1994, ARA&A, 32, 277
- Fabian, A.C. 1997, Science, 275, 48
- Fabian, A.C. & Daines, S. J. 1991, MNRAS, 252, 17p
- Feretti, L. 1999, in *Diffuse thermal and relativistic plasma in galaxy clusters*, eds. H. Böhringer, L. Feretti & P. Schuecker, MPE Report 271, 1
- Feretti, L. 2001, in *The Universe at Low Frequencies*, Pune 1999, ASP Conference Series, in press, astro-ph/0006379
- Fusco-Femiano, R., dal Fiume, D., Feretti, L., Giovannini, G., Grandi, P., Matt, G., Molendi, S. & Santangelo, A. 1999, ApJL, 513, L21
- Fusco-Femiano, R., De Grandi, S., Feretti, L., Giovannini, G., Grandi, P., Malizia, A., Matt, G. & Molendi, S. 2000, ApJL, 534, L7
- Ginzburg, V.L. & Syrovatskii, S.I. 1964, *The Origin of Cosmic Rays*, Publ. Macmillan, New York
- Giovannini, G., Feretti, L., Venturi, T., Kim, K.-T. & Kronberg, P.P. 1993, ApJ, 406, 399

- Goldoni, P., Goldwurm, A., Laurent, P., Casse, M., Paul, J. & Sarazin, C.L. 2001, in *Exploring the Gamma-ray Universe*, ESA-SP series, in press, astro-ph/0102363
- Gómez, P.L., Loken, C., Roettiger, K. & Burns, J.O. 2001, ApJ, in press, astro-ph/0009465
- Guy, T.B. 1974, Amer. Inst. Aero. Astro. J., 12, 380
- Henriksen, M.J. 1988, ApJL, 407, L13
- Hwang, C.-Y. 1997, Science, 278, 1917
- Kaastra, J.S., Lieu, R., Mittaz, J.P.D., Bleeker, J.A.M., Mewe, R., Colafrancesco, S. & Lockman, F.J. 1999, ApJL, 519, L119
- Kang, H., Rachen, J.P. & Biermann, P.L. 1997, MNRAS, 286, 257
- Kang, H., Ryu, D. & Jones, T.W. 1996, ApJ, 456, 422
- Kempner, J. & Sarazin, C.L. 2000, ApJ, 530, 282
- Kempner, J., Sarazin, C.L. & Ricker, P.R. 2001, ApJ submitted
- Kitayama, T. & Suto, Y. 1996, ApJ, 469, 480
- Lacey, C. & Cole, S. 1993, MNRAS, 262, 627
- Landau, L.D. & Lifshitz, E.M. 1959, *Fluid Mechanics*, Publ. Pergamon Press, Oxford
- Lieu, R., Mittaz, J.P.D., Bowyer, S., Breen, J.O., Lockman, F.J., Murphy, E.M. & Hwang, C.-Y., 1996b, Science, 274, 1335
- Lieu, R., Mittaz, J.P.D., Bowyer, S., Lockman, F.J., Hwang, C.-Y. & Schmitt, J. 1996b, ApJL, 458, L5
- Lieu, R., Bonamente, M. & Mittaz, J. 1999a, ApJL, 517, L91
- Lieu, R., Bonamente, M., Mittaz, J.P.D., Durret, F., Dos Santos, S. & Kaastra, J.S. 1999b, ApJL, 527, L77
- Markevitch, M., Forman, W.R., Sarazin, C.L. & Vikhlinin, A. 1998, ApJ, 503, 77
- Markevitch, M., Sarazin, C.L. & Vikhlinin, A. 1999, ApJ, 521, 526
- Markevitch, M. et al. 2000, ApJ, 541, 542
- Markevitch, M., Vikhlinin, A., Mazzotta, P. & Van Speybroeck, L. 2001, in *X-ray Astronomy 2000*, eds. R. Giacconi, L. Stella & S. Serio, ASP Conference Series, in press, astro-ph/0012215
- Mazzotta, P., Markevitch, M., Vikhlinin, A., Forman, W. R., David, L. P., & Van Speybroeck, L. 2001, ApJ, 555, 205
- McGlynn, T.A. & Fabian, A.C. 1984, MNRAS, 208, 709
- Mittaz, J.P.D., Lieu, R. & Lockman, F.J. 1998, ApJL, 498, L17
- Moekel, W.E. 1949, *Approximate Method for Predicting Forms and Location of Detached Shock Waves Ahead of Plane or Axially Symmetric Bodies*, NACA Technical Note 1921
- Navarro, J.F., Frenk, C.S. & White, S.D.M. 1997, ApJ, 490, 493
- Owen, F.N., Ledlow, M.J., Morrison, G.E. & Hill, J.M. 1997, ApJL, 488, L15

- Peebles, P.J.E. 1969, ApJ, 155, 393
- Peebles P.J.E. 1980, *The Large Scale Structure of the Universe*, Princeton University Press, Princeton, NJ
- Press, W.H. & Schechter, P. 1974, ApJ, 187, 425
- Radvogin, Y.B. 1974, Sov. Phys. Dokl., 19, 179
- Randall, S.W., Sarazin, C.L. & Ricker, P.M. 2001, ApJ submitted
- Rephaeli, Y. 1979, ApJ, 227, 364
- Rephaeli, Y., Gruber, D. & Blanco, P. 1999, ApJL, 511, L21
- Ricker, P. M. & Sarazin, C. L. 2001, ApJ, 561, in press (astro-ph/0107210)
- Roettiger, K., Burns, J. & Stone, J.M. 1999a, ApJ, 518, 603
- Roettiger, K., Stone, J.M. & Burns, J. 1999b, ApJ, 518, 594
- Rusanov, V.V. 1976, Ann. Rev. Fluid Mech., 8, 377
- Sarazin, C.L. 1999a, ApJ, 520, 529
- Sarazin, C.L. 1999b, in *Diffuse thermal and relativistic plasma in galaxy clusters*, eds. H. Böhringer, L. Feretti & P. Schuecker, MPE Report 271, 185
- Sarazin, C.L. & Kempner, J. 2000, ApJ, 533, 73
- Sarazin, C.L. & Lieu, R. 1998, ApJL, 494, L177
- Schindler, S. & Müller E. 1993, A&A, 272, 137
- Schreier, S. 1982, *Compressible Flow*, Publ. Wiley & Sons, New York, 182
- Siemienieć-Oziębło, G. & Ostrowski, M. 2000, A&A, 355, 51
- Spitzer, L. 1962, *Physics of Fully Ionized Gases*, Publ. Wiley & Sons, New York
- Sreekumar, P. et al. 1996, ApJ, 464, 628
- Sugerman, B., Summers, F.J. & Kamionkowski, M. 2000, MNRAS, 311, 762
- Takizawa, M. 1999, ApJ, 520, 514
- Takizawa, M. 1999, ApJ, 532, 183
- Takizawa, M. & Naito, T. 2000, ApJ, 535, 586
- Vestrand, W.T. 1982, AJ, 87, 1266
- Vikhlinin, A., Markevitch, M. & Murray, S.M. 2001a, ApJL, 549, L47
- Vikhlinin, A., Markevitch, M. & Murray, S.M. 2001b, ApJ, 551, 160
- White, S.D.M. 1984, ApJ, 286, 38

Chapter 2

OPTICAL ANALYSIS OF CLUSTER MERGERS

Marisa Girardi

Dipartimento di Astronomia

Università degli Studi di Trieste

Via Tiepolo 11

I-34100 Trieste, Italy

girardi@ts.astro.it

Andrea Biviano

Osservatorio Astronomico di Trieste

INAF

Via Tiepolo 11

I-34100 Trieste, Italy

biviano@ts.astro.it

Abstract An increasing amount of data has revealed that many clusters are very complex systems. Optical analyses show that several clusters contain subsystems of galaxies, suggesting that they are still in the phase of dynamical relaxation. Indeed, there is a growing evidence that these subsystems arise as the consequence of group/cluster mergers. We here review the state of art of optical search and characterization of cluster substructures. We describe the effects cluster mergers have on optical measures of cluster dynamics, and on the properties of cluster member galaxies. We also discuss cluster mergers in relation to the large scale structure of the universe.

Introduction

Until the 80's clusters have been modeled as virialized spherically symmetric systems (e.g., Kent & Gunn 1982). Rather, clusters often contain subsystems of galaxies, usually called substructures or subclusters. Indeed, in the hierarchical scenario of large scale formation it is

quite natural to expect that clusters form from the merger of small sub-clumps (e.g., Colberg et al. 1999). In this context, the presence of substructures is indicative of a cluster in an early phase of the process of dynamical relaxation, or of secondary infall of clumps of galaxies into already virialized clusters.

The presence of substructures complicates the theoretical modeling of cluster dynamics. On the other hand the existence of substructures is probably an essential ingredient in the formation and evolution processes of clusters and their components, so that the analysis of substructures could provide useful cosmological constraints.

Historically, the discovery of substructure occurred in the optical band, via the analysis of the projected distribution of cluster galaxies (e.g., Wolf 1902; Shane & Wirtanen 1954). In the X-ray, Jones et al.'s (1979) Einstein IPC images first showed the complex structure of the hot intra-cluster gas of many clusters. In the radio, Hanisch (1982) and Vestrand (1982) were the first to suggest that the presence of a radio-halo in clusters was related to a short-lived dynamical configuration (see also Feretti 2001). Only recently, new insights into the subclustering phenomenon have come from optical observations of gravitational lensing in galaxy clusters (e.g., Kneib et al. 1996; Pierre et al. 1996; Abdelsalam et al. 1998; Clowe et al. 2000; Hoekstra et al. 2000; Metzger & Ma 2000).

In this review, we consider substructures from the point of view of the analysis of cluster members. Strictly speaking, “optical analysis” of substructures should cover also the weak lensing analyses mentioned before, but the application of this technique to the detection of subclusters is quite recent, and we have decided not to consider it here. Weak lensing analyses are likely to become more and more important in the near future, as they directly detect subclustering in the mass component, rather than relying on galaxies as tracers of the potential. The most exciting possibility is the existence of “dark clumps” of matter traced by no galaxies (Erben et al. 2000; Umetsu & Futamase 2000). We refer the interested reader to Fort & Mellier (1994) and Mellier (1999) for a general review on gravitational lensing from clusters, and to Fitchett (1988a) and West (1994a) for previous reviews on the topic of subclustering.

This review is organized as follows. In § 1 we review the techniques used for the detection of substructure and their results; in § 2 we describe the physical nature of substructures and their connection with ongoing cluster mergers; in § 3 we describe the effects of mergers on estimates of the dynamical properties of clusters; in § 4 we discuss substructure in relation to cosmology and the large scale structure of the Universe (LSS hereafter); finally, in § 5 we review our current knowledge of the

relation between cluster mergers and the properties and evolution of cluster galaxies.

A Hubble constant of $50 \text{ km s}^{-1} \text{ Mpc}^{-1}$ and a deceleration parameter $q_0 = 0.5$ are used throughout.

1. DETECTING AND QUANTIFYING SUBSTRUCTURE

While the first indications of the existence of subclusters were already present in the maps of Wolf (1902), and Shane & Wirtanen (1954), the first modern analyses of the subclustering phenomenon date to the early 60's. Van den Bergh (1960, 1961) compared the observed distributions of velocity differences among galaxy pairs in Virgo and Coma to those obtained from azimuthal scramblings of the data-sets, and found evidence of subclustering in both clusters, on scales $\sim 0.15 \text{ Mpc}$. In the same period, de Vaucouleurs (1961) suggested that Virgo was not a single cluster but the overlap of two subclumps with different galaxy populations and kinematics. Substructure in the two-dimensional (2D) distribution of galaxies was examined for other clusters by Abell et al. (1964). In the 70's, White's (1976) numerical simulations indicated that clusters form by the coalescence of subclusters, and this prompted several authors (most notably Baier & Ziener 1977; Baier 1984; Geller & Beers 1982) to undertake a systematic analysis of substructure in the galaxy distributions of several clusters. Following these preliminary studies, many new techniques have been developed to analyze the problem of substructures. Despite an increased sophistication in the analysis, subclustering remains difficult to measure in a meaningful, quantitative, and unambiguous way. Due to the lack of full kinematical and dynamical information, all statistical methods need to rely on simulations to quantify the significance levels of the detected substructures.

Some of the techniques that have been developed for the detection of substructure in the distribution of galaxies in clusters only provide the probability that a given cluster contains significant substructures; others are able to characterize the properties of the detected substructures, and even to assign the probability of individual galaxies to belong to a given subcluster. Most methods only use the positions and velocities of cluster galaxies, but some do make use of internal galaxy properties – such as their morphologies, luminosities, colours, and star formation rates – to better characterize the substructures (see, e.g., Gurzadyan et al. 1994; Serna & Gerbal 1996). These more sophisticated methods have so far been applied only to a few clusters. A further step in improving the characterization of subclusters consists in using the relative distances of

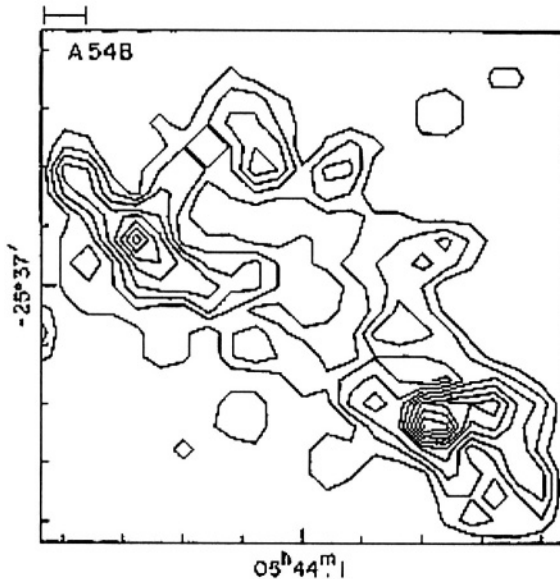


Figure 2.1. Galaxy surface number density diagram of A 548. The bar to the upper left represents 0.48 Mpc at the cluster distance. Courtesy of Geller & Beers (1982).

galaxies in a cluster, in lieu of their relative velocities. So far, this has been possible only for very nearby clusters, such as Virgo (Federspiel et al. 1998; Neilsen & Tsvetanov 2000) and Centaurus (Lucey et al. 1986).

Powerful constraints on cluster substructures come from the comparison of the distribution of cluster galaxies with the surface brightness and temperature maps in the X-ray (e.g., Bird et al. 1995; Arnaud et al. 2000; Gómez et al. 2000; Kolokotronis et al. 2001; Shibata et al. 2001). We discuss the results of these comparisons in more detail in § 3.

The most commonly used statistical methods for the detection of substructure can be grouped in three classes: (a) methods in which only the galaxy positions are used, (b) methods in which only the galaxy redshifts are used, or (c) methods in which the combined spatial and kinematical galaxy properties are used. Several methods can be equally applied to the distribution of galaxy positions, of galaxy velocities, or both, so that the above distinction is rather artificial, and we adopt it here for our convenience.

1.1. SPATIAL SUBSTRUCTURE

The main advantage of searching for substructures in the projected distribution of galaxies, is the availability of large data-sets, reaching

thousands of galaxy positions for nearby clusters. On the other hand, these methods suffer from contamination by fore/background galaxies, groups, and other clusters.

Geller & Beers (1982) were the first to systematically address the evidence of substructures in the projected distributions of cluster galaxies. Using smoothed density–contour maps in 65 clusters, they identified substructures as regions where the local density contrast was more than $3\text{--}\sigma$ above the background fluctuations (see Fig. 2.1).

West et al. (1988) developed three new statistical tests: the *β statistics* measures departures from mirror symmetry in clusters; the *angular separation test* detects subclustering by looking for significant galaxy overdensities at similar polar angles relative to the cluster centre; the *density contrast test* is similar to the method of Geller & Beers (1982).

The application of the *Lee–method* (Lee 1979) to clusters of galaxies is described in Fitchett & Webster (1987; see also Fitchett 1988b). The method optimally splits a data–set into two or more groups using a maximum–likelihood statistics. In practice, the method is only used for the partition of a sample into two subsamples, as the detection of more than two clumps is computer–time consuming. The method measures the clumpiness, L , of the 2D data projected onto a line, with a given orientation, α . The analysis of the function $L(\alpha)$ allows one to define the two groups. The significance of L is established by comparison to Monte Carlo simulations, in which the simulated galaxy distributions can be drawn from several kinds of surface density profiles. While initially applied to 2D data–sets, the *Lee–method* method has later been used also in its 1D and 3D versions (Fitchett & Merritt 1988).

The *Wavelet transform* method is described by Slezak et al. (1990). The basic idea is to convolve the 2D Dirac distribution of galaxy positions with a chosen zero–mean function of position and scale (the Wavelet), on a grid of pixels. There are different kinds of Wavelet function; the so–called 2D radial “Mexican Hat” (the second derivative of a Gaussian) is often used for studies of galaxy clusters (e.g., Escalera & Mazure 1992; Escalera et al. 1992). By varying the scale of the Wavelet function, one is able to test for the presence of substructure of different sizes (a multi–scale analysis). A given substructure can only be detected if its characteristic size is of the order of the scale of the Wavelet. It is worth pointing out that, despite of being circularly symmetric, the radial Wavelet can detect non–circular substructures. As usual, Monte Carlo simulations are needed to establish the statistical significance of the detected substructures. The method also provides the likelihood of individual galaxies to belong to given substructures, thus in practice allowing a decomposition of the cluster into its component subclusters.

A variant of the classical *Wavelet* method has been recently discussed by Shao & Zhao (1999). An extension of the *Wavelet* method to 3D is discussed below (see § 1.3).

Starting from statistical techniques generally used in the analysis of the LSS of the universe, Salvador–Solé et al. (1993a,b) implemented and applied the *average two point correlation function* to the study of cluster substructures. This method provides an estimate of the scale length of typical substructures.

The *KMM* mixture–modeling algorithm for the decomposition of a given data–set in two or more groups, described by Ashman et al. (1994), has been applied to the spatial distribution of cluster galaxies by, e.g., Kriessler & Beers (1997), Maurogordato et al. (2000). Since the simpler implementation of *KMM* is for a 1D distribution, we describe it at length in the next section.

1.2. VELOCITY SUBSTRUCTURE

Models for cluster evolution predict that a system of gravitationally bound particles relaxes into a Maxwellian velocity distribution. A Gaussian distribution of line–of–sight velocities is therefore expected (e.g., Ueda et al. 1993). A non–Gaussian distribution of the observed cluster member velocities is therefore indicative of a non–relaxed dynamical state. For this reasons, *shape estimators* have been used for the detection of substructure in the velocity distribution of cluster members. The classical shape estimators are the kurtosis and the skewness; more robust estimators are the asymmetry– and tail–index (Bird & Beers 1993). The main problem of this method is that the shape of the velocity distribution is not only affected by the presence of substructures, but also by velocity anisotropies (which change the kurtosis, see Merritt 1987), and by the inevitable contamination of the cluster velocity distribution by foreground and background galaxies. In this sense, an improved technique has been developed by Zabludoff et al. (1993). Their technique only works properly for well–sampled data–sets (at least 100 galaxies with velocities). It works by a decomposition of the cluster velocity distribution into a sum of orthogonal Gauss–Hermite functions, and it provides an estimation of the 3rd and 4th order moments, robust against the effect of interlopers.

An alternative way to look for deviation from a relaxed velocity configuration, is to compare the mean cluster velocity with the velocity of the cD galaxy (if present). In fact it has been argued by Beers et al. (1991) that cD galaxies with velocity offsets are only found in clusters with substructures (but see Lazzati & Chincarini 1998 for a different point of

view). There are clusters where significant substructure has been found and yet display a Gaussian velocity distribution, but, at the same time, with a significant cD velocity offset (e.g., Pinkney et al. 1993). We will develop this topic further in § 5.1.

More sophisticated methods have been developed for the detection of multi-modality in the velocity distribution of cluster galaxies. Ashman et al. (1994) described the use of the *KMM algorithm*, a mixture-modeling algorithm, for the detection of substructures in galaxy clusters. *KMM* uses maximum likelihood statistics to determine the optimal partition of a given data-set into an *a priori* chosen number N of Gaussian distributions. The method provides the relative probabilities of group memberships for all galaxies in the data-set. Using the maximum-likelihood ratio test, it estimates the probability that the given partition into N groups is a significantly better description of the distribution than the single group hypothesis. The correct number of groups N corresponds to the solution with the highest probability. *KMM* has also been applied to the distribution of galaxy positions (e.g., Kriessler & Beers 1997) and to the distribution of galaxy positions and velocities (e.g., Bird 1994a; Colless & Dunn 1996, see Fig. 2.2). The *Dedica* method, based on adaptive-kernels, developed by Pisani (1993), has the advantage of giving a non-parametric estimate of the clustering pattern of a data sample, without any *a priori* hypothesis neither on the number of groups, nor on the group distribution function. *Dedica* provides the significance of each subcluster in the velocity distribution, and the membership probability of each galaxy. Non-member galaxies are naturally rejected in this method (see Fadda et al. 1996 and Girardi et al. 1996 for an application of this method to a large cluster sample, see Fig. 2.3). *Dedica* has been extended to the analysis of subclustering in the combined spatial and velocity distributions by Pisani (1996; see Bardelli et al. 1998a for a recent application). Other non-parametric density estimators are the *Maximum Penalized Likelihood* technique (Merritt & Tremblay 1994) and the *Wavelet* method (see, e.g., Fadda et al. 1998 and § 1.1).

1.3. SPATIAL-VELOCITY SUBSTRUCTURE

The existence of correlations between the positions and velocities of cluster galaxies is a footprint of real substructures. Those methods that make use of both positions and velocities of cluster galaxies to search for substructures, are certainly the most reliable, but they are also the most demanding in terms of observational data.

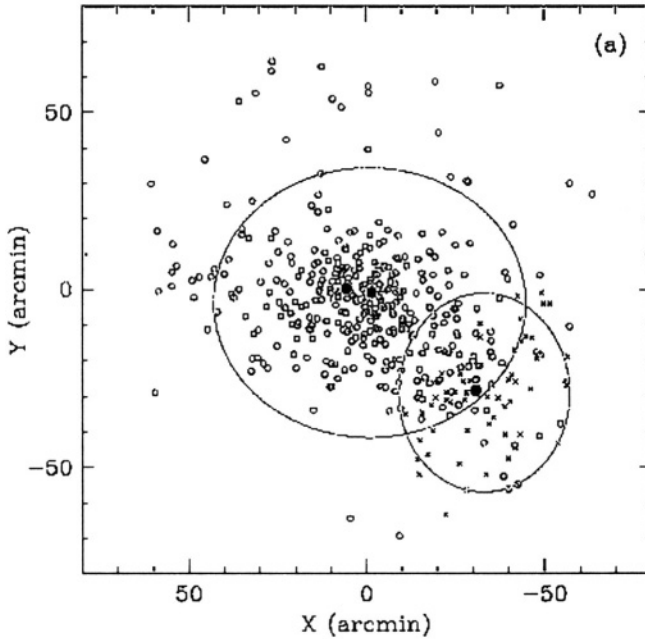


Figure 2.2. The partition of Coma into two subclusters by the *KMM algorithm*. Galaxies belonging to the main cluster are shown as circles and those in the NGC 4839 subcluster are shown as crosses. The dotted ellipses are the 2σ contours of the fitted Gaussians. Courtesy of Colless & Dunn (1996).

The most widely used of these methods is the Δ *statistics* devised by Dressler & Shectman (1988). The method considers all possible subgroups of 10 neighbours around each cluster galaxy, and computes the cumulative difference of these group mean velocities and velocity dispersions from the global cluster values. Galaxies located in groups with significantly different kinematical properties give a higher signal in the Δ *statistics*, see Fig. 2.4. Monte Carlo simulations are run to establish the significance of the Δ *statistics*, by randomly shuffling the velocities and positions of the cluster galaxies. Another method that makes use of both galaxy positions and velocities is the *non-hierarchical taxonomical method* of Perea et al. (1986a,b), where the relative variance of positions and velocities is used for scaling these coordinates. To our knowledge, this method has only been applied to the Coma/A 1367 supercluster complex and to the Cancer cluster.

Other methods are 3D versions of previously described methods (see § 1.1 and 1.2). In the 3D implementation of the *Lee-method* (see, e.g.,

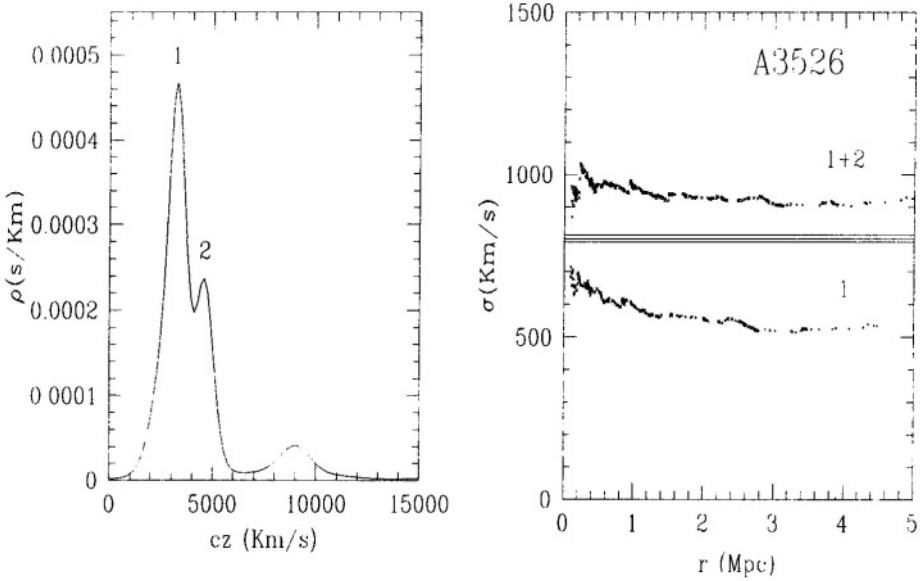


Figure 2.3. The double peaked velocity–space galaxy density of A 3526 (Centaurus), as provided by *Dedica* (Pisani 1993), where the y-axis is in arbitrary units (left panel) The integral velocity dispersion profiles corresponding to the most important peak and the two peaks together; the horizontal lines give the value of the velocity dispersion and 1σ confidence levels, obtained from the X-ray temperature under the condition of perfect galaxy/gas energy equipartition, i.e. $\beta_{spec} = 1$ (right panel). Courtesy of Girardi et al. (1996).

Fitchett & Webster 1987), the data are projected onto a line, allowed to rotate in a volume, rather than in a plane as in its 2D version. The *3D Lee-method* has two interesting properties: it combines the spatial information with the line-of-sight velocity information without any arbitrary scaling; it is independent of linear coordinate transformation, so that it does not artificially detect substructure in an elliptical cluster. The *3D Wavelet* analysis uses spatial and kinematic information by weighting each galaxy (represented by a Dirac function) with a “local kinematic estimator” borrowed from the Dressler & Shectman test (Escalera & Mazure 1992; Escalera et al. 1992). Escalera et al. (1994) and Girardi et al. (1997a) applied this method to large cluster samples (see Fig. 2.5). Needless to say, for both tests, the significance level of detected substructures is again established through the comparison with Monte-carlo simulations. Another test originally developed for the analysis of 1D data-sets, *Dedica*, has been extended to 3D by Pisani (1996). In this method the locally optimal metric is estimated, thus improving the

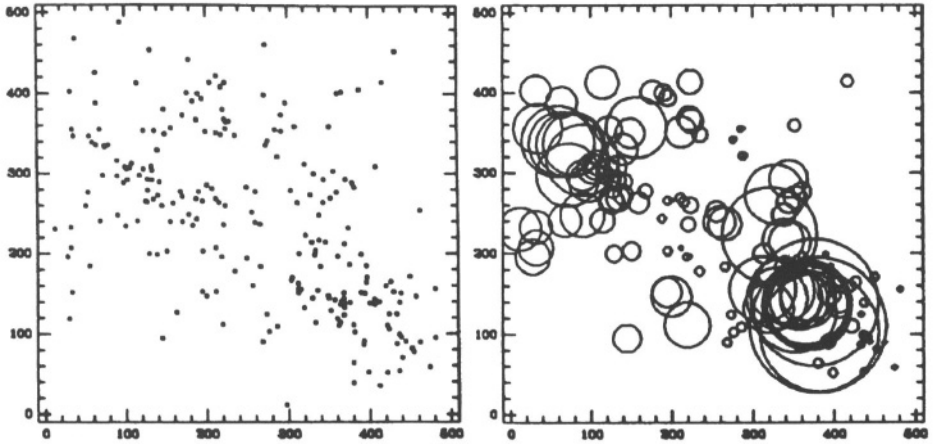


Figure 2.4. Map of the cluster A 548 analyzed using Δ -statistics. Distribution of all galaxies in the cluster (left panel), and galaxies with known velocities marked by a circle whose diameter scales with the deviation of the local kinematics (right panel). Courtesy of Dressler & Shectman (1988).

performance of the density estimator. Within *Dedica* it is also possible to examine to what extent the large and small scale structures affect the estimation of the cluster dynamical parameters (e.g., the virial mass).

Other methods try to establish the presence of substructures by the direct dynamical influence they have on the cluster. These are the *S-tree technique* of Gurzadyan et al. (1994) and the *h-method* of Serna & Gerbal (1996). These methods assume a proportionality between a galaxy luminosity and its mass, and therefore need galaxy magnitudes. The *S-tree technique* is based on the properties of the flow of geodesics in phase space, and uses the so-called 2D curvature for evaluating how strongly bound is a subsystem. The *h-method* by Serna & Gerbal (1996) uses the relative binding energy in the hierarchical clustering method.

1.4. DIFFERENT METHODS COMPARED

Pinkney et al. (1996) tested the efficiency of several methods for the detection of substructure via the analysis of N-body numerical simulations of cluster mergers. Only the simplest methods were considered, those which do not try to detect and characterize the individual subclusters, but which simply provide a probability for a given cluster to contain significant substructures. In particular, the *Wavelet* method, *KMM*, and *Dedica* were *not* considered by Pinkney et al. (1996). In general, these authors found that the higher the dimensionality of the test, the more

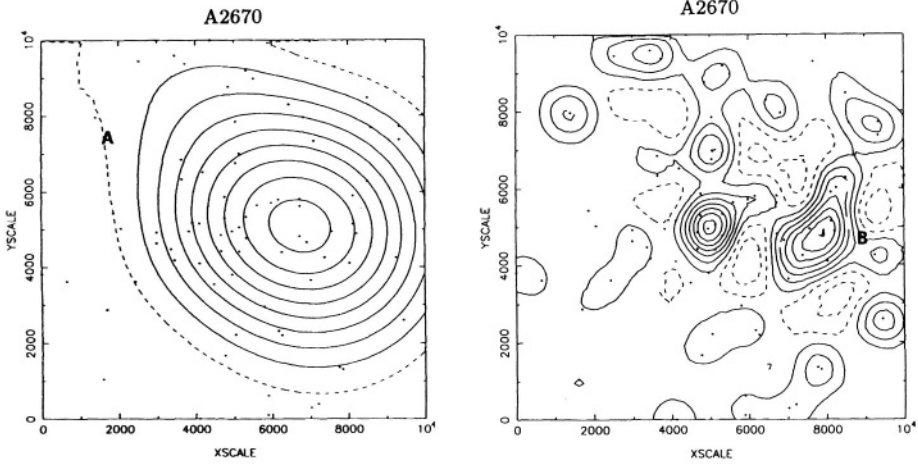


Figure 2.5. Results of the *Wavelet* analysis applied to a 3D sample of A 2670. Left panel: the *Wavelet* image on large scales; right panel: the *Wavelet* image on small scales. The cluster appears unimodal at large scales, but shows a structure in the core when examined at small scales. Courtesy of Escalera et al. (1994).

sensitive it is to substructure. However, the test sensitivity depends on the angle between the line of sight and the merger axis (e.g., those tests that consider galaxy positions only are most sensitive to line of sight perpendicular to the merger axis). As a consequence, a suite of tests is recommended when searching for cluster substructures.

According to Pinkney et al. (1996), the most sensitive of the tests they considered turned out to be Dressler & Shectman's (1988) Δ statistics. In agreement with Pinkney et al.'s result, Flores et al. (2000) found evidence for substructure in the cluster A 3266 with the Δ statistics, whereas the velocity distribution was found to be Gaussian. The N-body simulations of Crone et al. (1996) and Knebe & Müller (2000) confirmed the good overall performance of Dressler & Shectman's (1988) test, particularly for the case of recent big mergers, whereas small infalling groups remain difficult to detect.

For what concerns the comparison of more sophisticated tests, Fadda et al. (1998) found that the *Wavelet* technique and *Dedica* perform similarly, although Bardelli et al. (1998a) found the latter to be faster and more efficient. The *Wavelet* technique was found to give similar results to those of the *Lee-method*, when applied to detection of substructures

in the Coma cluster (Escalera et al. 1992). The good performance of the *Lee* test was also confirmed in Crone et al.'s analysis of their numerical simulated clusters. The 2D *KMM* test was used by Maurogordato et al. (2000) to establish the presence of substructures in the cluster A521, whose galaxy velocity distribution is nevertheless Gaussian.

2. FREQUENCY AND NATURE OF SUBCLUSTERS

The analysis of subclustering aims at answering the following main questions: (i) what is the fraction of clusters harbouring substructure, and (ii) which are the subcluster properties. Here we try to summarize the results obtained in the most extensive and accurate investigations of cluster substructures, but we note that the answers to the above questions depend somewhat upon the amount of photometric and spectroscopic data available for the galaxies of the clusters considered (cf. the Coma cluster, Biviano 1998).

There is a general agreement that substructures concern 30 – 60 % of all clusters (with a few notable exceptions: West & Bothun 1990; Rhee et al. 1991). This general consensus is built upon the independent results obtained from the analysis of substructures in the projected distribution of cluster galaxies (see, e.g., Geller & Beers 1982, who considered a sample of 65 clusters; Salvador–Solé et al. 1993a, 14 clusters; Kriessler & Beers 1997, 56 clusters), in the velocity distribution (e.g., Bird & Beers 1993, who analysed 14 clusters), and in the combined spatial and kinematical distribution (e.g., Dressler & Shectman 1988, who considered 15 clusters; Biviano et al. 1997, 25 clusters; Girardi et al. 1997a, 48 clusters; Stein 1997, 12 clusters; Solanes et al. 1999, 67 clusters). A higher frequency, ~ 80%, is sometimes found when considering a suite of tests (see, e.g., Bird 1994b who considered 25 cluster; Escalera et al. 1994 who considered 16 clusters).

The detected substructures generally have sizes of 0.4–0.6 Mpc (e.g., Geller & Beers 1982; Salvador–Solé et al. 1993b; Escalera et al. 1994; Girardi et al. 1997a), and their masses and richnesses are typically ~ 10% those of their parent cluster (Escalera et al. 1994; Girardi et al. 1997a). Larger size substructures (e.g. bimodal clusters) are less common and concern 10 – 20 % of clusters (e.g., Girardi et al. 1997a, 1998). Subclusters of smaller sizes, ~ 0.2 Mpc, composed by a bright galaxy surrounded by dwarf companions, have been described by Ferguson (1992), Conselice & Gallagher (1998) and Kambas et al. (2000). After all, it might well be that a whole hierarchy of subclustering exists; Tully (1987) and Zabludoff & Mulchaey (1998) presented evidence for

substructures in poor groups, and, on the largest scales, the superclusters are found to be substructured in clusters and groups (see § 4.1).

What is the physical nature of these subclusters? As pointed out by West & Bothun (1990), one can assign substructures to one of the following classes: (1) subclusters which are the surviving remnants of galaxy systems which have merged (or are in the merging phase) to form a rich cluster; (2) subclusters which presently reside within an otherwise relaxed cluster, perhaps arising from secondary infall of bound groups, in the phase of tidal disruption within the cluster; (3) galaxy groups which are bound to the cluster but are still outside the cluster virial region; (4) groups of galaxies dynamically disjoint from the cluster, which appear as substructures because of chance projection along the line of sight. Only substructures of the first class are truly representative of a young cluster dynamical status. For the sake of completeness, one should also mention the possibility that a specific type of substructure, the galaxy *aggregates* of Conselice & Gallagher (1998), i.e. clouds of dwarfs around a bright central galaxy, are just a manifestation of gravitational lensing of background galaxies by the mass of the bright central galaxy.

In principle, independent distance information is needed to assess the nature of the detected substructure (see Lucey et al. 1986; Federspiel et al. 1998; Neilsen & Tsvetanov 2000), but the inclusion of velocity data in the substructure analysis already reduces the probability of a chance projection.

The case of bimodal clusters, in particular, can be reduced to a simple two-body problem with linear motion (i.e., no rotational support) with a boundary value of separation $R = 0$ at time $T = 0$ (see, e.g., Gregory & Thompson 1984; Beers et al. 1992). Based on observational quantities (i.e. line-of-sight velocity, projected separation, and total mass of the system) one can then estimate the probability that: (a) the system is bound but still expanding, (b) the system is collapsing, or (c) the two clumps are not bound (see Lubin et al. 1998 for a recent application of this method to a bimodal cluster at $z \sim 0.8$). In more complicated cases of subclustering, it is possible to try to reproduce the observed galaxy distributions in positions and velocities, with numerical simulations, see e.g., Roettiger et al. (1997); Lubin et al. (1998); Flores et al. (2000); Roettiger & Flores (2000).

Cosmological N-body simulations have been used to test the sensitivity to projection effects of classical tests for substructure detection. Some have found the tests to be quite robust (e.g., Crone et al. 1996), but others (e.g., Cen 1997; Knebe & Müller 2000) have instead found that projection effects significantly inflate the estimation of the frequency of cluster substructure. These discrepant results can partly be ascribed to

the difficulty of analysing simulated clusters in the same way as real clusters, in particular for what cluster member identification is concerned. Kolokotronis et al. (2001), in a recent analysis of 22 rich clusters, found evidence of substructures in 10 of them, both in X-rays and optical, while in another 5 clusters, the optical evidence for substructure is not supported by the X-ray analysis. Taken at face value, their result implies that 1/3 of the optically detected substructures are due to projection effects, but we note that their observed frequency of optically detected substructures is above the average found in other studies.

Assuming that most optically-detected substructures are real, what are they? Substructure of large sizes, i.e. bimodal clusters, are clearly equal-mass clusters caught in the process of merging. Smaller size substructures, on the other hand, could be identified either with small groups accreted by the cluster, or with the dense cores of clusters which have survived tidal disruption during the merger with a similar mass cluster (González-Casado et al. 1994). In the Virgo cluster, Schindler et al. (1999) noted a trend concerning subcluster richness and spatial extent. The compactness of systems, in both optical and X-ray light, increases with decreasing optical richness (i.e., poorer systems are more compact), as expected if subclusters originate from virialized groups. This issue is critical, since the accretion rate required for explaining the frequency of observed substructures depends on their survival time within the cluster, which is larger for dense cluster cores than for loose poor groups (see also § 4.2). In general, numerical simulations (see, e.g., Burns et al. 1994) have indicated that after a collision the group galaxies are dispersed over a very wide area. Many subcluster particles disperse on both sides of the cluster along the merger axis. It is therefore generally assumed that compact subclusters, with a velocity dispersion characteristic of groups, are pre-merger. It is also instructive to compare the subcluster galaxy distribution with the gas surface brightness, since the collisional gas component is expected to be displaced downstream during the infall (see, e.g., Donnelly et al. 1999; Neumann et al. 2001).

3. DYNAMICAL EFFECTS OF CLUSTER MERGERS

Much of our knowledge on the dynamical effects of cluster mergers is based on the results of N-body simulations (see, e.g., Schindler & Bohringer 1993; Pinkney et al. 1996; Roettiger et al. 1996, 1997). The simulations have shown that during a cluster merger the global velocity dispersion of system galaxies can be strongly enhanced, up to a factor two, depending on the relative position of the merging axis

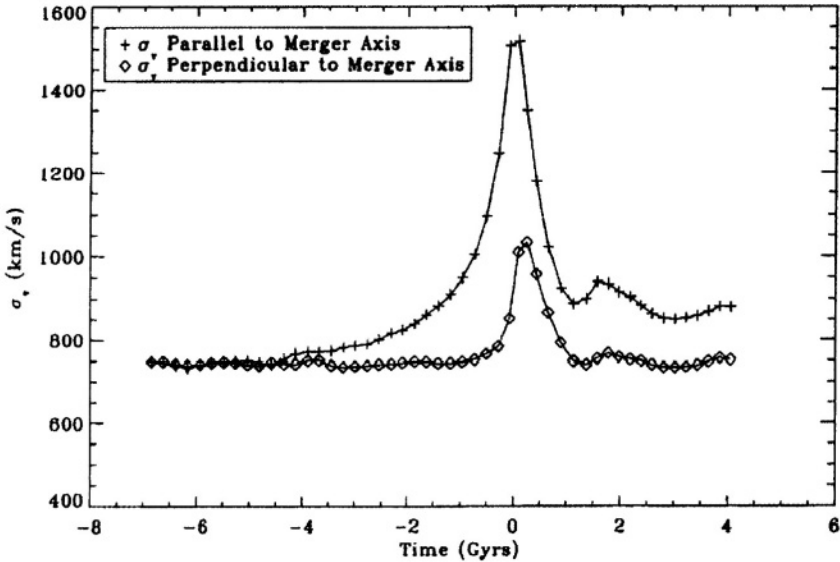


Figure 2.6. Velocity dispersion vs. time for a 3:1 mass ratio merger simulation and for two different viewing angles. Courtesy of Pinkney et al. (1996).

to the line of sight, the relative masses of the two clumps, and the epoch of merging (see Fig. 2.6). Part of the (huge) large-scale motion energy of the subcluster (10^{50-60} erg, see, e.g., Bardelli et al. 2001) is converted into random motion of the galaxies of both the infalling group and the main cluster (Pinkney et al. 1996). Significant mass overestimation might result from a simplistic application of the virial theorem if the system is observed within ± 1 Gyr from the epoch of core passage, the line of sight is close to the merger axis, and the mass ratio of the merging units is close to unity. For these extreme cases of mergers, in agreement with the results of numerical simulations, observational studies have indicated that the virial theorem would overestimate the mass of a cluster, typically by a factor 2, if subclustering is ignored in the analysis (Beers et al. 1991, 1992; Escalera et al. 1994; Girardi et al. 1997a; Flores et al. 2000; Maurogordato et al. 2000). Since the luminosity functions of galaxies in and outside subclusters are similar (Bardelli et al. 1998b), the mass-to-light ratio is similarly affected as the virial mass.

However, in such merging conditions, the distribution of galaxy velocities is strongly affected, and becomes skewed or double-peaked, so that a careful analysis of the velocity distribution can reveal the ongoing

merger, and the mass estimate can be corrected accordingly (see, e.g. Girardi et al. 1998). As an example, Fadda et al. (1996), using the adaptive kernel method (Pisani 1993), treated separately those peaks in the velocity distribution of cluster members, which are more distant than 1000 km s^{-1} and overlap for less than 20% of their galaxy population. However, as noted by Pinkney et al. (1996), during the core passage the two clumps could be so far apart in velocity ($\sim 3000 \text{ km s}^{-1}$) that the real issue is to understand whether the clumps are physically associated or seen in projection, rather than to provide a correct estimate of the velocity dispersion of the systems.

For what concerns the more common small substructures, Escalera et al. (1994) and Girardi et al. (1997a) showed that the effect of substructure on the virial mass estimation is marginal, $\sim 10\%$. Bird (1995) however found a much larger effect of substructures on the estimations of cluster masses. The discrepancy arises from the different methods of rejection of interlopers, Bird's method being much less sophisticated and less efficient than the methods adopted by Escalera et al. and Girardi et al. As a consequence, Bird tended to detect substructures in clusters where Girardi et al. did not, because of the much stronger contamination by interlopers that Bird considered as members of the main system along the line of sight. In other words, this is a typical case of contamination of the substructure analysis by projection effects. As a matter of fact, also Bird found that the effect of substructure is much reduced when only the central part of the cluster is considered (thus effectively reducing the influence of projection effects).

The limited effect of substructure on the mass estimates in the majority of clusters found by Escalera et al. (1994) and Girardi et al. (1997a) was confirmed in the cosmological simulations of Tormen et al. (1998), and Brainerd et al. (1999). Similarly, Xu et al. (2000) showed that, while the internal structure of a cluster may depart from dynamical relaxation, some statistical properties of clusters are approximately the same as for virialized systems (the "quasi-virialization" scenario). The mass estimates of groups were also found to be robust against the influence of substructures by Zabludoff & Mulchaey (1998).

The accretion of subclusters from the projected filaments along the line of sight (see § 4.1) could lead to overestimate a cluster velocity dispersion even before the merger event occurs. A detailed dynamical and structural analysis of the cluster and its surrounding LSS is needed to identify the accreting groups and projected filaments and return a reliable cluster velocity dispersion estimate (see, e.g., the case of A 1689, Girardi et al. 1997b; Centaurus, Churazov et al. 1999; and, in particular, A 85, Durret et al. 1998).

Apart from the effects on the velocity dispersion of a cluster, substructures have a more general influence on the global distribution of cluster galaxy velocities and positions. The velocity distribution of galaxies within a subcluster can be displaced with respect to the mean velocity of the cluster (Zabludoff & Franx 1993; Scodreggio et al. 1995; Quintana et al. 1996). Zabludoff & Franx (1993) argued that such asymmetries in the velocity distribution last until the subclusters merge with the central cluster. Substructures therefore produce asymmetries in the velocity distribution, precluding a reliable determination of the galaxy orbits based on the shape of the velocity distribution profile (Merritt 1987).

The effect of cluster substructures is evident in the velocity vs. clustercentric radius (R, v) distribution for cluster galaxies. The theory of spherical infall predicts the existence of caustics of infinite galaxy density in the (R, v) -space, but substructures make a substantial contribution to the amplitude of the caustics, which are related to the escape velocity from the cluster (Rines et al. 2000). When averaging over many clusters, the velocity asymmetries are largely erased, but galaxies in subclusters still have a different (R, v) -distribution from galaxies outside substructures (Biviano et al., 2001).

A dynamical consequence of an off-axis cluster merger is the transfer of the angular momentum of the infalling subcluster to the system. Roettiger & Flores (2000) found that the transfer of angular momentum is more efficient towards the collisional component (the intra-cluster gas), and this can explain the velocity gradient in the intra-cluster gas of Perseus (Dupke & Bregman 2001). On the other hand, the simulations of Caldwell & Rose (1997), Lima-Neto & Baier (1997), and Gómez et al. (2000) all found that significant angular momentum is also transferred to the galaxy component, resulting in a velocity gradient of the galaxy population. Apart from the obvious cases of bimodal clusters, only few clusters show a significant velocity gradient and the relative correction to the global value of velocity dispersion is very small (some tens of km s^{-1} , Girardi et al. 1996). In Coma, Biviano et al. (1996) and Colless & Dunn (1996) provided evidence for a significant velocity gradient in the core region. Of course, a technical problem in these studies is that only the line-of-sight component of the velocity tensor is observable.

Even more extreme are the consequences of merging on the velocity distribution of the members of the accreting clump. In particular, it is expected that tidal stripping affects more strongly the less bound galaxies in the group, so that the groups tend to develop truncated velocity distributions (see Gurzadyan & Mazure 1998, 2001).

The effects of substructures on the projected distribution of cluster members are less important than the effects on their kinematics (but

see Bird 1995 for a different opinion). However, it has been suggested that fictitious cores in the cluster galaxy distribution can be produced by the presence of subclusters in the central cluster regions (Fitchett & Webster 1987; Mohr et al. 1996). Roettiger et al.'s (1993) simulations showed that as a consequence of a cluster–subcluster merger, the cluster core is elongated by 10% in the direction perpendicular to the merger axis, and by 30% in the direction parallel to the merger axis. Several simulations and observations indicated that the elongation of a cluster is induced by the accretion of groups along filaments (e.g., Roettiger et al. 1997; Durret et al. 1998; see § 4.1).

It is interesting to compare the mass estimates obtained from the virial analysis of the galaxy distribution, with those inferred from X–ray and gravitational lensing analyses. In fact, the two former methods assume that the cluster is in dynamical equilibrium, while the latter only requires some assumptions on the geometry of the cluster, so that a discrepant result could be a signature of the presence of substructure. If a cluster is out of equilibrium, the optical and X–ray analyses can lead to serious discrepancies.

Observationally, optical and X–ray subclustering are generally well correlated (Kolokotronis et al. 2001, but see Baier et al. 1996 for a different view) but in a few individual cases the galaxies and the IC gas have different distributions. In addition the peak of the X–ray surface brightness does not coincide with the peak of the galaxy distribution (Zabludoff & Zaritsky 1995: A 754; Barrena et al., 2001: 1E 0657–56).

Indeed, numerical simulations have shown that the galaxies and the IC gas react on different time scales during a merger, e.g. two clusters can pass through one another without destroying the individual optical components while the gas is strongly affected (e.g., White & Fabian 1995; Roettiger et al. 1997). The shocks from the infalling subcluster create temperature and density gradients that can lead to an overestimation of the mass determined assuming hydrostatic equilibrium for the X–ray emitting gas by up to a factor 2 (e.g., Schindler 2000). On the other hand, substructures also flatten the density profile and this could lead to a mass underestimation by a similar factor. According to Roettiger et al.'s (1997) hydro/N–body simulations much of the heating of the merger goes into energy of the IC gas, while the heating of the dark matter component is minimal, and the dark matter component can efficiently redistribute energy through violent relaxation. On the other hand, Lewis et al. (1999) suggested that merging affects the optical estimates of a cluster mass much more than the X–ray estimates mainly because of the different nature of measurements which, in the

optical case, have the added difficulty of determining the interlopers. Lewis et al. also pointed out that substructure could boost the lensing (in particular strong lensing) mass estimates up by a factor 1.6. King & Schneider (2001) found that substructure increases the dispersion of all recovered parameters from weak lensing technique. It is therefore difficult to predict *a priori* which kind of mass estimate is more reliable.

Several discrepancies in the mass estimates from the different methods were pointed out in the past (e.g., Miralda–Escudé & Babul 1995; Smail et al. 1997; Wu & Fang 1997). Recent results have suggested that, when clear bimodal clusters are excluded from the sample, the mass estimates from the virial analysis, X–ray and weak lensing methods are in reasonable agreement except, perhaps, for the central cluster regions, possibly because of the effect of small–size substructures (see, e.g., Allen 1998; Girardi et al. 1997b, 1998; Lewis et al. 1999). However more difficulties remain in the task of correctly estimating the masses of subclusters, which are even more affected by the merger process than the main cluster (see, e.g., the case of the NGC4839 group in Coma – Colless & Dunn 1996 vs. Neumann et al. 2001).

Other global cluster properties are affected by the presence of substructures. This is particularly evident when considering the X–ray vs. optical properties, since these properties are affected in different ways due to the collisional nature of the IC gas and the non–collisional nature of the cluster galaxies. Substructure has been invoked to explain observed departures from the L_X – σ_v relation (e.g., for A 1060, Fitchett 1988a), and from the σ_v – T_X relation. High values of $\beta_{spec} = \sigma_v^2 / (kT_X / \mu m_p)$ (where μ and m_p are the molecular weight and the proton mass respectively) are suggestive of the presence of substructure since $\beta_{spec} \sim 1$ if only gravitational processes are important (e.g., Edge & Stewart 1991). However, even anomalously low values of β_{spec} have been found in merging clusters (e.g., in A 754, Girardi et al. 1996). The value of β_{spec} can thus provide useful insight into the evolutionary stage of a merger (e.g., Bird et al. 1995; Shibata et al. 2001). On the other hand, both the velocity dispersion and the X–ray temperature of a cluster tend to increase during a merger, so that there is a chance to observe $\beta_{spec} \simeq 1$ also for non–relaxed clusters.

4. SUBSTRUCTURE AND COSMOLOGY

4.1. ACCRETION FROM THE LSS

In hierarchical clustering cosmological scenarios clusters of galaxies form by accretion of subunits. Numerical simulations show that clusters form preferentially through anisotropic accretion of subclusters along

large scale filaments (West et al. 1991; Katz & White 1993; Cen & Ostriker 1994; Colberg et al. 1998, 1999). The infall of matter onto clusters arises from clumpy, inhomogeneous, filaments and sheets (Colberg et al. 1999). The signature of this anisotropic cluster formation is the cluster elongation along the main accretion filament (e.g., Roettiger et al. 1997). This is certainly true for the collisionless component, while the IC gas is first elongated similarly, and then is pushed outwards perpendicular to the merger axis (e.g., Schindler 2000).

There is a wealth of observational data supporting the anisotropic cluster formation scenario borne out of numerical simulations. The LSS topology is characterized by large filamentary structures (e.g., the Perseus–Pisces supercluster, described by Haynes & Giovanelli 1986, and the Great Wall, described by Geller & Huchra 1990). The cluster main axes are oriented along the main directions of the surrounding LSS (Gregory & Thompson 1978; Binggeli 1982; Fontanelli 1984; Rhee et al. 1992; Plionis 1994; West et al. 1995; Dantas et al. 1997; Bardelli et al. 2001). Zabludoff & Franx (1993; see also Neill et al. 2001) showed that galaxies of different morphological types have different mean velocities in some clusters. This fact was interpreted as evidence for anisotropic accretion of clumps of (mostly) spirals onto these clusters.

Several detailed studies have recently added further evidence for the infall of groups into clusters along preferential directions. Girardi et al. (1997b) showed that A 1689 is composed of two main structures aligned along the line of sight that add to three small foreground groups already identified by Teague et al. (1990). The A 85/87/89 complex analyzed by Durret et al. (1998) is one of the most striking examples of structure alignments (see Fig. 4.1). Using both optical and X-ray data, these authors showed that A 89 is a line-of-sight superposition of two groups which are located in intersecting sheets on opposite sides of a large galaxy bubble. A 87 is resolved into individual groups, organized as a filament almost perpendicular to the plane of the sky, possibly falling onto A 85. Remarkably, the alignment goes from small to very large scales: the A 85/87 filament is coaligned both with the cD galaxy of A 85 and with a structure that extends over more than 5 degrees on the sky (corresponding to 28 Mpc at the redshift of A 85), and which includes A 70, 85, 89, 87, 91 and some other groups. A strongly supporting evidence for the formation of rich clusters at the intersection of filaments has come from the study of Arnaud et al. (2000). They identified in A 521 a young cluster in formation at the crossing of two filaments, one pointing towards A 517 and the other in the direction of A 528/518 (see Fig. 2.8). They splitted A 521 into a main structure, A 521S, onto which a smaller group, A 521N, is infalling.

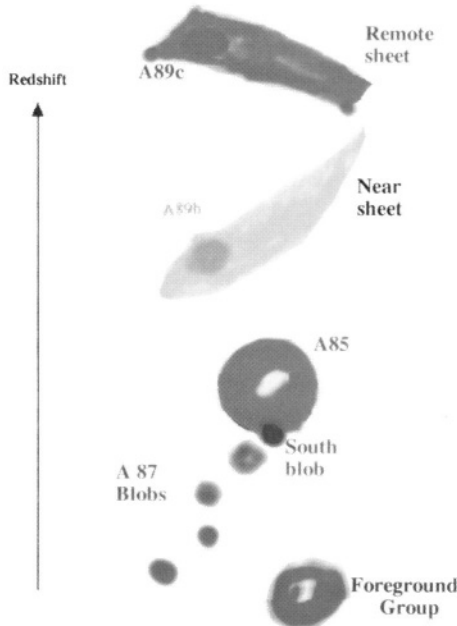


Figure 2.7. An artist's view of the A 85/87/89 complex. Courtesy of Durret et al. (1998).

West & Blakeslee (2000) have been able to determine the principal axis of the Virgo cluster in 3D, by determining galaxy distances with the surface-brightness fluctuations method. This axis joins a filamentary bridge of galaxies connecting Virgo to A 1367. The Virgo ellipticals themselves have their axes aligned along this same direction. Since the Coma cluster is also embedded in the LSS at the intersection of filaments pointing to other clusters, and, in particular, to A 1367, Virgo and Coma are themselves connected (West 1998). West (1998) also presented evidence that the distribution of groups around Coma (from Ramella et al. 1997) is suggestive of future infall onto the cluster along the same direction traced by Coma galaxies. Finally, direct evidence that the LSS filaments are clumpy has come from weak lensing analyses (Clowe et al. 2000). Rich superclusters of galaxies are the ideal environment for studying major cluster mergers. In fact, the high local overdensity of the superclusters implies higher relative velocities for clusters, which in turn increase the cross-section for cluster-cluster collisions (Bardelli et al. 2001). Most remarkable is the central region of the Shapley Concentration, where three rich clusters (A 3556, 3558, and 3562) and several

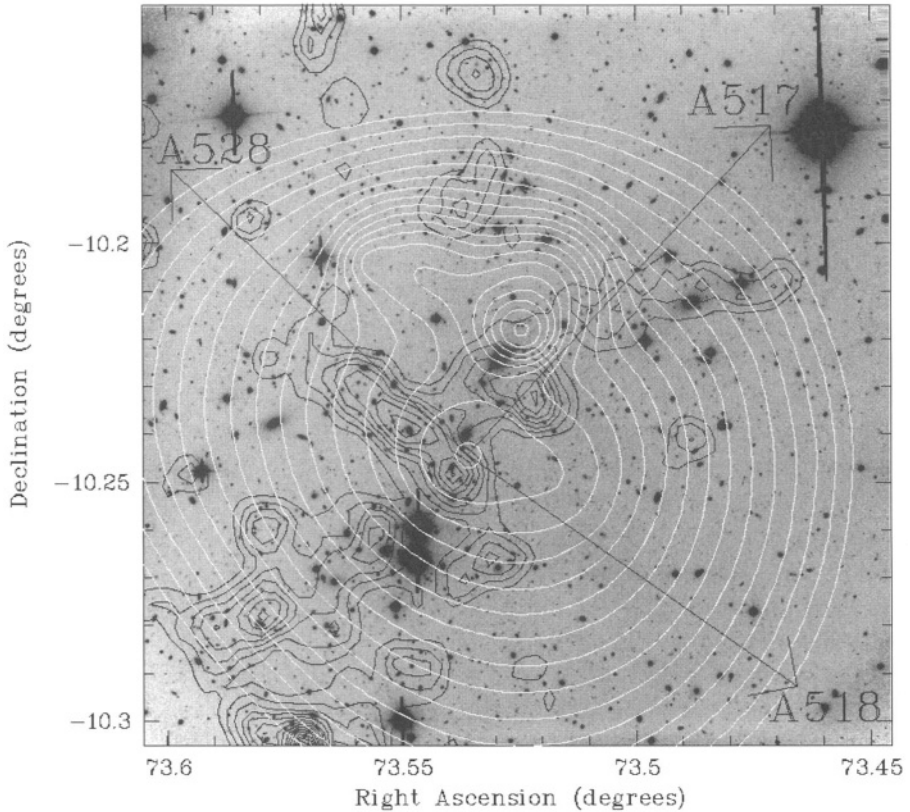


Figure 2.8. A521 galaxy isodensity contours in black, and X-ray isointensity contours in white, are superimposed on the V-band image. The direction towards the clusters A 517, A 528, and A 518 are also indicated. Courtesy of Arnaud et al. (2000).

poor clusters or groups are aligned. Bardelli and collaborators have described the properties of this complex in a series of papers. In particular, for what concerns the optical analysis of substructures, Bardelli et al. (1998a) used *Dedica* (Pisani 1996) to identify a large number of substructures and drew two alternative scenarios for the structure and dynamical evolution of this cluster complex (see Fig. 2.9). In one scenario the core of the Shapley Concentration would correspond to a cluster–cluster collision seen just after the first core passage. In the alternative scenario this structure would result from a series of incoherent group–group and cluster–group merging. A similar study – but using *KMM* instead of

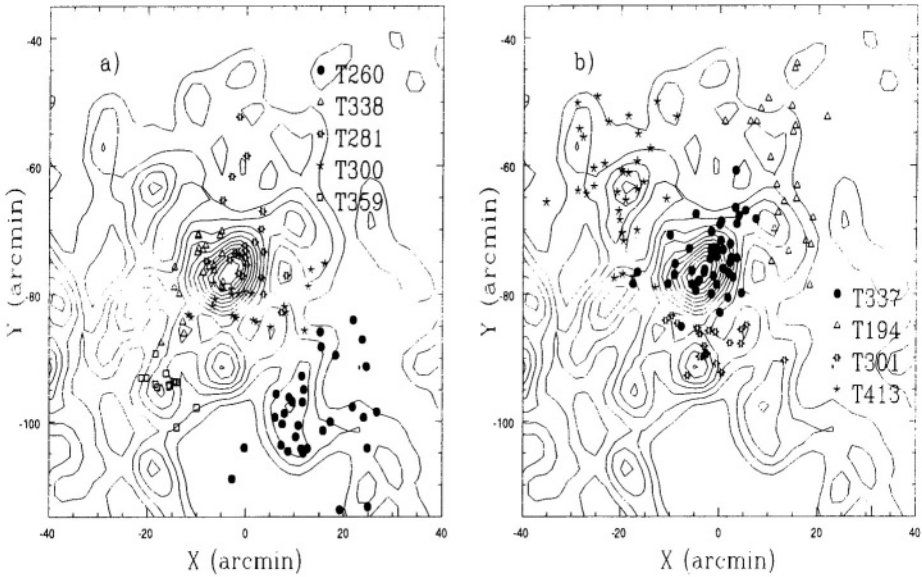


Figure 2.9. Groups found in the A 3558 cluster region. The positions of sub-cluster galaxies found by using *3D Dedic*a (Pisani 1996) are overplotted onto the smoothed 2D isodensity contours. Different symbols label galaxies in different groups. For cleanliness the group members are splitted in two panels. Courtesy of Bardelli et al. (1998a).

*Dedic*a – has been performed by Barmby & Huchra (1998) in the Hercules Supercluster.

4.2. ESTIMATING Ω

Since the frequency of subclustering at the present epoch is set by the mean density at recombination, substructure analyses in clusters can be used to constrain Ω_m with little influence from Ω_Λ (Richstone et al. 1992; Lacey & Cole 1994; Thomas et al. 1998). In fact, in a low density Universe the structure formation tends to freeze at $z = 1/\Omega_m - 1$, while in a 5–8 Gyr (Brainerd et al. 1998). From the observed degree of high density Universe clusters accrete 50% of their mass in the last subclustering, Richstone et al. (1992) concluded that a high density Universe was implied, unless substructures can survive longer than expected, or projected groups along the line of sight are mistaken for subclusters.

Following analyses produced contradictory results. Later results of cosmological simulations have suggested that low-density models are

able to produce a fraction of clusters with substructure in substantial agreement with the observations when proper account is taken for projection effects and the (in)efficiencies of substructure–detection methods (Jing et al. 1995; Jing & Borner 1996; Cen 1997; Knebe & Müller 2000). Dutta (1995) suggested that at least 500 galaxies per clusters are needed to discriminate between a low and high Ω_m universe by using the Δ -*statistics* test. Knebe & Müller (2000), however, provided a more optimistic estimate. In general the dark matter component, rather than galaxies, is traced by the cosmological simulations, thus complicating the direct comparison with observations.

The main unknown in this approach is the survival time of the substructure within a cluster. If substructures are long-lived, a high fraction of clusters with substructure can be reconciled with a low-density Universe. Bimodal configurations, and off-axis mergers, in particular, can last long (Cavaliere et al. 1986; Cavaliere & Colafrancesco 1990; Roettiger & Flores 2000), up to 4 Gyr (Nakamura et al. 1995). The compactness of the infalling groups helps them to survive for a significant fraction of the Hubble time (Tormen et al. 1998). Since hierarchical clustering predicts smaller systems to be more compact, Tormen et al. suggested a longer survival time for smaller groups, while the larger groups rapidly sink into the cluster centre and lose their identity. On the other hand, González-Casado et al. (1993, 1994) suggested that the longest lasting subclusters are detached cores of colliding clusters. In general, several investigations have agreed that the presence of subclustering significantly slows down the collapse and virialization of a cluster (Cavaliere et al. 1986; Thomas & Couchman 1992; Schindler & Böhringer 1993; Antonuccio-Delogu & Colafrancesco 1994; Roettiger et al. 1998) with respect to the classical homogeneous spherical infall model of Gunn & Gott (1972).

Possibly, a more interesting approach comes from the comparison of the dynamical status of nearby and distant clusters. In particular, there is a growing evidence that distant clusters (at $z > 0.8$) display a young dynamical state. Smail et al. (1997) presented weak lensing results for 12 distant clusters and interpreted their high velocity dispersions as overestimates induced by subclustering. Lubin et al. (1998) showed that the cluster Cl J0023+0423 at $z = 0.84$ is a candidate ongoing merger of two low-dispersion groups. Both RX J1716.6 + 6708 at $z = 0.81$ and MS 1054.4 – 0321 at $z = 0.83$ have a filamentary morphology, which is suggestive of a young dynamical status (Gioia et al. 1999, see Fig. 2.10; van Dokkum et al. 2000). RX J1716.6+6708 has a β_{spec} in excess of one, indicative of an ongoing merger (see § 3). Several distant clusters have been found to have companions (e.g., the supercluster at $z = 0.91$ found

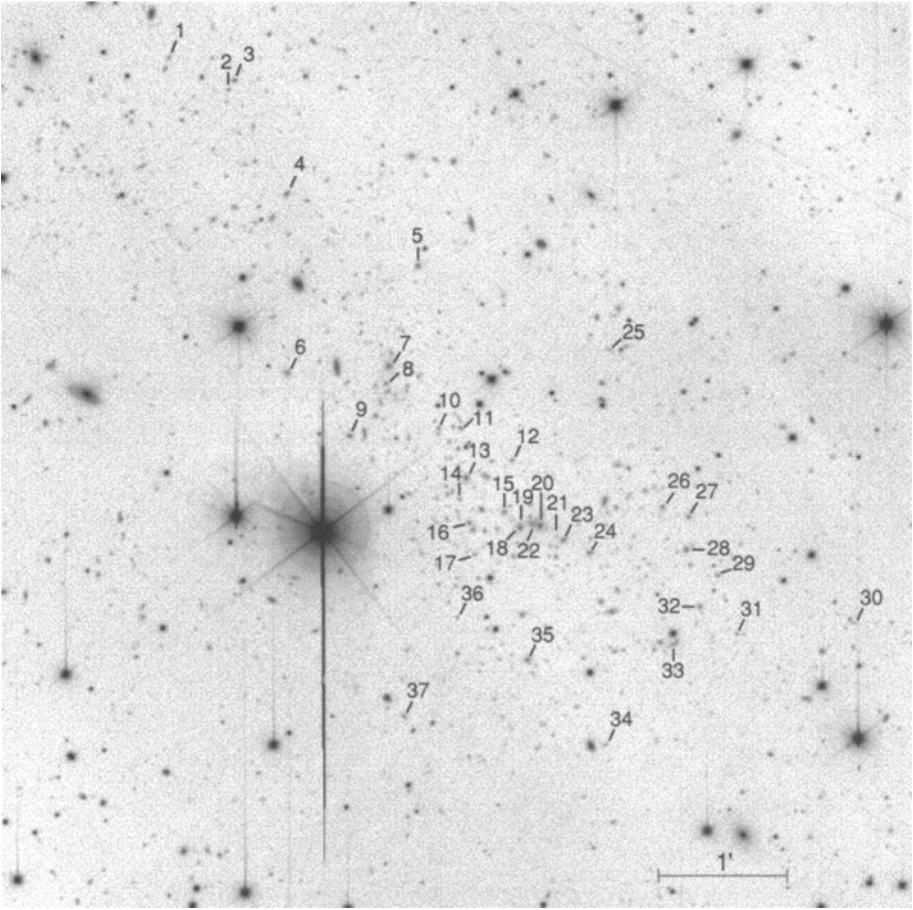


Figure 2.10. The I-band image of *RXJ1716.6 + 6708*. The cluster galaxies are marked and show the filamentary morphology of this cluster. Courtesy of Gioia et al. (1999).

by Lubin et al. 2000, and the two clusters at $z = 1.26$ discovered by Rosati et al. 1999). Analyses of the environment around distant quasars and radio-galaxies have also indicated the presence of subclustering. In particular, the study of the 104420.8 + 055739 quasar at $z = 1.23$ suggested the presence of a merger among two compact groups (Haines et al. 2001, see Fig. 2.11). Pentericci et al. (2000) found a structure in the Ly α emitters around a radio-galaxy at $z = 2.16$, that they splitted into two groups with velocity dispersions of 530 and 280 km s $^{-1}$. By approaching the epoch of cluster formation, it will be possible to follow the evolution of clustering and set useful constraints on cosmological models.

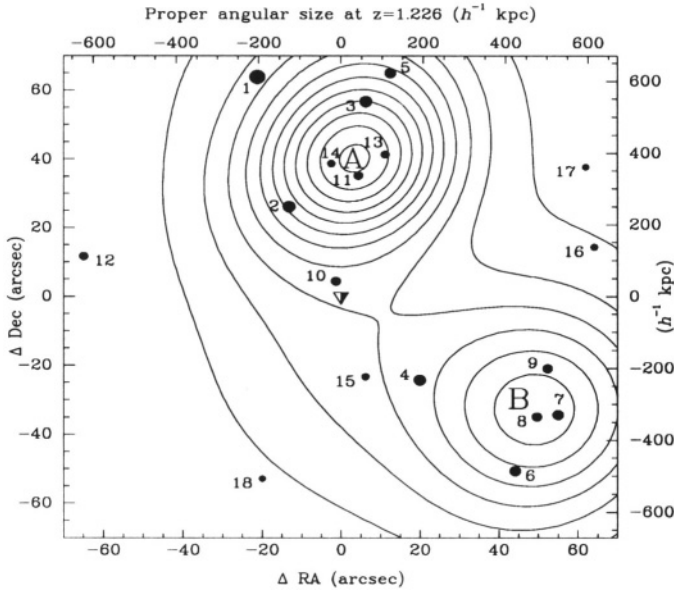


Figure 2.11. Isodensity contours of the red galaxies (dots) in the field of quasar 104420.8 + 055739 (triangle). The galaxies are numbered in order of increasing K magnitude. Courtesy of Haines et al. (2001).

5. CLUSTER MERGERS AND GALAXY PROPERTIES

5.1. BRIGHTEST CLUSTER MEMBERS

Cluster mergers are intimately connected with the properties of cluster galaxies. We start by considering the brightest cluster members (BCMs in the following). Their abnormal luminosities have long been thought to result from repeated galaxy merging and cannibalism (e.g., Hausman & Ostriker 1978; Bhavsar & Barrow 1985; but see Merritt 1984). The fact that larger BCMs are found in higher density environments, suggests the growth of these galaxies is governed by their local environment (within 400 kpc; see Fisher et al. 1995).

Both Hill et al. (1988) and Sharples et al. (1988; see also Malumuth 1992) argued that BCMs form in groups via merging of smaller galaxies, before the cluster virialization effectively renders merging impossible (due to the high velocity dispersion of cluster galaxies). While most BCMs are located very close to the centre of their parent cluster (e.g., Adami et al. 1998; Adami & Ulmer 2000), several observations have identified BCMs displaced from the cluster centre, sitting at the

bottom of local potential wells. Examples include the three BCMs in Coma (Biviano et al. 1996; Colless & Dunn 1996), the cD in A 2634 (Pinkney et al. 1993), the cD in A 754 (Zabludoff & Zaritsky 1995), the cD in A 2670 (Bird 1994a), the three BCMs in A 521 (Maurogordato et al. 2000), and the extensive analysis of several BCMs by Kriessler & Beers (1997). The merger of the BCM host group with the cluster naturally produces a velocity offset of the BCM with respect to the cluster, until dynamical friction puts the BCM at rest at the bottom of the cluster potential (see, e.g., Pinkney et al. 1993). In general, first observational results have overestimated the number of BCMs with significant different velocities from the cluster mean, but a significant number of BCMs with velocity offsets persist (Beers et al. 1991; Gebhardt & Beers 1991; Bird 1994b). These offsets could be partly produced by an oscillatory motion of the BCM around the bottom of the cluster potential (Lazzati & Chincarini 1998) and partly by gravitational redshift (Cappi 1995). However, the global observational evidence is suggestive of the formation of at least some BCMs in groups which later infall onto clusters. Consistently, Beers et al. (1991) found that only in clusters with independent evidence for substructure, do the BCMs have a significant velocity offset.

Whether the BCM retains (or not) its original galaxy group while approaching the cluster centre is debatable. Evidence for bound populations around some BCMs has been provided by observations of local overdensities of galaxies around the BCM with a velocity dispersion lower than that of the host cluster. Subclusters around BCMs were detected in e.g. the core of the Coma cluster (see Biviano et al. 1996 and references therein), in A 2634 (Bothun & Schombert 1990), in A 496 (Quintana & Ramírez 1990), but most BCMs are *not* accompanied by a bound population of satellite galaxies (e.g., Bower et al. 1988; Gebhardt & Beers 1991; Merrifield & Kent 1991).

There is strong observational evidence for the alignment of the BCM major axis with the major axis of its cluster and the surrounding LSS (e.g., Binggeli 1982; Lambas et al. 1990; Johnstone et al. 1991; Rhee et al. 1992; Dantas et al. 1997; Durret et al. 1998). This fact is difficult to explain if the formation of the BCM is totally uncorrelated to the cluster formation. According to the simulations of Rhee & Roos (1990), West (1994b) and Dubinski (1998), the alignment effect is explained by the formation of BCMs through the merging of several massive galaxies accreted along a filament early in the cluster history. This scenario can also account for the correlation of the BCM and cluster properties (Edge 1991).

An alternative scenario for the formation of BCMs is the coalescence of the central brightest galaxies of merging subclusters (Johnstone et al. 1991). Since groups infall onto clusters along filaments defined by the surrounding LSS, this scenario can also naturally account for the observed axes alignments. Within this scenario it is easy to explain the distorted morphology of the cD galaxy in A 697 (Metzger & Ma 2000), as well as the multiple nuclei of some BCMs, in terms of ongoing mergers of the brightest galaxies of individual subgroups (Tremaine 1990). The high relative speed of the galaxies making up a dumbbell galaxy may be the result of the orbital motions of their subclusters within the cluster (Beers et al. 1992). It is remarkable that dumbbell dominant galaxies are often found in clusters with a significant degree of subclustering (e.g.: A 3530 and 3532 in the Shapley concentration, see Bardelli et al. 2001; A 521, see Maurogordato et al. 2000; A 3266, see Quintana et al. 1996). As argued by Merritt (1984), accretion of galaxies onto the central BCM of a cluster is not easy, because of the high velocity dispersion of cluster galaxies, but when two clusters merge, the two cluster BCMs rapidly sink to the bottom of the common potential well, because of dynamical friction (Valentijn & Casertano 1988). It takes several Gyr for the two BCMs to merge (Rix & White 1989; Cavaliere & Colafrancesco 1990) and therefore many dumbbell galaxies can be observed. Note, however, that the observed number of multiple-nuclei BCMs is boosted up by projection effects (see, e.g., Hoessel & Schneider 1985; Blakeslee & Tonry 1992; Gregorini et al. 1992).

If groups are the site of BCM formation, significant dynamical evolution has occurred in them prior to their infall onto the cluster core. Significant luminosity segregation could then be expected, with the most massive galaxies forming a dense core, surrounded by fainter galaxies. When the groups enter the cluster, they are tidally truncated, and the less bound population of faint galaxies is dispersed throughout the cluster, while the detached core maintains its identity for several crossing times (see also González-Casado et al. 1994; Tormen et al. 1998; Balogh et al. 2000). This scenario would account for the observations of Biviano et al. (1996) who showed that substructures in the Coma cluster core are better traced by the bright galaxy populations, while faint galaxies have a much smoother distribution. The same is true in Virgo, where dE's and dS0's describe a smoother distribution than bright galaxies, which instead are sub-clustered around the brightest galaxies (see Fig.3 of Schindler et al. 1999).

5.2. GALAXY STAR-FORMATION

Recent results from numerical simulations have shown that cluster mergers can influence the evolution of the cluster galaxy population.

Bekki's (1999) simulations showed that mergers induce a time-dependent gravitational field that stimulates non-axisymmetric perturbations in disk galaxies, leading to starbursts (SBs in the following) in the central parts of these galaxies. Gnedin (1999) showed that the infall of groups onto a cluster induces a temporal variation of the cluster gravitational potential, as well as shocks, that enhance the galaxy-galaxy interactions and produce SB in gas-rich infalling galaxies. After collision, the SB (or post-starburst, PSB in the following) galaxies would remain well outside the cluster, and near the developed substructure for a few Gyr. Moore et al. (1999) found that low-surface brightness galaxies evolve dramatically as a result of rapid encounters with substructures and strong tidal shocks. Similar results are found in the simulations of Dubinski (1999).

In their numerical SPH simulations, Fujita et al. (1999) found that cluster mergers suppress, rather than trigger, star formation in galaxies because of increasing ram pressure during cluster-cluster collisions. However, before stripping, the formation activity *is increased* even if for a short period (≤ 0.4 Gyr). A more detailed description of the full process of ram pressure stripping during cluster-cluster mergers is given by Roettiger et al.'s (1996) simulations. They showed that a bow shock forms on the leading edge of an infalling subcluster which reduces effectively the ram pressure and protects the gas-rich subcluster galaxies. This protection fails at core crossing. Galaxies passing through the shock initiate a burst of star formation followed by rapid stripping. Similarly, Tomita et al. (1996) argued that in a merging cluster there are regions overdense in IC gas. Some galaxies may experience a rapid increase of external pressure, leading to compression of molecular clouds and SB. An excess of star-forming galaxies is therefore expected in the region between two colliding subclusters.

The first observational evidence for a correlation between cluster mergers and star formation activity in cluster galaxies has come from the observations of the Coma cluster. As shown by Biviano et al. (1996), Coma is currently undergoing accretion of several groups (centred on the bright galaxies NGC 4874, 4889, 4839, 4911), and can therefore be suspected to host significant merger-induced activity. Strong Balmer absorption, consistent with a PSB phase of star formation, was first detected in disk galaxies in Coma by Bothun & Dressler (1986). In the Coma centre most bright galaxies have uniform old ages (Bower et al. 1990, 1992; Rose et al. 1994) while the age-range among brighter galax-

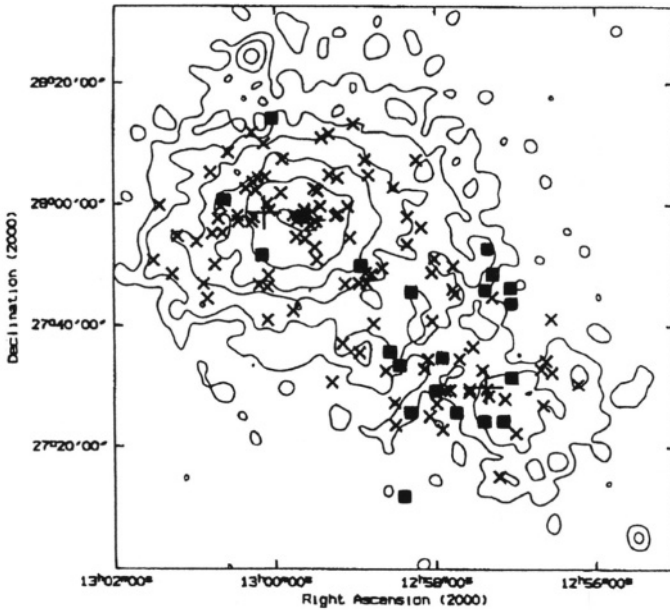


Figure 2.12. Positions of spectroscopically observed galaxies in Coma overlaid on the ROSAT X-ray isocontours. Abnormal-spectrum galaxies are denoted by filled squares. Courtesy of Caldwell et al. (1993).

ies in the SW Coma region close to the subcluster around NGC 4839 was found to be large by Caldwell & Rose (1998). Caldwell et al. (1993) found that 30% of the early-type galaxies in SW Coma concentration have enhanced Balmer absorption lines or even emission lines. Similar abnormal spectrum early-type galaxies are found scattered all around Coma (Caldwell & Rose 1997) but the excess of this kind of galaxies in the SW region is remarkable (see Fig. 2.12). The spectral features are indicative of a SB which ceased 1 Gyr ago (Caldwell et al. 1996). The disk morphology of PSB galaxies in Coma indicates that, whatever the mechanism inducing the SB, it mainly affects the internal gas rather than the structure of these galaxies (Caldwell et al. 1999). Learning from the results of the numerical simulations, the most straightforward interpretation of this excess is that of an induced SB activity – followed by a PSB phase – in galaxies located along the merger axis of the NGC 4839 group with Coma.

Caldwell & Rose (1997) found abnormal-spectrum early-type galaxies in many other clusters, all with substructures. Although not al-

ways located close to the substructures, these galaxies are often found in the tails of the cluster velocity distribution. In Coma the abnormal-spectrum galaxies are mostly in a PSB phase, but there are clusters (e.g., DC0326 – 53/0329 – 52) where most abnormal-spectrum early-type galaxies are star-forming, possibly indicating that the merger is in an earlier phase. Similarly, Drinkwater et al. (2001) speculated that the high fraction of SB galaxies in the SW group of Fornax indicates that this group has not yet crossed the cluster core.

According to Moss & Whittle (2000) SB galaxies are found mostly in the richest clusters with substructure. They identified the mechanism responsible for the SB phase in subcluster merging, and suggest this as a plausible explanation for the lack of the morphology–density relation in irregular clusters at intermediate redshift (Dressler et al. 1997). The increased star formation activity of galaxies in substructured, vs. relaxed, clusters was also found in clusters from the ENACS collaboration (Biviano et al. 1997), and in a sample of distant clusters analysed by Wang & Ulmer (1997). Clusters from the CNOC collaboration (e.g., Yee et al. 1996) are found to have a lower fraction of PSB and SB galaxies than clusters from the MORPHS collaboration (Dressler et al. 1997). A possible explanation of this difference is that MORPHS clusters are generally more substructured than CNOC clusters (which are all X-ray selected), and the presence of substructures enhances the frequency of SB (Ellingson et al. 2001).

It is not certain that the interaction with the cluster environment is essential for the formation of SB and PSB galaxies. According to Hashimoto et al. (1998), in groups or poor clusters the level of normal star formation and starburst is higher than in rich clusters and the field, in clear disagreement with Moss & Whittle (2000). Zabludoff et al. (1996) and Ellingson et al. (2001) argued that galaxy–galaxy interactions and mergers happen more frequently in groups (because of their lower velocity dispersion). In clusters with substructures the number of recently accreted groups is higher, and this would naturally explain the higher fraction of “cluster” galaxies in a SB or PSB phase. Consistently, the high fraction of ongoing mergers in the distant rich cluster MS 1054.4 – 0321 is mainly located in small infalling groups (van Dokkum et al. 1999).

Nevertheless, this scenario can hardly explain the excess of these galaxies in the region *between* two merging groups. For example, the bluest galaxies in the complex A 3558/3562 are found in the region between the two colliding clusters (Bardelli et al. 1998a), and the emission-line galaxies in A 3266 are mainly located on one side of the cluster, tracing the direction of a subclump crossing the cluster core (Flores et

al. 2000). Similarly, Abraham et al. (1996) found that [OII] emitters in A 2390 have a spatial and velocity distribution which is related to infall pattern of the NW group, which is itself populated mostly by red evolved galaxies. Moreover, if infalling groups are originally composed of star-forming galaxies, these galaxies must suffer a morphological modification in order to account for the observed morphological fractions of galaxy samples in substructures (Beers et al. 1992; Biviano et al., 2001). Possibly, both near-neighbour interaction and the tidal field of the cluster play a significant role in triggering star formation (Moss et al. 1998).

Acknowledgments

We wish to dedicate this paper to the memory of our friend and colleague Giuliano Giuricin.

References

- Abdelsalam, H.M., Saha, P. & Williams, L.L.R. 1998, *AJ*, 116, 1541
Abell, G.O., Neyman, J. & Scott, E.L. 1964, *AJ*, 69, 529
Abraham, R.G. et al. 1996, *ApJ*, 471, 694
Adami, C., Mazure, A., Katgert, P. & Biviano, A. 1998, *A&A*, 336, 63
Adami, C. & Ulmer, M.P. 2000, *A&A*, 361, 13
Allen, S.W. 1998, *MNRAS*, 296, 392
Antonuccio-Delogu V. & Colafrancesco, S. 1994, *ApJ*, 427, 72
Arnaud, M., Maurogordato, S., Slezak, E. & Rho, J. 2000, *A&A*, 355, 461
Ashman, K., Bird, C. M. & Zepf, S. 1994, *AJ*, 108, 2348
Baier, F.W. 1984, *Astron. Nachr.*, 305, 175
Baier, F.W., Lima-Neto, G.B., Wipper, H. & Braun, M. 1996, *Astron. Nachr.*, 317, 77
Baier, F.W. & Ziener, R. 1977, *Astron. Nachr.*, 298, 87
Balogh, M.L., Navarro, J.F. & Morris, S.L. 2000, *ApJ*, 540, 113
Bardelli, S., Pisani, A., Ramella, M., Zucca, E. & Zamorani, G. 1998a, *MNRAS*, 300, 589
Bardelli, S., Zucca, E. & Baldi, A. 2001, *MNRAS*, 320, 387
Bardelli, S., Zucca, E., Zamorani, G., Vettolani, G. & Scaramella, R. 1998b, *MNRAS*, 296, 599
Barmby, P. & Huchra, J.P. 1998, *AJ*, 115, 6
Barrena, R., Biviano, A., Ramella, M., Falco, E. & Seitz, S. 2001, *A&A* submitted
Beers, T.C., Forman, W., Huchra, J.P., Jones, C. & Gebhardt, K. 1991, *AJ*, 102, 1581

- Beers, T.C., Gebhardt, K., Huchra, J.P., Forman, W., Jones, C. & Bothun, G.D. 1992, ApJ, 400, 410
- Bekki, K. 1999, ApJL, 510, L15
- Bhavsar, S.P. & Barrow, J.D. 1985, MNRAS, 213, 857
- Binggeli, B. 1982, A&A, 107, 338
- Bird, C.M. 1994a, ApJ, 422, 480
- Bird, C.M. 1994b, AJ, 107, 1637
- Bird, C.M. 1995, ApJL, 445, L81
- Bird, C.M. & Beers, T.C. 1993, AJ, 105, 1596
- Bird, C.M., Davis, D.S. & Beers, T.C. 1995, AJ, 109, 920
- Biviano, A. 1998 in *A New Vision of an Old Cluster: Untangling Coma Berenices*, eds. A. Mazure, F. Casoli, F. Durret & D. Gerbal, World Scientific Publishing, 1
- Biviano, A., Durret, F., Gerbal, D., Le Fevre, O., Lobo, C., Mazure, A. & Slezak, E. 1996, A&A, 311, 95.
- Biviano, A., Katgert, P., Mazure, A., Moles, M. den Hartog, R., Perea, J. & Focardi, P.. 1997, A&A, 321, 84.
- Biviano, A., Katgert, P., Thomas, T. & Adami, C. 2001, A&A submitted
- Blakeslee, J.P. & Tonry, J.L. 1992, AJ, 103, 1457
- Bothun, G.D. & Dressler, A. 1986, ApJ, 301, 57
- Bothun, G.D. & Schombert, J.M. 1990, ApJ, 360, 436
- Bower, R.G., Ellis, R.S. & Efstathiou, G. 1988, MNRAS, 234, 725
- Bower, R.G., Ellis, R.S., Rose, J.A. & Sharples, R.M. 1990, AJ, 99, 530
- Bower, R.G., Lucey, J.R. & Ellis, R.S. 1992, MNRAS, 254, 601
- Brainerd, T.G., Goldberg, D.M. & Villumsen, J.V. 1998, ApJ, 502, 505
- Brainerd, T.G., Oaxaca Wright, C., Goldberg, D.M. & Villumsen, J.V. 1999, ApJ, 524, 9
- Burns, J.O., Roettiger, K., Ledlow, M. & Klypin, A. 1994, ApJL, 427, L87
- Caldwell, N. & Rose, J.A. 1997, AJ, 113, 492
- Caldwell, N. & Rose, J.A. 1998, AJ, 115, 1423
- Caldwell, N., Rose, J.A. & Dendy, K. 1999, AJ, 117, 140
- Caldwell, N., Rose, J.A., Franx, M. & Leonardi, A.J. 1996, AJ, 111, 78
- Caldwell, N., Rose, J.A., Sharples, R.M., Ellis, R.S. & Bower, R.G. 1993, AJ, 106, 473
- Cappi, A. 1995, A&A, 301, 6
- Cavaliere, A. & Colafrancesco, S. 1990, in *Clusters of Galaxies*, STScI Symp. 4, eds. W.R. Oegerle, M.J. Fitchett & L. Danly, Cambridge University Press: Cambridge, 43
- Cavaliere, A., Santangelo, P., Tarquini, G. & Vittorio, N. 1986, ApJ, 305, 651
- Cen, R. 1997, ApJ, 485, 39

- Cen, R. & Ostriker, J.P. 1994, ApJ, 429, 4
- Churazov, E., Gilfanov, M., Forman, W. & Jones, C. 1999, ApJ, 520, 105
- Clowe, D., Luppino, G.A., Kaiser, N. & Gioia, I.M. 2000, ApJ, 539, 540
- Colberg, J.M. et al. 1998, in *Wide Field Surveys in Cosmology*, eds. Publ. Editions Frontieres, 247
- Colberg, J.M., White, S.D.M., Jenkins, A. & Pearce, F.R. 1999, MNRAS, 308, 593
- Colless, M. & Dunn, A. 1996, ApJ, 458, 435
- Conselice, C.J. & Gallagher, J.S. III 1998, MNRAS, 297, L34
- Crone, M.M., Evrard, A.E. & Richstone, D.O. 1996, ApJ, 467, 489
- Dantas, C.C., de Carvalho, R.R., Capelato, H. V. & Mazure, A. 1997, ApJ, 485, 447
- de Vaucouleurs, G. 1961, ApJS, 6, 213
- Donnelly, R.H., Markevitch, M., Forman, W., Jones, C., Churazov, E. & Gilfanov, M. 1999, ApJ, 513, 690
- Dressler, A. et al. 1997, ApJ, 490, 577
- Dressler, A. & Shectman, S.A. 1988, AJ, 95, 985
- Drinkwater, M.J., Gregg, M.D. & Colless, M. 2001, ApJL, 548, L139
- Dubinski, J. 1998, ApJ, 502, 141
- Dubinski, J. 1999, in *Galaxy Dynamics*, eds. D.R. Merritt, M. Valluri & J.A., Sellwood, ASP Conference Series, 182, 491
- Dupke, R.A. & Bregman, J.N. 2001, ApJ, 547, 705
- Durret, F., Forman, W., Gerbal, D., Jones, C. & Vikhlinin, A. 1998, A&A, 335, 41
- Dutta, S.N. 1995, MNRAS, 276, 1109
- Edge, A.C. 1991, MNRAS, 250, 103
- Edge, A.C. & Stewart, G.C. 1991, MNRAS, 252, 414
- Ellingson, E., Lin, H., Yee, H.K.C. & Carlberg, R.G. 2001, ApJ, 547, 609
- Erben, T., van Waerbeke, L., Mellier, Y., Schneider, P., Cuillandre, J.-C., Castander, F.J. & Dantel-Fort, M. 2000, A&A, 355, 23
- Escalera, E., Biviano, A., Girardi, M., Giuricin, G., Mardirossian, F., Mazure, A. & Mezzetti, M. 1994, ApJ, 423, 539
- Escalera, E. & Mazure, A. 1992, ApJ, 388, 23
- Escalera, E., Slezak, E. & Mazure, A. 1992, A&A, 264, 379
- Fadda, D., Girardi, M., Giuricin, G., Mardirossian, F. & Mezzetti, M. 1996, ApJ, 473, 670
- Fadda, D., Slezak, E. & Bijaoui, A. 1998, A&AS, 127, 335
- Federspiel, M., Tammann, G.A. & Sandage, A. 1998, ApJ, 495, 115
- Feretti, L. 2001, in *The Universe at Low Frequencies*, Pune 1999, ASP Conference Series, in press, astro-ph/0006379

- Ferguson, H.C. 1992, MNRAS, 255, 389
- Fisher, D., Illingworth, G. & Franx, M. 1995, ApJ, 438, 539
- Fitchett, M.J. 1988a, in *The Minnesota Lectures on Clusters of Galaxies and Large-Scale Structures*, ed. J.M. Dickey ASP Conference Series, 5, 143
- Fitchett, M.J. 1988b, MNRAS, 230, 161
- Fitchett, M.J. & Merritt, D. 1988, ApJ, 335, 18
- Fitchett, M.J. & Webster, R. 1987, ApJ, 317, 653
- Flores, R.A., Quintana, H. & Way, M.J. 2000, ApJ, 532, 206
- Fontanelli, P. 1984, A&A, 138, 85
- Fort, B. & Mellier, Y. 1994, ARA&A, 5, 239
- Fujita, Y., Takizawa, M., Nagashima, M. & Enoki, M. 1999, PASJ, 51, L1
- Gebhardt, K. & Beers, T.C. 1991, ApJ, 383, 72
- Geller, M.J. & Beers, T.C. 1982, PASP, 94, 421
- Geller, M.J. & Huchra, J.P. 1990, Scientific American, 262, 19
- Gioia, I.M., Henry, J.P., Mullis, C.R. & Ebeling, H. 1999, AJ, 117, 2608
- Girardi, M., Escalera, E., Fadda, D., Giuricin, G., Mardirossian, F. & Mezzetti, M. 1997a, ApJ, 482, 41
- Girardi, M., Fadda, D., Escalera, E., Giuricin, G., Mardirossian, F. & Mezzetti, M. 1997b, ApJ, 490, 56
- Girardi, M., Fadda, D., Giuricin, G., Mardirossian, F., Mezzetti, M. & Biviano, A. 1996, ApJ, 457, 61
- Girardi, M., Giuricin, G., Mardirossian, F., Mezzetti, M. & Boschin, W. 1998, ApJ, 505, 74
- Gnedin, O. 1999, PhD Thesis, Princeton Univ.
- Gómez, P.L., Hughes, J.P. & Birkinshaw, M. 2000, ApJ, 540, 726
- González-Casado, G., Mamon, G. & Salvador-Solé, E. 1994, ApJL, 433, L61
- González-Casado, G., Solanes, J.M. & Salvador-Solé, E. 1993, ApJ, 410, 15
- Gregorini, L., Vettolani, G., de Ruiter, H.R. & Parma, P. 1992, A&AS, 95, 1
- Gregory, S.A. & Thompson, L.A. 1978, ApJ, 222, 784
- Gregory, S.A. & Thompson, L.A. 1984, ApJ, 286, 422
- Gunn, J.E. & Gott, J.R. III 1972, ApJ, 176, 1
- Gurzadyan, V.G., Harutyunyan, V.V. & Kocharyan, A.A. 1994, A&A, 281, 964
- Gurzadyan, V.G. & Mazure, A. 1998, MNRAS, 295, 177
- Gurzadyan, V.G. & Mazure, A. 2001, New Astron., 6, 43
- Haines, C.P., Clowes, R.G., Campusano, L.E. & Adamson, A.J. 2001, MNRAS, 323, 688

- Hanisch, R.J. 1982, *A&A*, 111, 97
- Hashimoto, Y., Oemler, A., Lin, H. & Tucker, D.L. 1998, *ApJ*, 499, 589
- Hausman, M.A. & Ostriker, J.P. 1978, *ApJ*, 224, 320
- Haynes, M.P. & Giovanelli, R. 1986, *ApJL*, 306, L55
- Hill, J.M., Hintzen, P. & Oegerle W.R. 1988, *ApJL*, 332, L23
- Hoekstra, H., Franx, M. & Kuijken, K. 2000, *ApJ*, 532, 88
- Hoessel, J.G. & Schneider, D.P. 1985, *AJ*, 90, 1648
- Jing, Y.P. & Borner, G. 1996, *MNRAS*, 278, 321
- Jing, Y.P., Mo, H.J., Borner, G. & Fang, L.Z. 1995, *MNRAS*, 276, 417
- Johnstone, R.M., Naylor, T. & Fabian, A.C. 1991, *MNRAS*, 248, 18
- Jones, C., Mandel, E., Schwarz, J., Forman, W., Murray, S.S. & Harnden, F.R. 1979, *ApJL*, 234, L21
- Kambas, A., Davies, J.I., Smith, R.M., Bianchi, S. & Haynes, J.A. 2000, *AJ*, 120, 1316
- Katz, N. & White, S.D.M. 1993, *ApJ*, 412, 455
- Kent, S.M. & Gunn, J.E. 1982, *AJ*, 87, 945
- King, L.J. & Schneider, P. 2001, *A&A*, 369, 1
- Knebe, A. & Müller, V. 2000, *A&A*, 354, 761
- Kneib, J.-P., Ellis, R.S., Smail, I., Couch, W.J. & Sharples, R.M. 1996, *ApJ*, 471, 643
- Kolokotronis, V., Basilakos, S., Plionis, M. & Georgantopoulos, I. 2001, *MNRAS*, 320, 49
- Kriessler, J.R. & Beers, T.C. 1997, *AJ*, 113, 80
- Lacey, C. & Cole, S. 1994, *MNRAS*
- Lambas, D. G., Nicotra, M., Muriel, H. & Ruiz, L. 1990, *AJ*, 100, 1006
- Lazzati, D. & Chincarini, G. 1998, *A&A*, 339, L52
- Lee, K.L. 1979, *J. Am. Stat. Assoc.*, Vol. 74, No. 367, 708
- Lewis, A.D., Ellingson, E., Morris, S.L. & Carlberg, R.G. 1999, *ApJ*, 517, 587
- Lima-Neto, G. & Baier, F.W. 1997, *A&A*, 320, 717
- Lubin, L.M., Brunner, R., Metzger, M.R., Postman, M. & Oke, J.B. 2000, *ApJL*, 531, L5
- Lubin, L.M., Postman, M. & Oke, J.B. 1998, *AJ*, 116, 643
- Lucey, J.R., Currie, M.J. & Dickens, R.J. 1986, *MNRAS*, 221, 453
- Malumuth, E.M. 1992, *ApJ*, 386, 420
- Maurogordato, S., Proust, D., Beers, T.C., Arnaud, M., Pelló, R., Cappi, A., Slezak, E. & Kriessler, J. R. 2000, *A&A*, 355, 848
- Mellier, Y. 1999, *ARA&A*, 37, 127
- Merrifield, M.R. & Kent, S.M. 1991, *AJ*, 101, 783
- Merritt, D. 1984, *ApJL*, 280, L5
- Merritt, D. 1987, *ApJ*, 313, 121
- Merritt, D. & Tremblay, B. 1994, *AJ*, 108, 514

- Metzger, M. & Ma, C.-P. 2000, *AJ*, 120, 2879
- Miralda-Escudé, J. & Babul, A. 1995, *ApJ*, 449, 18
- Mohr, J.J., Geller, M.J., Fabricant, D.G., Wegner, G., Thorstensen, J. & Richstone, D.O. 1996, *ApJ*, 470, 724
- Moore, B., Lake, G., Quinn, T. & Stadel, J. 1999, *MNRAS*, 304, 465
- Moss, C. & Whittle, M. 2000, *MNRAS*, 317, 667
- Moss, C., Whittle, M. & Pesce, J.E. 1998, *MNRAS*, 300, 205
- Nakamura, F.E., Hattori, M. & Mineshige, S. 1995, *A&A*, 302, 649
- Neill, J.D., Brodie, J.P., Craig, W.W., Hailey, C.J. & Misch, A.A. 2001, *ApJ*, 548, 550
- Neilsen, E.H. & Tsvetanov, Z.I. 2000, *ApJ*, 536, 255
- Neumann, D.M. et al. 2001, *A&A*, 365, L74
- Pentericci, L. et al. 2000, *A&A*, 361, L25
- Perea, J., del Olmo, A., Moles, M. 1986a, *MNRAS*, 219, 511
- Perea, J., del Olmo, A., Moles, M. 1986b, *MNRAS*, 222, 49
- Pierre, M., LeBorgne, J.F., Soucail, G. & Kneib, J.-P. 1996, *A&A*, 311, 413
- Pinkney, J., Hill, J.M., Oegerle, W., Batuski, D. & Hintzen, P. 1993, *ApJ*, 416, 36
- Pinkney, J., Roettiger, K., Burns, J.O. & Bird, C. M. 1996, *ApJS*, 104, 1
- Pisani, A. 1993, *MNRAS*, 265, 706
- Pisani, A. 1996, *MNRAS*, 278, 697
- Plionis, M. 1994, *ApJS*, 95, 401
- Quintana, H. & Ramírez, A. 1990, *AJ*, 100, 1424
- Quintana, H., Ramírez, A. & Way, M.J. 1996, *AJ*, 112, 36
- Ramella, M., Pisani, A. & Geller, M.J. 1997, *AJ*, 113, 483
- Rhee, G. & Roos, N. 1990, *MNRAS*, 243, 629
- Rhee, G., van Haarlem, M.P. & Katgert, P. 1991, *A&A*, 246, 301
- Rhee, G., van Haarlem, M.P. & Katgert, P. 1992, *AJ*, 103, 1721
- Richstone, D., Loeb, A. & Turner, E.L. 1992, *ApJ*, 393, 477
- Rines, K., Geller, M.J., Diaferio, A., Mohr, J.J. & Wegner, G.A. 2000, *AJ*, 120, 2338
- Rix, H.-W.R. & White, S.D.M. 1989, *MNRAS*, 240, 941
- Roettiger, K., Burns, J.O. & Loken, C. 1993, *ApJL*, 407, L53
- Roettiger, K., Burns, J.O. & Loken, C. 1996, *ApJ*, 473, 651
- Roettiger, K. & Flores, R. 2000, *ApJ*, 538, 92
- Roettiger, K., Loken, C. & Burns, J.O. 1997, *ApJS*, 109, 307
- Roettiger, K., Stone, J.M. & Mushotzky, R.F. 1998, *ApJ*, 493, 62
- Rosati, P., Stanford, S.A., Eisenhardt, P.R., Elston, R., Spinrad, H., Stern, D. & Dey, A. 1999, *AJ*, 118, 76

- Rose, J.A., Bower, R.G., Caldwell, N., Ellis, R.S., Sharples, R.M. & Teague, P. 1994, *AJ*, 108, 2054
- Salvador-Solé, E., González-Casado, C. & Sanromá, M. 1993a, *ApJ*, 410, 1
- Salvador-Solé, E., Sanromá, M. & González-Casado, C. 1993b, *ApJ*, 402, 398
- Schindler, S. 2000, in *Frontier Objects in Astrophysics and Particle Physics*, eds. F. Giovannelli & G. Mannocchi, astro-ph/0010006
- Schindler, S., Binggeli, B. & Böhringer, H. 1999, *A&A*, 343, 420
- Schindler, S. & Böhringer, H. 1993, *A&A*, 269, 83
- Scodreggio, M., Solanes, J.M., Giovanelli, R. & Haynes, M.P. 1995, *ApJ*, 444, 41
- Serna, A. & Gerbal, D. 1996, *A&A*, 309, 65
- Shane, C.D. & Wirtanen, C.A. 1954, *AJ*, 59, 285
- Shao, Z.-Y. & Zhao, J.-L. 1999, *Chinese A&A*, 23, 159
- Sharples, R.M., Ellis, R.S. & Gray, P.M. 1988, *MNRAS*, 231, 479
- Shibata, R., Matsushita, K., Yamasaki, N.Y., Ohashi, T., Ishida, M. & Kikuchi, K. 2001, *ApJ*, 549, 228
- Slezak E., Bijaoui, A. & Mars, G. 1990, *A&A*, 227, 301
- Smail, I., Ellis, R.S., Dressler, A., Couch, W.J., Oemler, A., Sharples, R.M. & Butcher, H. 1997, *ApJ*, 479, 70
- Solanes, J. M., Salvador-Solé, E. & González-Casado, G. 1999, *A&A*, 343, 733
- Stein, P. 1997, *A&A*, 317, 670
- Teague, P.F., Carter, D. & Gray, P.M. 1990, *ApJS*, 72, 715
- Thomas, P.A. et al. 1998, *MNRAS*, 296, 1061
- Thomas, P.A. & Couchman, H.M.P. 1992, *MNRAS*, 257, 11
- Tomita, A., Nakamura, F.E., Takata, T., Nakanishi, K., Takeuchi, T., Ohta, K. & Yamada, T. 1996, *AJ*, 111, 42
- Tormen, G., Diaferio, A. & Syer, D. 1998, *MNRAS*, 299, 728
- Tremaine, S. 1990, in *Dynamics and Interactions of Galaxies*, ed. R. Wielen, Springer-Verlag, Berlin, 394
- Tully, B. 1987, *ApJ*, 321, 280
- Ueda, H., Itoh, M. & Suto, Y. 1993, *ApJ*, 408, 3
- Umetsu, K. & Futamase, T. 2000, *ApJL*, 539, L5
- Valentijn, E.A. & Casertano, S. 1988, *A&A*, 206, 27
- van den Bergh, S. 1960, *MNRAS*, 121, 387
- van den Bergh, S. 1961, *PASP*, 73, 46
- van Dokkum, P.G., Franx, M., Fabricant, D., Illingworth, G.D. & Kelson, D.D. 2000, *ApJ*, 541, 95
- van Dokkum, P.G., Franx, M., Fabricant, D., Kelson, D.D. & Illingworth, G.D. 1999, *ApJL*, 520, L95

- Vestrand, W.T. 1982, *AJ*, 87, 1266
- Wang, Q.D. & Ulmer, M.P. 1997, *MNRAS*, 292, 920
- West, M.J. 1994, in *Clusters of Galaxies*, 29th Recontres de Moriond, eds. F. Durret, A. Mazure & J. Trân Thanh Vân, Publ. Frontier Editions, 23
- West, M.J. 1994, *MNRAS*, 268, 79
- West, M.J. 1998, in *A New Vision of an Old Cluster: Untangling Coma Berenices*, eds. A. Mazure, F. Casoli, F. Durret & D. Gerbal, Publ. World Scientific, 36
- West, M.J. & Blakeslee, J.P. 2000, *ApJL*, 543, L27
- West, M.J. & Bothun, G.D. 1990, *ApJ*, 350, 36
- West, M.J., Jones, C. & Forman, W. 1995 *ApJL*, 451, L5
- West, M.J., Oemler, A. & Dekel, A. 1988, *ApJ*, 327, 1
- West, M.J., Villumsen, J.V. & Dekel, A. 1991, *ApJ*, 369, 287
- White, S.D.M. 1976, *MNRAS*, 177, 717
- White, D.A. & Fabian, A.C. 1995, *MNRAS*, 273, 72
- Wolf, M. 1902, *Pub. Astr. Obs. Königstuhl-Heidelberg*, I, 127
- Wu, X.-P. & Fang, L.-Z. 1997, *ApJ*, 483, 62
- Xu, W., Fang, L.-Z. & Wu, X.-P. 2000, *ApJ*, 532, 728
- Yee, H.K.C., Ellingson, E. & Carlberg, R.G. 1996, *ApJS*, 102, 269
- Zabludoff, A.I. & Franx, M. 1993, *AJ*, 106, 1314
- Zabludoff, A.I., Franx, M. & Geller, M.J. 1993, *ApJ*, 419, 47
- Zabludoff, A.I. & Mulchaey, J.S. 1998, *ApJL*, 498, L5
- Zabludoff, A.I. & Zaritsky, D. 1995, *ApJL*, 447, L21
- Zabludoff, A.I., Zaritsky, D. & Lin, H. 1996, *ApJ*, 466, 104

This page intentionally left blank

Chapter 3

X-RAY OBSERVATIONS OF CLUSTER MERGERS

Cluster Morphologies and Their Implications

David A. Buote

Department of Physics and Astronomy

University of California at Irvine

4129 Frederick Reines Hall

Irvine, CA 92697-4575, USA

buote@uci.edu

Abstract X-ray observations have played a key role in the study of substructure and merging in galaxy clusters. I review the evidence for cluster substructure and mergers obtained from X-ray observations with satellites that operated before *Chandra* and *XMM*. Different techniques to study cluster mergers via X-ray imaging and spectral data are discussed with an emphasis on the quantitative analysis of cluster morphologies. I discuss the implications of measurements of cluster morphologies for cosmology and the origin of radio halos.

Introduction

“Substructure” in a galaxy cluster is defined as multiple peaks in the cluster surface density on scales larger than the constituent galaxies; the “cluster surface density” refers either to the galaxies, the X-ray emission from hot gas, or the dark matter. Today we take it for granted that many galaxy clusters exhibit substructure and thus are in early stages of formation. This, of course, was not always the case. In the 1980s there were several searches for cluster substructure in the optical, but their results were controversial, primarily because of the difficulty in assessing the importance of projection effects and the statistical significance of substructure (see reviews by West 1990, 1995 and Girardi & Biviano, this volume).

X-ray studies of clusters are less susceptible to contamination from foreground and background objects than optical studies. The X-ray luminosity is a strong function of the temperature, or mass, which means that, e.g., foreground groups contribute proportionally less to the X-ray emission than they do to the galaxy surface density. X-ray studies of clusters also have the advantage that the signal is limited only by the effective area of the detector and exposure time of an observation whereas optical studies are limited by the finite number of cluster galaxies.

The reality of substructure in clusters was firmly established with *ROSAT* observations in the early 1990s. The watershed example is that of A2256 which had long been thought to be a prototypical relaxed cluster when examined from the perspective of its galaxy isopleths. However, in a controversial optical study of A2256, Fabricant et al. (1989) proposed the existence of an infalling subcluster from analysis of the galaxy velocities even though they detected no such evidence from the galaxy positions alone.

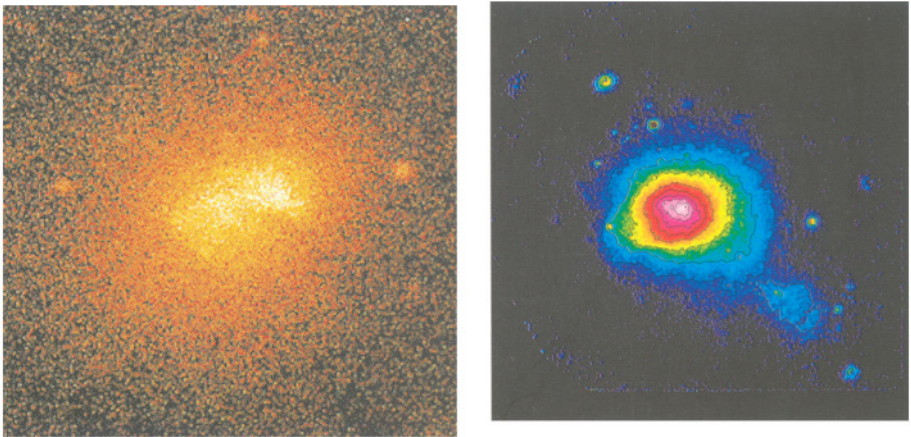


Figure 3.1. (Left) *ROSAT* PSPC image of A2256 (Briel et al. 1991). (Right) *ROSAT* PSPC image of Coma (Briel & Henry 1998).

The existence of a subcluster in A2256 was confirmed by the stunning *ROSAT* PSPC image (Briel et al. 1991) that showed a subcluster¹ offset from the main cluster by a few hundred kpc (Figure 3.1, left). *ROSAT* also clearly demonstrated significant subclustering in the Coma cluster (Briel et al. 1992) which had been presumed to be the quintessential

¹This X-ray substructure in A2256 could have been discovered ten years before *ROSAT* since the *Einstein* image reveals the presence of the subcluster albeit at a lower level of significance (Buote 1992; Davis & Mushotzky 1993).

relaxed cluster (Figure 3.1, right). Hence, *ROSAT* images confirmed and clearly established the existence of substructure in clusters, and thus showed that such clusters are really still forming.

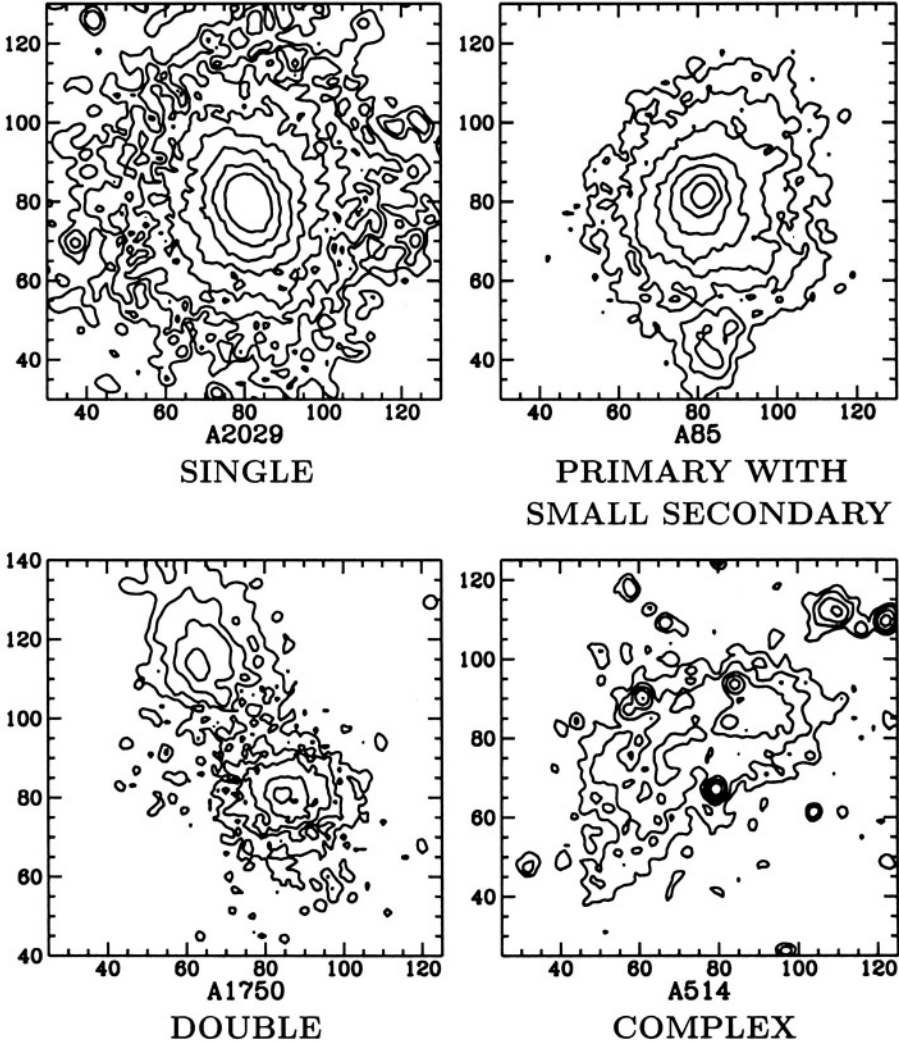


Figure 3.2. Contour plots of *ROSAT* PSPC images (see Buote & Tsai 1995) of four Abell clusters labeled according to the Jones & Forman (1992) morphological classification scheme.

The fundamental question raised by these early *ROSAT* observations is how widespread is merging in clusters? Are clusters generally young or old? Or is there an equal distribution of cluster ages in a given cluster

sample? To address this issue one needs to have measurements of the subclustering properties of a large cluster sample and, of equal importance, a precise definition of the “age” of a cluster. The first systematic X-ray study of cluster merging was by Jones & Forman (1992). From visual inspection of ~ 200 *Einstein* cluster images, Jones & Forman separated the clusters into 6 morphological classes (see Figure 3.2). These classes range from relaxed single-component systems to systems with a large degree of substructure. From the relative populations of these classes they deduced that $\sim 30\%$ of clusters have substructure, which is actually a lower limit because of the limited resolution of the *Einstein* IPC. This study established that merging and substructure are very common in clusters. Consequently, the need arose for a more precise assignment of the age of a cluster; e.g., how much older or younger are clusters in the Jones & Forman classes? Hence, Jones & Forman (1992) ushered in the era of quantitative X-ray cluster morphology.

1. QUANTITATIVE ANALYSIS OF INDIVIDUAL SUBSTRUCTURES

Quantitative studies of cluster X-ray morphologies have traveled down two distinctly different paths. The first path is that of the detailed structural analysis of clusters to determine the number of substructures, their fluxes, spatial properties, etc.. A popular approach is to examine the residuals obtained from subtracting a smooth model representing a relaxed cluster from the X-ray cluster image (e.g., Davis & Mushotzky 1993; White et al. 1994; Davis 1994; Prestwich et al. 1995; Neumann & Böhringer 1997, 1999; Böhringer et al. 2000). Usually this smooth model is obtained by fitting a set of perfect elliptical isophotes or an elliptical β model to the cluster surface brightness; i.e., the X-ray emission of a relaxed cluster is assumed to be elliptical in shape.

In hydrostatic equilibrium the surfaces of constant X-ray emissivity are identical in shape to the surfaces of constant gravitational potential regardless of the temperature profile of the gas (Buote & Canizares 1994, 1998). And since the isopotential surfaces generated by an elliptical matter distribution (which is assumed to be the most general stable, relaxed, non-rotating, self-gravitating configuration) are not perfect ellipses (e.g., Binney & Tremaine 1987), neither are the X-ray isophotes. Consequently, the residuals obtained from subtracting elliptical models from the X-ray surface brightness of clusters need to be carefully considered. This procedure is most appropriately applied as a simple, approximate indicator of substructure.

A more general and powerful method to identify and quantify substructures is to perform a wavelet decomposition of the X-ray image. The wavelet analysis is a powerful multi-scale technique to detect sources embedded in the bright diffuse background cluster emission which has been successfully applied to many clusters (e.g., Slezak et al. 1994; Vikhlinin et al. 1994; Grebenev et al. 1995; Biviano et al. 1996; Pislar et al. 1997; Lima-Neto et al. 1997; Pierre & Starck 1998; Lemonon et al. 1997; Dantas et al. 1997; Vrtilik et al. 1997; Lazzati & Chincarini 1998; Lazzati et al. 1998; Arnaud et al. 2000). Wavelet analysis locates substructures on different scales and allows separate spatial analysis (e.g., flux, extent etc.) of each detected structure. The statistical significance of the substructures can be assessed rigorously via Monte Carlo simulations.

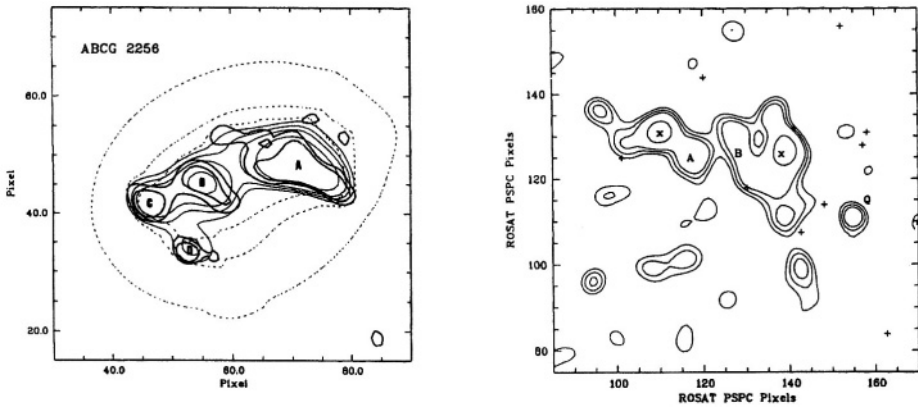


Figure 3.3. Wavelet decomposition of *ROSAT* images of (Left) A2256 by Slezak et al. (1994) and (Right) of Coma by Biviano et al. (1996).

Applications of wavelets to the *ROSAT* images of A2256 and Coma (Figure 3.1) are shown in Figure 3.3. In the case of A2256 Slezak et al. (1994) establish that the core is more than a simple bimodal system since the bottom-left region consists of at least three subclusters. The wavelet analysis of Coma by Biviano et al. (1996) shows that the core consists of two subclusters surrounding each of the large galaxies NGC 4874 and NGC 4889. Apparently both Coma and A2256 are far from relaxed systems.

Wavelets are particularly useful for less-massive systems like A1367 where the emission from several galaxies or groups needs to be separated from the diffuse cluster background. In Figure 3.4 is shown the wavelet analysis by Grebenev et al. (1995) who analyzed both the *ROSAT* PSPC and HRI images and detected 16 extended sources embedded in the

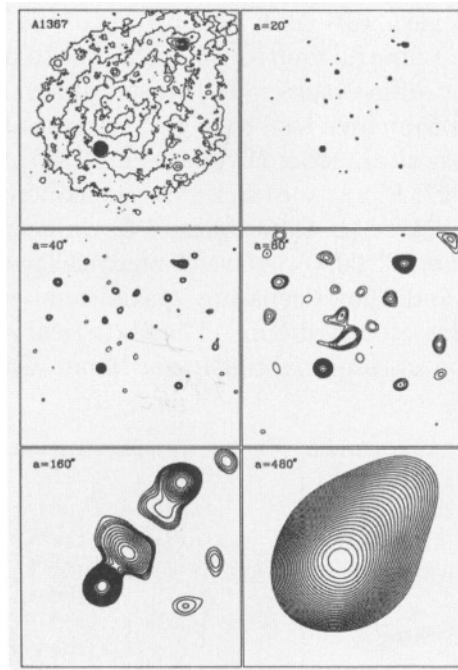


Figure 3.4. ROSAT image of A1367 and a wavelet decomposition on different scales by Grebenev et al. (1995).

diffuse ICM of A1367. Not only does the wavelet analysis allow the fluxes and extents of each of these sources to be quantified, but the larger scale wavelets (see Figure 3.4) show that the cluster is bimodal with subclusters centered about what are likely to be galaxy groups.

The power of the wavelet technique is also demonstrated by the analysis of the ROSAT HRI image of A521 by Arnaud et al. (2000). From visual inspection of the HRI image of A521 one notices asymmetric isophotes such that the emission peak appears to be offset from the centers of the fainter isophotes (see left panel in Figure 3.5). Application of the wavelet technique to this image reveals two distinct structures (see right panel of Figure 3.5). The main cluster appears to be oriented along a line connecting two adjacent clusters. Nearly perpendicular to this line is the line connecting the subcluster to the main cluster. This other line appears to lie nearly parallel to the line pointing to another adjacent cluster. Consequently, Arnaud et al. conjecture that A521 lies at the intersection of two large-scale filaments.

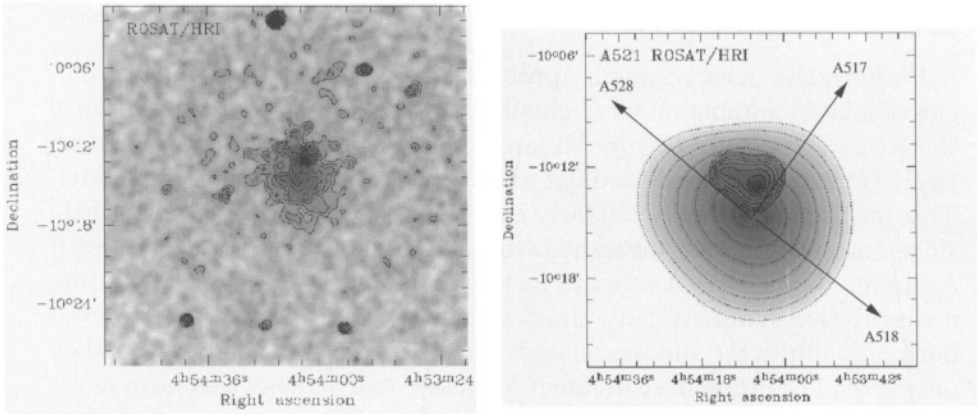


Figure 3.5. (Left) ROSAT HRI image of A521 and (Right) the wavelet transformed image (Arnaud et al. 2000).

2. QUANTITATIVE CLASSIFICATION OF GLOBAL MORPHOLOGY

The other path taken by studies of quantitative X-ray cluster morphology is to build on the work of Jones & Forman (1992) and to devise a quantitative scheme for classifying the morphologies of X-ray images of galaxy clusters. As with any classification system in astronomy the principal motivation for classifying cluster morphologies is to elucidate fundamental physical properties, in particular those associated with cluster formation and evolution.

The presence of substructure in clusters implies they are still forming and evolving dynamically, and thus a logical candidate for a fundamental parameter is the current dynamical state. The dynamical state of a cluster is related to the amount of time required for the cluster to virialize; i.e., a time of order a crossing time. But for a cluster of a given total mass one can imagine many different morphological configurations – and formation histories – that would lead to similar relaxation timescales. Hence, to classify clusters having different formation histories but similar dynamical states we also require one or more fundamental parameters to specify the type of merger (e.g., bimodal, many small subclusters) as indicated qualitatively by the classes of Jones & Forman (1992).

2.1. METHODS

Perhaps the most common approach used to quantify the morphologies of a large number of X-ray cluster images has been with a measure of the X-ray ellipticity (e.g., McMillan et al. 1989; Davis 1994; Mohr et al. 1995; Gómez et al. 1997; Gómez et al. 2000; Kolokotronis et al. 2001). This method is not a particularly good indicator of the dynamical state since both relaxed and disturbed clusters can have significant ellipticity. And even disturbed clusters can have small ellipticity if the substructure is distributed symmetrically about the cluster center. Moreover, even if both the ellipticity and associated position angles are considered they only provide a crude measurement of cluster morphology and have never been shown to provide an interesting distinction between the variety of morphologies exemplified by the Jones & Forman classes.

A better method is the center-shift introduced by Mohr et al. (1993). This popular method has been applied in various forms to X-ray cluster images in several studies (e.g., Mohr et al. 1995; Gómez et al. 1997, 2000; Rizza et al. 1998; Kolokotronis et al. 2001). The basic idea is to divide up a cluster image into a series of circular annuli having different radii but with centers located initially at a guess for the cluster center. The center-shift is then given by the rms difference between the centroid computed for each of these annuli and the weighted average centroid for all annuli.

Since the center-shift is sensitive only to asymmetries in the X-ray images (in particular non-ellipsoidal configurations) it is much more reliable than the ellipticity as an indicator for when a cluster is relaxed. However, it is not transparent how the center shift translates into a physical measure of the dynamical state. And since the center-shift is most sensitive to mergers of equal-mass subclusters, it cannot by itself distinguish the full range of structures exhibited by the Jones & Forman morphological classes.

If the only objective were to distinguish the full range of cluster morphologies then the logical procedure would be to decompose cluster images into a set of orthogonal basis functions of which wavelets (see § 1) are the probably best example. The wavelet coefficients would then define the parameter space of cluster morphologies. Unfortunately, there is no obvious connection (of which I am aware) between wavelet coefficients and a physical measure of the dynamical state.

One method that is both closely related to the cluster dynamical state and provides a quantitative description of the full range of Jones & Forman morphological classes is the “power ratio” method (Buote & Tsai 1995, 1996; Buote 1998). The power ratios are constructed from

the moments of the two-dimensional gravitational potential. Specifically, one evaluates the square of the moments over a circle of radius, R , where the origin is located at the center of mass or at the largest mass peak. The ratio of term, m , to the monopole term is called a “power ratio”,

$$\frac{P_m}{P_0} \equiv \frac{\langle (\Psi_m^{\text{int}})^2 \rangle}{\langle (\Psi_0^{\text{int}})^2 \rangle}, \quad (1)$$

where Ψ_m^{int} is the m th multipole of the two-dimensional gravitational potential due to matter interior to the circle of radius, R , and $\langle \dots \rangle$ represents the azimuthal average around the circle. In detail we have,

$$P_0 = [a_0 \ln(R)]^2, \quad (2)$$

for $m = 0$,

$$P_m = \frac{1}{2m^2 R^{2m}} (a_m^2 + b_m^2) \quad (3)$$

for $m > 0$. The moments a_m and b_m are given by,

$$\begin{aligned} a_m(R) &= \int_{R' \leq R} \Sigma(\vec{x}') (R')^m \cos m\phi' d^2x', \\ b_m(R) &= \int_{R' \leq R} \Sigma(\vec{x}') (R')^m \sin m\phi' d^2x', \end{aligned}$$

where $\vec{x}' = (R', \phi')$.

These ratios are directly related to the 2D gravitational potential if one has a map of the 2D surface mass density such as provided by weak gravitational lensing studies. For X-ray studies Σ is replaced with the X-ray surface brightness, Σ_x , and therefore the power ratios in X-ray studies are really derived from a pseudo potential. These ratios are most sensitive to structures on the same scale as the aperture radius, R .

When the aperture is located at the peak of the X-ray emission the dipole power ratio, P_1/P_0 , provides structural information similar to the center shift discussed above (see also Dutta 1995). For an aperture located at the centroid of the surface brightness the dipole moment vanishes. In this case the quadrupole power ratio, P_2/P_0 , is sensitive to the degree of flattening and is related to the ellipticity. But unlike ellipticity P_2/P_0 is also sensitive to the radial profile of the X-ray emission.

The primary physical motivation behind the power ratios is that they are related to potential fluctuations. And since it is thought that large potential fluctuations drive violent relaxation in clusters, the power ratios are closely related to the dynamical state of a cluster (Buote 1998). The other motivation is that the multipoles are a complete orthogonal

set of basis functions for the (pseudo) potential and thus are well suited to classify the wide range of observed cluster morphologies.

To get a feel for the power ratios let us see how they behave on the *ROSAT* PSPC images of clusters in the different Jones & Forman morphological classes shown in Figure 3.2. The four clusters inhabit the extreme Jones & Forman classes. A2029 is a smooth, single component system apparently in a relaxed state. A85 has a regular dominant component but with a small structure ~ 0.6 Mpc to the S. A1750 is a double cluster consisting of two roughly equal-sized components separated by ~ 1 Mpc. A514 is a highly irregular aggregation of structures.

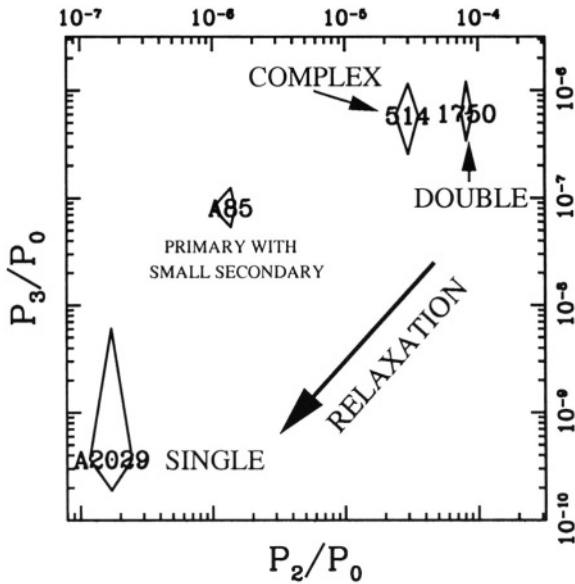


Figure 3.6. Power ratios (from Buote & Tsai 1996) for the clusters in Figure 3.2 computed within a circular aperture of 1 Mpc radius located at the centroid of the X-ray emission.

In Figure 3.6 I show the power ratios, P_2/P_0 and P_3/P_0 , of these clusters computed for a 1 Mpc aperture² where the aperture is located at the centroid of the X-ray emission (i.e., analog of the center of mass). It can be seen that the single-component cluster is well separated from the primary with small secondary. And each of these classes is clearly distinguished from the disturbed complex and double clusters. In effect the power ratios have defined a morphological evolutionary track where the young, unrelaxed clusters are born at the top right of the figure.

²In Buote & Tsai (1995, 1996) $H_0 = 80 \text{ km s}^{-1} \text{ Mpc}^{-1}$ and $q_0 = 0$ were assumed.

As they relax and erase their substructure they pass through a phase similar to A85 until they are old and evolved systems like A2029.

Although we have succeeded in obtaining a successful broad classification according to dynamical states, we have not distinguished clearly between the different classes of highly disturbed clusters (i.e., complex and double). Since there is nothing special about the 1 Mpc aperture it is sensible to explore the effects of using different apertures. The result of computing the power ratios in a 0.5 Mpc aperture is displayed in Figure 3.7

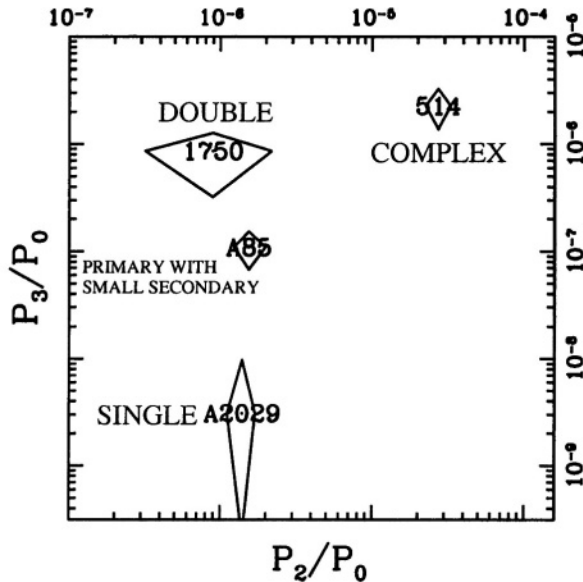


Figure 3.7. As Figure 3.6 but for the 0.5 Mpc aperture.

By focusing initially on P_2/P_0 it can be seen that three of the clusters appear to be relaxed systems (i.e., small P_2/P_0). This is because the 0.5 Mpc aperture only encloses 1 component of the double cluster and only the primary component of A85. The single component cluster A2029 appears relaxed on both the 0.5 and 1 Mpc scales. However, A514 is complex on many scales and it is easily distinguished from the other reference clusters as a disturbed system in the 0.5 Mpc aperture. Of course, one only needs to appeal to P_3/P_0 to verify that both the double and complex clusters are actually in a younger dynamical state than the others. Hence, the power ratios represent a quantitative implementation of the Jones & Forman classification scheme, particularly on the 0.5 Mpc scale.

2.2. MERGER FREQUENCY OF ROSAT CLUSTERS

The result of computing power ratios for the brightest ~ 40 *ROSAT* clusters is displayed in Figure 3.8. It is immediately apparent that there is a marked deficiency of highly disturbed clusters (complex and double). These brightest clusters therefore lack young members and are instead dominated by mostly evolved clusters with only small-scale (< 500 kpc) substructure. Since such highly evolved clusters are usually associated with cooling flows it should be expected that cooling flows dominate the brightest clusters as has been suggested before on different grounds (e.g., Arnaud 1988; Forman & Jones 1990; Edge et al. 1992; Peres et al. 1998).

In Figure 3.9 the quantitative connection between cooling flows and cluster morphology is shown by the anti-correlation of the mass deposition rate (M) and P_2/P_0 . This represents the first quantitative description of the anti-correlation of substructure with the strength of a cooling flow. Note the large scatter for systems that have significant substructure (i.e., large P_2/P_0). Analysis of this correlation and its large scatter should shed light on how cooling flows are disrupted by mergers and are subsequently re-established.

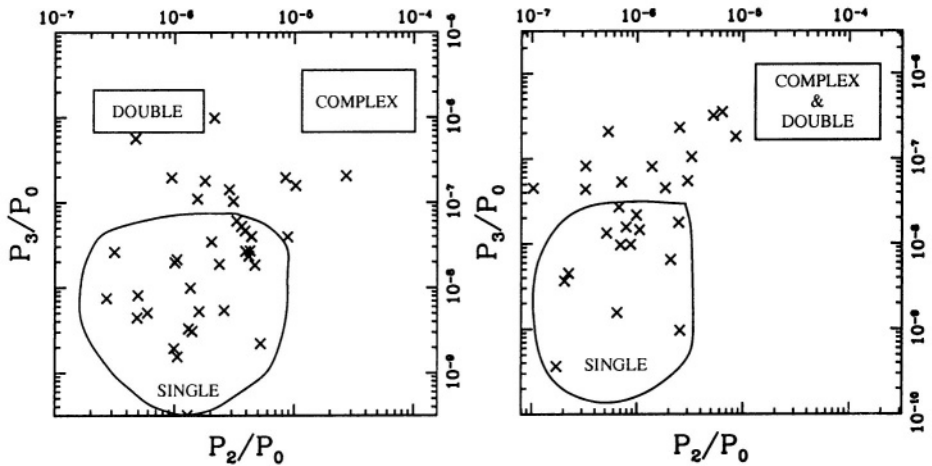


Figure 3.8. Power ratios of the brightest ~ 40 clusters (Buote & Tsai 1996) computed within apertures of 0.5 Mpc (Left) and 1 Mpc (Right).

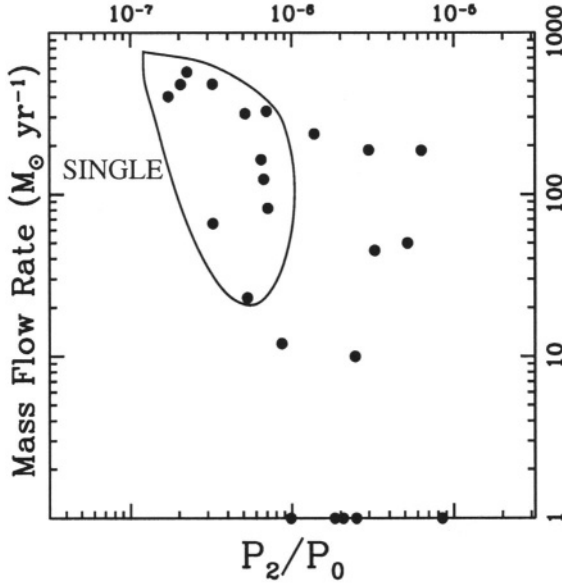


Figure 3.9. As Figure 3.8 for the 1 Mpc aperture except that the cooling flow mass deposition rate has been plotted on the vertical axis.

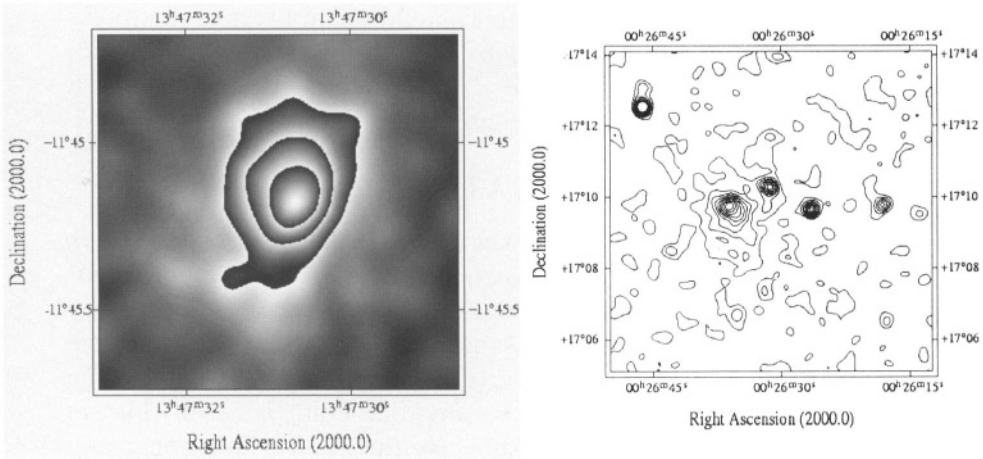


Figure 3.10. ROSAT HRI images of (Left) RX J1347.5-1145 from Schindler et al. (1997) and (Right) Cl 0024+17 from Böhringer et al. (2000).

3. HIGH-REDSHIFT CLUSTERS

Unfortunately, because of the limited resolution and collecting area of *ROSAT* it has been difficult to study the morphologies of distant clusters. Two of the best examples ($z \sim 0.4$) imaged with the *ROSAT*

HRI are displayed in Figure 3.10. The cluster RX J1347.5-1145 appears to be a relaxed, cooling flow (Schindler et al. 1997) while the cluster Cl 0024+17 may have substantial substructure as quantified by a center shift (Böhlinger et al. 2000). These tantalizing glimpses demonstrate the need for a systematic study at high resolution with *Chandra*.

4. MORPHOLOGY AND COSMOLOGY

Fossil imprints of the process of formation are retained in the cluster substructure. In the standard hierarchical paradigm of structure formation the mass spectrum of subclusters is related to the power spectrum of mass density fluctuations which is a key distinguishing property of cosmological models (e.g., Peacock 1999). As clusters evolve dynamically the mass spectrum of subclusters changes. In a standard Friedmann-Robertson-Walker universe with $\Omega_m < 1$ and $\Omega_\Lambda = 0$, the linear growth of density fluctuations becomes strongly suppressed when the curvature term in the Friedmann equation exceeds the matter term. The redshift delineating this transition from an Einstein - de Sitter phase to one of free expansion is then $1 + z_{\text{trans}} = \Omega_m^{-1} - 1$; i.e. when the matter density $\Omega(z_{\text{trans}}) = 0.5$. Hence, in a low-density universe ($\Omega_m \ll 1$) where the growth of structure is sharply suppressed at late times, objects formed a long time in the past and then clusters should be on average in a more relaxed and stable state. In a high density universe ($\Omega_m \approx 1$), instead, structures continue to form indefinitely, giving rise to the existence of a significant number of young and currently accreting galaxy clusters.

4.1. SEMI-ANALYTICAL MODELS

Richstone et al. (1992) presented the first theoretical model relating Ω_m to the observed frequency of substructure in clusters. In their semi-analytical calculations they avoided the issue of the power spectrum by concentrating on clusters having the same total mass. The collapse time of a $10^{15} h^{-1} M_\odot$ spherical density perturbation (taken to be twice the turn around time) was defined to be the dividing point between clusters that do and do not possess substructure. By further assuming that any substructure is erased on a crossing time (taken to be $0.1/H_0$), Richstone et al. computed the quantity δF , the fraction of present-day clusters which formed within the last time interval, $0.1/H_0$, as a function of Ω_m and Ω_Λ . They found $\delta F \sim \Omega_m$ (see Figure 3.11). When compared to the estimates of $\gtrsim 30\%$ for the frequency of substructure in nearby clusters (Jones & Forman 1992) Richstone et al. concluded that $\Omega_m \gtrsim 0.5$.

Follow up theoretical studies by Kauffmann & White (1993), Lacey & Cole (1993), and Nakamura et al. (1995) emphasized that the time

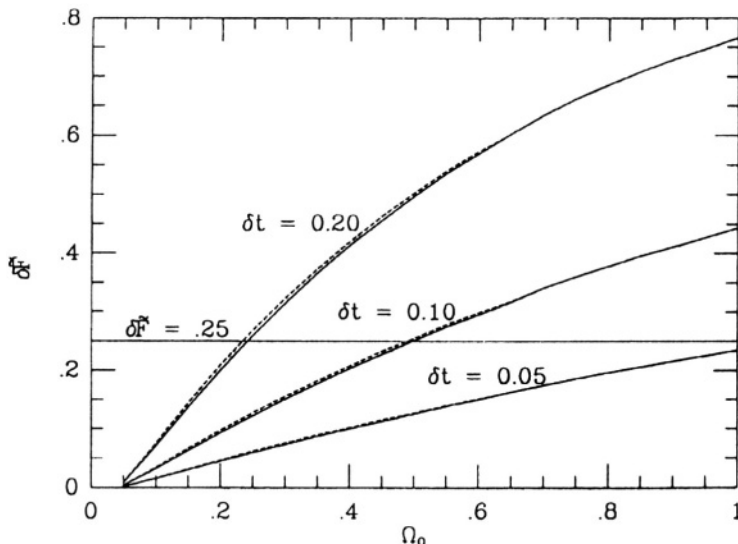


Figure 3.11. Figure 3 from Richstone et al. (1992). Fraction of present-day clusters which formed within the last time interval, δt , as a function of Ω_m . The time intervals are in units of H_0^{-1} . The horizontal line represents a conservative observational estimate of the frequency of substructure.

for substructure to be erased is variable and can be especially long for substructures with compact cores. The relationship between the collapse time of a spherical density perturbation and subclustering, though qualitatively reasonable, is ambiguous. Consequently, it is difficult to compare directly the frequency of observed substructure to predictions of semi-analytic models based on Richstone et al.’s idea.

Thus, a fundamental limitation of these studies is that they only predict the ambiguous “frequency of substructure” rather than a well-defined quantitative measure of cluster morphology such as the power ratios. Since Richstone et al.’s idea is really a statement about the dynamical states of clusters, in Buote (1998) I used a related (but more detailed) semi-analytical approach to study the behavior of cluster power ratios in different cosmologies. Violent relaxation (Lynden-Bell 1967) is the key process driving the elimination of large potential fluctuations. It operates on a timescale of $\sim 1 - 2$ crossing times and proceeds independently of the masses of the constituents. Consequently, I argued that a plausible definition of the dynamical state of a cluster is,

$$\frac{\langle (\Delta \Phi^{\text{int}})^2 \rangle}{\langle (\bar{\Phi}^{\text{int}})^2 \rangle} \approx \left(\frac{\Delta M}{\bar{M}} \right)^2 + \sum_{l>0} \frac{\langle (\Phi_l^{\text{int}})^2 \rangle}{\langle (\bar{\Phi}_0^{\text{int}})^2 \rangle}, \quad (4)$$

where Φ^{int} is the gravitational potential arising from material interior to a radius r , \bar{M} is the average mass and ΔM is the mass accreted over a relaxation time, typically assumed to be a crossing time; $\Delta M/\bar{M}$ is called the “fractional accreted mass”. This equation states that over the duration of a crossing time the fractional increase in the rms spherically averaged potential is approximately equal to the fractional increase in the mass added in quadrature to the ratios of the increases of the rms spherically averaged higher order potential multipoles to the monopole.

The key premise is that the amount of accreted mass over the previous relaxation timescale determines the amount of substructure (or non-ellipsoidal distortions) which is similar to the premise of Richstone et al. that substructure is related to the collapse and crossing times. This premise requires that $\Delta M/\bar{M}$ be strongly correlated with the other low-order terms, which are approximately, $\langle (\Phi_l^{\text{int}})^2 \rangle / \langle (\Phi_0^{\text{int}})^2 \rangle$, defined at the epoch of interest. These terms are just the 3D versions of the power ratios (see equation 1).

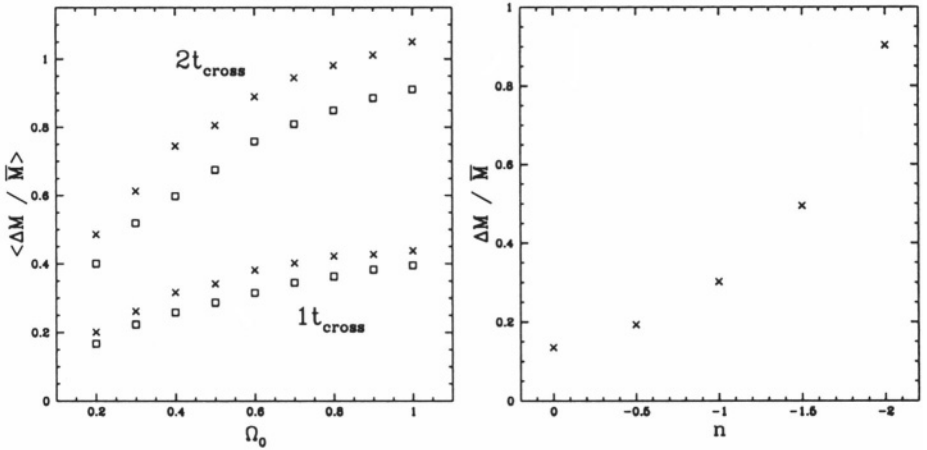


Figure 3.12. From Buote (1998): (Left) The mass-averaged fractional accreted mass evaluated for $r = 1h^{-1}$ Mpc at $z = 0$ for CDM models as a function of $\Omega_0 = \Omega_m$ ($\Omega_\Lambda = 0$). The crosses indicate a mass average over the full range $(0.35 - 3) \times 10^{15} h^{-1} M_{\odot}$, and the boxes indicate a lower limit of $7 \times 10^{14} h^{-1} M_{\odot}$. Relaxation timescales of 1 and 2 crossing times are shown. (Right) $\Delta M/\bar{M}$ for clusters of mass $7 \times 10^{14} h^{-1} M_{\odot}$ evaluated for $r = 1h^{-1}$ Mpc at $z = 0$ for models with $\Omega_m = 1$ and power spectra $P(k) \propto k^n$ as a function of spectral index n .

The dependence of $\Delta M/\bar{M}$ on Ω_m and the power spectrum is shown in Figure 3.12. We see the expected increase in fractional accreted mass with increasing Ω_m where $\Delta M/\bar{M} \propto \sqrt{\Omega_m}$, but the normalization does depend sensitively on the assumed relaxation timescale similarly to the

previous related studies by Richstone et al. and others. Also shown is the dependence on n , the spectral index of models with $P(k) \propto k^n$, which is considerably steeper, $\Delta M/\bar{M} \propto (-n)^{2.5}$. Since the observable low-order power ratios should behave as $P_m/P_0 \sim (\Delta M/\bar{M})^2$ (see section 2.2 of Buote 1998), the power-ratio distribution for a large sample of clusters should be an interesting probe of Ω_m and the power spectrum.

4.2. N-BODY SIMULATIONS

N-body simulations of CDM clusters confirm that the mean value of P_m/P_0 for small m in a cluster sample increases with Ω_m (Buote & Xu 1997; Thomas et al. 1998). But Buote & Xu (1997) also perform simulations with $P(k) \propto k^n$ for different n and find that the mean value of P_m/P_0 is barely affected by n . On the other hand they find that n does affect significantly the variance of P_m/P_0 . (Ω_m does not seem to affect the variance.) These conclusions have to be viewed with some caution because these dark-matter-only simulations analyze the projected square of the mass density in an attempt to mimic X-ray observations. Further work with large high-resolution N-body simulations is required to establish precisely the relationships between $\Delta M/\bar{M}$, P_m/P_0 , Ω_m , and $P(k)$ (and Ω_Λ).

Other N-body simulations with and without gas show that center-of-mass shifts are also sensitive to Ω_m (Jing et al. 1995; Crone et al. 1996). Generally both semi-analytic models and dark-matter-only N-body simulations agree that center shifts and power ratios can distinguish between CDM models with different values of Ω_m . The same holds for gas-dynamical N-body simulations (Evrard et al. 1993; Mohr et al. 1995).

However, when the N-body simulations (with or without gas) are compared to X-ray observations of clusters conflicting results are obtained (Figure 3.13). Mohr et al. (1995) compare center shifts of clusters formed in hydrodynamical simulations to *Einstein* clusters and conclude that $\Omega_m \approx 1$ whereas Buote & Xu (1997) compare power ratios of the projected square of the dark matter density to *ROSAT* clusters and conclude $\Omega_m < 1$. Furthermore, the clusters formed in the hydrodynamical simulations by Valdarnini et al. (1999) give power ratios different from those obtained by Buote & Xu (1997).

All of these simulations have deficiencies. The most important deficiency in the hydrodynamical simulations is the poor force resolution for the gas: softening lengths of ~ 80 kpc for Valdarnini et al. (1999) and over $100h^{-1}$ kpc for Mohr et al. (1995). The simulations of Mohr et al. also contained only six clusters which is too small for statistical

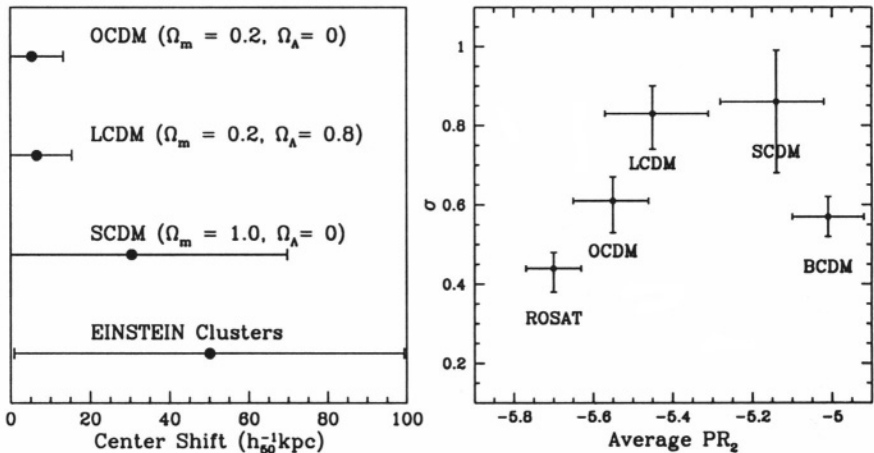


Figure 3.13. (Left) Center shifts obtained by Mohr et al. (1995) from simulated and *Einstein* clusters. (Right) Power ratios ($PR_2 = \log_{10}(P_2/P_0)$) obtained by Buote & Xu (1997) for *ROSAT* and simulated clusters: OCDM ($\Omega_m = 0.35$), LCDM ($\Omega_m = 0.35, \Omega_\Lambda = 0.65$), and SCDM ($\Omega_m = 1.0$).

studies. Finally, the simulations of Buote & Xu (1997) approximated the gas distribution using the dark matter.

Clearly until appropriate simulations are applied to this problem we will not have a reliable constraint on Ω_m or $P(k)$ from cluster morphologies. What is needed are high-resolution ($\lesssim 20$ kpc) three-dimensional gas-dynamical simulations of a large number ($\gtrsim 50$) of clusters. The existing observational samples of *Einstein* data (Mohr et al. 1995) and *ROSAT* data (Buote & Tsai 1996) also need to be expanded and re-analyzed with new high-resolution, high S/N *Chandra* and *XMM* data. These requirements are not excessive for a problem that deserves serious attention.

5. MORPHOLOGY AND RADIO HALOS

It has been noticed for some time that X-ray observations provide circumstantial evidence for a connection between cluster merging and radio halos (see Feretti 2001 and references therein) because, in particular, radio halos are only found in clusters possessing X-ray substructure and weak (or non-existent) cooling flows. However, it has been argued (e.g., Giovannini & Feretti 2000; Liang et al. 2000; Feretti 2001) that merging cannot be solely responsible for the formation of radio halos because at least 50% of clusters show evidence for X-ray substructure (Jones & Forman 1999) whereas only $\sim 10\%$ possess radio halos. (Note

X-ray and optical substructures are well-correlated – Kolokotronis et al. 2001.)

Unfortunately, it is difficult to interpret the importance of merging using the observed frequency of substructure as it does not itself quantify the deviation of an individual cluster from a virialized state. And the shocks that could be responsible for particle acceleration will be proportionally stronger in clusters (of the same mass) with the largest departures from a virialized state. To measure the dynamical states of clusters from X-ray images it is necessary to quantify the cluster morphologies using statistics such as the center-shift and the power ratios.

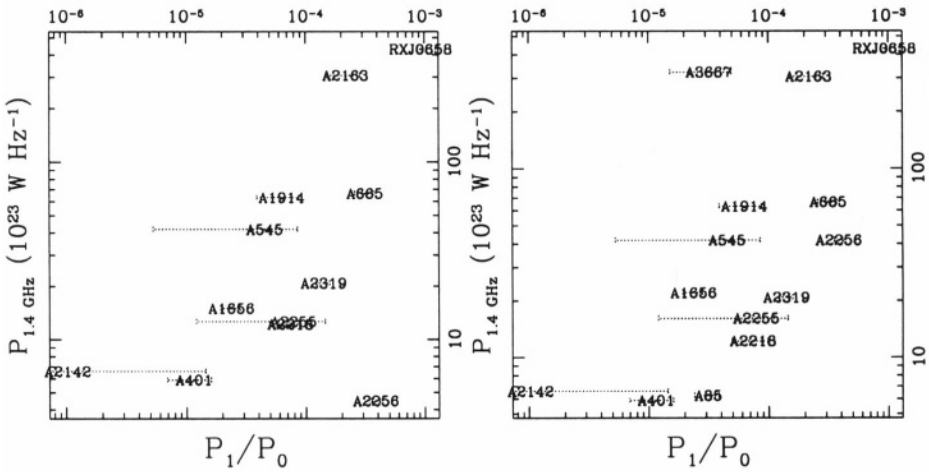


Figure 3.14. From Buote (2001): Radio power ($P_{1.4}$ – 1.4 GHz rest frame) versus dipole power ratio (P_1/P_0) where $P_{1.4}$ includes emission from (Left) only radio halos and (Right) the total diffuse emission from halos and relic sources. The power ratios are computed within a 0.5 Mpc aperture centered on the X-ray emission peak with estimated 1σ errors shown. (Uncertainties on $P_{1.4}$ are believed to be $\lesssim 10\%$ and are not shown.)

In Buote (2001) I used power ratios to provide the first quantitative comparison of the dynamical states of clusters possessing radio halos. A correlation between the 1.4 GHz power ($P_{1.4}$) of the radio halo (or relic) and the magnitude of the dipole power ratio (P_1/P_0) was discovered such that approximately $P_{1.4} \propto P_1/P_0$ (see Figure 3.14). The $P_{1.4} - P_1/P_0$ correlation not only confirms previous circumstantial evidence relating the presence of radio halos to mergers but, more importantly, establishes for the first time a quantitative relationship between the “strength” of radio halos and relics ($P_{1.4}$) and the “strength” of mergers (P_1/P_0); i.e., the strongest radio halos appear only in those clusters currently experiencing the largest departures from a virialized state. Moreover,

in the $P_{1.4} - P_1/P_0$ plane both radio halos and relics may be described consistently which provides new evidence that both halos and relics are formed via mergers. The $P_{1.4} - P_1/P_0$ correlation supports the idea that shocks in the X-ray gas generated by mergers of subclusters accelerate (or re-accelerate) the relativistic particles responsible for the radio emission.

From additional consideration of a small number of highly disturbed clusters without radio halos detected at 1.4 GHz, and recalling that radio halos are more common in clusters with high X-ray luminosity (Giovannini et al. 1999), I argued that radio halos form preferentially in massive ($L_x \gtrsim 0.5 \times 10^{45} \text{ erg s}^{-1}$) clusters experiencing violent mergers ($P_1/P_0 \gtrsim 0.5 \times 10^{-4}$) that have seriously disrupted the cluster core. The association of radio halos with massive, large- P_1/P_0 , core-disrupted clusters is able to account for both the vital role of mergers in accelerating the relativistic particles responsible for the radio emission as well as the rare occurrence of radio halos in cluster samples.

On average P_1/P_0 is expected to increase with increasing redshift owing to the higher incidence of merging (Buote 1998) which would lead to a higher incidence of radio halos. However, on average cluster masses are lower at earlier times implying a lower incidence of radio halos. Each of these factors is dependent on the assumed cosmology, and future theoretical work is therefore required to establish whether the abundance of radio halos (1) increases or decreases with redshift, and (2) provides an interesting test of cosmological models.

6. TEMPERATURE SUBSTRUCTURE

The morphologies of X-ray images of clusters suggest that clusters span a wide range of dynamical states and merger configurations. During such violent mergers the gas should be shock-heated at various locations between an infalling subcluster and the center of the primary cluster. In contrast to the azimuthally symmetric temperature profile expected of a relaxed system, two-dimensional temperature variations both represent a necessary confirmation of the merger picture obtained from images and also provide a complementary view of the cluster dynamical state and merger history.

6.1. X-RAY TEMPERATURE MAPS

In the era before *Chandra* and *XMM* it was exceedingly difficult to obtain accurate two-dimensional X-ray temperature maps of clusters. The *ROSAT* PSPC had sufficient spatial and spectral resolution but its bandpass cut off sharply just beyond 2 keV. Since massive clusters have temperatures above ~ 5 keV the temperatures could not be constrained

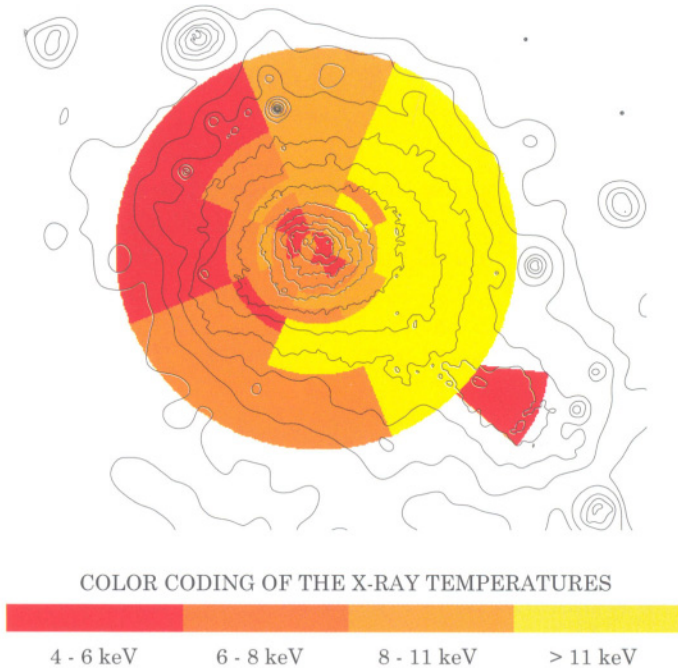


Figure 3.15. *ROSAT* temperature map of the Coma cluster (Briel & Henry 1998).

with any precision for all but a small number of the brightest clusters. For these clusters the S/N was so high that the data from the spectra below 2 keV managed to place interesting constraints on the temperature.

For example, the *ROSAT* temperature map of Coma (Briel & Henry 1998) displayed in Figure 3.15 shows significant temperature variations. The region of hotter gas in between the main cluster and the NGC 4839 subcluster is consistent with shock heating during the passage of the subcluster through the main cluster (e.g., Burns et al. 1994; Ishizaka & Mineshige 1996). However, further simulations are required to establish whether the subcluster is currently falling in or has already passed through the main cluster. As noted by Briel & Henry (1998) if the subcluster already passed through the main body then it is unclear why the subcluster still has retained its halo of hot gas. Other *ROSAT* temperature maps of mergers display similar evidence for shock-heating (e.g., Briel & Henry 1994; Henry & Briel 1995, 1996; Ettori et al. 2000).

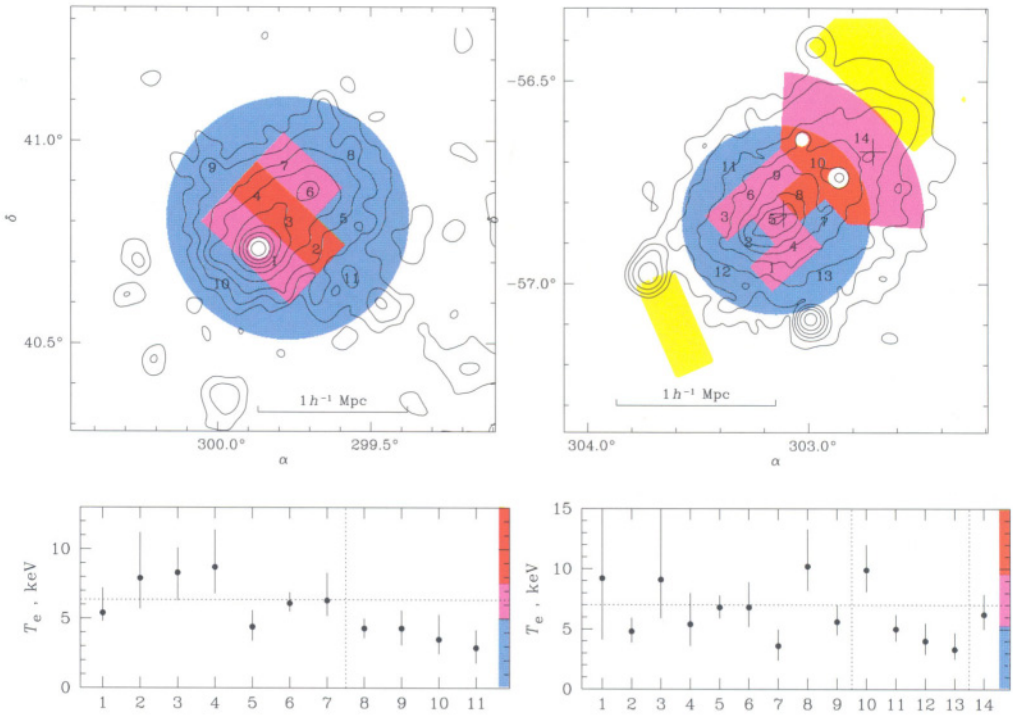


Figure 3.16. ASCA temperature maps of (Left) Cygnus-A and (Right) A3667 from Markevitch et al. (1999).

The qualitative features in the temperature maps derived from *ROSAT* were also found with data from the *ASCA* satellite. The higher energy resolution and larger bandpass (up to 10 keV) of *ASCA* provided a distinct advantage over *ROSAT* studies, but the poor spatial resolution ($\gtrsim 1.5'$ FWHM) and highly energy dependent point spread function (PSF) seriously hampered two-dimensional spatial-spectral analysis. To obtain physical results with *ASCA* data the PSF needs to be incorporated into the analysis.

When incorporating the PSF into modeling of the *ASCA* data of mergers two-dimensional temperature variations similar to those obtained by *ROSAT* are found. For example, in Figure 3.16 the results of the analysis of Cygnus-A and A3667 by Markevitch et al. (1999) are shown. Although some of the detailed results for a particular cluster differ between studies using different deconvolution procedures, the basic idea that non-azimuthal temperature variations exist in mergers seems to be supported by most *ASCA* and *BeppoSAX* studies (e.g., Markevitch et al. 1998, 1999; Churazov et al. 1999; Donnelly et al. 1999; Molendi et

al. 1999; Shibata et al. 1999; De Grandi & Molendi 1999; Henriksen et al. 2000; Iwasawa et al. 2000).

Since there are some differences in the radial temperature profiles obtained from *ASCA* data depending on the PSF deconvolution procedure used (see White 2000; Irwin & Bregman 2000 and references therein) the detailed temperature features obtained with *ASCA* do need to be confirmed with *Chandra* and *XMM* (as do those with *BeppoSAX* because of its low spatial resolution.) Nevertheless, the overall trend of non-azimuthal temperature structures and the shock-heating of the intra-cluster medium are supported by the available *ROSAT*, *ASCA*, and *BeppoSAX* data.

6.2. QUANTITATIVE CLASSIFICATION OF TEMPERATURE MORPHOLOGY

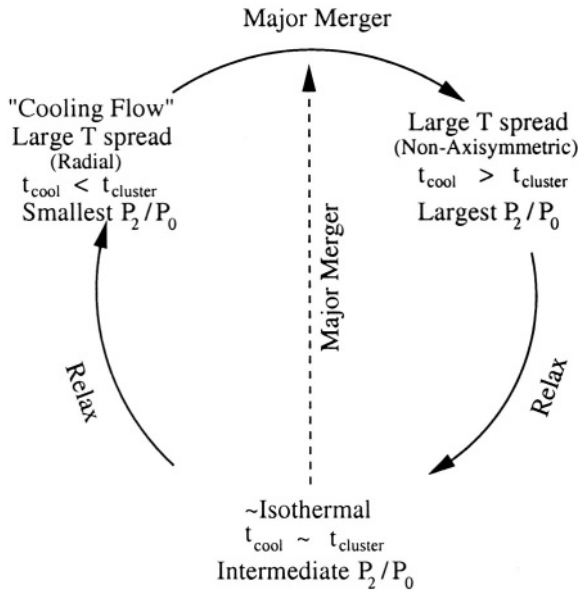


Figure 3.17. A possible description of the evolution of the X-ray temperature structure and image morphology during the formation and evolution of a cluster.

To obtain a more complete picture of the current dynamical states and the merger histories of clusters the global morphological classification of cluster images discussed in § 2 should also incorporate the morphologies of X-ray temperature maps. In Figure 3.17 I show an idealized picture of how the temperature morphology of a cluster might evolve during a merger. At early times there is a large spread of temperatures dis-

tributed spatially in a non-azimuthally symmetric fashion. At this time the cluster is far from a virialized state. It possesses obvious substructure and a disturbed spatial morphology quantified by, e.g., a large value for the P_2/P_0 power ratio. The disturbed morphology implies there is no cooling flow at this early time (see Figure 3.9), and the cooling time (t_{cool}) is longer than the cluster age (t_{cluster}) (e.g., Fabian 1994).

As the system relaxes image substructure and the spatial fluctuations in the temperature are gradually erased until the system is approximately isothermal and on the verge of establishing a cooling flow. At this time $t_{\text{cool}} \sim t_{\text{cluster}}$ and there is only a small amount of substructure (i.e., intermediate P_2/P_0 values – see § 2). If the cluster now experiences a major merger it will begin again at the top of Figure 3.17 with a lot of temperature variations and image substructure. If instead the system relaxes further without being disturbed then a cooling flow will develop ($t_{\text{cool}} < t_{\text{cluster}}$) and the image substructure should be mostly erased (smallest values of P_2/P_0). Although the azimuthal temperature variations will also be erased, a radial temperature gradient will be established where the temperature rises from the center out to an approximately isothermal plateau.

Such radial temperature gradients are characteristic of cooling flows (e.g., White 2000 and references therein). Whether the temperature profile is caused by cooling gas or a two-phase medium (e.g., Ikebe et al. 1997; Xu et al. 1998) is not important for the arguments presented here. All that is required is that relaxed systems (particularly those with cD galaxies) tend to have characteristic radial temperature structure.

Therefore, for the merger scenario displayed by Figure 3.17 the amount of image substructure (P_2/P_0) falls continuously as the cluster relaxes, but the overall spread in temperatures falls and then rises again at late times. One possible way to quantify the temperature morphology is with the multiphase strength (Buote et al. 1999) which essentially measures the width of the differential emission measure, $\xi(T)$,

$$\sigma_\xi = \frac{1}{2\langle T \rangle \xi_{\text{max}}} \int_{T_{\text{min}}}^{T_{\text{max}}} \xi(T) dT, \quad (5)$$

where ξ_{max} is the maximum value of $\xi(T)$ and $\langle T \rangle$ is the emission-measure weighted value of T . This statistic ignores the spatial information and is therefore intended as a relatively crude measure of the temperature variations in a cluster appropriate when the data do not allow precise temperature estimates in small spatial regions. In such cases where the integrated cluster spectrum is modeled with a simple cooling flow spectral model plus an isothermal component then equation 5 is modified to $f\sigma_\xi$, where f is the relative fraction of the cooling

flow to the total emission measure (see section 5.2 of Buote et al. 1999). A variation on this prescription using the breaks in cooling flow mass deposition profiles has been used to determine the “ages” of some bright cooling flow clusters with *ROSAT* (Allen et al. 2000).

Joint consideration of σ_ξ and P_m/P_0 should provide a more precise indicator of the current cluster dynamical state and merger configuration than P_m/P_0 alone. For high precision temperature maps adding a first or second radial moment to equation (5) may be sufficient to capture the spatial dependences accounted for in the scenario represented in Figure 3.17.

Finally, the scenario described by Figure 3.17 will be complicated if there are important dynamical contributions from non-thermal processes such as AGN feedback (e.g., Owen et al. 2001). Empirical studies of the spatial and spectral morphologies of a large number of clusters using the improved instruments on *Chandra* and *XMM* will help to elucidate the importance of these and other process associated with cluster formation and evolution.

7. CONCLUSIONS

X-ray images of clusters obtained by *Einstein* and *ROSAT* have established that substructure and merging are common in nearby galaxy clusters. This evidence is reinforced by the X-ray temperature maps of a smaller number of bright clusters analyzed by *ROSAT*, *ASCA*, and *Bep-poSAX*. The study of substructure and morphology has evolved beyond detection and visual classification to that of quantitative morphological statistics that probe the dynamical states and the power spectrum of density fluctuations.

Unfortunately, the present status of cosmological studies of cluster morphologies is ambiguous. Although theoretical studies agree that cluster morphologies are sensitive to the cosmology (particularly to Ω_m and $P(k)$), the nature of the agreement and the relationship to observations have been often in conflict. It is difficult to interpret these disagreements because all of the N-body simulations applied to this problem have been inadequate. Large volume, high-resolution gas dynamical N-body simulations are required to obtain definitive answers. A larger observational sample of cluster morphologies with higher S/N data is also needed.

A quantitative connection between cluster mergers and the formation of radio halos has now been established. The strength of a merger indicated by the dipole power ratio (P_1/P_0) is approximately proportional to the power of the radio halo. Radio halos form preferentially in mergers of massive clusters with large values of P_1/P_0 where the merger has

proceeded fully into the core of the cluster. Larger samples are needed to understand the relative importance of the mass and P_1/P_0 on the strength of the radio halo and to clarify the connection between the formation of radio halos and relics.

Acknowledgments

I am grateful to the editors for the invitation to provide this review. I thank J. Tsai and G. Xu for previous collaboration on studies of cluster morphologies. I also thank the IAU, AAS, and a *Chandra* Fellowship for travel assistance to the IAU meeting in Manchester in August, 2000 where I presented the material that formed the basis for this review.

References

- Allen, S.W., Fabian, A.C., Johnstone, R.M., Arnaud, K.A. & Nulsen, P.E.J. 2001, *MNRAS*, 322, 589
- Arnaud, K.A., 1988, in *Cooling Flows in Clusters of Galaxies*, ed. A.C. Fabian, Kluwer Academic Publishers, 31
- Arnaud, M., Maurogordato, S., Slezak, E. & Rho, J. 2000, *A&A*, 355, 461
- Binney, J. & Tremaine, S. 1987, *Galactic Dynamics*, Princeton University Press, Princeton, NJ
- Biviano, A., Durret, F., Gerbal, D., Le Fèvre, Lobo, C., Mazure, A. & Slezak, E. 1996, *A&A*, 311, 95
- Böhringer, H., Soucail, G., Meiller, Y., Ikebe, Y. & Schuecker P. 2000, *A&A*, 353, 124
- Briel, U.G. et al. 1991, *A&A*, 246, L10
- Briel, U.G. & Henry, J.P. 1994, *Nature*, 372, 439
- Briel, U.G. & Henry, J.P. 1998, in *A New Vision of an Old Cluster: Untangling Coma Berenices*, eds. A. Mazure, F. Casoli, F. Durret & D. Gerbal, Publ. World Scientific, 170
- Briel, U.G., Henry, J.P. & Böhringer, H. 1992, *A&A*, 259, L31
- Buote, D.A. 1992, M.S. Thesis, Massachusetts Institute of Technology
- Buote, D.A. 1998, *MNRAS*, 293, 381
- Buote, D.A. 2001, *ApJL*, 553, L15
- Buote, D.A. & Canizares, C.R., 1994, *ApJ*, 427, 86
- Buote, D.A. & Canizares, C.R., 1998, in *Galactic Halos*, UC Santa Cruz Workshop, ed. D. Zaritsky, ASP Conf. Series 136, 289
- Buote, D.A. & Tsai, J.C. 1995, *ApJ*, 452, 522
- Buote, D.A. & Tsai, J.C. 1996, *ApJ*, 458, 27
- Buote, D.A. & Xu, G. 1997, *MNRAS*, 284, 439
- Buote, D.A., Canizares, C.R. & Fabian, A.C. 1999, *MNRAS*, 310, 483

- Burns, J.O., Roettiger, K., Ledlow, M. & Klypin, A. 1994, *ApJ*, 427, 87
- Churazov, E., Gilfanov, M., Forman, W. & Jones, C. 1999, *ApJ*, 520, 105
- Crone, M.M., Evrard, A.E. & Richstone, D.O. 1996, *ApJ*, 467, 489
- Dantas, C.C., de Carvalho, R.R., Capelato, H.V. & Mazure, A. 1997, 485, 447
- De Grandi, S. & Molendi, S. 1999, *ApJL*, 527, L25
- Davis, D.S. 1994, Ph.D. Thesis, University of Maryland
- Davis, D.S. & Mushotzky, R.F. 1993, *AJ*, 105, 409
- Donnelly, R.H., Markevitch, M., Forman, W., Jones, C., Churazov, E. & Gilfanov, M. 1999, *ApJ*, 513, 690
- Dutta, S.N. 1995, *MNRAS*, 276, 1109
- Edge, A.C., Stewart, G.C. & Fabian, A.C. 1992, *MNRAS*, 258, 177
- Ettori, S., Bardelli, S., De Grandi, S., Molendi, S., Zamorani, G. & Zucca, E. 2000, *MNRAS*, 318, 239
- Evrard, A.E., Mohr, J.J., Fabricant, D.G. & Geller, M.J. 1993, *ApJL*, 419, L9
- Fabian A.C. 1994, *AR&AA*, 32, 277
- Fabricant, D.G., Kent, S.M. & Kurtz, M.J. 1989, *ApJ*, 336, 77
- Feretti, L. 2001, in *The Universe at Low Radio Frequencies*, IAU 199, in press, astro-ph/0006379
- Forman, W. & Jones, C. 1989, in *Clusters of Galaxies*, STScI Symp. 4, eds. W.R. Oegerle, M.J. Fitchett & L. Danly, Cambridge University Press: Cambridge, 257
- Giovannini, G. & Feretti, L. 2000, *New Astron.*, 5, 355
- Giovannini, G., Tordi, M. & Feretti, L. 1999, *New Astron.*, 4, 141
- Gómez, P.L., Pinkney, J., Burns, J.O., Wang, Q., Owen, F.N. & Voges, W. 1997, *ApJ*, 474, 580
- Gómez, P.L., Hughes, J.P. & Birkinshaw, M. 2000, *ApJ*, 540, 726
- Grebenev, S.A., Forman, W., Jones, C. & Murray, S. 1995, *ApJ*, 445, 607
- Henriksen, M.J., Donnelly, R.H. & Davis, D.S. 2000, *ApJ*, 529, 692
- Henry J.P. & Briel U.G., 1995, *ApJL*, 443, L9
- Henry, J.P. & Briel U.G. 1996, *ApJ*, 472, 137
- Ikebe Y. et al. 1997, *ApJ*, 481, 660
- Irwin, J.A. & Bregman, J.N. 2000, *ApJ*, 538, 543
- Ishisaka, C. & Mineshige, S. 1996, *PASJ*, 48, L37
- Iwasawa, K., Ettori, S., Fabian, A.C., Edge, A.C. & Ebeling H. 2000, *MNRAS*, 313, 515
- Jing Y.P., Mo H.J., Börner G. & Fang L.Z. 1995, *MNRAS*, 276, 417
- Jones, C. & Forman W. 1992, in *Clusters and Superclusters of Galaxies* ed. A.C. Fabian, Kluwer Academic Publishers, 366, 49

- Jones, C. & Forman, W. 1999, ApJ, 511, 65
- Kauffmann G. & White S. D. M. 1993, MNRAS, 261, 921
- Kolokotronis, V., Basilakos, S., Plionis, M. & Georgantopoulos, I. 2001, MNRAS, 320, 49
- Lacey C. & Cole S. 1993, MNRAS, 262, 627
- Lazzati, D. & Chincarini, G. 1998, A&A, 339, 52
- Lazzati, D., Campana, S., Rosati, P., Chincarini, G. & Giacconi, R. 1998, A&A, 331, 41
- Liang, H., Hunstead, R.W., Birkinshaw, M. & Andreani, P. 2000, ApJ, 544, 686
- Lima-Neto, G.B., Pislár, V., Durret, F., Gerbal, D. & Slezak, E. 1997, A&A, 327, 81
- Lemonon, L., Pierre, M., Hunstead, R., Reid, A., Mellier, Y. & Böhringer, H. 1997, A&A, 326, 34
- Lynden-Bell D. 1967, MNRAS, 136, 101
- Markevitch, M., Sarazin, C.L. & Vikhlinin, A. 1999, ApJ, 521, 526
- Markevitch, M., Forman, W., Sarazin, C.L. & Vikhlinin, A. 1998, ApJ, 503, 77
- McMillan, S.L.W., Kowalski, M.P. & Ulmer, M.P. 1989, ApJS, 70, 723
- Mohr, J.J., Fabricant, D.G. & Geller, M.J. 1993, ApJ, 413, 492
- Mohr, J.J., Evrard, A.E., Fabricant, D.G. & Geller, M.J. 1995, ApJ, 447, 8
- Molendi, S., De Grandi, S., Fusco-Femiano, R., Colafrancesco, S., Fiore, F., Nesci, R. & Tamburelli, F. 1999, ApJL, 525, L73
- Nakamura, F.E., Hattori, M. & Mineshige, S. 1995, A&A, 302, 649
- Neumann, D. & Böhringer, H. 1997, MNRAS, 289, 123
- Neumann, D. & Böhringer, H. 1999, ApJ, 512, 630
- Owen, F.N., Eilek, J.A. & Kassim, N. E. 2000, ApJ, 543, 611
- Peacock, J.A. 1999, *Cosmological Physics*, Cambridge University Press, Cambridge, UK
- Peres, C.B., Fabian, A.C., Edge, A.C., Allen, S.W., Johnstone, R.M. & White, D.A. 1998, MNRAS, 298, 416
- Pierre, M. & Starck, J.-L. 1998, A&A, 330, 801
- Pislár, V., Durret, F., Gerbal, D., Lima-Neto, G.B. & Slezak, E. 1997, A&A, 322, 53
- Prestwich, A.H., Guimond, S.J., Luginbul, C.B. & Joy, M. 1995, ApJL, 438, L71
- Richstone, D.O., Loeb, A. & Turner, E.L. 1992, ApJ, 393, 477
- Rizza, E., Burns, J.O., Ledlow, M.J., Owen, F.N., Voges, W. & Bliton, M. 1998, MNRAS, 301, 328
- Schindler, S. et al. 1997, A&A, 317, 646

- Shibata, R., Honda, H., Ishida, M., Ohashi, T. & Yamashita, K. 1999, *ApJ*, 524, 603
- Slezak, E., Durret, F. & Gerbal, D. 1994, *AJ*, 108, 1996
- Thomas, P.A. et al. 1998, *MNRAS*, 296, 1061
- Valdarnini, R., Ghizzardi, S. & Bonometto, S. 1999, *New Astron.*, 4, 71
- Tsai, J.C. & Buote, D.A. 1996, *MNRAS*, 282, 77
- Vikhlinin, A., Forman, W. & Jones, C. 1994, *ApJ*, 435, 162
- Vrtilek, J.M., David, L.P., Vikhlinin, A., Forman, W. & Jones, C. 1997, *A&AS*, 191, 5304
- West, M.J. 1989, in *Clusters of Galaxies*, STScI Symp. 4, eds. W.R. Oegerle, M.J. Fitchett & L. Danly, Cambridge University Press: Cambridge, 65
- West, M. J. 1995, in *Clusters of Galaxies*, 29th Recontres de Moriond, eds. F. Durret, A. Mazure & J. Trân Thanh Vân, Publ. Frontier Editions, 23
- White, D.A., 2000, *MNRAS*, 312, 663
- White, D.A., Fabian, A.C., Allen, S.W., Edge, A.C., Crawford, C.S., Johnstone, R.M., Stewart, G.C. & Voges, W. 1994, *MNRAS*, 269, 589
- Xu, H., Makishima, K., Fukazawa, Y., Ikebe, Y., Kikuchi, K., Ohashi, T. & Tamura, T. 1998, *ApJ*, 500, 738

This page intentionally left blank

Chapter 4

HIGH ANGULAR RESOLUTION CLUSTER OBSERVATIONS WITH CHANDRA

A New View

W. Forman, C. Jones, M. Markevitch, A. Vikhlinin*

Smithsonian Astrophysical Observatory
60 Garden St., Cambridge, MA 02138, USA
wforman@cfa.harvard.edu, cjones@cfa.harvard.edu,
mmarkevitch@cfa.harvard.edu, alexey@hea.iki.rssi.ru

E. Churazov*

Max-Planck-Institut für Astrophysik
Karl-Schwarzschild-Strasse 1
Garching, D-85741, Germany
churazov@mpa-garching.mpg.de

Abstract Chandra’s high angular resolution has provided a surprising new view of clusters of galaxies. First, we discuss the newly discovered “cold fronts”, sharp, edge-like surface brightness structures in clusters. These sharp features, previously suggested to be shock fronts, probably arise from cluster mergers. We review Chandra observations of merging clusters with radio halos that provide new insights into the particle acceleration mechanisms for producing the energetic electrons responsible for the radio halos. Second, we describe the interactions of buoyant, radio emitting plasma bubbles with the hot gas in cluster, and galaxy, atmospheres.

*also at Space Research Institute, Moscow

Introduction

The Chandra X-ray Observatory provides X-ray imaging and imaging spectroscopy capabilities with $\sim 1''$ angular resolution, comparable to that familiar to ground-based optical observers. With this improvement in angular resolution, previously unseen, or rarely seen, phenomena have been detected in many clusters. We focus on two areas of cluster research where high angular resolution is significantly improving our understanding of the properties of galaxy clusters. First, we review the surprising “edges”, the boundaries between cold clouds traversing cluster cores, which Chandra has shown are a common feature of clusters. We review the observations of merging clusters with radio halos, which suggest that the synchrotron emitting electrons are accelerated by merger shocks. Second, we describe the interaction between plasma bubbles, ejected from active galactic nuclei, and the surrounding cluster atmospheres and review a model for the evolution of buoyant bubbles in cluster and galaxy atmospheres.

The phenomena observed in the hot intracluster medium (ICM) are often similar to those seen in their smaller cousins, the gaseous atmospheres around early-type galaxies. For example, radio emitting plasmas energized by active galactic nuclei can affect the hot gas in both individual galaxies and the intracluster medium. Therefore, we illustrate and discuss new results for individual galaxies when these are relevant for understanding the processes that occur in the ICM.

1. CLUSTER MERGERS

For many years clusters were thought to be dynamically relaxed systems evolving slowly after an initial, short-lived episode of violent relaxation. However, in a prescient paper, Gunn & Gott (1972) argued that, while the dynamical timescale for the Coma cluster, the prototype of a relaxed cluster, was comfortably less than the Hubble time, other less dense clusters had dynamical timescales comparable to or longer than the age of the Universe. Gunn and Gott concluded that “The present is the epoch of cluster formation”. The launch of the Einstein Observatory provided the capability to “image” the gravitational potential around clusters. Many papers in the 1980’s, exploited the imaging of the Einstein Observatory and showed the rich and complex structure of present epoch galaxy clusters (Jones et al. 1979; Jones & Forman 1984, 1999; Forman et al. 1981; Escalera et al. 1994; Slezak et al. 1994; Salvador-Solé et al. 1993; Mohr et al. 1993, 1995). Along with the X-ray observations, optical surveys delineated the large scale structure and

elucidated the filamentary structure of the Universe (e.g., de Lapparent et al. 1986; Kirschner et al. 1981).

ROSAT and ASCA provided a tantalizing view of the rich physics expected from detailed studies of cluster mergers (e.g., Briel et al. 1991; Briel & Henry 1992; White et al. 1993; Böhringer et al. 1994; Vikhlinin et al. 1994; Henry & Briel 1995; Honda et al. 1996; Henriksen & Markevitch 1996; Churazov et al. 1999; Markevitch et al. 1999; Donnelly et al. 1998; Schindler et al. 1999; Henriksen et al. 2000). An example showing the relationship between large scale structure and cluster merging is seen in the ROSAT image of A85 (see Fig. 4.1 from Durret et al. 1998). Such filaments are the high density end of the structures seen in numerical simulations and represent the densest component of the “missing” baryons (e.g., Cen & Ostriker 1999; Hellsten et al. 1998). As we observe in A85, many clusters may grow from accretion of relatively

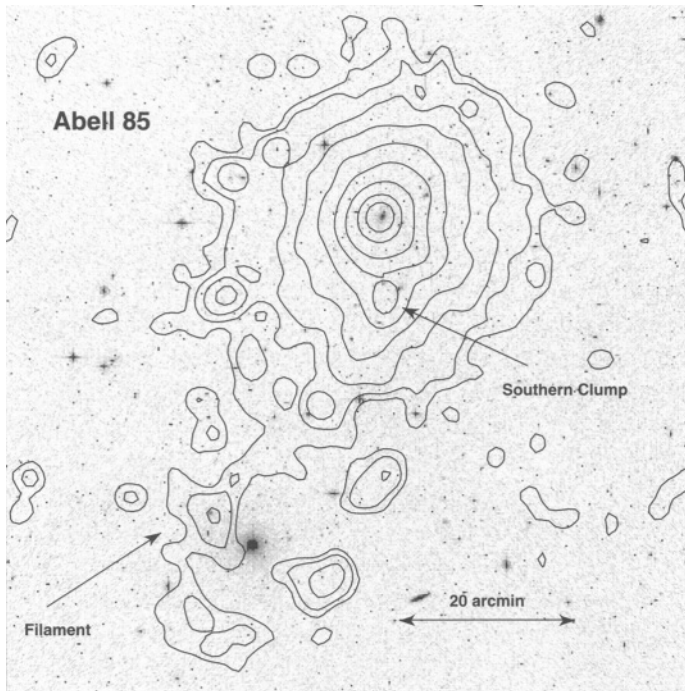


Figure 4.1. Smoothed, flat-fielded ROSAT PSPC contours (0.4-2.0 keV) are shown superposed on the optical digitized sky survey of the A85 region (adapted from Durret et al. 1998). A filamentary structure to the southeast can be seen, aligned at the same position angle (160° , measured counter clockwise from North) as the central cD galaxy (coincident with the X-ray peak). A much larger structure of clusters and groups spanning 5° on the sky, almost 30 Mpc at the redshift ($z = 0.0555$) of A85 lies at the same angle.

small mass concentrations along filamentary structures (Van Haarlem & Van de Weygaert 1993). However, during their evolution, other clusters may undergo major mergers of two nearly equal components. These major mergers are the most energetic events since the Big Bang involving kinetic energies as large as $\sim 10^{64}$ ergs (see Sarazin, this volume, for a discussion of the growth of clusters).

Chandra's high angular resolution has further illuminated the merging process and the complexity of the ICM. Prior to the launch of Chandra, sharp gas density discontinuities had been observed in several clusters (Markevitch et al. 1999). Since these clusters were undergoing major mergers, these features were expected to be shock fronts. However, the first Chandra observations showed that these were not shocks, but a new kind of structure – cold fronts.

We also describe the effects of the shocks that precede the cold fronts. Such shocks can accelerate electrons, whose synchrotron emission is observed as radio halos in some merging clusters.

1.1. MULTIPLE COLD FRONTS IN A2142

A2142 is a hot ($kT \sim 9$ keV), X-ray-luminous cluster at a redshift of $z = 0.089$. Two bright elliptical galaxies lie near the center and are aligned in the general direction of the X-ray brightness elongation. Furthermore, the line-of-sight velocities of these galaxies differ by 1840 km s $^{-1}$ (Oegerle et al. 1995), consistent with an unrelaxed cluster. In earlier work, the ROSAT PSPC image was used to argue for a late merger stage (Buote & Tsai 1996) and Henry & Briel (1996) used a ROSAT temperature map to suggest an ongoing merger.

The Chandra 0.3-10 keV band ACIS image of A2142, shown in Fig. 4.2, exhibits two sharp surface brightness edges – one lies $\sim 3'$ northwest of the cluster center (seen earlier in the ROSAT image) and a second lies $\sim 1'$ south of the center (see Markevitch et al. 2000 for details). To determine the nature of the edges, Markevitch et al. (2000) derived the gas density, temperature, and pressure distributions across each of the edges in the cluster. The gas temperature distribution across the edges (increasing distance from the cluster center) shows a sharp and significant *increase* as the surface brightness (gas density) decreases. For the edge south of the cluster center, the gas temperature rises by about a factor of 2 from ~ 5 keV to ~ 10 keV (Fig. 4.3 top left). For the north-western edge, the surface brightness is lower and the uncertainties are larger, but the temperature change is comparable. The X-ray brightness profile (Fig. 4.3, top right panel) is derived using sectors parallel to the elliptical boundaries of the edges. The lower left panel shows the gas

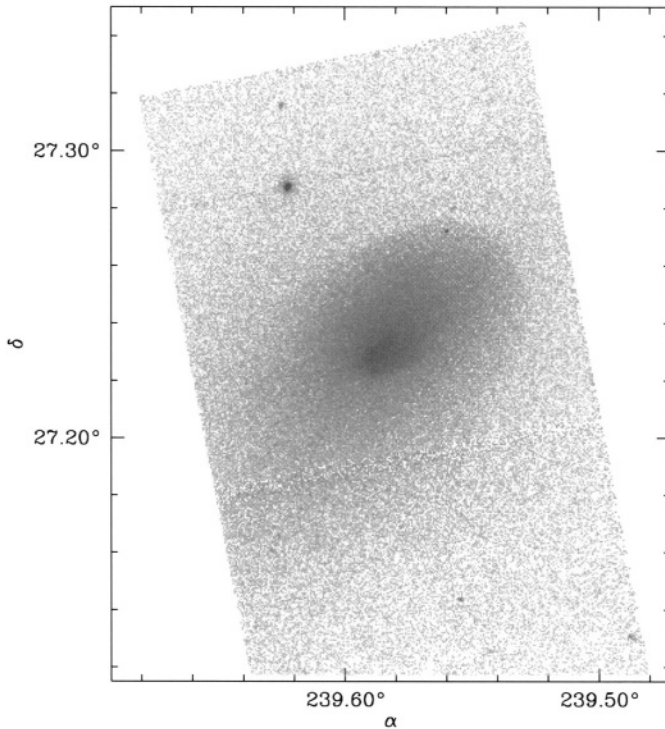


Figure 4.2. The 0.3–10 keV band ACIS image of A2142 shows two sharp elliptical brightness edges, cold fronts, northwest and south of the cluster center. The bright point source to the northeast is a Seyfert galaxy and a cluster member.

density model fit with two power laws and a discontinuity. The right bottom panel shows the pressure distribution across the edges derived by combining the gas density and gas temperature distributions. The vertical dashed lines indicate the best-fit positions of the density jumps.

One possibility for the formation of the two sharp density and temperature discontinuities, presented by Markevitch et al. (2000), is that the A2142 structures arise from the merger of two systems. The dense cores have survived the passage of the shock of the other merger component. We observe A2142 as it would appear after the merger (see Fig. 4.4). The outer, lower density gas has been shock heated, but the dense cores remain “cold”. Each sharp edge is then a boundary between the ram pressure-stripped subcluster remnant and the ICM. Alternatively, the edges in A2142 could arise from the impact of an unequal mass merger

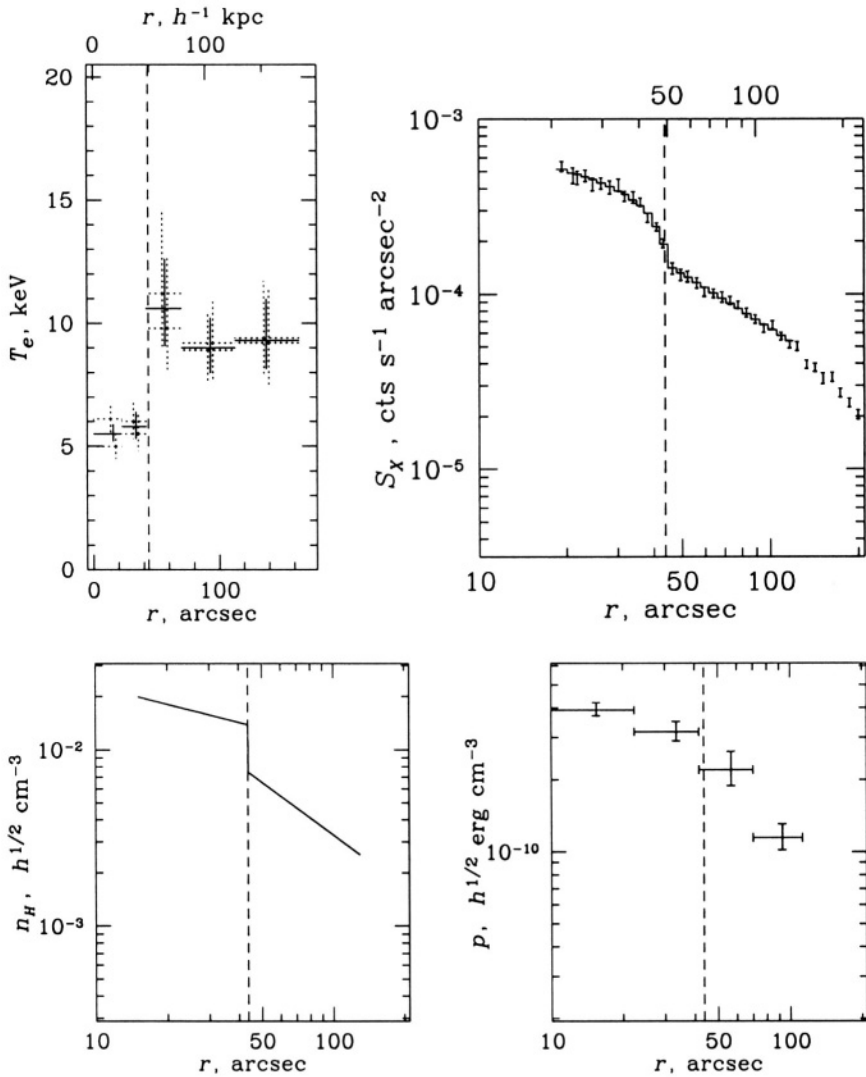


Figure 4.3. Each of the four figure panels shows a physical quantity for the southern edge in A2142. Top left shows the gas temperature, top right shows the X-ray surface brightness, bottom left shows the fitted gas density, and bottom right shows the calculated gas pressure. All quantities are shown as a function of the average radius from the cluster center of elliptical sectors that match the shape of the edges. The figure shows the typical behavior at an edge. As a function of increasing radius, the temperature abruptly increases, the surface brightness, and therefore gas density, abruptly decrease, while the gas pressure decreases continuously. Within the uncertainties (90% confidence), the gas is in pressure equilibrium across the edge. Note that A2142 was observed in two separate pointings and in the top left panel, solid crosses show simultaneous temperature fits to both pointings and dashed crosses show separate fits to each observation (see Markevitch et al. 2000 for details).

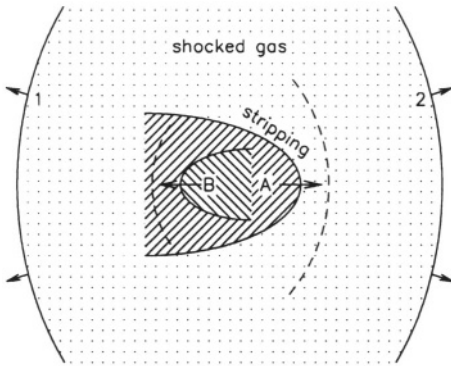


Figure 4.4. A possible model for the origin of the features in A2142 showing the merger of two components. Shock fronts 1 and 2 have crossed the cluster and are now in the cluster outskirts. The shocks are unable to penetrate the dense cores that continue to move through the shocked gas. The cores may develop additional leading shock fronts (dashed lines). The “edges” correspond to the leading sides, cold fronts, of the cores of the original merging clusters.

with the smaller system incoming from the northwest. The northwest edge could be the fossil remains of the initial impact.

Despite the uncertainties in the interpretation of the A2142 observation and the formation of the multiple edges, one conclusion is clear – the edges do *not* arise from shocks. If these edges were shocks, the gas temperature in front of the shock (i.e. away from the cluster center) would be lower than that behind the shock. This is exactly the opposite of what Markevitch et al. found. The observed features were called “cold fronts”.

1.2. CLUSTER PHYSICS AND COLD FRONTS

The detailed study of cluster cold fronts provides an opportunity to explore the physics of cluster mergers and to determine parameters of the ICM that cannot be determined in any other way (e.g., Sarazin, this volume). Deep Chandra observations of the cluster A3667 were analyzed by Vikhlinin et al. (2001a, b) who showed the potential of quantitative analyses of the cold fronts. A3667 is a moderately distant cluster ($z = 0.055$; 1.46 kpc per arcsec). The sharp edge in this cluster was observed with ROSAT by Markevitch et al. (1999) who suggested that this feature was a shock front. However, as with A2142, this feature

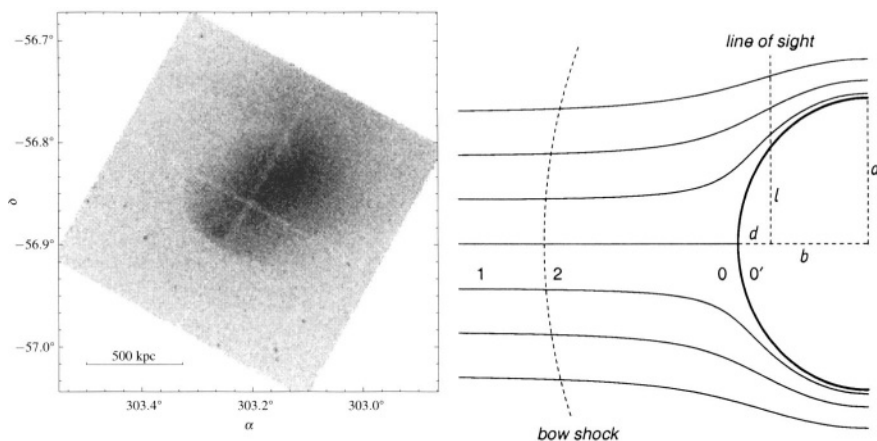


Figure 4.5. Left: The 0.5-4.0 keV Chandra image of A3667 shows the sharp surface brightness discontinuity, cold front, to the southeast. Right: This schematic shows the important features of the cold front and its interaction with the ICM in A3667. The boundary of the cold front and its geometry (semi-major axes a and b), the direction of the line-of-sight, the location of the bow shock, the stagnation region (zone 0; where gas piles up in front of the moving cold front) are shown. Region 1 is the free streaming zone, while region 2 lies behind a possible bow shock (weakly detected in the X-ray data).

is the boundary of a dense cold cloud, a merger remnant, as it traverses the hotter ICM.

Fig. 4.5 (left panel) shows the Chandra ACIS-I image of A3667 in the 0.5-4.0 keV energy band. To the southeast, the surface brightness shows a sharp decrease. Because A3667 is relatively bright and the exposure relatively long (49 ksec), Vikhlinin et al. were able to determine physical properties of the cluster merger that gives rise to the various features described below.

Vikhlinin et al. (2001a) showed that the edge can be accurately modeled as a spheroid (see right panel of Fig. 4.5 and left panel of Fig. 4.6). From the surface brightness profile, converted to gas density, and precise gas temperatures, the gas pressure on both sides of the cold front can be accurately calculated. Using the ratio of the pressures in the free streaming region and the stagnation point (see right panel of Fig. 4.5), the factor of two difference in pressure across the front yields a Mach number for the cloud of 1 ± 0.2 ($v = 1430 \pm 290 \text{ km s}^{-1}$). Thus, the precise measurement of the gas parameters allows the calculation of the cloud velocity in the plane of sky.

As Vikhlinin et al. (2001a) point out, such motion should produce a weak shock preceding the cold front and such a feature is detected.

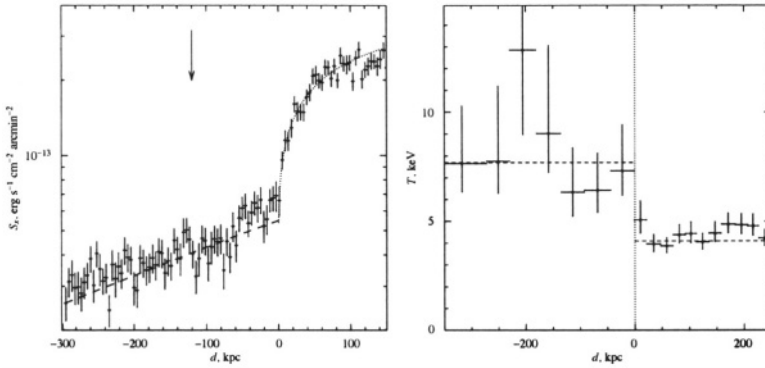


Figure 4.6. For A3667, the X-ray surface brightness and gas temperature profiles across the cold front. Left: The 0.5-2.0 keV surface brightness profile extracted in elliptical regions across the cold front. The large, sharp drop is clearly seen. The dashed line is the ROSAT PSPC fit to the outer surface brightness distribution and agrees well with the Chandra observation. The dotted curve is a fit to a spheroid with a sharp boundary. As discussed by Vikhlinin et al. (2001a), the excess at distances of 0-50 kpc in advance of the front represents gas that accumulates in the stagnation region. Right: The temperature profile across the cold front. The temperature *increases* from ~ 4 keV to ~ 8 keV across the front.

Furthermore, the distance from the cold front to the shock (~ 350 kpc) and the observed gas density jump (a factor of 1.1-1.2) yield the shock propagation velocity of ~ 1600 km s $^{-1}$, in good agreement with the independently derived cold front velocity calculated from the pressure difference across the front.

Finally, the A3667 observation provides important information on the efficiency of transport processes in clusters. As the temperature and surface brightness profiles show (see Fig. 4.6), the front is quite sharp. Quantitatively, Vikhlinin et al. showed that the width of the front was less than $3.5''$ (5 kpc). This sharp front requires that transport processes across the front must be suppressed, presumably by magnetic fields. Without such suppression, the front should be broader since the Coulomb mean free path for electrons is about 13 kpc, several times the width of the cold front.

Vikhlinin et al. (2001b) also observed that the cold front appears sharp only over a sector of about $\pm 30^\circ$ centered on the direction of motion. Beyond this sector, the sharp boundary disappears. The disappearance can be explained by the onset of Kelvin-Helmholtz instabilities, as the ambient gas flows past the moving cold front. To explain the limited extent of the sharp boundary, the Kelvin-Helmholtz instability must be partially suppressed, e.g., by magnetic fields parallel to the boundary.

The strength of such a field is $7 - 16\mu\text{G}$ (Vikhlinin et al. 2001b). This measured value of the magnetic field in the cold front implies that the pressure from magnetic fields is small (only 10-20% of the thermal pressure) and, hence, adds confidence to calculations of cluster gravitating masses from X-ray measurements that assume that the X-ray emitting gas is in hydrostatic equilibrium and supported by thermal pressure.

1.3. COLD FRONTS IN OTHER CLUSTERS

Sharp edges are a new cluster phenomenon that are being studied in considerable detail with Chandra. Edges are a common feature of clusters, but they exhibit a variety of morphologies.

1.3.1 RX J1720.1+2638. Chandra observations of the cluster RX J1720.1+2638 ($z = 0.164$) showed the presence of two surface brightness discontinuities – the first, an edge about 250 kpc to the southeast of the cluster center and the second, a plateau about 130 kpc to the northwest. The gas temperature distributions suggest that these features represent the boundaries of a central, group-sized cold ($kT = 4$ keV) cloud within a hot ($kT = 10$ keV) ICM (Mazzotta et al. 2001a). Despite the presence of these sharp features, the cluster otherwise appears rather regular with a single central bright optical galaxy that is coincident with the peak in the X-ray surface brightness. Mazzotta et al. suggest that RXJ1720.1+2638, an apparently relaxed cluster on large scales with a rapidly moving core, could be produced from the collapse of two nearly co-located mass perturbations. In this scenario, initially, a group mass scale perturbation collapses and, at nearly the same location but later in time, a larger cluster scale perturbation collapses. Thus, the effects of a strong merger would not be apparent, but one could still observe a cold front, associated with a collapsed group formed within, but not at the exact center of, a cluster, and traversing the larger cluster core.

1.3.2 ZW3146 – A Cluster with Three Edges. ZW3146 is a moderately distant ($z = 0.2906$; 5.74 kpc per arcsec) cluster with a remarkably high mass deposition rate that is estimated to exceed $1000 M_{\odot} \text{ yr}^{-1}$ (Edge et al. 1994). The Chandra image further demonstrates the remarkable nature of this cluster – on scales from $3''$ to $30''$ (~ 20 kpc to 170 kpc), three separate edges are detected (see Fig. 4.7 and Forman et al., in preparation). At the smallest radii, two edges are seen to the northwest and north (see left panel of Fig.4.7). The first, at a radius of $\sim 3''$ (17 kpc), spans an angle of nearly 180° with a surface brightness drop of almost a factor of 2. The second edge, at a radius of $\sim 8''$ (45 kpc) spans only 90° but has a surface brightness drop of almost a factor

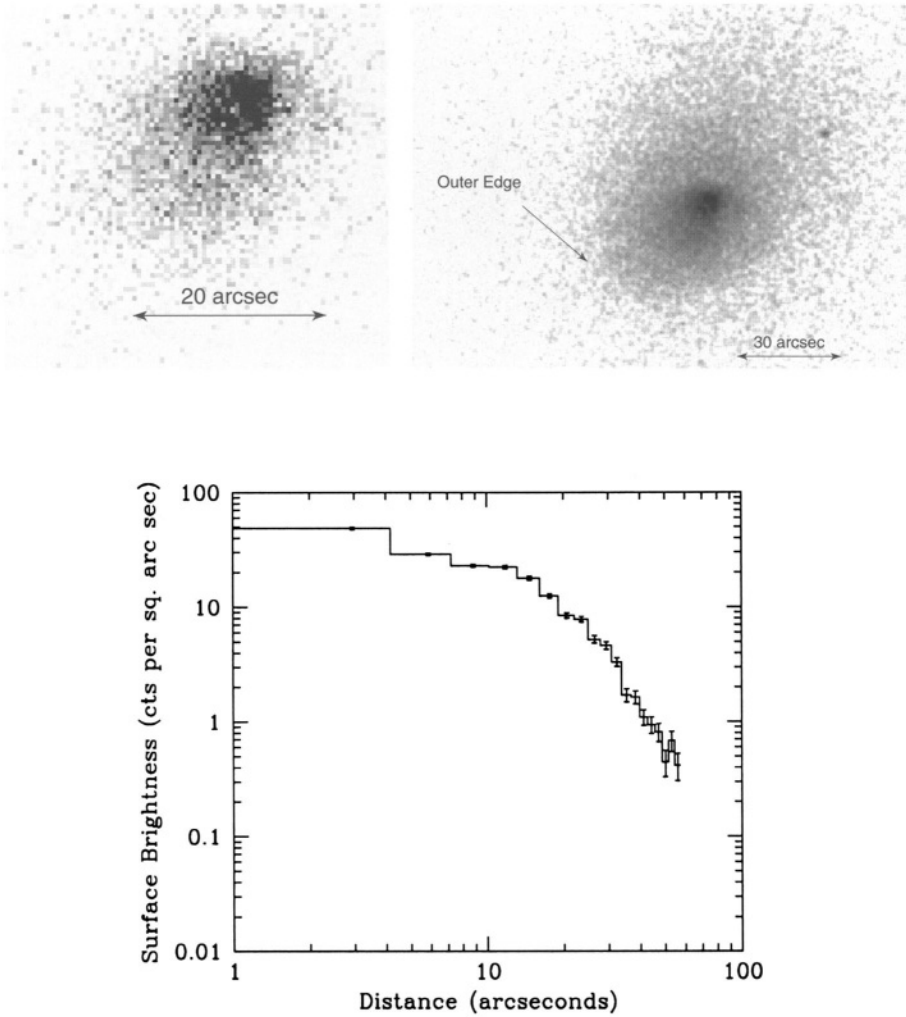


Figure 4.7. Edges in ZW3146. Top left, a 0.5-2.0 keV image of the central region of ZW3146 shows the two inner edges at 3'' and 8''. The top right panel shows the edge at 35''. The lower panel shows the surface brightness profile in a sector of width about 20° to the southeast. The factor of 2 discontinuity at 35'' is clearly seen.

of 4. The third (see right panel of Fig. 4.7) lies to the southeast, about 35'' (200 kpc) from the cluster center, and, as with the first, extends over an angle of almost 180°. The surface brightness distribution for the third edge is shown in the bottom panel of Fig. 4.7. Measured in

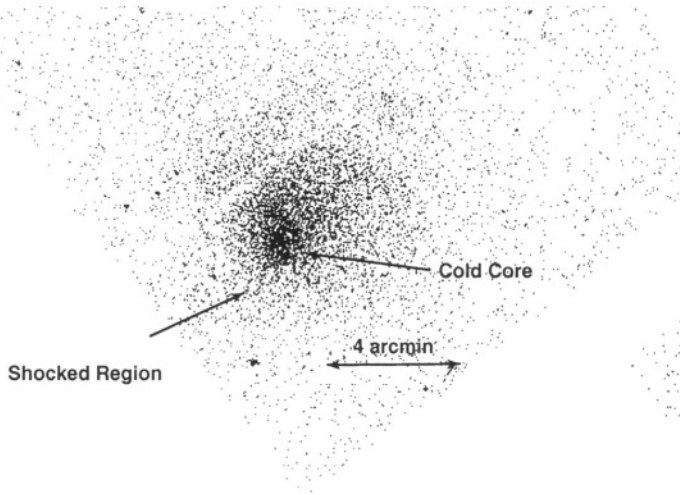


Figure 4.8. The 0.5-4.0 keV Chandra image of A665 shows the bright cold, core with a tail of apparently stripped material to the northwest. This suggests the cold front is moving to the southeast. The cold front is not as sharp as other fronts, e.g., A3667, and hence the front is probably moving at some modest angle with respect to the plane of the sky. The region to the southeast of the cold core is shock heated by the supersonic motion of the core (see Markevitch & Vikhlinin 2001).

a sector of about 20° to the southeast, the surface brightness drops by almost factor of 2.

Thus, the variety of morphologies and scales exhibited by these sharp edges or cold fronts is quite remarkable. Possibly the edges may arise from moving cold gas clouds that are the remnants of merger activity. They may arise either from massive mergers as in A2142, multiple collapses as suggested for RXJ1720.1+2638, or oscillations of gas clouds before finally coming to rest (Markevitch 2001). Alternatively, some edges could arise from the interaction of surviving cold, dark matter halos as they move within the cluster potential. High resolution, large scale structure simulations show that dense halos, formed at very early epochs, would not be disrupted as clusters collapse (Ghigna et al. 1998; Ghigna et al. 2000). While most of the dark matter halos, having galaxy size masses, are associated with the sites of galaxy formation, the larger mass halos also may survive or may have fallen into the cluster only recently. Hence, we might expect to find a range of halo mass distributions moving within the cluster potential. As these halos move, they could give rise to the multiple surface brightness edges observed in some clusters.

1.4. MERGER SHOCKS AND CLUSTER RADIO HALO SOURCES

While many of the expected surface brightness discontinuities observed with Chandra were discovered to be “cold” fronts, Chandra has seen evidence of shock fronts in merging clusters. Markevitch & Vikhlinin (2001) studied two clusters, A2163 and A665, undergoing major mergers. We present their results for A665 ($z = 0.01829$) that shows the clearest relationship between the merger shock and a low frequency radio halo.

Gómez et al. (2000) argued that A665 is a major merger of two components with masses in the ratio of 1:1 or 1:2 based on extensive optical spectroscopy and the ROSAT image that shows isophotal twists and centroid variations (see also Buote & Tsai 1996). The ROSAT images (both PSPC and HRI) clearly show the cool core, just like those seen in the clusters discussed above. The Chandra image (see Fig. 4.8) shows the northwest to southeast elongation of the cluster core, which is similar to that seen in the optical galaxy distribution (Geller & Beers 1982; Beers & Tonry 1986) and that suggests a merger in the direction of the elongation.

To investigate the merger, Markevitch & Vikhlinin (2001) derived the cluster temperature map that is shown in Fig. 4.9 (left panel). The gas immediately in front (southeast) of the X-ray bright, cold cloud is shock heated to a temperature of approximately 15 keV (based on a spectral fit to the data extracted from the hot region identified in the temperature map). While Markevitch & Vikhlinin could not exclude a power law spectrum for these data, the emission is not associated with any point source, but is extended (see Fig. 4.8). Hence, the scenario of a cold core moving rapidly to the southeast is consistent with both the appearance of the X-ray surface brightness map and the spectral data.

A665 is one of the clusters that hosts a centrally located, low frequency, diffuse radio source (see Moffet & Birkinshaw 1989; Giovannini & Feretti 2000; see Feretti (2001) and Sarazin (this volume) for a discussion and reviews of radio halos and particle acceleration). Cluster merger shocks are one mechanism for accelerating the electrons whose synchrotron emission could produce the radio halo. Recently, Buote (2001) argued that those luminous clusters whose morphology was indicative of a major merger were statistically more likely to harbor radio halos (see also Buote, this volume, and Feretti 2001).

Markevitch & Vikhlinin (2001) showed that the radio halo emission in A665 is closely correlated with the hot, shocked gas. Fig. 4.9 shows the radio contour map (from Giovannini & Feretti 2000) divided by the square root of X-ray brightness superposed on the gas temperature map.

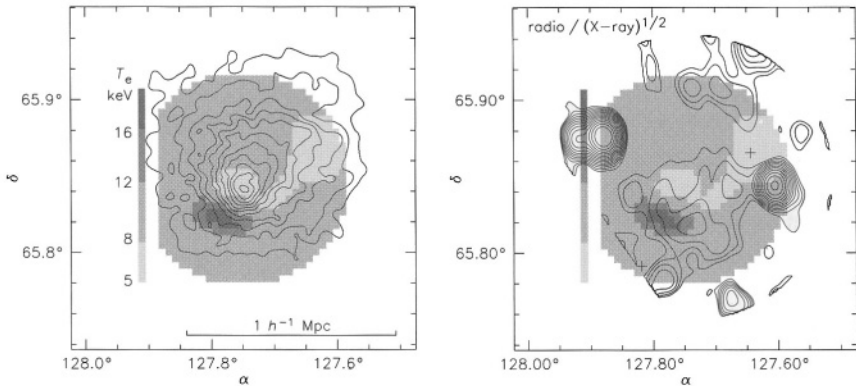


Figure 4.9. The left panel shows the smoothed, 0.5-4.0 keV band X-ray surface brightness contours (after removing point sources) superposed on the greyscale Chandra temperature map for A665. Each shade of gray approximately corresponds to a significantly different temperature. The right panel shows a representation of the VLA 1.4 GHz contours of the radio halo from Giovannini & Feretti (2000) overlaid on the greyscale A665 temperature map. The contours the radio brightness divided by the square root of the X-ray brightness. The two crosses indicate positions of two excised radio point sources; the angular resolution of the radio images is $45''$. Contours in both the left and right panels are log-spaced by a factor of $2^{1/2}$ and figures are from Markevitch & Vikhlinin (2001).

The contours thus approximate the number of radio-emitting relativistic electrons per X-ray emitting thermal electron along the line of sight (assuming a reasonably uniform magnetic field). The contours peak at the location of the shock identified from the X-ray temperature map. Thus, Markevitch & Vikhlinin suggest that the shock, produced by the rapidly moving, cold core, accelerates particles as it crosses the cluster from northwest to southeast. As the authors note, this model predicts that the most recently accelerated particles should lie closest to the shock and the effects of aging of the particle energy spectra could be measured from radio observations.

2. THE RADIO—X-RAY CONNECTION

Prior to the launch of Chandra, ROSAT observations of NGC1275 and M87 provided hints of complex interactions between radio emitting plasmas ejected from central galaxies in clusters (e.g., Bohringer et al. 1993, 1995; Churazov et al. 2000, 2001). With the launch of Chandra, the interaction between the radio emitting plasma and the hot intraclus-

ter medium (ICM) has been observed in many systems and has begun to be investigated in detail.

2.1. A FIRST LOOK AT RADIO EMITTING PLASMA BUBBLES IN CLUSTER ATMOSPHERES

One of the first, and clearest, examples of the effect of plasma bubbles on the hot intracluster medium was found in the Perseus cluster whose bright active, central galaxy is NGC1275 (3C84). First studied in ROSAT images (Böhringer et al. 1993), the radio emitting cavities to the north and south of NGC1275 are clearly seen in the Chandra images (Fabian et al. 2000). Bright X-ray emitting rims surround the cavities that coincide with the inner radio lobes. For NGC1275/Perseus, the radio lobes are in approximate pressure equilibrium with the ambient, denser and cooler gas and the bright X-ray rims surrounding the cavities are softer than the ambient gas. Therefore, the radio cavities are not likely to be a major source of shock heating.

The Chandra images of Perseus/NGC1275 also suggest the presence of older bubbles produced by an earlier outburst (Fabian et al. 2000). These older bubbles appear as X-ray surface brightness “holes”, but unlike the inner bubbles, these outer holes show no detectable radio emission, suggesting that the synchrotron emitting electrons have decayed, leaving a heated, plasma bubble. Such bubbles, with no attendant radio emission, are seen by Chandra in other systems. In particular, the galaxy groups HCG 062 (Vrtilek et al. 2001) and MKW 03s (Mazzotta et al. 2001b) show clear evidence of X-ray holes, but have no detected radio emission from the cavities.

Around the central galaxy in the Hydra A cluster, Chandra observations show cavities, similar to those described above for Perseus, created by the inner radio lobes as they displace the X-ray gas (McNamara et al. 2000). As with Perseus, the X-ray emission in Hydra A shows no evidence for shock heating.

While all these examples show no evidence for strong shock heating of the gas by the radio plasma ejected from the active nucleus, MKW 03s does indicate that energy is being transferred from the radio plasma to the thermal gas. Mazzotta et al. (2001b) showed that the X-ray emission from the cavity in MKW3s is most likely thermal emission and that its spectrum is harder than that of the surrounding ICM. Hence, the gas in the bubble has been heated, presumably by the now decayed relativistic plasma.

2.2. BUBBLES IN A GALAXY ATMOSPHERE – M84

The examples above have concentrated on the radio–X-ray connection around central galaxies in clusters and groups. These galaxies are clearly the brightest cluster members and lie at the cluster center, a special position in the cluster’s gravitational potential. However, a notable example of the influence of radio plasma on the X-ray emitting gas in a more typical early-type galaxy is M84 (NGC4374, 3C272.1), an E1 galaxy, within the core of the Virgo cluster, but not at its center.

Finoguenov & Jones (2001) found very complex structure in the soft X-ray emitting gas around the Virgo galaxy M84 (NGC4374) whose appearance is completely explained by the morphology of the radio lobes. Fig. 4.10 shows the strong influence of radio bubbles on the X-ray emitting gas distribution. The X-ray emission appears \mathcal{H} -shaped, with a bar extending east-west and two filaments roughly perpendicular to this bar. The complex X-ray surface brightness distribution arises from the presence of two radio lobes (approximately north and south of the galaxy) that produce two low density cavities surrounded by higher density X-ray filaments. As with Perseus/NGC1275 and Hydra A, the filaments, defining the \mathcal{H} -shaped emission, have gas temperatures comparable to the gas in the central and outer regions of the galaxy and hence argue against any strong shock heating of the galaxy atmosphere by the radio plasma.

From the gas density distribution surrounding the radio lobes and the observed Faraday rotation, Finoguenov & Jones (2001) determined the strength of the magnetic field. A simple model of the X-ray gas distribution gave an integrated electron density of $\sim 0.04 \text{ cm}^{-3} \text{ kpc}$. From the observed Faraday rotation, Finoguenov & Jones (2001) inferred a line-of-sight magnetic field of $0.8 \mu \text{ Gauss}$ (below the equipartition value of $20 \mu \text{ Gauss}$; Laing & Bridle 1987).

In summary, the high resolution Chandra image of M84 shows the remarkable interaction between the radio plasma and the X-ray emitting interstellar medium (ISM). The radio lobes have created cavities in the ISM that are surrounded by higher density shells and, with some assumptions, the magnetic field overlying the radio bubbles can be calculated.

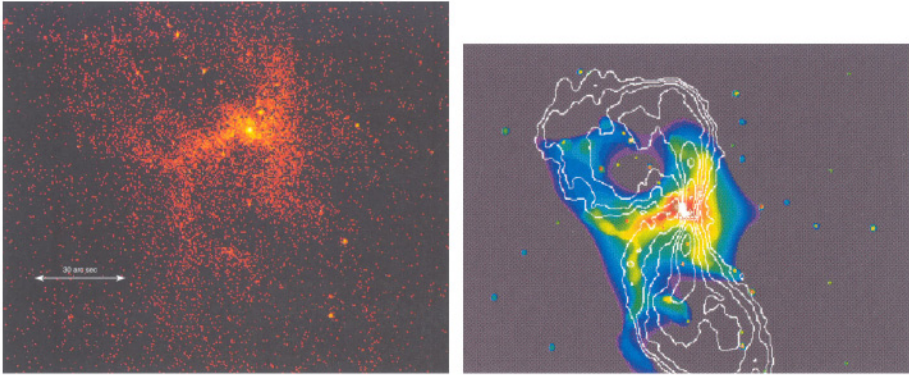


Figure 4.10. Left: H -shaped X-ray emission from M84 image (0.5–2.0 keV band) as observed with Chandra. The X-ray emission shows an east-west bar and two filaments extending from each end. The galaxy nucleus lies in the bright region at the west end of the bar. Right: Radio emission overlaid on the smoothed Chandra image. (Finoguenov & Jones 2001) “explains” the unusual X-ray morphology – the radio plasma has displaced the hot X-ray emitting gas.

2.3. EVOLUTION OF BUOYANT PLASMA BUBBLES IN HOT GASEOUS ATMOSPHERES

Buoyant bubbles, as described above, are a common feature of central galaxies in groups and clusters and are being detected around individual early-type galaxies. In a study of M87, Churazov et al. (2001) combined the new radio image of Owen et al. (2000) with the ROSAT HRI data to propose a scenario for the interaction of buoyant bubbles with the X-ray emitting hot gas and to explain many features seen in clusters and around galaxies.

Owen et al. (2000) made a high resolution, high dynamic range, 327 MHz map of the halo of M87 (see Fig. 4.11, left panel). The high surface brightness center is the inner lobe structure (oriented approximately north-south) with the famous jet pointing west north-west (approximately bottom-right for the orientation of images adopted in Fig. 4.11). Surrounding this, the highly structured outer halo is much fainter and consists of the torus-like eastern bubble, the much less well-defined western bubble, both of which are connected to the central emission by a column, and the two very faint almost circular emission regions northeast and southwest of the center. Fig. 4.11 (right panel) shows the X-ray surface brightness distribution of the same region (with similar orientation) from a 200 ksec ROSAT/HRI image. As pointed out by a number of

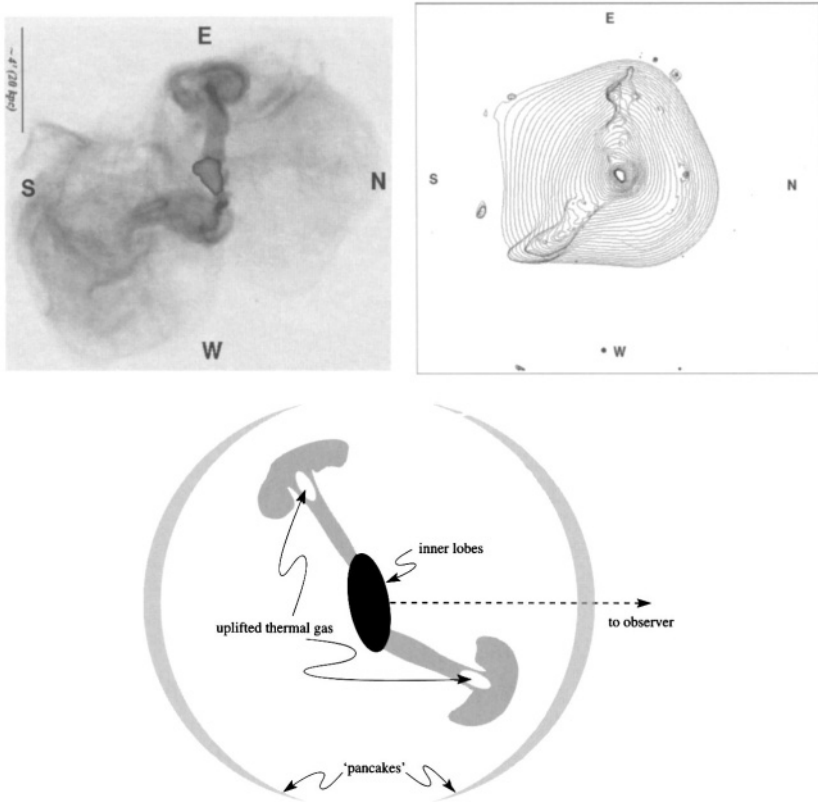


Figure 4.11. Left: $14'.6 \times 16'.0$ radio map of M87 (North to the right, East is up) (from Owen et al. 2000). Right: Contour map of the smoothed ROSAT HRI X-ray image (same size and orientation as the radio image). Bottom: Suggested source geometry. The central black region denotes the inner radio lobes, the gray “mushrooms” correspond to buoyant bubbles, transformed into tori, and the gray lens-shaped structures are “pancakes” (seen edge-on) formed by older bubbles.

authors (Feigelson et al. 1987; Böhringer et al. 1995; Owen et al. 1999; Harris et al. 1999), there is evidence for a correlation between the X-ray and radio emitting features. The simplest explanation for this correlation is that the excess X-ray emission is produced by inverse Compton scattering of cosmic microwave background photons by the same relativistic electrons that produce the synchrotron radio emission (Feigelson et al. 1987). However, ROSAT PSPC observations have shown that the excess emission has a thermal spectrum (Böhringer et al. 1995) and the X-ray emitting gas in these regions has a lower temperature than that in the surrounding regions. Three fundamental properties emerge – 1)

the radio image shows prominent “torus-like” features; 2) the X-ray and radio bright images show correlations, but often not one-to-one; 3) the X-ray emission, associated with the radio bubbles and attached columns, is thermal in nature and the gas temperature is lower than that of the ambient X-ray emitting gas.

The “torus-like” radio features are strikingly similar to hot buoyant bubbles formed by powerful nuclear atmospheric explosions. Initially a spherical bubble is formed that transforms into a torus and appears as a characteristic “mushroom” cloud as the bubble, lacking strong surface tension, rises in the ambient medium. The important role of buoyancy in the evolution of radio lobes was first proposed by Gull & Northover (1973). The similarity of M87’s “torus-like” features to Rayleigh–Taylor mushrooms was discussed by Churazov et al. (2001) and their similarity to subsonic vortex rings by Owen et al. (2000). Another property of powerful atmospheric explosions and buoyant bubbles is that as the bubble transforms to a torus, the rising bubble/torus entrains and uplifts ambient gas. This may qualitatively explain the correlation of the radio and X-ray emitting plasmas and naturally accounts for the thermal nature of the excess emission.

In an atmospheric explosion, the final evolutionary phase occurs when the bubble reaches a height at which the ambient gas density equals that of the bubble. The bubble no longer rises, but expands laterally (forming a “pancake”) and occupies a thin layer in the atmosphere. The bubbles/tori in M87 may undergo the same evolutionary phases. In a spherically symmetric gravitational potential, the bubble will try to fill a segment of a sphere. The large low surface brightness features in the radio map could be bubbles transformed into thin “pancakes” (see Fig. 4.11). A sketch of a possible overall source structure of M87, based on the evolution of buoyant bubbles, is shown in Fig. 4.11.

Churazov et al. (2001) simulated their qualitative picture described above. A spherical bubble was inflated in an atmosphere defined by the gravitational potential of M87. The bubble has an initial radius of $r_b = 5$ kpc and is centered 9 kpc from the gravitational center of M87. The bubble density is 1/100 of the ambient density, making the bubble buoyant, and the bubble temperature is 100 times the ambient value, establishing pressure equilibrium. The evolution of the gas temperature distribution is illustrated in 5 snapshots spanning the 67 million year simulation with steps at 0, 8.4, 21, 42 and 67 Myrs shown in Fig. 4.12 (Churazov et al. 2001). The initially spherical bubble flattens and develops a “cone” at the rear, that is filled with entrained gas. The bubble then transforms into a torus. Ambient gas (gas captured during the transformation of the bubble into a torus) occupies the central part of the rising struc-

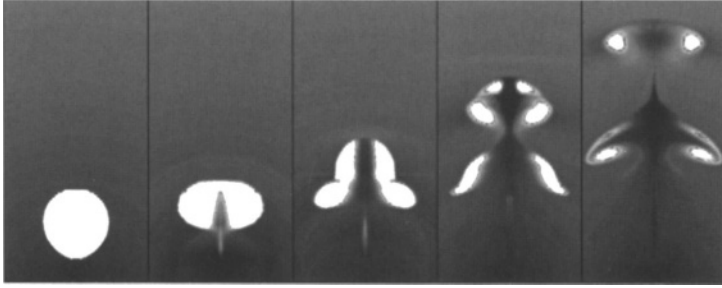


Figure 4.12. The gas temperature distribution (from Churazov et al. 2001) in 5 time steps— 0, 8.4, 21, 42 and 67 Myrs after the start of the simulation. Each box is 40 by 20 kpc. The center of the cluster is at the bottom of the box. Temperature is color coded in the 0.7 (black) to 5 keV (white) range. The temperature of the cluster thermal gas (blue) changes from ~ 1 keV at the center to ~ 1.7 keV at a distance of 40 kpc. All temperatures above 5 keV are white. Thus, the hot “radio-emitting plasma” that initially has a temperature of order of 100 keV is white. At later stages, the coldest gas is associated with the rising bubble.

ture. In the last evolutionary stages (shown in Fig. 4.12), the coldest gas is found not at the center of the cluster, but within the rising bubble/torus. Although the simulations did not include radiative cooling, this cool gas in the rising torus is that which has been uplifted from the regions closest to the galaxy center. Adiabatic expansion further cools the uplifted gas as it expands to match the ambient gas pressure at the current location of the bubble.

Churazov et al. (2001) also computed the effect of the rising bubble on the X-ray surface brightness. The X-ray surface brightness map shown in Fig. 4.13 is the excess above the unperturbed surface brightness. As shown in the X-ray and radio surface brightness maps (Fig. 4.13), in general where the radio is brightest, the X-ray is faintest. The holes in the early stages of the simulation are remarkably similar to the radio/X-ray features seen in Perseus, Hydra A, and M84. During the later stages, the tori form and separate from the main bubble. As expected the “stem” of the mushroom is brighter than the surrounding regions.

Models, like that described above, can be applied to the increasing number of examples of radio plasma – cluster/galaxy atmosphere interactions. How much matter is uplifted by the rising, buoyant bubbles? How much energy is transferred from the relativistic plasma to the thermal plasma? How do mergers and the turbulence they cause in the cluster core affect the appearance of both the thermal and relativistic plasmas? With Chandra, we have the ability to address these issues

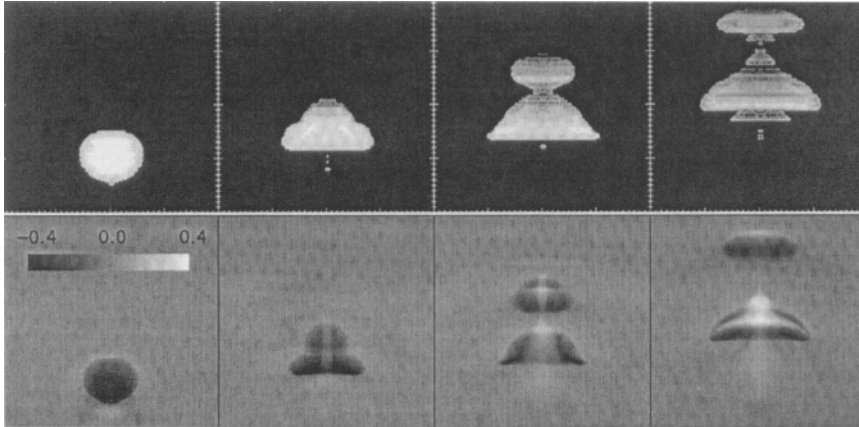


Figure 4.13. Top: The 327 MHz radio surface brightness of M87 calculated at four time steps (4.2, 21, 42, and 67 Myrs after the start of the simulation). Each snapshot of the simulation is 40 kpc on a side. Bottom: Calculated X-ray morphology of the bubble for the same times as in the upper panel. Each box is 40 by 40 kpc. The figure shows the relative deviation of the X-ray surface brightness (in the ROSAT energy band) with respect to the unperturbed X-ray emission of the cooling flow at the same distance from the center of M87. The darker regions are X-ray underluminous and lighter regions are X-ray bright. Black corresponds to regions dimmer by 40% (or more) than the unperturbed value and white corresponds to regions brighter by 40% (or more) than the unperturbed value. The figure is adapted from Churazov et al. 2001)

in detail and can expect to better understand the detailed evolution of buoyant bubbles in galaxy and cluster atmospheres.

3. CONCLUSIONS

The full import of Chandra cluster observations has only recently begun to be understood. The rich variety of the interaction between radio emitting plasmas and the X-ray emitting ICM in clusters (and hot gaseous atmospheres in galaxies) are only beginning to be appreciated. What were believed to be shock fronts are instead a new phenomenon – cold fronts. High angular resolution can provide unique insights into cluster mergers and the physics of the ICM. With sufficiently high signal-to-noise, magnetic field strengths and cloud velocities can be calculated. Detailed models to fully exploit the high angular resolution of Chandra are required both for understanding the very complex behaviors of bubbles in hot atmospheres and cold fronts traversing clusters. Chandra observations are allowing a deep, and quantitative, physical understanding of the processes in clusters and galaxies. We can expect new insights

and more surprises as the observations are better understood and we understand how better to utilize the new observational tools provided by the Chandra X-ray Observatory.

Acknowledgments

We acknowledge support from NASA contract NAS8 39073, NASA grants NAG5-3065 and NAG5-6749 and the Smithsonian Institution.

References

- Beers, T.C. & Tonry, J.L. 1986, *ApJ*, 300, 557
- Böhringer, H., Briel, U.G., Schwarz, R.A., Voges, W., Hartner, G. & Trümper J. 1994, *Nature*, 368, 828
- Böhringer, H., Nulsen, P., Braun, R. & Fabian, A. 1995, *MNRAS*, 274, L67
- Böhringer, H., Voges, W., Fabian, A.C., Edge, A.C. & Neumann, D. M. 1993, *MNRAS*, 264, L25
- Briel, U.G. et al. 1991, *A&A*, 246, L10
- Briel, U.G. & Henry, J.P. 1992, *A&A*, 259, L31
- Buote, D. A. 2001, *ApJL*, 553, L15
- Buote, D. & Tsai, J. 1996, *ApJ*, 458, 27
- Cen, R. & Ostriker, J. 1999, *ApJ*, 514, 1
- Churazov, E., Brügggen, M. Kaiser, C. R., Böhringer, H. & Forman, W. 2001, *ApJ*, 554, 261
- Churazov, E., Forman, W., Jones, C. & Böhringer, H. 2000, *A&A*, 356, 788
- Churazov, E., Gilfanov, M., Forman, W. & Jones, C. 1999, *ApJ*, 520, 105
- de Lapparent, V., Geller, M. & Huchra, J. 1986, *ApJL*, 302, L1
- Donnelly, R.H., Markevitch, M., Forman, W., Jones, C., David, L.P., Churazov, E. & Gilfanov, M. 1998, *ApJ*, 500, 138
- Durret, F., Forman, W., Gerbal, D., Jones, C. & Vikhlinin, A. 1998, *A&A*, 335, 41
- Edge, A.C., Fabian, A.C., Allen, S.W., Crawford, C.S., White, D.A., Böhringer, H. & Voges, W. 1994, *MNRAS*, 270, L1
- Escalera, E., Biviano, A., Girardi, M., Giuricin, G., Mardirossian, F., Mazure, A. & Mezzetti, M. 1994, *ApJ*, 423, 539
- Fabian, A.C., et al. 2000, *MNRAS*, 318, L65
- Feigelson, E.D., Wood, P., Schreier, E., Harris, D. & Reid, M. 1987, *ApJ*, 312, 101
- Feretti, L. 2001, in *The Universe at Low Frequencies*, Pune 1999, ASP Conference Series, in press, astro-ph/0006379

- Finoguenov, A. & Jones, C. 2001, ApJL, 547, L107
- Forman, W., Bechtold, J., Blair, W., Giacconi, W., van Speybroeck, L. & Jones, C. 1981, ApJL, 243, L133
- Geller, M.J. & Beers, T.C. 1982, PASP, 94, 421
- Ghigna, S., Moore, B., Governato, F., Lake, G., Quinn, T. & Stadel, J. 1998, MNRAS, 300, 146
- Ghigna, S., Moore, B., Governato, F., Lake, G., Quinn, T. & Stadel, J. 2000, ApJ, 544, 616
- Giovannini, G. & Feretti, L. 2000, New Astron., 5, 335
- Giovannini, G., Tordi, M. & Feretti, L. 1999, New Astron., 4, 141
- Gómez, P. L., Hughes, J. P. & Birkinshaw, M. 2000, ApJ, 540, 726
- Gull, S. & Northover, K. 1973, Nature, 244, 80
- Gunn, J.E. & Gott, J.R. 1972, ApJ, 176, 1
- Harris, D.E., Owen, F.N., Biretta, J.A. & Junor, W. 1999, in *Diffuse Thermal and Relativistic Plasma in Galaxy Clusters*, eds. H. Böhringer, L. Feretti & P. Schuecker, MPE Report 271, 111
- Hellsten, U., Gnedin, N.Y. & Miralda-Escudé, J. 1998, ApJ, 509, 56
- Henriksen, M. & Markevitch, M. 1996, ApJL, 466, 79
- Henriksen, M., Donnelly, H. & Davis, D. 2000, ApJ, 529, 692
- Henry, J.P. & Briel, U.G. 1995, ApJL, 443, L9
- Henry, J.P. & Briel, U.G. 1996, ApJ, 472, 137
- Honda, H. et al. 1996, ApJL, 473, L71
- Jones, C. & Forman, W. 1984, ApJ, 276, 38
- Jones, C. & Forman, W. 1999, ApJ, 511, 65
- Jones, C., Mandel, E., Schwarz, J., Forman, W., Murray, S.S. & Harnden, F.R., Jr. 1979, ApJL, 234, L1
- Kirshner, R., Oemler, G., Schechter, P. & Shectman, S. 1981, ApJL, 248, L57
- Laing, R. & Bridle, A. 1987, MNRAS, 228, 557
- Markevitch, M. 2001, in *Galaxy Clusters and the High Redshift Universe Observed in X-rays*, XXI Moriond Astrophysics Meeting (March 2001), eds. D. Neumann, F. Durret, & J. Tran Thanh Van, in press
- Markevitch, M. & Vikhlinin, A. 2001, ApJ, in press, astro-ph/0105093
- Markevitch, M. et al. 2000, ApJ, 541, 542
- Markevitch, M., Sarazin, C.L. & Vikhlinin, A. 1999, ApJ, 521, 526
- Mazzotta, P., Kaastra, J.S., Paerels, F.B., Ferrigno, C., Colafrancesco, S., Mewe, R., Forman, W.R. 2001b, ApJL, in press, astro-ph/0107557
- Mazzotta, P., Markevitch, M., Vikhlinin, A., Forman, W.R., David, L.P. & Van Speybroeck, L. 2001a, ApJ, 555, 205
- McNamara, B. et al. 2000, ApJL, 534, L135
- Moffet, A.T. & Birkinshaw, M. 1989, AJ, 98, 1148
- Mohr, J., Evrard, G., Fabricant, D. & Geller, M. 1995, ApJ, 447, 8

- Mohr, J., Fabricant, D. & Geller, M. 1993, ApJ, 413, 492
- Oegerle, W., Hill, J. & Fitchett, M.J. 1995, AJ, 110, 32
- Owen, F., Eilek, J. & Kassim, N. 1999, in *Diffuse Thermal and Relativistic Plasma in Galaxy Clusters*, eds. H. Böhringer, L. Feretti & P. Schuecker, MPE Report 271, 107
- Owen, F., Eilek, J. & Kassim, N. 2000, ApJ, 243, 611
- Salvador-Solé, E. Sanroma, M. & Gonzalez-Casado, G. 1993, ApJ, 402
- Schindler, S., Binggeli, B. & Böhringer, H. 1999, A&A 343, 420
- Slezak, E., Durret, F. & Gerbal, D. 1994, AJ, 108, 1996
- Van Haarlem, M. & Van de Weygaert, R. 1993, ApJ, 418, 544
- Vikhlinin, A., Forman, W. & Jones, C. 1994, ApJ, 435, 162
- Vikhlinin, A., Markevitch, M. & Murray, S. 2001a, ApJ, 551, 160
- Vikhlinin, A., Markevitch, M. & Murray, S. 2001b, ApJL, 549, L47
- Vrtilek, J.M., David, L.P., Grego, L., Jerius, D., Jones, C., Forman, W., Donnelly, R.H. & Ponman, T.J., in *Constructing the Universe with Clusters of Galaxies*, eds. F. Durret & D. Gerbal, available on CD-Rom and at <http://www.iap.fr/Conferences/Colloque/coll2000/>, contributions Reference: 6.10
- White, S.D.M., Briel, U.G. & Henry, J.P. 1993, MNRAS, 261, L8

Chapter 5

OBSERVATIONAL SIGNATURES AND STATISTICS OF GALAXY CLUSTER MERGERS

Results from X-ray observations with ROSAT, ASCA, and XMM-Newton

Hans Böhringer

Max-Planck-Institut für extraterrestrische Physik

D-85741 Garching, Germany

hxb@mpe.mpg.de

Peter Schuecker

Max-Planck-Institut für extraterrestrische Physik

D-85741 Garching, Germany

peters@mpe.mpg.de

Abstract In this chapter we focus on the discussion of observational data on cluster mergers. The majority of the results shown comes from observations with the *ROSAT* observatory. Results from *ASCA*, *BeppoSAX* and from very recent observations performed with *XMM-Newton* are also included. We discuss the signature and diagnostics of the merger process in galaxy clusters. We show some observable effects caused by mergers. Based on large statistically complete samples of X-ray selected galaxy clusters we consider the frequency and statistics of cluster mergers and compare them to predictions of cosmological models.

Introduction

It has been well established by now that the structure we observe in our Universe today was formed by a hierarchical structure formation process (e.g., White 1997). In this scenario smaller units formed first through gravitational instabilities from positive primordial density fluctuations and merged to larger and larger units in the course of time.

The largest units that have merged and have formed nearly dynamical-equilibrium objects by today are clusters of galaxies with masses covering the range from about $10^{14} - 6 \times 10^{15} M_{\odot}$. The observed and expected space density of clusters is a very steeply decreasing function of mass (e.g., Reiprich & Böhringer 2001) and the probability to observe a virialised object with a mass much larger than $6 \times 10^{15} M_{\odot}$ is negligible.

It is obvious, even intuitively, that the most massive objects form the youngest population in the hierarchical merging process. Therefore if the growth of structure has not stopped yet, we should expect to see many clusters still growing today, where the most massive objects should show the most violent growth. The degree of cluster growth at the present day depends on the current mean density of the universe, with an unimpeded growth for $\Omega_m = 1$ and a decreasing growth rate with decreasing cosmic density (the characteristic formation redshift of clusters is $z_f \sim \Omega_m^{-1} - 1$). There is still a considerable growth rate expected for the current favoured value of $\Omega_m \sim 0.3$ cosmology. Thus we can expect to observe many clusters in the state of merging. The qualitative picture described here can of course be cast into quantitative models either in the form of analytical calculations (e.g., Lacey & Cole 1993) or in the form of numerical simulations as described in the contributions by Schindler, and by Evrard & Gioia in this volume.

Therefore mergers are very important processes in the formation of clusters and many of the observed properties of clusters depend on the physics of the merging process. These observed properties are: density profiles, intracluster plasma temperature and entropy structure, mixing of heavy elements within the intracluster medium, possible acceleration of high energy particles and formation of radio halos, and possible destruction of cooling flows. Furthermore, the gravitational mass is the most fundamental physical parameter characterizing a galaxy cluster and its measurement is of prime importance. Conventionally the mass is measured either based on a virial equilibrium assumption from the spatial distribution and velocity dispersion of the cluster galaxies, as observed in the optical, or based on a hydrostatic equilibrium assumption from the density and temperature distribution of the intracluster gas as observed in X-rays. In both cases the assumption of an equilibrium configuration is violated in the case of a cluster merger. This has been used as an argument for the discrepancy of the mass determination based on the above mentioned methods compared to gravitational lensing studies (e.g., Squires et al. 1996; Böhringer et al. 2000). Good observational diagnostics of the effects of merging processes is important to recognize cases where the mass determination is problematic. Therefore the study of merging processes in clusters is receiving increasing attention.

Since theoretical aspects as well as simulations of cluster mergers are described in detail in other chapters of this book, we concentrate on the observational aspects of the merging process, on its diagnostics and consequences, and on the statistics of cluster mergers as observed in well characterized flux limited X-ray cluster samples.

For the scaling of distance dependent physical parameters of clusters we use a Hubble constant of $H_0 = 50 \text{ km s}^{-1} \text{ Mpc}^{-1}$ throughout this chapter.

1. X-RAY DIAGNOSTICS FOR CLUSTER MERGERS

While the study of cluster mergers is quite difficult at optical wavelength (see Girardi & Biviano, this volume), deep X-ray images can provide more detailed insight into the merger configuration. The X-ray emission originates from hot intracluster gas which is thermally emitting in X-rays and which is trapped in the gravitational potential well of the clusters. The X-ray emission is proportional to the square of the density (emission measure) of the hot gas and the X-ray surface brightness distribution provides an image of the projection of the emission measure distribution. If the cluster is in a relaxed state, the gas density is an ideal tracer of the shape of the gravitational potential and X-ray images are expected to show spherical or elliptical symmetry. In a merging process we expect to see a strong distortion of this symmetry, however, and in an early phase of the merging process we can hope to still recognize the basic structure and the dense central regions of the two or more merging components.

Figures 5.1 and 5.2 show a sequence of merger stages in clusters as observed by *ROSAT* and analysed by Briel & Henry (1998). While the X-ray images provide a good first impression of the merger stage, the X-ray temperature maps, shown along with the images in the figures, give further details of the merger process.

The upper panels of Fig. 5.1 show the Coma cluster illustrating an early stage of a merger of a smaller component in the south-west of the center with a quite massive main cluster (see Briel et al. 1992; White et al. 1993; Briel & Henry 1998 for X-ray observations - and Mellier et al. 1988; Colless & Dunn 1996 for optical observations). Additional substructure has been identified in this X-ray image by White et al. (1993), and it was interpreted as the signature of past mergers of several groups dominated by bright elliptical galaxies with the main cluster. An alternative interpretation of the X-ray system as a post-merger configuration, where the group has passed through the center already once,

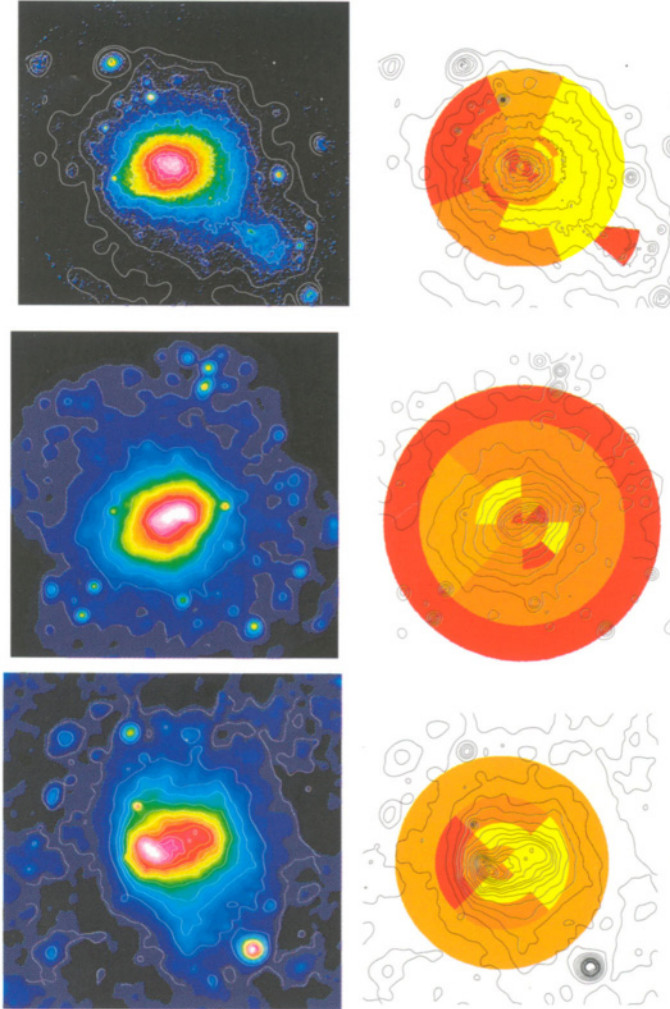


Figure 5.1. ROSAT PSPC images and color-coded temperature maps of a sequence of merging clusters in different stages of merging. Temperature increases going from red to yellow. The clusters are Coma (Briel & Henry 1998), A2256 (Briel & Henry 1994), and A754 (Henry & Briel 1995).

was given by Burns et al. (1994). New *XMM-Newton* data shown in Fig. 5.3 (left panel) provide fresh insight into this system (Neumann et al. 2001). The dominant galaxy NGC 4839, featuring an X-ray emitting

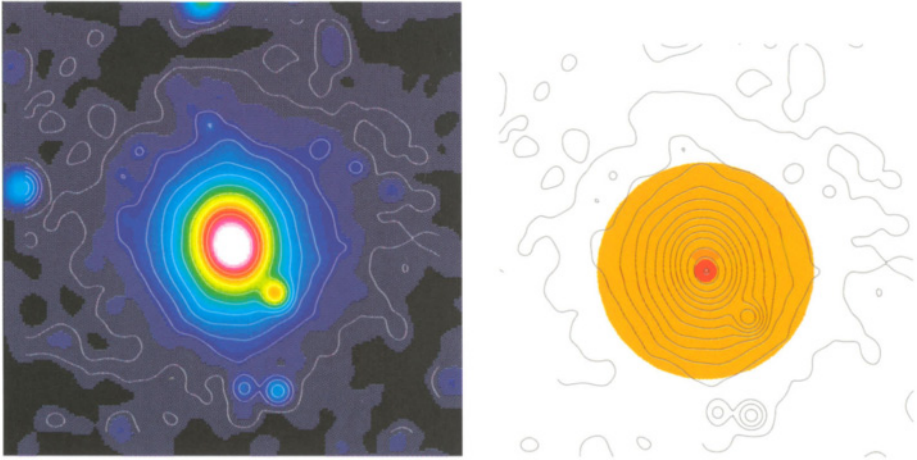


Figure 5.2. ROSAT PSPC image and temperature map of the fairly relaxed galaxy cluster A1795 from Briel & Henry 1996.

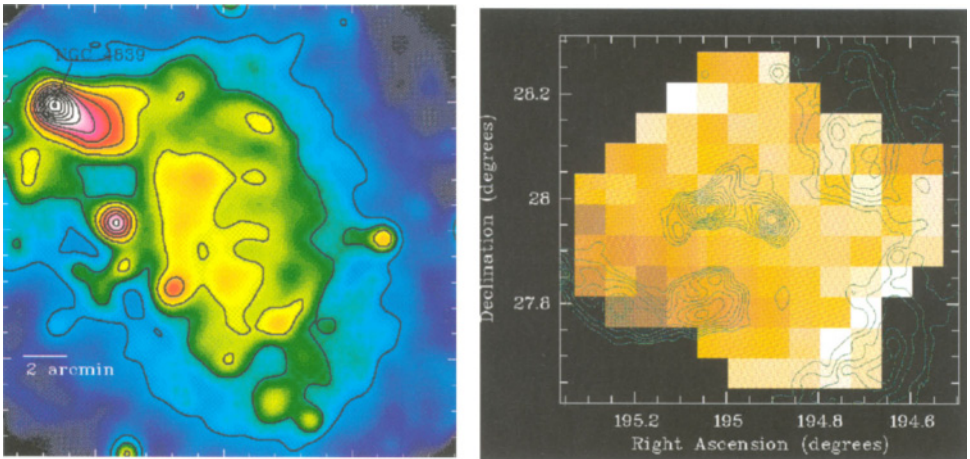


Figure 5.3. **left:** *XMM-Newton* image in the energy band 0.5 to 2.0 keV of the south-western group in the Coma cluster including the bright elliptical galaxy NGC 4839 which is in the stage of merging with the main body of Coma (Neumann et al. 2001) **right:** Temperature map of the central region of the Coma cluster as obtained from the hardness ratio of *XMM-Newton* images by Arnaud et al. (2001). The superposed contours show the deviation in the X-ray surface brightness from a symmetric β -model image of the cluster.

gaseous tail and an associated concentration of galaxies (Mellier et al. 1988), is falling into Coma ahead of the bulk of the X-ray emitting gas. This was interpreted by Neumann et al. (2001) as a deceleration of the intracluster gas associated with the galaxy group in its infall velocity by

the interaction with the intracluster medium of Coma while the infalling galaxies continue to fall undisturbed. This interpretation is supported by the *XMM* observations which clearly indicate an early merger stage. A further signature of the merger process is the increased temperature shown in the interaction region as found in the analysis of the *XMM-Newton* observation of Coma by Arnaud et al. (2001) and Briel et al. (2001) (see Fig. 5.3, right panel). The heating should be the result of adiabatic compression in the contact region of the cluster and the infalling group. A more diffuse signature of the temperature enhancement may be even seen in the *ROSAT* temperature map of Fig. 5.1 (upper right panel).

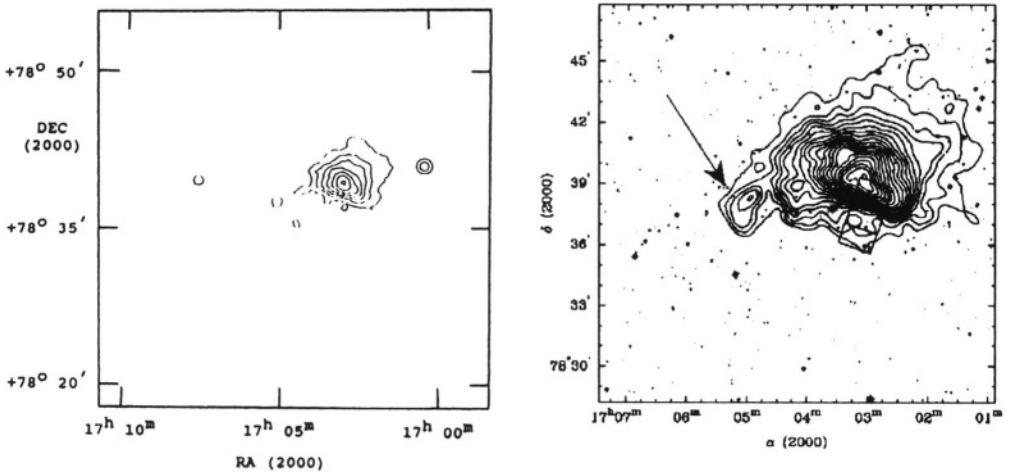


Figure 5.4. **left:** Residual image of the *ROSAT* PSPC X-ray surface brightness distribution in A2256 after subtracting an azimuthally symmetric model image for the main part of the cluster system (Briel et al. 1991). **right:** Similar residual image after subtraction of a symmetric model from the high resolution *CHANDRA* image of A2256 (from Sun et al. 2001). The arrow marks another substructural feature noted by Sun et al. and termed “shoulder” with a lower temperature than the ambient one.

The middle panel in Fig. 5.1 shows the merger in A2256. Also here the two merging components are still quite well separated. This point was illustrated (see Briel et al. 1991) by a decomposition of the image into two components, a main azimuthally symmetric cluster and the residual component (see Fig. 5.4, left panel). There is an indication of a compression of the gas density distribution in the smaller north-eastern component due to the interaction (Briel et al. 1991). In this colliding system the central density of the X-ray emitting gas is higher in the smaller cluster component while the main cluster has a low central

density comparable to the classical non-cooling flow cluster, Coma. The high central gas density of the smaller subcluster is consistent with the standard cooling flow model with a mass flow rate of the order of $10 M_{\odot} \text{ yr}^{-1}$ (see also Fabian & Daines 1991). This may imply that the merger has not reached the stage where the cooling flow is disrupted. However, if the central gas density enhancement would survive the cluster merger, it could introduce a cooling flow into the newly forming cluster. The temperature map in the central right panel of Fig. 5.1 shows that a new feature appears with the progression of the merger. This feature consists of two hot regions close to the center. The hot regions most probably result from heating by an emerging shock which comes out perpendicular to the merger axis.

The recently obtained *CHANDRA* observation of A2256 provides a sharper image and more detailed features of the morphology of this merger system (Sun et al. 2001). The *CHANDRA* temperature map shown in Fig. 5.5 is indeed similar to the *ROSAT* map. The two hot spots seen in the *ROSAT* map (central right panel in Fig. 5.1) are not as pronounced but they coincide with the hottest regions seen in the *CHANDRA* temperature map. The good resolution of *CHANDRA* allows to resolve in more detail the southern edge of the subcluster infalling from the west. The edge is even sharper (Fig. 5.4, right panel) than seen with *ROSAT*. The temperature map shows that the surface brightness edge, which originates in a steep density gradient, is also associated with a strong temperature gradient with an opposite sign. This implies that the discontinuity is approximately in pressure equilibrium. This configuration has been seen in other clusters observed by *CHANDRA* and it has been termed “cold front” (see Forman et al., this volume, and references therein). For a more detailed modeling of this merger system done with simulations see e.g., Schindler & Müller (1993), Roettiger et al. (1995) and Ricker & Sarazin (2001).

In the case of A754, shown in the lower panel of Fig. 5.1, the merger has further progressed making it difficult to recognize the properties of the pre-merging components. The temperature map shows that the hot region has increased in size implying that the shock region has significantly expanded. The cluster is elongated in the east-west direction which is probably the merger axis. There is a dense region of gas which has shifted to the west of the center and with a pronounced elongation perpendicular to the merger axis. The hot region, recognizable in the temperature map as yellowish region to the west of the highest density peak, has a roughly fan shaped appearance. These features are similar to the structure seen in N-body and hydrodynamical simulations of cluster mergers (Evrard 1990; Schindler & Müller 1993; Roettiger et

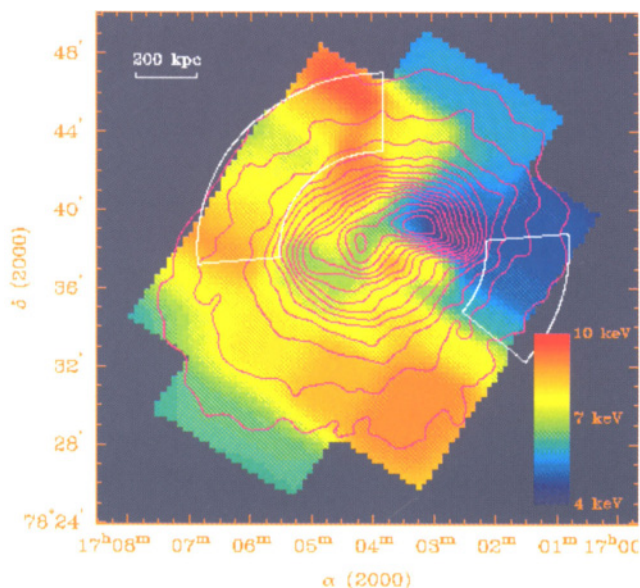


Figure 5.5. Temperature map of the central part of the A2256 merger system obtained from a *CHANDRA* observation by Sun et al. (2001).

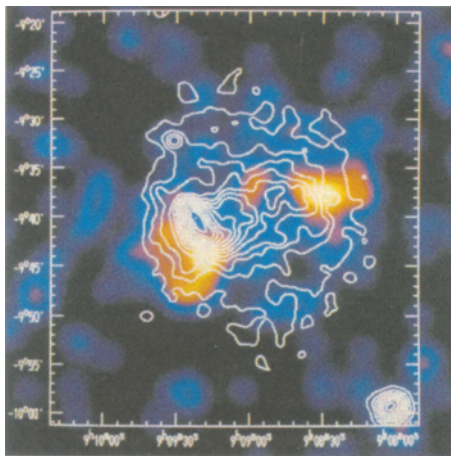


Figure 5.6. Image of the projected galaxy density in A754 obtained from galaxy redshift measurements by Zabludoff & Zaritsky (1995). Superposed in the form of contour lines is the X-ray surface brightness distribution.

al. 1993) which show similar X-ray morphologies. The dense elongated region could be identified as the remnant of the central collision of the two densest gas halo regions of the colliding clusters. The hot region is

the expanding shock wave which starts moving outwards effectively after the central collision has happened. This region is quite one-sided, probably due to the fact that the merger component coming from the west is considerably smaller, and that the eastern part is the more massive collision partner. Therefore the shock wave expands more readily to the west into the region of lower gas density. Such one-sided hot structures are a typical signature of unequal mass mergers and most probably the sites where radio relics develop (see contribution by Giovannini & Feretti in this volume).

Zabludoff and Zaritsky (1995) obtained 341 galaxy redshifts for A754 and made a detailed comparison of the optical and X-ray appearance of this cluster. The projected galaxy density distribution with the *ROSAT* X-ray image superposed is shown in Fig. 5.6. There is a striking offset between the densest galaxy concentrations (both marked by a dominant bright elliptical) and the X-ray peaks which mark the densest gas concentrations - a clear sign that the gas is not in hydrostatic equilibrium. This morphology adds to the interpretation that the cluster is in an advanced stage of merging. The picture is the following: the densest galaxy concentrations may have already crossed the center region; the cores of the gas halos have formed the shock compressed and elongated core; the shock wave has heated the gas halo to the west.

Henricksen & Markevitch (1996) have analysed *ASCA* observations of A754 and found a temperature structure very similar to the one seen in the *ROSAT* data. Henricksen & Markevitch compared their results to a simulation performed by Evrard et al. (1996) of an off-axis merger. A striking similarity was found between the X-ray morphology and the predicted X-ray appearance in the simulations. Following this suggestion Roettiger et al. (1998) performed detailed simulations tailored to the A754 system, including an impact parameter in the collision. The galaxy counts and velocity dispersions around 800 and 900 km s⁻¹ (Escalera & Mazure 1992, Zabludoff & Zaritsky 1995) suggest an almost twice as massive SE component. Based on these optical properties, Roettiger et al. chose a mass ratio of the merging units of 2.5:1, a merger plane perpendicular to the line-of-sight, an impact parameter of about 120 kpc, and a total mass of the system of $1.12 \times 10^{15} M_{\odot}$ resulting in an actual velocity difference of 2500 km s⁻¹. An important ingredient of the model is the more massive gas core of the main component, with central density up to 1.5 times higher than that of the smaller component. Such a complex merger system is very difficult to understand and model, since there are many unknown physical parameters controlling the resulting morphology. Therefore such simulation can only provide a plausible (but not unique) interpretation of the observations. Nevertheless, Roettiger

et al. (1998) found a convincing similarity between the simulations and the observations for an interval of time of about 0.3 Gyr after the core passage when the main clump has entered from the west. The smaller unit has partially gone through the main clump and is now forming the western extension. Another part of the gas of the smaller unit is still streaming against the gas in the X-ray peak. The smaller unit gas is compressing the dense core thus producing a sharp eastern edge by ram pressure. We have described this complex merger system in detail here to illustrate how it is possible to understand such advanced mergers by combining X-ray and optical data and benefitting from N-body-hydrodynamic simulations (for further simulations see, e.g., Ricker & Sarazin 2001).

Fig. 5.2 shows a *ROSAT* X-ray image and temperature map for A1795, a fairly relaxed cluster which has started to cool in the center (Briel & Henry 1996). The central gas temperature has decreased from a mean value of about 6 keV (the main cluster temperature) to a minimum value of about 3 keV. The *ROSAT* result has been recently confirmed by the detailed spectroscopic analysis of the cluster system by Tamura et al. (2001). From their *XMM-Newton* data a value of 6.4 keV is obtained for the mean outer temperature. No significant variation within the error limits (± 1 to ± 1.5 keV) is detected in the outer part the gas. According to the standard cooling flow scenario the dense cool region corresponds to a cooling flow with a mass deposition rate of about $\dot{M} \sim 500 M_{\odot} \text{ yr}^{-1}$ (Allen et al. 2001). A new interpretation of these results may be necessary after the non-detection of cooling gas below about 3 keV in the *XMM* spectra (Tamura et al. 2001). Independent of this interpretation it would take a few Gyr for the gas to cool down to the observed temperature in the central region, assuming that no heating processes are involved (i.e. no major merger). Therefore, the almost spherical symmetry (with a small ellipticity and an extremely small surface brightness enhancement to the north) coupled with the nearly isothermal outer atmosphere and the dense cool region in the center can be interpreted as a clear signature that the cluster has experienced no major merger process for at least the last ~ 4 Gyr (Briel & Henry 1996).

2. THE VIRGO CLUSTER AS A LABORATORY FOR DETAILED MERGER STUDIES

The Virgo cluster, with a distance of about 17 Mpc, is the nearest massive and X-ray bright galaxy cluster. Due to its proximity we can

study its physical processes, including merging and mass accretion, in much more detail than in any other system. At large scales Virgo is a very irregular and unrelaxed system. Fig. 5.7 (left panel) shows a 10×10 degree² X-ray image from the *ROSAT* All-Sky Survey (Böhringer et al. 1994). More than 80% of the X-ray luminosity comes from a spherically symmetric, and centrally peaked, X-ray halo centered on M87, the second brightest elliptical galaxy in Virgo. The central part of the cluster has been interpreted as the relaxed core of the cluster by Böhringer et al. (1994). The southern part is less luminous and has a very low X-ray surface brightness, except for a compact luminous X-ray halo around the brightest galaxy in Virgo, M49. A detailed study of deeper *ROSAT* X-ray images by Irwin & Sarazin (1996) indicate that M49 is attracted towards the northern part of Virgo and the M87 region. Thus this southern unrelaxed part of the Virgo cluster may eventually merge with the northern main cluster body within the next Gyrs.

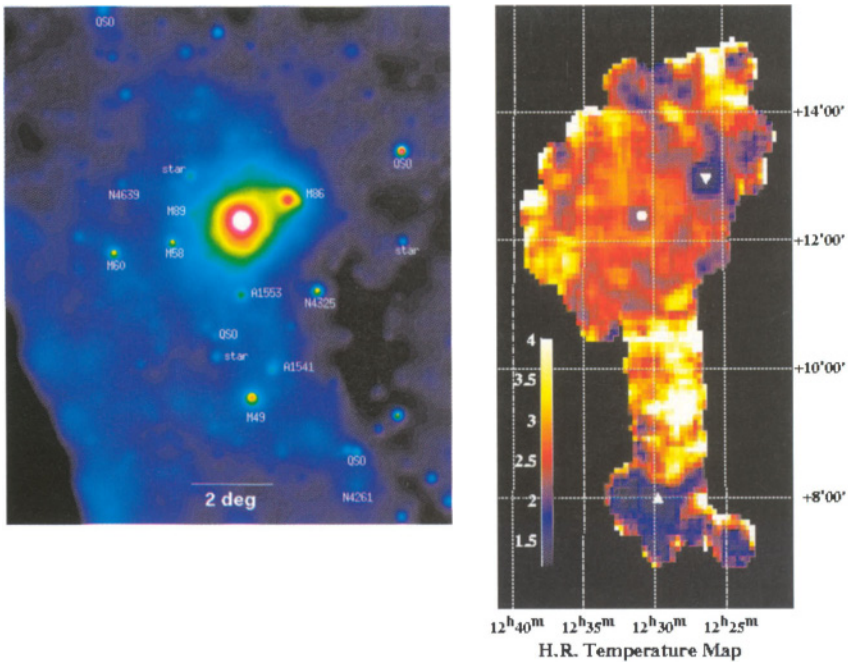


Figure 5.7. **left:** X-ray image of the Virgo cluster from the *ROSAT* All-Sky Survey in the energy band 0.5 to 2 keV (Böhringer et al. 1994). The image covers a region of about 10×10 degree² in the sky. **right:** Temperature map of the Virgo cluster obtained with a mosaic of *ASCA* observations by Shibata et al. (2001). The temperatures have been determined on the basis of hardness ratios. The scale of the individual pixels is 5×5 arcmin². The amplitude of the fluctuations is about 2 keV.

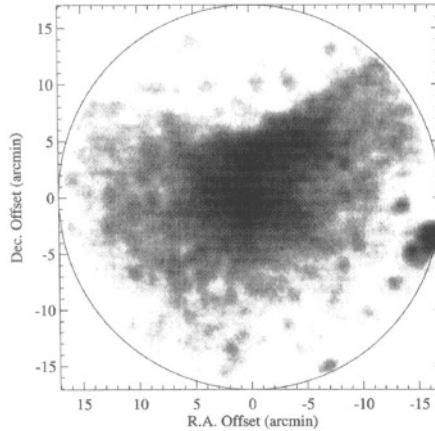


Figure 5.8. ROSAT PSPC X-ray image of the M86 region in the Virgo cluster showing the merging of a galaxy group with the main body of the cluster (Rangarajan et al. 1995).

A more spectacular signature of the merging of a subgroup with the main part of Virgo is seen to the north-west where a galaxy group, associated to the bright elliptical galaxy M86, is falling into the cluster in projection along the line of sight. M86 has a blue-shifted spectrum as seen from Earth with an infall velocity along the line-of-sight into the Virgo cluster of about 1200 km s^{-1} . This infalling galaxy is most probably part of a group composed by several galaxies, mostly dwarf galaxies, with similar infall velocities (see the imaging and redshift survey of the Virgo cluster by Binggeli et al. 1987). An X-ray image of this spectacular merger is shown in Fig. 5.8 (from Rangarajan et al. 1995). The group is far from showing a symmetrical morphology in X-rays. Clear interaction effects are present. The observed X-ray morphology - in particular the very sharp surface brightness edge towards the north - does not have a detailed and satisfactory explanation yet.

A very detailed study of the temperature distribution in the Virgo cluster has recently been performed by Shibata et al. (2001) on the basis of extensive mosaic observations performed with the *ASCA* satellite. A temperature map of the area covered by *ASCA* is shown in Fig. 5.7 (right panel). The map is based on hardness ratio values obtained from a very fine grid with pixel size equal to $5 \times 5 \text{ arcmin}^2$. Small scale temperature variations with amplitude of 2 keV are observed. An autocorrelation analysis of the two-dimensional image shows that these fluctuations have a typical scale of about 300 kpc. The features are interpreted as the signature of several small galaxy groups that have recently

merged with the Virgo cluster (see Shibata et al. 2001 for details). The fluctuations seen are probably the smallest merging features that have been discovered so far.

The merging signatures shown in this section and in the previous one have mostly been observed with the *ROSAT* and *ASCA* observatories. While *ROSAT* has a low energy resolution, *ASCA* has a low angular resolution which gives serious limitations in the construction of temperature maps. Nevertheless results from data taken with *ASCA* and *ROSAT* have already provided interesting insight into the physics of mergers. The new generation of X-ray telescopes, such as *CHANDRA* and *XMM-Newton* observatories, now offers simultaneous good spectral and angular resolution together with increased sensitivity. Therefore a major breakthrough in the understanding of galaxy cluster mergers is expected from the two observatories. The first results from *CHANDRA* and *XMM* shown in this book demonstrate this potential.

3. OBSERVATIONAL CONSEQUENCES OF CLUSTER MERGERS

Cluster mergers have interesting consequences for the observable properties of galaxy clusters. The most important effect is the heating of the cluster gas during the merger event. During this process temperature gradients, in particular the temperature drop caused by the cooling of the dense central gas, seem to be leveled out over a large part of the cluster volume. Thus less strong radial temperature gradients are observed in clusters which have undergone recent mergers. A similar effect is the mixing of the heavy element distribution in clusters.

In very relaxed clusters with central cDs, an increasing abundance gradient of elements (heavier than, and including, Si) as a function of decreasing radius is observed. Fig. 5.9 shows such a dramatic abundance increase at the center of the M87 halo (Böhringer et al. 2001a). The abundance gradient can be explained in terms of recent enrichment of the central intracluster medium mainly by supernovae Type Ia from the stellar population of M87 (see also Matsushita et al. 2001, Finoguenov et al. 2001). The increased metal abundance will only accumulate in the central region with the largest light-to-gas mass ratio as long as the gas is more or less at rest in the cluster. If the cluster is suffering a merger, large enough to strongly affect the central region, the gas will be redistributed. Observations indicate that as a consequence flat metal distributions in merger systems are observed. A recent detailed abundance analysis of *XMM-Newton* data by Arnaud et al. (2001) shows that this is the case for Coma (see Fig. 5.10).

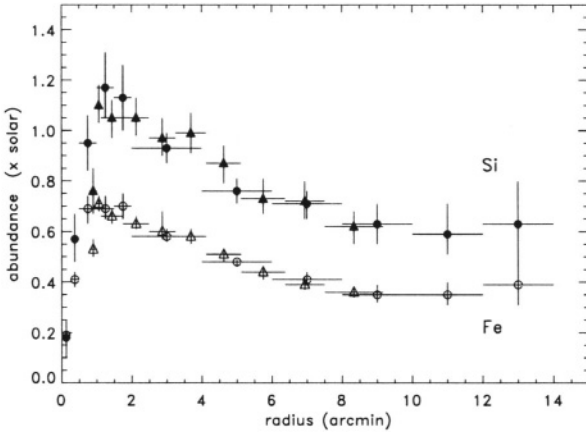


Figure 5.9. Abundance profiles of the elements Fe and Si observed in the X-ray halo of M87 at the center of the Virgo cluster with *XMM-Newton* (Böhringer et al. 2001a). The steep increase of the heavy element abundances towards the center is mainly the result of recent supernova Type Ia enrichment. The abrupt decrease of the abundances in the very central region is most probably an artefact due to resonant line scattering.

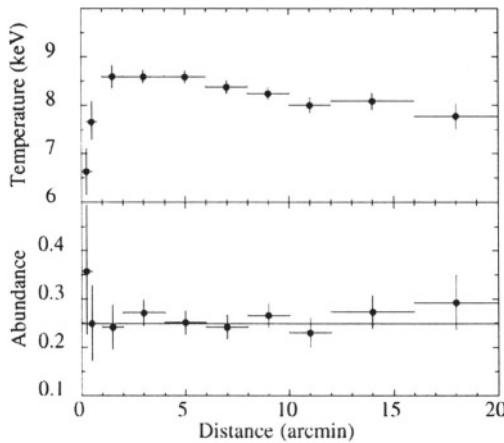


Figure 5.10. Flat metal abundance profile observed in the Coma cluster with *XMM-Newton* by Arnaud et al. (2001)

A systematic study of this effect has been performed by De Grandi & Molendi (2001) for 17 X-ray bright galaxy clusters observed with the *BeppoSAX* observatory. The results, shown in Fig. 5.11, clearly indicate increasing iron abundance profiles in cooling flow clusters which are supposed to be undisturbed by recent mergers. In non-cooling flow clus-

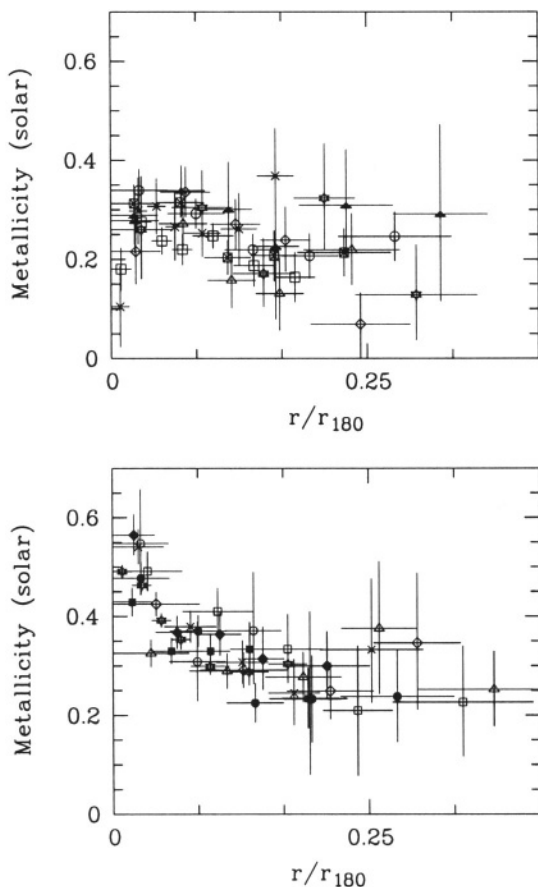


Figure 5.11. Metal density gradients in non-cooling flow clusters (upper panel) and cooling flow clusters (lower panel) as obtained by De Grandi & Molendi (2001) from *BeppoSAX* observations of 17 nearby clusters.

ters (many of which are believed to be merging systems) the metallicity profiles are flat (see also Irwin & Bregman 2001). Similar results have been obtained by Fukazawa et al. (2000) through a systematic analysis of *ASCA* observations of bright, nearby clusters.

Additional important effects caused by mergers are the destruction of cooling flows and the creation of radio synchrotron halos as discussed in detail in the contribution by Sarazin in this volume. One of the most important reasons why cluster mergers are crucial for the formation of radio halos is the release of enormous quantities of energy during the cluster collision. This is the only process known to supply more than sufficient energy over a widespread volume that can easily power the

high energy particle population of a radio halo (e.g., Böhringer et al. 1992; Tribble 1993).

4. MERGER STATISTICS

Differently from the Einstein-de Sitter case, clusters in low- Ω_m universes are expected to be more relaxed, less substructured, and less elongated as shown by the simulations of the Virgo Consortium (Thomas et al. 1998; see also Evrard et al. 1993; Crone et al. 1996; Mohr et al. 1995; Evrard & Gioia, this volume). The violent processes during the merging of subclumps are expected to be detectable in X-rays on time scales of several Gyrs after first core passage, and even 15 Gyr seems to be insufficient for the merger remnants to come to equilibrium (e.g., Ricker & Sarazin 2001). The frequency of these long-lived structures – substructure occurrence rate (SOR) – is thus an important statistical quantity with a direct relation to cosmology. Further discussions of theoretical SORs can be found in Richstone et al. (1992) and Lacey & Cole (1993), partially based on Press Schechter-like theories as presented in Bond et al. (1991) (see also its extension to non-sharp k -space filters in Schuecker et al. 2001a).

The cosmological effects as indicated by mergers are difficult to measure, thus the resulting constraints on structure formation models are currently less stringent than, for instance, the direct measurements of power spectra of cluster number density fluctuations (e.g., Schuecker et al. 2001b). However, a proper evaluation of SORs is very important to understand the processes which are related to the expected hierarchical growth of structure in the Universe, possibly triggering the formation of cluster radio halos and relics, and disrupting cluster cooling flows.

The effects of mergers on spatial X-ray surface brightness and temperature maps are discussed in several chapters of this book (see for instance contributions by Buote and by Forman et al.). Unfortunately, detailed substructure measurements are obtained from interesting but not necessarily representative clusters of galaxies. Examples of projects which aim to get information on merging clusters in a more statistical manner are given in Mohr et al. (1993, 1995); Buote & Tsai (1995, 1996); Slezak et al. (1994); Lazzati et al. (1998); Rizza et al. (1998).

A systematic and comprehensive study of substructure properties compiled in an homogeneous way for a large set of clusters is clearly needed.

One of the first systematic studies of cluster X-ray morphologies for a large statistically representative sample was undertaken by Jones & Forman (1999). These authors used the spatial emissivity distributions

of targeted and serendipitous clusters obtained with the *Einstein* imaging proportional counter (IPC). The X-ray iso-intensity contours of 208 clusters with redshifts $z \leq 0.15$ were classified by visual inspection into the following categories (occurrence rates are given in parenthesis):

Single: no substructure or departures from symmetry (56%). *Double*: two subclusters of comparable size and luminosity (6%). *Primary with small secondary*: main subcluster at least two times brighter than secondary (3%). *Complex*: more than two subclusters (13%). *Elliptical*: elliptical X-ray surface brightness contours (14%). *Offcenter*: peak emission not in center defined by lower surface brightness emission (5%). *Galaxy*: emission dominated by a galaxy (3%).

Jones & Forman (1999) found that 41% of the examined clusters presents asymmetric or otherwise distorted X-ray contours. Such high substructure occurrence rate suggests that a significant fraction of groups and clusters are still forming in the present Universe, and that the idealization of a relaxed, virialized structure is somewhat unrealistic.

The classification of Jones & Forman, though useful, is subjective and should be supplemented by a more homogeneous sample selection and by a more objective, quantitative method to analyse the cluster morphology. A method to quantify substructures in the ROSAT All-Sky Survey (RASS, Trümper 1993; Voges et al. 1999) is described in the following sections.

4.1. ROBUST SUBSTRUCTURE TESTS TO MEASURE SUBSTRUCTURE OCCURENCE RATES

Several substructure tests applicable to deep pointed X-ray data containing a large number of X-ray photons are described in this volume by Buote. Representative SORs can only be obtained with large cluster samples. Unfortunately, the RASS X-ray images which can be used for this purpose have on average a quite low number of X-ray photons (about 300). Therefore, more robust tests for substructure are needed. The relation between substructure, as defined by robust tests, and physical substructure is less direct thus a bigger effort is needed for the physical interpretation of the results. The link between SORs and theoretical merger rates can be obtained when the mass scales of the subclumps and the time scales needed for the merged cluster to reach dynamical equilibrium are known.

Many observational effects become apparent when statistical samples are analysed (see § 4.2) which complicates the interpretation of SORs. After proper correction, semi-analytic Press Schechter-like theories, as

presented for instance in Lacey & Cole (1993), can in principle be applied to understand the rates within a cosmological context (see § 4.3).

The relation between observed SORs and true substructure becomes secondary when SORs obtained for different subsamples drawn from the same parent distribution are compared. In this case the tests define substructure more operationally than what they measure. Thus these tests can serve as a mere link between different cluster types like, for instance, halo/relic clusters, cooling flow clusters, clusters located in high and in low-density regions (see § 4.4 and § 4.5).

N-body simulations of merging clusters of galaxies favour three tests for substructure analysis of two-dimensional distributions: beta test, FEL test and LEE statistic (Pinkney et al. 1996). Translated to the case of X-ray images, the β statistic compares the X-ray emissivity measured around the i th X-ray photon with the emissivity measured in the diametrically opposite site. The emissivities are obtained by weighting each photon with the corresponding exposure time. The final β value is the average of the ratios obtained over all photons (West et al. 1988). The β value is sensitive to deviations from mirror symmetry, independent of the actual elongation of the target. The statistic becomes rather ineffective as the mass ratio of the sub-components approaches 1:1.

Deviations from circular symmetry might indicate merger events (e.g., Roettiger et al. 1997, see also Buote, this volume), although even relaxed clusters can show significant ellipticities (see below). Recent simulations by Thomas et al. (1998), for example, show a dependency of the frequency distribution of cluster major axial ratios on cosmology where the rounder X-ray isophotes in the low Ω_m models result primarily from the scarcity of recent mergers (Evrard et al. 1993). We thus regard elongation as a useful cosmological quantity, although its relation to substructure is not unambiguous. Following Rhee et al. (1991), the azimuthal number counts of X-ray photons are approximated to first order by a constant density, modulated by a double sine. Under this assumption the normalized amplitude (FEL) of this modulation gives a measure of the elongation strength. N-body simulations show that FEL is the most sensitive of the three tests used to check for substructure if elongation is to be considered as substructure.

In the Lee statistic (LEE) the X-ray photons are projected onto lines with different inclination angles, ϕ . In general, for all ϕ and for all partitions of the set of photons, the ‘within-class’ scatter and the ‘between-class’ scatter are determined and their ratios maximized (Fitchett 1988). Fitchett & Webster (1987) successfully applied the method for substructure detection in the core of the Coma galaxy cluster. The Lee likelihood value, L , is most sensitive if two substructure components are present,

especially when they are very compact. It is not sensitive to any elongation, and it loses sensitivity if more than two subclumps are visible. Compared to the other two tests the Lee statistic is thus the most conservative.

To decide whether a cluster shows significant substructure, probabilities are computed that the actual values of the substructure parameters described could be obtained just by chance from an X-ray image satisfying the null hypothesis of a circular symmetric, mirror-symmetric, and unimodal emissivity distribution. The statistical significances, S , thus correspond to the confidence probability, $(1 - S)$, that the null hypothesis can be rejected. The significance values, S_β , S_{FEL} , S_{LEE} , are computed by comparing the β , FEL, and L values obtained for the programme cluster with the corresponding values obtained with a large set of unstructured photon distributions derived from the same cluster. These smooth and symmetric distributions are obtained by azimuthal randomization (West et al. 1988) without the need to choose a specific model cluster profile.

Schuecker et al. (2001c) compares deep *ROSAT* PSPC pointings and the corresponding RASS-3 (third processing of the *ROSAT* All-Sky Survey)¹ images of well-known regular and substructured clusters. It is seen that β and LEE statistics detect substructure under realistic conditions. Tests of FEL suggest that also many regular cooling flow clusters exhibit significant elongation whereas β and LEE statistics do not show any sign of irregularity or multi-modality in these cases. Elongation might thus not be a sufficient criterion for substructure.

4.2. OBSERVED SUBSTRUCTURE OCCURRENCE RATES

Following Jones & Forman (1999) and Mohr et al. (1995), the morphological analyses presented in Schuecker et al. (2001c) is another attempt to measure the substructure occurrence rate for a large sample of X-ray galaxy clusters in a systematic way. Other projects have significantly smaller number of clusters (below 30) so that it is questionable whether they provide a statistically representative census of cluster substructure (see, e.g., Neumann 1997; Rizza et al. 1998; Rhee & Rogers 1998; Kolokotronis et al. 2001).

¹The main advantage of RASS-3 compared to RASS-2 (second processing of the RASS) is that its less stringent constraints on the attitude solutions yield a larger number of accepted X-ray photon events resulting in a higher signal-to-noise without a significant increase of the measurement errors of the individual photons. The advantages of RASS second processing versus the first processing are discussed in Voges et al. (1999).

In Schuecker et al. (2001c) the two largest and almost complete X-ray cluster surveys available to date are used. The working sample counts 452 clusters from the ROSAT-ESO Flux-Limited X-ray (REFLEX) cluster survey (Böhringer et al. 2001b), and 201 clusters from the Brightest Cluster Sample (BCS, Ebeling et al. 1998). The occurrence rates of substructure and elongation are determined within a metric aperture of 1 Mpc using data from the RASS-3. The rates are compared with those obtained for clusters with radio halo/relic and cooling flow signatures (see § 4.5).

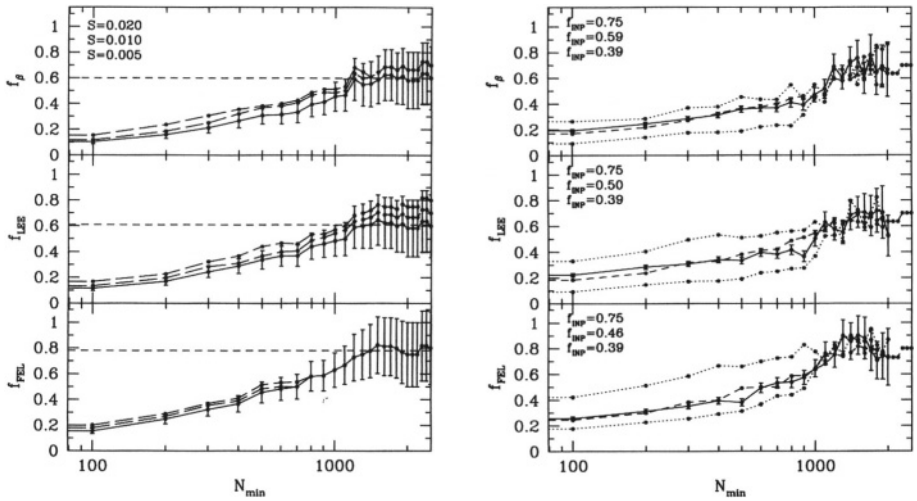


Figure 5.12. **Left:** Fraction, f , of REFLEX+BCS clusters obtained from the RASS-3 as a function of the minimum number of X-ray photons, N_{\min} , with significances less or equal the $S = 0.005$ (lower curves with formal Poisson error bars), 0.01 (middle curves) and 0.02 (upper curves) level. **Right:** Observed significance curves for the REFLEX+BCS clusters with redshifts $z \leq 0.08$ (dashed lines) compared to curves obtained with an empirical model described in the text (continuous lines) covering the same redshift range. The input substructure fractions, f_{INP} , of the template sample used to fit the observations are shown in the upper left of each panel. The central continuous lines represent the best fits of the substructure fraction to the observed curves. All curves are given for the 99% confidence limit.

The observed substructure and elongation occurrence rates, f , of the REFLEX+BCS clusters obtained with β , LEE, and FEL statistics are plotted in Fig. 5.12 (left). The observed fraction of substructured and

elongated clusters increases with the minimum number of X-ray photons, N_{\min} . Similar curves determined for subsamples with upper redshift limits between $z = 0.04$ and 0.40 show z -dependent effects on the 10 % level and must be taken into account.

The observed fractions range between lower limits of 10% to 20% and plateau values of 60% to 78%. As expected, the number of X-ray photons per cluster is an important factor which clearly biases observed SORs. Similar biases are expected when optical galaxies instead of X-ray photons are used to trace substructure. However, the smoothing introduced in X-rays by the pointspread function of the X-ray telescope and detector leads to stronger redshift-dependent effects in X-rays compared to analyses of optical cluster galaxies.

Less biased SORs can be determined from $f(N_{\min})$ curves shown in Figs. 5.12 (left) by the comparison with template samples with known fractions of substructured clusters, f_{INP} . In order to estimate the SOR this input fraction is varied iteratively until good fits of the REFLEX+BCS curves are obtained (see Schuecker et al. 2001c for more details). The best fits (continuous lines in Fig. 5.12, right) give SORs ranging from 46% to 59%. The flatter dotted reference lines obtained for FEL suggest that elongation is less affected at small N_{\min} . This is of great interest when alignment effects of cluster major axes are studied. The final estimate of the ‘true’ SOR as obtained from the formal mean of the three results is $(52 \pm 7)\%$.

How does this SOR estimate compares to results obtained with similar projects in X-rays? As mentioned above, Jones & Forman (1999) find a substructure occurrence rate of 41% by visual inspecting 208 *Einstein* IPC images. Mohr et al. (1995) analysed 65 *Einstein* IPC images using the emission-weighted centroid variation for substructure detection. Kolmogorov-Smirnov tests suggest that the sample is representative. They found a SOR of 61% for the same confidence level (99%) as used for the REFLEX+BCS sample.

It is thus seen that the three largest presently available systematic X-ray cluster works give SORs of about 50 %. However, the conservative (formal) 3σ standard deviation of 30 % between the three estimates already indicates that there is still considerable scatter between different samples and methods. The conservative interval of substructure occurrence rates

$$20 \leq f \leq 80 \text{ percent (99\% confidence range)}, \quad (1)$$

for nearby clusters with $z < 0.15$ might give a realistic picture of the current situation of statistical work on X-ray SORs.

The next step towards a physical understanding of the observed SOR should be the determination of the mass scales of the subclumps and the dynamical time scales involved. Note that the individual contributions of major mergers and accretion to (1) are not given by the measurements. Obtaining quantitative estimates appears to be quite difficult, even if the analysis would have been done with better data and refined substructure tests. However, large sample sizes offer the possibility to calibrate the substructure events at least in a statistical way by the application of the same substructure tests to both observed and simulated cluster X-ray images distributed in flux and redshift in the same way. This would establish the link between substructure as defined by the various measures and the dynamical state of a cluster. Some interesting statistical results obtained from the combination of observational work and numerical experiments can be found, for instance, in Mohr et al. (1995).

Depending on the accuracy of this comparison one should also try to investigate redshift-dependent effects where no information is available. High-resolution N-body simulations of Gottlöber et al. (2001) suggest an increase of major merger rates by a factor of about 2 between redshift $z = 0$ and 0.25.

4.3. THEORETICAL ASPECTS

On the theoretical side SORs are discussed analytically in more detail in Bond et al. (1991), Bower (1991), Richstone et al. (1992), Lacey & Cole (1993, 1994), Kauffmann & White (1993), Kitayama & Suto (1996a,b), Tormen (1998), Percival & Miller (1999), Somerville et al. (2000), Cohn et al. (2001). A frequently applied formalism is the excursion set variant of the Press-Schechter prescription, i.e., the extended Press-Schechter (EPS) formalism which is expected to provide a full theoretical treatment of hierarchical structure formation.

The idea is to describe the hierarchical growth of structure as an abstract diffusion process in a density-contrast/mass space (see also Sarazin, this volume). Here the fraction of trajectories reaching specific density-contrast/mass points are used to derive analytic formulae for mass functions and merger rates. The basic conclusion of the investigations mentioned above is that numerical N-body simulations and EPS semi-analytic estimates of merger counts do roughly agree.

In order to illustrate the inferred results, one can use within the framework of EPS the simplified counting arguments of diffusion trajectories, first discussed in Bond et al. (1991) and Lacey & Cole (1993). The semi-analytic estimate of the conditional probability that a halo of

mass M_2 observed at the cosmic time t_2 has a parent in the mass range $M_2/2 < M_1 < M_2$ at the time $t_1 < t_2$ can thus be used to estimate the fraction of clusters that are formed, i.e., assembled at least half of their mass on the past dynamical time scale of the cluster between t_1 and t_2 (today), where $\Delta t = t_2 - t_1$ represents the time scale over which significant distortions of the cluster potential are detectable.

Assuming that all substructures detected in the observations mentioned in § 4.2 are major merger events in the sense described above (a quite crude assumption), one can compute for a typical cluster with $M_2 = 10^{15} M_\odot$ the SOR for different structure formation scenarios. The theoretical SORs appear to be consistent with the estimate (1) for a standard Cold Dark Matter (CDM) model with $\Omega_0 = \Omega_m = 1$ and dynamical time scales in the range $1.5 \leq \Delta t \leq 3.0$ Gyr. The presently favoured CDM variant with a large cosmological constant (Λ CDM) and $\Omega_m = 0.3$ appears to be consistent with (1) and dynamical time scales > 2.5 Gyr. If we assume that significant distortions of X-ray emissivity distribution of cluster merger are still seen at least 3.5 Gyr after first core passage as suggested by numerical experiments (e.g., Ricker & Sarazin 2001) one could conclude that the presently observed SORs support low-density structure formation models.

However, in addition to the problem that the observed merger events might not necessarily be of the same type as assumed by EPS, the question arises whether the application of EPS is appropriate in general. The similarity of the *statistical* results obtained with N-body simulations and EPS appears to be quite surprising since many assumptions of EPS are expected to be incorrect in detail (see also Conn et al. 2001): spherical collapse (Sheth et al. 2001), monotonic growth of halos (Tormen 1998), association of initial density peaks with final halos (Frenk et al. 1988; Carlberg 1990; Katz et al. 1993), application of sharp k -space filters to frame the region of primordial material that ultimately collapses to form a virialized halo (e.g., Schuecker et al. 2001a). It also appears questionable whether Markovian processes, used to derive EPS, provide the correct theoretical framework (White 1997, Schuecker et al. 2001a).

Note also that in contrast to the general agreement of statistical quantities of simulations and EPS predictions, on the halo-by-halo basis the mass assignment scheme of EPS clearly contradicts numerical experiments (see Fig. 8 in White 1996). Therefore, much work has been done in order to improve the original formalism (see, e.g., Lucchin & Matarrese 1988; Lilje 1992; Cavaliere & Menci 1994; Jedamzik 1995; Monaco 1995, 1997a,b; Yano et al. 1996; Valageas & Schaeffer 1997; Lee & Shandarin 1998; Gross et al. 1998; Sheth et al. 2001; Sheth & Tormen 1999; Jenkins et al. 2001), but without performing the critical halo-by-halo

test (see also Gottlöber et al. 2001). More realistic comparisons of observation and theoretical expectation in the sense described in § 4.2 are clearly needed.

4.4. SUBSTRUCTURE DENSITY RELATION

Clusters in dense supercluster environments are expected to have a higher probability to interact with neighbouring clusters or filamentary structures connecting the cluster centers. If this hypothesis is correct, then larger fractions of clusters with distorted X-ray surface brightness distributions and thus with subclusters are expected in dense environments. To detect this effect, mean significances of β , LEE, and FEL are computed for different local cluster number densities.

As a measure of the local cluster number density around each cluster one can use \bar{d}^{-3} , where \bar{d} is the mean of its five nearest neighbour distances. For flux-limited samples, however, this approach introduces redshift-dependent effects. Therefore the number densities are normalized by the average density obtained with the same density estimator using all clusters in a thin redshift shell centered on the cluster's z value. The normalization has the additional effect of compensating also for edge effects which are known to distort next neighbour statistics (e.g., Cressie 1993).

Figure 5.13 shows the average substructure significances as a function of the normalized cluster number density of REFLEX+BCS clusters excluding the very extreme densities where sample sizes are small and the results quite noisy. It is seen that the average significances of β and LEE decrease with density, indicating that the fraction of substructured clusters increases with local density. The effect is supported by subsamples of nearby clusters with comparatively large numbers of X-ray photons. Even stronger dependencies of the average significances on density are found when the aperture radius used for substructure detection is increased from 1 Mpc to 3 Mpc. For the latter case, however, it cannot be ruled out that neighbouring clusters, not necessarily in the process of merging with the programme cluster, might artificially increase SOR.

Contrary to the results obtained with β and LEE, the elongation significances, S_{FEL} , are found to be almost insensitive to local cluster number density. It should be mentioned that a strong density-dependence is still present for FEL when 3 Mpc aperture radii are used for substructure analyses.

This substructure density relation of clusters appears to be analogous to the morphology density relation of galaxies. A related effect, namely that dynamically young optical APM clusters are more clustered than

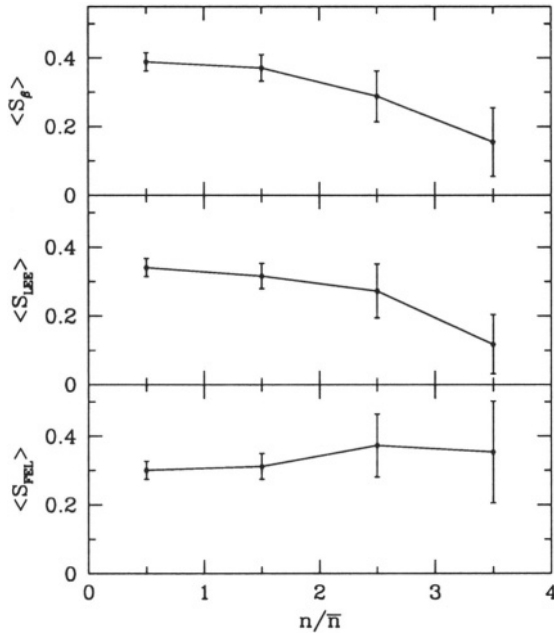


Figure 5.13. Average significances and standard deviations for the three statistical tests as a function of the local cluster number density, normalized to the average density obtained with the 238 REFLEX+BCS clusters with at least 150 X-ray photons.

the overall cluster population, was recently found by Plionis (2001) thus supporting the present findings.

4.5. SUBSTRUCTURES IN HALO, RELIC, AND COOLING FLOW CLUSTERS

In many deep X-ray pointed observations, clusters with radio halos/relics show indication for substructure whereas clusters with cooling flow signatures usually show quite regular X-ray surface brightness distributions. The question is whether these differences can be regarded as statistically significant when compared to large reference samples assumed to be representative.

For a sample of 53 halo and relic clusters compiled by Feretti (private communication), 22 clusters with cooling flow mass deposition rates $\geq 100 M_\odot \text{ yr}^{-1}$, selected from the list presented in Peres et al. (1998), and 470 REFLEX+BCS clusters, the significance histograms and their 1σ errors (points with error bars) are given in Figs. 5.14. Note that large count rates in the first S_β bin indicates a high fraction of irregular clusters. Similarly, high rates in the first bin of the S_{LEE} and S_{FEL}

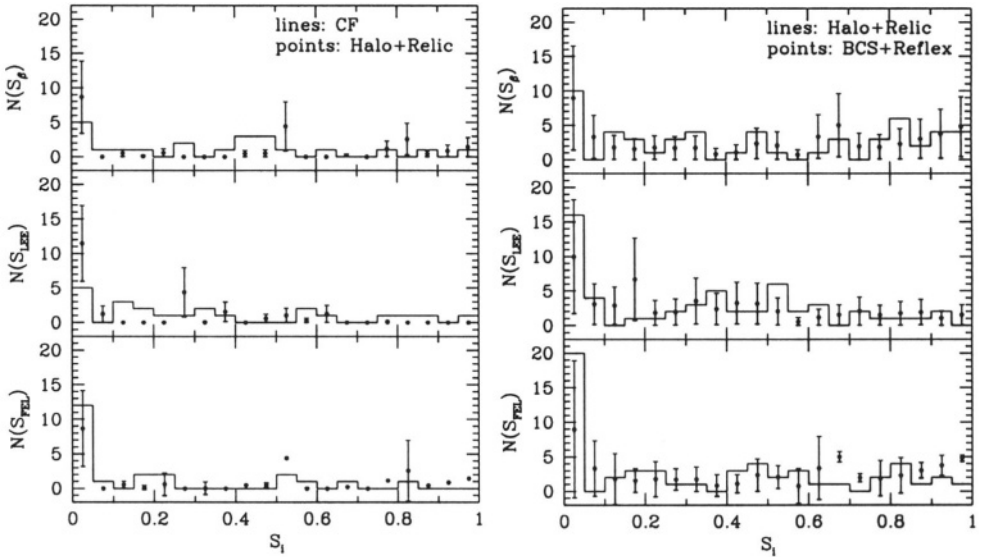


Figure 5.14. **Left:** Frequency distributions of substructure significances for cooling flow clusters (lines) and halo+relic clusters (points). **Right:** Same as left for halo/relic clusters (lines) and BCS+Reflex clusters (points).

histograms suggest large fractions of bi-modal and elongated X-ray surface brightness distributions, respectively. The computations of the histograms take into account the different ‘sensitivities’ for substructure detection of the different samples in a similar way as in § 4.2.

The comparison indicates that halo/relic, cooling flow, and REFLEX+BCS clusters differ in their substructure behaviour on the $1-2\sigma$ level. Although the difference is not strong, the general picture that cooling flow clusters appear to be more regular and halo/relic clusters more often substructured is clearly supported.

To be more specific, the largest differences between the substructure occurrence rates are found when halo/relic and cooling flow clusters are compared (see Fig. 5.14, left panel). It is seen that even after proper equalization of the different sensitivities for substructure detection, the radio halo/relic clusters are more often irregular and bi-modal. However, elongated isophotes appear to be a common feature for both cluster types with a marginally higher fraction for cooling flow clusters. The same trends are found when cooling flow clusters are compared with REFLEX+BCS clusters (not shown here) increasing the significance of the effect because an independent reference sample is used.

Figure 5.14 (right panel) shows that the fraction of bi-modal and elongated halo/relic clusters is higher compared to the REFLEX+BCS reference sample. However, for irregularity (β statistic) almost the same high substructure occurrence rates are found.

It is thus seen that basically all measurements, although each on a marginal significance level, are found to be consistent with the idea that radio halos and relics are triggered by merger events (Harris et al. 1980; Burns et al. 1995; Feretti & Giovannini 1996; Sarazin, this volume; Giovannini & Feretti, this volume), and that pre-existing cooling flows might be disrupted by recent major merger events.

Acknowledgments

The authors wish to thank U.G. Briel and J.P. Henry for providing the beautiful *ROSAT* illustrations of cluster mergers.

References

- Allen, S.W., Fabian, A.C., Johnstone, R.M., Arnaud, K.A. & Nulsen, P.E.J. 2001, MNRAS, 322, 589
- Arnaud, M. et al. 2001, A&A, 365, L67
- Binggeli, B., Tammann, G.A. & Sandage, A. 1987, AJ, 94, 251
- Böhringer, H. et al. 2001a, A&A, 365, L181
- Böhringer, H., Briel, U.G., Schwarz, R.A., Voges, W., Hartner, G. & Trümper, J. 1994, Nature, 368, 828
- Böhringer, H. et al. 2001b, A&A, 369, 826
- Böhringer, H., Schwarz, R.A., Briel, U.G., Voges, W., Ebeling, H., Hartner, G. & Cruddace, R.G. 1992, in *Clusters and Superclusters of Galaxies*, ed. A.C. Fabian, Kluwer Academic Publishers, 71
- Böhringer, H., Soucail G., Mellier Y., Ikebe Y. & Schuecker P. 2000, A&A, 353, 124
- Bond, J.R., Cole, S., Efstathiou, G. & Kaiser, N. 1991, ApJ, 379, 440
- Bower, R.J. 1991, MNRAS, 248, 332
- Briel, U.G. et al. 1991, A&A, 246, L10
- Briel, U.G., Henry, J.P., & Böhringer, H. 1992, A&A, 259, L31
- Briel, U.G. & Henry, J.P. 1994, Nature, 372, 439
- Briel, U.G. & Henry, J.P. 1996, ApJ, 472, 137
- Briel, U.G. & Henry, J.P. 1998, in *A New Vision of an Old Cluster: Untangling Coma Berenices*, eds. A. Mazure, F. Casoli, F. Durret & D. Gerbal, World Scientific Publishing, 170
- Briel, U.G. et al. 2001, A&A, 365, L60
- Buote, D.A. & Tsai, J.C. 1995, ApJ, 452, 522
- Buote, D.A. & Tsai, J.C. 1996, ApJ, 458, 27

- Burns, J. O., Roettiger, K., Ledlow, M. & Klypin, A. 1994, ApJ, 427, L87
- Burns, J.O., Roettiger, K., Pinkney, J. Perley, R.A., Owen, F.N. & Voges, W. 1995, ApJ, 446, 583
- Carlberg, R.G. 1990, ApJ, 350, 505
- Cavaliere, A. & Menci, N. 1994, ApJ, 435, 528
- Cohn, J.D., Bagla, J.S. & White, M. 2001, MNRAS, 325, 1053
- Colless, M. & Dunn, A.M. 1996, ApJ, 458, 435
- Cressie, N.A.C. 1993, *Statistics for Spatial Data*, Publ. Wiley & Sons, New York, 602
- Crone, M.M., Evrard, A.E. & Richstone, D.O. 1996, ApJ, 467, 489
- De Grandi, S. & Molendi, S. 2001, ApJ, 551, 153
- Ebeling, H., Edge, A.C., Böhringer, H., Allen, S.W., Crawford, C.S., Fabian, A.C., Voges, W. & Huchra, J.P. 1998, MNRAS, 301, 881
- Escalera, E. & Mazure, A. 1992, ApJ, 388, 23
- Evrard, A.E. 1990, ApJ, 363, 349
- Evrard, A.E., Metzler, C.A., Navarro, J.F. 1996, ApJ, 469, 494
- Evrard, A.E., Mohr, J.J., Fabricant, D.G. & Geller, M.J. 1993, ApJL, 419, L9
- Fabian, A.C. & Daines, S.J., 1991, MNRAS, 252, 17
- Feretti, L. & Giovannini, G. 1996, in *Extragalactic Radio Sources*, eds. R. Ekers, C. Fanti & L. Padrielli, Kluwer Academic Publishers, 333
- Finoguenov, A., Matsushita, K., Böhringer, H., Ikebe, Y. & Arnaud, M. 2001, A&A, in press, astro-ph/01110516
- Fitchett, M.J. 1988, MNRAS, 230, 161
- Fitchett, M.J. & Webster, R.L. 1987, ApJ, 317, 653
- Frenk, C.S., White, S.D.M., Davis, M. & Efstathiou, G. 1988, ApJ, 327, 507
- Fukazawa, Y., Makishima, K., Tamura, T., Nakazawa, K., Ezawa, H., Ikebe, Y., Kikuchi, K. & Ohashi, T. 2000, MNRAS, 313, 21
- Gottlöber, S., Klypin, A. & Kravtsov, A.V. 2001, ApJ, 546, 223
- Gross, M.A.K. et al. 1998, MNRAS, 301, 81
- Harris, D.E., Lari, C., Vallee, J.P. & Wilson, A.S. 1980, A&AS, 42, 319
- Henriksen, M.J. & Markevitch, M.L. 1996, ApJL, 466, L79
- Henry, J.P. & Briel, U.G. 1995, ApJL, 443, L9
- Irwin, J.A. & Sarazin, C.L. 1996, ApJ, 471, 683
- Irwin, J.A. & Bregman, J.N. 2001, ApJ, 546, 150
- Jedamzik, K. 1995, ApJ, 448, 1
- Jenkins, A., Frenk, C.S., White, S.D.M., Colberg, J.M., Cole, S., Evrard, A.E., Couchman, H.M.P. & Yoshida, N. 2001, MNRAS, 321, 372
- Jones, C. & Forman, W. 1999, ApJ, 511, 65
- Katz, N., Quinn, T. & Gelb, J.M. 1993, MNRAS, 265, 689

- Kauffmann, G. & White, S.D.M. 1993, MNRAS, 261, 921
- Kitayama, T. & Suto, Y. 1996a, MNRAS, 280, 638
- Kitayama, T. & Suto, Y. 1996b, ApJ, 469, 480
- Kolokotronis, V., Basilakos, S., Plionis, M. & Georgantopoulos, I. 2001, MNRAS, 320, 49
- Lacey, C. & Cole, S. 1993, MNRAS, 262, 627
- Lacey, C. & Cole, S. 1994, MNRAS, 271, 676
- Lazzati, D., Campana, S., Rosati, P., Chincarini, G. & Giacconi, R. 1998, A&A, 331, 41
- Lee, J. & Shandarin, S.F. 1998, ApJ, 500, 14
- Lilje, P.B. 1992, ApJL, 386, L33
- Lucchin, F. & Matarrese, S. 1988, ApJ, 330, 535
- Matsushita, K., Belsole, E., Finoguenov, A. & Böhringer, H. 2001, A&A submitted
- Mellier, Y., Mathez, G., Mazure, A., Chauvineau, B. & Proust, D. 1988, A&A, 199, 67
- Mohr, J.J., Evrard, A.E., Fabricant, D.G. & Geller, M.J. 1995, ApJ, 447, 8
- Mohr, J.J., Fabricant, D.G. & Geller, M.J. 1993, ApJ, 413, 492
- Monaco, P. 1995, ApJ, 447, 23
- Monaco, P. 1997a, MNRAS, 287, 753
- Monaco, P. 1997b, MNRAS, 290, 439
- Neumann, D.M. 1997, PhD thesis (Univ. München)
- Neumann, D.M. et al. 2001, A&A, 365, L74
- Percival, W.J. & Miller, L. 1999, MNRAS, 309, 823
- Peres, C.B., Fabian, A.C., Edge, A.C., Allen, S.W., Johnstone, R.M. & White, D.A. 1998, MNRAS, 298, 416
- Pinkney, J., Roettiger, K., Burns, J.O. & Bird, C.M. 1996, ApJS, 104, 1
- Plionis, M. 2001, in *Galaxy Clusters and the High Redshift Universe Observed in X-rays*, eds. D. Neumann, F. Durret & J. Tran Thanh Van, in press, astro-ph/0105522
- Rangarajan, F.V.N., White, D.A., Ebeling, H., Fabian, A.C. 1995, MNRAS, 277, 1047
- Reiprich, T.H. & Böhringer, H. 2001, ApJ submitted
- Rhee, G. & Rogers, P. 1998, Abstracts of the 19th Texas Symposium on *Relativistic Astrophysics and Cosmology*, eds. J. Paul, T. Montmerle & E. Aubourg, Publ. CEA, Saclay, 541
- Rhee, G.F.R.N., van Haarlem, M.P. & Katgert, P. 1991, A&AS, 91, 513
- Richstone, D., Loeb, A. & Turner, E. 1992, ApJ, 393, 477
- Ricker, P.M. & Sarazin, C.L., 2001, ApJ in press, astro-ph/0107210
- Rizza, E., Burns, J.O., Ledlow, M.J., Owen, F.N., Voges, W. & Bliton, M. 1998, MNRAS, 301, 328

- Roettiger, K., Burns, J.O. & Loken, C. 1993, ApJL, 407, L53
- Roettiger, K., Burns, J.O. & Pinkney, J. 1995, ApJ, 453, 634
- Roettiger, K., Loken, C. & Burns, J.O. 1997, ApJS, 109, 307
- Roettiger, K., Stone, J.M., Mushotzky, R.F. 1998, ApJ, 493, 62
- Schindler, S. & Müller, E. 1993, A&A, 272, 137
- Schuecker, P., Böhringer, H., Arzner, K. & Reiprich, T.H. 2001a, A&A, 370, 715
- Schuecker, P. et al. 2001b, A&A, 368, 86
- Schuecker, P., Böhringer, H., Reiprich, T.H. & Feretti, L. 2001c, A&A, 378, 408
- Sheth, R.K. & Tormen, G. 1999, MNRAS, 308, 119
- Sheth, R.K., Mo, H.J. & Tormen G. 2001, MNRAS, 323, 1
- Shibata, R., Matsushita, K., Yamasaki, N.Y., Ohashi, T., Ishida, M., Kikuchi, K., Böhringer, H. & Matsumoto, H. 2001, ApJ, 549, 228
- Slezak, E., Durret, F. & Gerbal, D. 1994, AJ, 108, 1996
- Somerville, R. et al. 2000, MNRAS, 316, 479
- Squires, G.G., Kaiser, N., Fahlman, G., Woods, D., Babul, A., Neumann, D. & Böhringer, H. 1996, ApJ, 461, 572
- Sun, M., Murray, S.S., Markevitch, M. & Vikhlinin, A. 2001, ApJ, in press, astro-ph/0103103
- Tamura, T. et al. 2001, A&A, 365, L87
- Thomas, P.A. et al. (the Virgo Consortium) 1998, MNRAS, 296, 1061
- Tormen, G. 1998, MNRAS, 297, 648
- Trümper J., 1993, Science, 260, 1769
- Tribble, P.C. 1993, MNRAS, 263, 31
- Valageas, P. & Schaeffer, R. 1997, A&A, 328, 435
- Voges, W. et al. 1999, A&A, 349, 389
- West, M.J., Oemler, A., Jr. & Dekel, A. 1988, ApJ, 327, 1
- White, S.D.M. 1996, in *Cosmology and Large-Scale Structure*, eds. R. Schaeffer, J. Silk, M. Spiro & J. Zinn-Justin, Publ. Elsevier, Dordrecht, 349
- White, S.D.M. 1997, in *The Evolution of the Universe*, eds. G. Börner & S. Gottlöber, Publ. Wiley & Sons, New York, 227
- White, S.D.M., Briel, U.G., Henry, J.P. 1993, MNRAS, 261, L8
- Yano, T., Nagashima, M. & Gouda, N. 1996, ApJ, 466, 1
- Zabludoff, A.I. & Zaritsky, D. 1995, ApJL, 447, L21

Chapter 6

RADIO GALAXIES AND THEIR ENVIRONMENT

Luigina Feretti

Istituto di Radioastronomia CNR

Via P. Gobetti 101

I-40129 Bologna, Italy

lferetti@ira.bo.cnr.it

Tiziana Venturi

Istituto di Radioastronomia CNR

Via P. Gobetti 101

I-40129 Bologna, Italy

tventuri@ira.bo.cnr.it

Abstract In this paper we review the properties of radio galaxies in connection to the effect of the dynamic gaseous environment inside clusters in which they are embedded. The external gas can interact with a radio source in different ways: modifying its morphology via ram-pressure, confining the radio lobes, possibly feeding the active nucleus, enhancing star formation, exerting stripping effects on the galaxy's gaseous component. We present the different classes of radio galaxy structures, and provide evidence that the presence of the intracluster gas and of cluster/subcluster mergers play an important role in their formation and evolution. The statistical characteristics of radio galaxies are described, and shown to be surprisingly similar for sources both in and outside of rich clusters. The effect of the environment on starburst emission and gas stripping is also described and results on late type galaxies, richer in gas content than ellipticals, are presented.

Introduction

The radio emission originating from individual elliptical galaxies, mapped over the last decades with sensitive radio telescopes, is frequently

found to extend well beyond the physical size of the host galaxy (≥ 100 kpc).

Radio galaxies of high and low luminosity have quite different radio morphologies on kiloparsec scale. A simple but important morphological classification of extended radio structures was made by Fanaroff & Riley (1974) who pointed out that low-power sources tend to be brightest close to their nuclei whereas high-power ones are brightest at their outer extremities. Sources with $P_{1.4 \text{ GHz}} \lesssim 10^{24.5} \text{ W Hz}^{-1}$ tend to have their brightness peaks less than half way from the nucleus to the outer edges (FRI, see Fig. 6.1) and those with $P_{1.4 \text{ GHz}} \gtrsim 10^{24.5} \text{ W Hz}^{-1}$ have the peaks more than half way out (classical doubles, FR II, Fig. 6.2). Further work has shown that the characteristic optical luminosity dividing FRIs from FR IIs is a function of galaxy magnitude, but the transition remains extremely sharp (Owen & Ledlow 1994).

In addition, the knowledge of the environment of radio galaxies has greatly increased in the past 20 or so years, thanks to the sensitivity achieved by X-ray satellites. Hot X-ray emitting gas is found to be associated with galaxy clusters and groups (see Sarazin 1986 for a review), so the possible effect of the gaseous environment on the extended radio sources can be investigated in detail. In particular, the properties of radio galaxies in and out of the rich cluster environment can be compared to look for differences in the host galaxies, the distribution of sources in morphology, radio luminosity, and size. Another important issue is to understand if and how the cluster environment plays any role in the statistical radio properties of galaxies, i.e. their probability of forming radio sources.

Our understanding of the dynamical evolutionary state of clusters of galaxies is undergoing major changes. Clusters are no longer believed to be simple relaxed structures but are interpreted in the framework of the hierarchical growth of rich clusters via mergers of poor groups. This merger activity appears to be continuing at the present time, and would explain the relative abundance of substructure in Abell clusters. It is also supported by temperature gradients detected in the cluster intergalactic medium by X-ray observations. The intracluster medium (ICM) within merging clusters is likely to be in a violent or turbulent dynamical state which may have a significant effect on the radio source morphology and the evolution of cluster radio galaxies.

Mergers generate expansion shocks in the ICM through which individual galaxies may pass. In doing so, they will experience an increase in ram pressure which can induce a burst of star formation changing the observed galaxy's colours and stellar content. The ram pressure may also strip the galaxy of its gas content reducing the potential for fu-

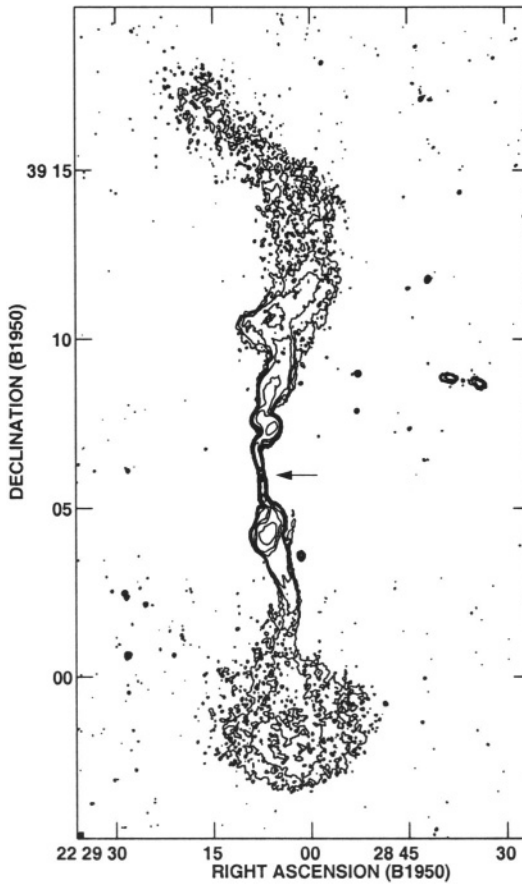


Figure 6.1. The radio galaxy 3C449 is an example of a FRI radio source. The arrow indicates the location of the radio nucleus and of the parent galaxy. The structure consists of two opposite jets, emanating from the nucleus, and two extended lobes of low brightness. The sources of the FRI class have low-intermediate radio luminosity.

ture star formation and thus altering the galaxy's observed colour and morphology.

In this paper, these effects are discussed in detail and the observational evidence in their support is reported. Results are given mostly for the radio sources associated with elliptical galaxies, i.e. the classical radio galaxies whose origin is due to an active galactic nucleus. Some results are also presented for spiral galaxies, which show fainter radio emission

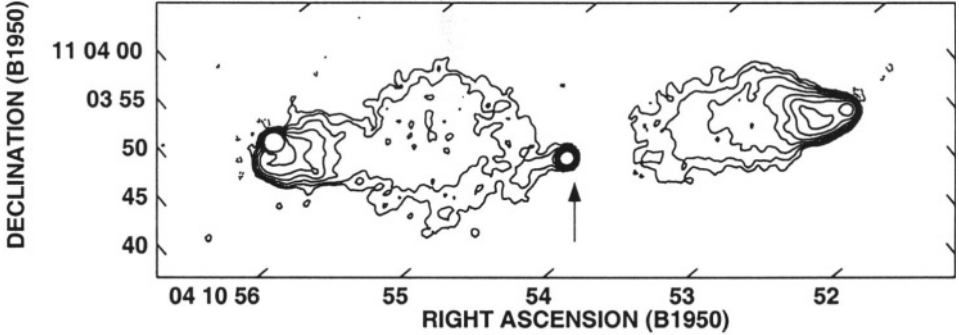


Figure 6.2. The radio galaxy 3C109 is an example of FR II radio source. The arrow indicates the location of the radio nucleus and of the parent galaxy. This structure, characterized by two bright hot-spots at the source extremes, is associated with powerful radio sources.

with respect to ellipticals, but are richer in gas and therefore suitable for studying the interaction with the environment.

A Hubble constant $H_0=50 \text{ km s}^{-1} \text{ Mpc}^{-1}$ and $q_0=0.5$ are used.

1. CLUSTER X-RAY EMITTING GAS

It is well established that a significant amount of hot gas is present within rich clusters of galaxies as well as in poor groups, as detected by the free-free emission in the X-ray band. The general morphology of the cluster gas can be approximated by the hydrostatic isothermal model (Cavaliere & Fusco-Femiano 1981), the density profile $n(r)$ can be described by the law

$$n(r) = n_0 \left(1 + \frac{r^2}{r_c^2}\right)^{-3\beta/2} \quad (1)$$

where n_0 is the central density, r_c is the core radius, and β is the slope parameter, originating from the ratio between kinetic energy in the galaxies and thermal energy of the gas.

Values of n_0 in clusters and groups are in the range 10^{-3} – 10^{-2} cm^{-3} and 10^{-4} – 10^{-3} cm^{-3} , respectively. Cluster core radii are typically of about 200 kpc. Gas temperatures are 2–10 keV in clusters and 1–3 keV in groups (Sarazin 1986, David et al. 1993, Mulchaey et al. 1993, Feretti et al. 1995).

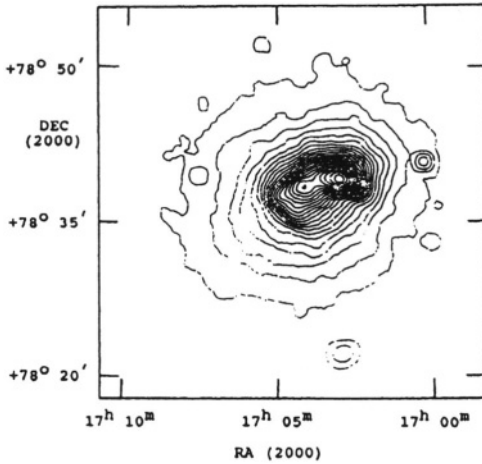


Figure 6.3. X-ray image of A2256 taken with the ROSAT PSPC in the energy band from 0.1-2.4 keV. The cluster shows two clumps of emission, indicative of two merging subclusters. The picture is from Briel et al. (1991).

Our view of galaxy clusters, however, has changed dramatically in the past decade with the detection of a significant amount of substructure, as indicated by the presence of X-ray clumps, twisted X-ray isophotes, central X-ray elongations, and temperature structure. Spatial substructure (“clumpiness”) was noted in early X-ray images of clusters (e.g., Forman & Jones 1982) and confirmed by a more recent analysis of Einstein images (Jones & Forman 1999, Mohr et al. 1993, Burns et al. 1994). Higher resolution ROSAT images have uncovered a great variety of X-ray substructures in clusters (Burns et al. 1994), in particular in Coma (White et al. 1993), which was previously believed to be a relaxed cluster, and A2256 (Briel et al. 1991, Fig. 7.6). These X-ray clumps have been interpreted as the remnants of cluster merger events. Therefore, clusters are very far from being simple spherical, isolated structures in virial and hydrostatic equilibrium. Rather, they are more dynamic, and younger systems whose intracluster medium and gravitational potential well continue to evolve even at the present epoch by accreting gas and galaxies and by merging with other clusters/groups (roughly every few Gyrs). Simulations suggest that the ICM within clusters is violent, filled with shocks, high winds and turbulence (see contributions by Sarazin and by Schindler, in this volume).

In addition, in the central regions of many clusters, the density of the ICM rises sharply and the inferred cooling time is significantly less than the Hubble time ($t_{cool} \geq 10^9 yr$; e.g., Edge et al. 1992). In the absence of

forces other than thermal pressure and gravity, the cooling of the ICM leads to a slow net inflow of material towards the cluster center, which is called a *cooling flow* (see Fabian 1994 for a review of the theory and observations). The environment at the centers of galaxy cluster cooling flows is extreme. The ICM thermal pressure is a factor of 10–100 times higher than that near other cluster galaxies. Any preexisting cooling flow may be disrupted by cluster mergers (Roettiger et al. 1993, Edge et al. 1992).

With such changes taking place in the cluster gas, one should ask what effect this will have on extended radio plasma associated with radio galaxies inside clusters.

2. RADIO STRUCTURES

Cluster radio galaxies are predominantly FR class I (i.e., low power, edge darkened). According to Prestage & Peacock (1988), FRIs are associated with giant ellipticals similar to first ranked galaxies, while FRIIs are identified with galaxies of lower optical luminosity and exist in poorer clusters. The FRI sources are typically found in regions of significantly enhanced galaxy density. Conversely, FRII sources appear to differ in their cluster environments only marginally from elliptical galaxies drawn at random from the whole population. The cluster environment of a statistical sample of nearby radio galaxies was investigated by Miller et al. (1999) in both the X-ray and the optical. They found that many of the nearby radio galaxies do in fact reside in cluster environments, with the FRI's more likely associated with some amount of clustering than FRII's.

In general, cluster radio sources are characterized by complex structures, with prominent distortions, resulting from the interaction between the radio emission regions and the ambient gas. A common morphology is represented by the *tailed radio galaxies*, i.e. FRI sources where the large scale low-brighthness emission is bent toward the same direction, forming features similar to tails. These radio galaxies were originally distinguished in 2 classes: narrow-angle tailed sources (NAT), which are "U" shaped, i.e. with a small angle between the tails, and wide-angle tailed sources (WAT), which are "V" shaped, i.e. with a larger angle between the tails. We note that distortions in FRIIs are marginal and only in weak structures.

2.1. NARROW-ANGLE TAILED RADIO GALAXIES

The most striking example of the interaction between the ICM and radio sources is provided by the head-tail, or NAT, sources (Rudnick & Owen 1976, O’Dea & Owen 1985). These sources have radio jets that are bent at extreme angles, up to 90° , from their original orientation. They have typical luminosities of FRI sources, and are identified with cluster galaxies located at any distance from the cluster center. The NAT radio sources generally show a high degree of polarization in the tails (up to 40–50%) with the intrinsic magnetic field parallel to the tail direction. Typical ages at the end of the tails, derived from spectral index arguments, are around 5×10^7 years (e.g., Feretti et al. 1998, 1999).

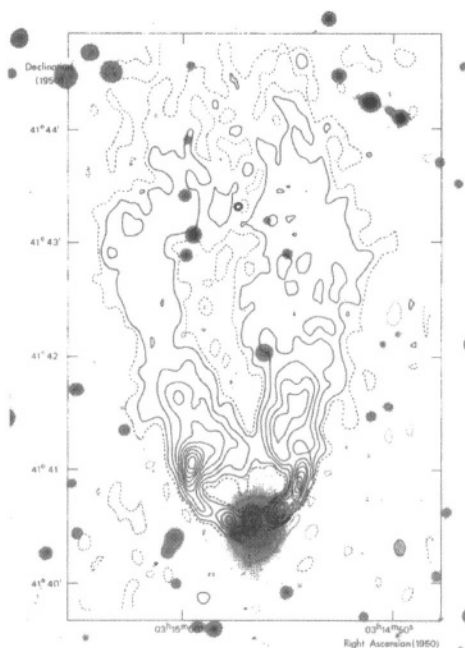


Figure 6.4. Radio image at 5 GHz of the Narrow Angle Tailed radio source NGC1265 (contours), superimposed on the blue Palomar Sky Survey print (grey-scale). The radio nucleus coincides with the optical galaxy. The two jets are bent backward and form low brightness tails in a common direction. The image is courtesy of Wellington et al. (1973).

The prototypical example of a NAT radio source is NGC1265 in the Perseus cluster (Wellington et al. 1973, see Fig. 6.4). The standard interpretation for this radio morphology is that the jets are curved by

ram pressure from the high-velocity host galaxy moving through the dense ICM (Miley et al. 1972), whereas the low brightness tails are material left behind by the galaxy's motion. The ram pressure model was first developed by Begelman et al. (1979), and studied in further detail by Vallée et al. (1981) and Baan & McKee (1985). Following dynamical arguments, the bending is described by the Euler equation

$$R \sim h(\rho_j/\rho_e)(v_j/v_g)^2 \quad (2)$$

where R is the radius of curvature, ρ is density, v is velocity (the subscript j refers to the jet, e to the external medium, g to the galaxy) and h is the scale height over which the ram pressure is transmitted to the jets. Thus, from the jet bending, important constraints on both the jet dynamics and the ICM can be placed. In some cases there is evidence that the radio jets travel first through the galactic atmosphere and then are sharply bent at the transition between the galactic atmosphere and the ICM (Venturi et al. 1989). Bends can occur very close to the nucleus, as in NGC 4869 in the Coma cluster (Feretti et al. 1990), indicating that the bulk of interstellar medium has been stripped by the galaxy during its motion.

The properties of nearby, rich clusters of galaxies containing NAT radio sources has been recently analyzed by Bliton et al. (1998), who derived that NATs are preferentially found in clusters with X-ray substructure. Additionally, NAT galaxies tend to have, on average, velocities similar to those of typical cluster members, instead of high peculiar motions expected if NATs were bent from ram pressure. Thus, they suggested a new model for the NAT formation, in which NATs are associated with dynamically complex clusters with possible recent or ongoing cluster-subcluster mergers. The U-shaped morphology is then suggested to be produced, at least in part, by the merger-induced bulk motion of the ICM bending the jets.

In an effort to understand the orbits of NAT galaxies, O'Dea et al. (1987) examined the directions of NATs with respect to the Abell cluster centres. Assuming that the NATs are indicators of the direction of motion of the host galaxies, the resulting random orientation led them to suggest that the overall distribution of NATs is consistent with isotropic galaxy orbits. However, only considering NATs located within 0.5 Mpc, the galaxies exhibited a trend towards radial orbits. Bliton et al. (1998) performed the same analysis and found that the direction of NAT tails are consistent with random orientations in clusters. We note, however, that some clusters show tailed radio galaxies with the tails oriented in the same direction (e.g., A119, Feretti et al. 1999, Fig. 6.5 and Fig. 6.6). This would support the interpretation that bulk gas motion is the

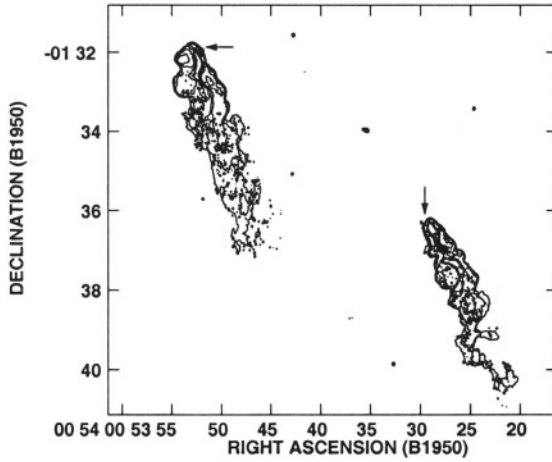


Figure 6.5. Radio image obtained with the VLA at 1.4 GHz of the two NAT radio sources in A119. The arrows indicate the location of the nucleus and of the host galaxy. The two tails show similar orientation.

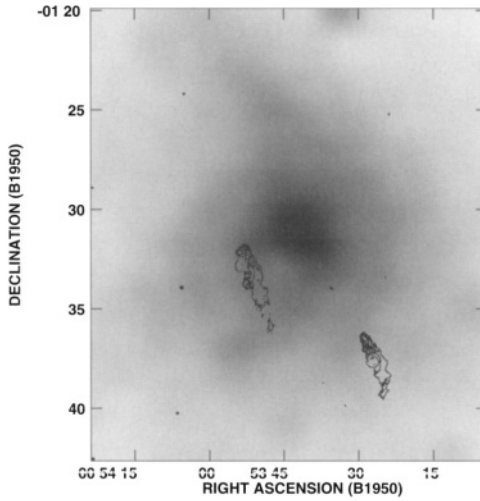


Figure 6.6. Overlay of the radio and X-ray emission of the cluster A119. The contours represent the two NAT radio galaxies, whereas the grey-scale refers to the X-ray emission from the ROSAT PSPC. The X-ray cluster structure is indication of a recent merger, which could have influence on the formation of the two tailed radio sources.

dominant effect in the formation of the tailed morphology at least in some clusters.

2.2. WIDE-ANGLE TAILED RADIO GALAXIES

Wide-angle tails (WAT), originally defined by Owen & Rudnick (1976), are V-shaped radio sources consisting of two, straight and narrow, jets that flare into broad tails. Like in NATs, the tails extend in a common direction, although forming a much larger angle between them. They are generally associated with D/cD or giant ellipticals at the optical centers of clusters (O'Donoghue et al. 1990). Despite the fact that D and cD galaxies are most likely to be found in cooling flow regions, WATs are rarely found in regions with cooling flows.

They show radio luminosities in the range 10^{42} to 10^{43} erg s⁻¹, i.e. intermediate values corresponding to the Fanaroff-Riley (1974) break between the FR class I and II. A characteristic of their jets is that they display a pronounced and abrupt transition from the well-collimated small-scale flow to the extended large-scale lobe structure. This transition is usually identified with a brightness flaring point, where the flow suddenly expands by a factor of 3–10 (O'Donoghue et al. 1993).

The prototypical example of WAT is 3C465 (Eilek et al. 1984, Leahy 1984), shown in Fig. 6.7. The polarization properties and source ages are similar to those of NATs.

From optical studies, it is derived that the WAT galaxies are generally moving very slowly (< 100 km s⁻¹) relative to the cluster velocity centroid (Quintana & Lawrie 1982, Bird 1994, Pinkney et al. 2000), as expected for dominant cluster galaxies. Such slow motion is insufficient to bend the jets/tails of WATs to their observed curvature by ram pressure (see Eq. 2). In fact, galaxy velocities of the order of 1000 km s⁻¹ are required from radio data to provide the necessary ram pressure to bend the jets, assuming typical central gas densities ($\sim 10^{-3}$ cm⁻³). Thus, an interesting puzzle emerges concerning the origin and shape of these relatively powerful cluster radio sources, and alternative mechanisms have been invoked (Eilek et al. 1984). A suggested possibility was an electromagnetic force arising from the interaction between a jet that carries a net electrical current and the magnetic field in the ICM. Given our poor understanding of currents in jets and magnetic field in clusters, this model has not been extensively explored. One problem with it is that it requires a highly and favourably ordered magnetic field in order to produce the symmetric shape of WATs. Alternatively, it was proposed that jets could be deflected by collisions with dense clouds in

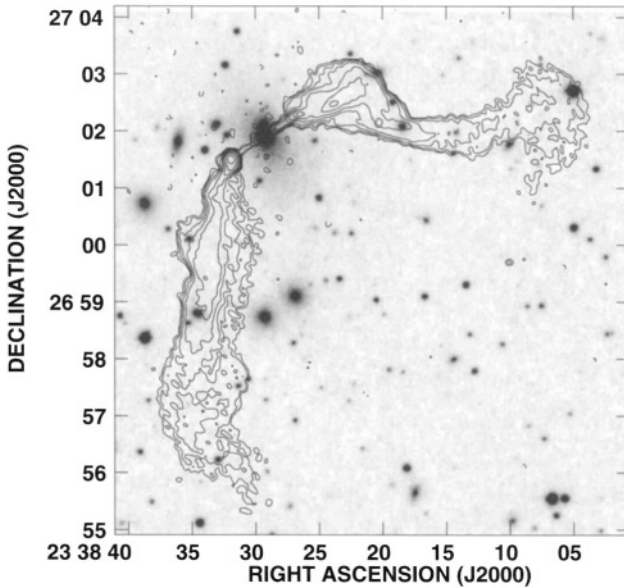


Figure 6.7. Contour image of the Wide Angle Tailed radio source 3C465 in the cluster A2634, superimposed onto the grey-scale optical image from the Digitized Palomar Sky Survey. The two opposite jets emanating from the radio nucleus show a sudden expansion, and then form two tails extended in a common direction, although with a much larger angle between the tails than in NAT sources.

the ICM. Although this process may be at work in some radio galaxies, again it has difficulty in producing the large-scale symmetric structure of WATs. Moreover, it has been ruled out for 3C75 and 3C465 by Owen et al. (1990), on the basis of long-slit spectroscopy observations.

Therefore, WATs must be shaped, at least in part, by other ram pressure gradients not arising from motion of the host galaxy. It has been suggested that the galaxy motions required to bend WATs by ram pressure are a by-product of mergers between clusters (Pinkney et al. 1993, Loken et al. 1995, Roettiger et al. 1996, Gomez et al. 1997). Major perturbations in merging clusters include shocks, turbulence and bulk flows. During the collision of a cluster with a second comparable system, the two gaseous components will rapidly dissipate their kinetic energy, merging into a single structure. The radio galaxy, on the other hand, will not be decelerated at the same rate as the surrounding ICM, being essentially a collisionless system. Therefore, the motion of the

galaxy relative to the ICM will generate the ram pressure needed to bend the radio jets.

Numerical simulations presented by Roettiger et al. (1993) add quantitative support to this idea. The linear scale of WATs, ranging from 100 kpc to 1 Mpc, gives some indication as to the required linear dimensions of the bulk flows. These conditions are met for extended periods during the evolution of a merger. Peak gas velocities well in excess of 1000 km s^{-1} at various stages of the merger evolution are found, which generally do not decay below 1000 km s^{-1} for nearly 2 Gyr after the core passage. This is much longer than the estimated ages of the radio source, 10^7 – 10^8 yr. Typically the bulk flow through the cluster core is greater than 200 kpc wide and can be ~ 1 Mpc wide.

The interstellar medium (ISM) of the central dominant galaxy in a merging cluster environment is likely to be separated from the ICM by a gas discontinuity, which may affect the propagation of a jet producing the observed strong decollimation (Loken et al. 1995, Sakelliou & Merrifield 1999). Since merger bulk flows may result in the disruption of cooling flows (Roettiger et al. 1996), the hypothesis also accounts for the lack of any strong cooling flow candidates in WAT clusters.

If the merger hypothesis is true, one would expect WAT clusters to exhibit other merger signatures, such as elongation of the X-ray morphology in the same direction as the radio tails, absence of cooling flows and velocity substructure. All of these are indeed observed. Fig. 6.8 shows that the direction of the tailed structure agrees well with the direction of the vectors representing the gas velocity field.

From the investigation of the properties of a sample of WAT sources, Sakelliou & Merrifield (2000) find that WATs are not generally located at the centres of their host clusters as defined by their X-ray emission, and that their orbits are predominantly radial, with more WATs traveling toward the centres of clusters than away from the centres. These findings are expected if the X-ray emission is disturbed as in a merger process, and are therefore strongly supporting the above model. Additional support to the model comes from the recent work of Novikov et al. (1999), who found that the WAT tails tend to be aligned with the local supercluster axis as defined by the distribution of nearby Abell clusters. It is along this axis that one would expect cluster mergers to occur preferentially (Colberg et al. 1999). Thus the large scale environment is having a direct impact on the central regions, including radio sources, within clusters.

In addition to the effect of cluster merger, because the jets lie inside the potential of the surrounding cluster of galaxies, one would expect gravitational forces to affect their dynamics. In particular, if the jets

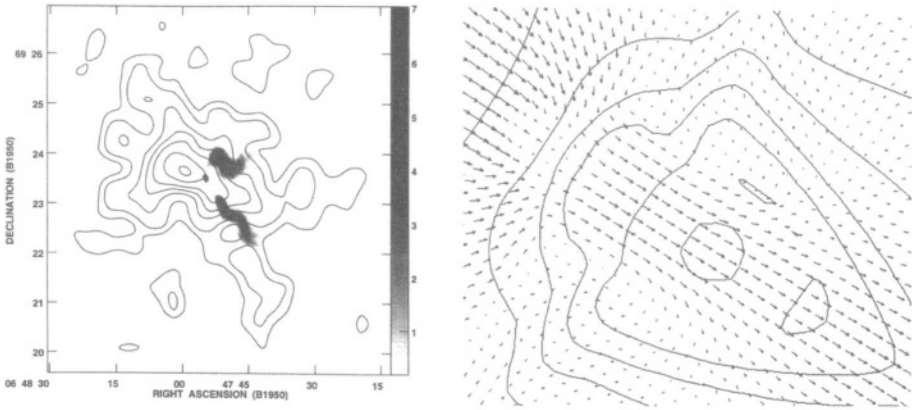


Figure 6.8. Left panel: overlay of a 6 cm radio map grey scale onto a ROSAT X-ray surface brightness contour map of A562. Right panel: Overlay of a synthetic X-ray image of a cluster merger onto a velocity vector field that represents the gas velocity. Note that the X-ray contours in the left panel look very similar to the synthetic X-ray image and that the radio tails are in the direction of the gas velocity. The figure is courtesy of Gómez et al. (1997)

are less dense than their surroundings, then buoyancy forces may play a role in bending the outer radio structures into directions of decreasing external gas pressure (e.g., NGC 326, Worrall et al. 1995, 3C 465, Sakelliou & Merrifield 1999).

2.3. RADIO GALAXIES IN COOLING FLOWS

A wide variety of morphologies are associated with cD galaxies in the centres of cooling flow clusters. The majority of sources are FRIs, but there are exceptions, like for example Cyg A and 3C295, which are FRII sources, and compact sources (<10 kpc), like for instance A496.

The FRI radio sources in cluster cooling flows may be subdivided further into two classes. The most common are the *lobe-dominated sources*, which exhibit a typical jet/lobe radio structure with jets leading from the nucleus to the outer lobes. Examples include the sources in A1795 and A2029. The second class of FRI radio sources in cooling flows are *amorphous sources* (Burns 1990, Baum & O’Dea 1991), which seem to be less common than the lobe-dominated sources, but, interestingly, appear to exist only in clusters with cooling flows. These sources are typically 100–400 kpc in diameter, have strong cores, and diffuse quasi-spherical structure with little signs of collimated emission such as jets or lobes.

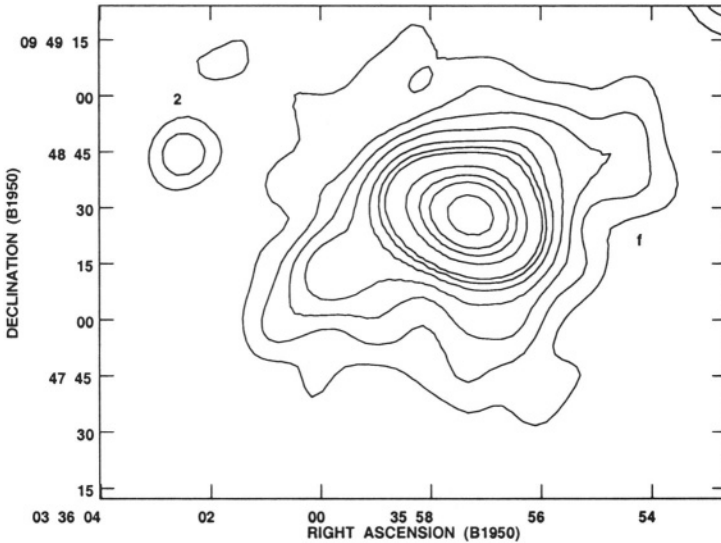


Figure 6.9. Contours of the radio emission from the center of the 2A 0335+096 cluster at 1.5 GHz, showing the amorphous structure at the center of a cooling flow cluster. The figure is from Sarazin et al. (1995).

Good examples are 2A 0335+096 (Fig. 6.9), PKS 0745-191 and 3C317 (Baum & O’Dea 1991, Sarazin et al. 1995, Roland et al. 1985). It appears that the cooling flows in such clusters have either disrupted the radio jets or prevented them from forming (Soker & Sarazin 1988, Loken et al. 1993).

Most of the radio sources associated with cDs in cooling flow clusters have exceptionally steep radio spectra ($\alpha \approx 1-2$ where $S(\nu) \propto \nu^{-\alpha}$). This suggests that the high thermal gas pressure at the cores of the cooling flows reduces the adiabatic expansion of the radio plasma and allows it to spectrally age.

For the lobe-dominated sources, the radio and X-ray emitting regions appear anticorrelated. The first dramatic example was presented by Böhringer et al. (1993), who showed that the thermal plasma in 3C84, in the Perseus cluster, is displaced by the inner parts of the radio lobes, causing “X-ray holes” at the position of the radio lobes. Also the X-ray image of Cyg A (Carilli et al. 1994) reveals clear signatures of hydrodynamic modification of the cluster gas by the jets and lobes of the radio source. Similar effect is seen in the ROSAT images of other clusters. The displacement of the X-ray gas from the radio jets and lobes is confirmed by very recent Chandra X-ray images of Perseus (3C84) and

Hydra A (Fabian et al. 2001, McNamara et al. 2000, see also Forman, this volume).

In the lobe-dominated cooling flow sources, strong polarization and very strong Faraday rotation are seen (e.g., Taylor et al. 1994), likely to originate in the external displaced plasma. On the other hand, well studied amorphous sources (e.g. PKS 0745-191 and 2A 0335+096) are unpolarized, possibly because of mixing of thermal plasma in the radio lobes. Thus, the comparison of X-ray and radio images, and the polarization properties are all consistent with a picture in which the lobes in the lobe-dominated radio sources have displaced the surrounding gas, while the radio plasma in the amorphous sources appears to be mixed with the X-ray emitting gas.

3. CONFINEMENT

An important connection between the intracluster medium and the radio galaxies is provided by the thermal pressure of the hot gas, which exerts static confinement on the radio structures. From the parameters given in § 1, it turns out that the pressure of the X-ray emitting gas is in the range 10^{-10} – 10^{-13} dyn cm⁻². Therefore, both the ICM in groups and clusters, and the hot gaseous coronae around early type galaxies are suitable to confine the radio components.

From the radio data, one can compute the non-thermal energy density, and the pressure within the radio source, when the contributions of the relativistic particles and the magnetic field are assumed to be approximately equal. This estimate is known as the *equipartition value* and depends on assumptions on the geometry, including the filling factor Φ , and the ratio k between the contributions of the electrons and the protons. The energy density is minimum when $\Phi=1$ and $k=1$.

From X-ray data, one can estimate the parameters (temperature, density and pressure) of the interstellar and intergalactic gas surrounding the radio components. A comparison between the internal pressure of the radio emitting plasma and the thermal pressure of the ambient gas provides information about the equilibrium between ambient gas and radio plasma.

In the case of low luminosity radio galaxies, it is found that the minimum internal pressure in low brightness features is generally lower than the outer pressure (see e.g., Morganti et al. 1988, Killeen et al. 1988, Feretti et al. 1992, 1995, Röttgering et al. 1994, Worrall et al. 1995, Schindler 1996, Feretti et al. 1997, Hardcastle et al. 1998, Worrall & Birkinshaw 2000). An example is shown in Fig. 6.10. The difference between internal and external pressure is likely to be due to the numer-

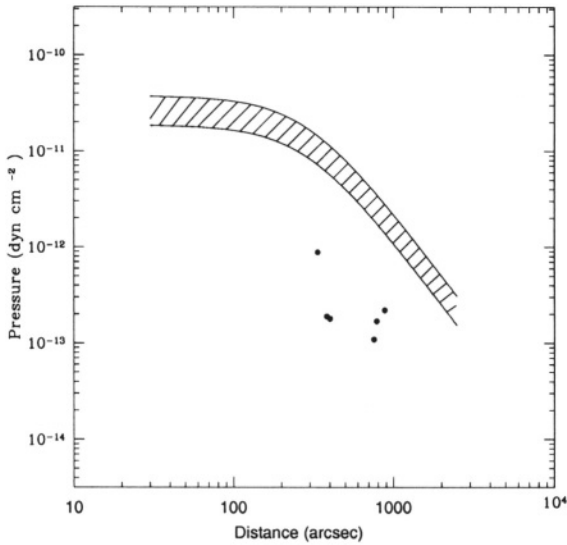


Figure 6.10. Pressure comparison for the radio sources in the cluster A2255 (Feretti et al. 1997): the dashed region is the range of pressure of the X-ray emitting gas versus the radial distance from the cluster center, whereas the dots represent the equipartition pressures in the tailed radio galaxies.

ous assumptions used for the calculation of equipartition parameters, in particular: i) the filling factor Φ is lower than 1; ii) the energy ratio k between relativistic protons and electrons is larger than 1, i.e. the non-thermal radio pressure is dominated by relativistic protons; iii) electrons significantly radiate below the adopted low-frequency cutoff; iv) equipartition conditions do not hold; v) thermal plasma is present within the radio lobes. In some cases, the pressure of the intracluster medium is found to be comparable to the minimum pressure of the radio sources (e.g., Birkinshaw & Worrall 1996, Liang et al. 1997). In conclusion, the FRI sources are likely to be confined by the outer medium, whose pressure is commonly in the range. 10^{-12} – 10^{-10} dyn cm $^{-2}$ (Feretti et al. 1992).

Similar results are obtained for the FRII radio sources. In Cyg A the pressure in the thermal gas is considerably larger than the minimum energy pressure in the radio bridge (Carilli et al. 1994) as recently found also in several other radio galaxies (Leahy & Gizani 2001, Hardcastle & Worrall 2000). In other sources, the non-thermal pressure of the radio bridges in FRIIs tends to be comparable to thermal pressures of the surrounding gas (Wan & Daly 1996). Values of thermal pressure around

FRII radio galaxies are between 10^{-12} – $5 \cdot 10^{-10}$ dyn cm $^{-2}$. These pressures are similar to those of the gas surrounding FRI sources, suggesting that FRI and FRII live in similar environments. This is unexpected, since most clusters with FRII sources appear to lie at the lower end of the cluster X-ray luminosity distribution, and are then likely to contain a lower density ICM (Wan & Daly 1996). A possibility is that the local medium around the radio sources is similar (Owen et al. 1996, see also the discussion in § 4.3).

The lobe-dominated radio sources at the cooling flow center have a radio pressure either comparable to or much lower than the X-ray pressure (Sarazin 1997, Taylor et al. 1994), whereas the amorphous sources always have much lower internal pressure (Sarazin 1997). More detailed analysis needs to be performed with the Chandra data and more sensitive radio data.

4. STATISTICS OF RADIO SOURCES: RADIO LUMINOSITY FUNCTIONS

The high density of galaxies within clusters, especially in the innermost cluster regions, and the peculiar velocities of galaxies, most extreme in merging clusters, enhance the probability of galaxy-galaxy interactions. These very special conditions raise the question whether cluster galaxies have enhanced probability of developing a radio source, or if they tend to have more powerful and long lived radio emission. This subject has been under investigation since the late seventies.

A powerful statistical tool to address the above question is the radio luminosity function (hereinafter RLF). Its classical definition was given by Longair (1966) as “the distribution of radio luminosity among a complete sample of galaxies within a unit volume at a given cosmological epoch”, $\rho(P, z)$. Later, a fractional luminosity function was introduced, defined as $f_i(P, z) = \rho_i(P, z)/\phi_i(z)$, where $\phi_i(z)$ is the density of objects of a particular class i at the epoch z .

From an operational point of view, we can express the fractional RLF $f(P)$ as the probability that a galaxy in a defined sample at a given epoch emits with radio power in the interval $P \pm dP$, i.e. $f(P) = \frac{n(\Delta P_i)}{N(\Delta P_i)}$, where n and N are respectively the number of detected radio galaxies in the power interval ΔP_i and the total number of optical galaxies which could have been detected in the same power bin. The integral form $F(> P)$ can be obtained simply summing over all radio power intervals up to the power P .

In order to take into account the correlation between the optical and radio properties of galaxies, it is useful to introduce the bivariate lumi-

osity function $f(P_i, M_j)$, which gives the probability that a galaxy with absolute magnitude in the range $M \pm dM$ be radio emitting in the radio power range $P \pm dP$.

4.1. LOCAL RLF FOR FIELD GALAXIES

An accurate determination of the local ($z < 0.1$) RLF for elliptical and S0 galaxies was carried out by Auriemma et al. (1977), who used a complete sample of objects selected from a variety of radio catalogues irrespective of their large scale environment, with optical magnitude $M_{pg} < -19.5$. Radio interferometric 1.4 GHz data was used to derive the RLF in the power range $21.1 \leq \log P \leq 27.1$, both for the whole sample and for different classes of optical magnitude. Similar studies were further carried out by other authors (e.g., Sadler et al. 1989, Calvani et al. 1989). Meier et al. (1979) investigated the evolutionary properties of the radio galaxy population and found no difference in the RLF calculated for $z < 0.1$ and $z > 0.1$.

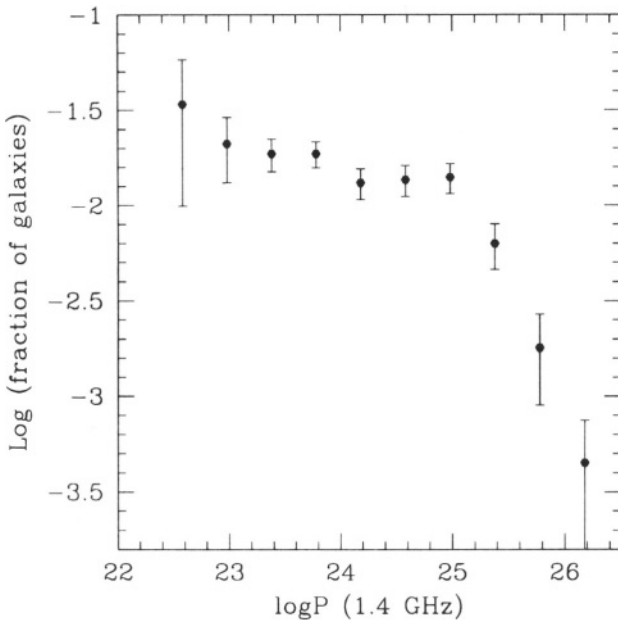


Figure 6.11. Typical shape of the fractional radio luminosity function for elliptical galaxies. The power break in this case occurs at $\log P^* \sim 25$.

The RLF (see Fig. 6.11) can be described by two exponential laws, with a break at a power P^* , which corresponds to the transition between

FRI and FRII radio galaxies. Comparison of the RLF in different magnitude ranges shows that the probability of a galaxy to develop a radio source is strongly dependent on the optical luminosity, in the sense that brighter, i.e. more massive, galaxies have a higher probability. Another interesting result is that for $P > P^*$ the shape of the RLF is the same for each magnitude class, but for powers $P < P^*$ it is steep at faint optical magnitudes, and flattens as the optical luminosity increases. Finally, these studies suggest that the power break in the RLF is a function of the optical magnitude, with P^* increasing for brighter galaxy samples.

4.2. LOCAL RLF FOR CLUSTER GALAXIES

It is reasonable to expect that any difference in the radio properties of a sample of galaxies should be reflected in the radio luminosity function, either as a change in the shape or in the power cutoff, so it is instructive to see how the RLF for elliptical and S0 galaxies selected in different environments compares to the RLF derived for field galaxies. We note that galaxies with radio emission $\log P_{1.4GHz} (W Hz^{-1}) \gtrsim 22$ owe the radio activity primarily to an AGN-type mechanism, i.e. accretion from a central black hole, therefore when we compare the RLF for field and cluster ellipticals and S0s we test if the cluster environment affects the probability of such galaxy types developing a radio source of nuclear origin, i.e. a radio AGN.

This was first investigated by Fanti (1984), who obtained a RLF for ellipticals and S0s in rich Abell clusters with distance class $D \leq 3$ ($z \leq 0.1$), using 1.4 GHz interferometric data available in the literature. The most striking result is that the RLF for ellipticals and S0s in rich clusters and in the field does not differ. Even for cluster galaxies the only relevant parameter seems to be the optical magnitude, i.e. brighter galaxies have a higher probability of developing a radio galaxy within a given power range. The radial distribution of radio galaxies in rich clusters reveals a segregation effect, i.e. powerful radio sources are centrally peaked (more than 50% of radio galaxies with $\log P_{1.4GHz} \gtrsim 24.5$ are located within $0.2 R_A$ from the cluster centre), and the distribution flattens at lower powers. This could, at least in part, reflect the well known segregation in the optical, and could be interpreted as due to the fact that brighter galaxies, which have a higher probability of producing a powerful radio galaxy, tend to be more concentrated towards the cluster centre. As expected on the basis of these results, the RLF is also independent of the richness class of the clusters.

Those early results were more recently confirmed and reinforced by Ledlow & Owen (1996) on the basis of a much larger sample of cluster

galaxies selected from the VLA 1.4 GHz survey of Abell clusters (Zhao et al. 1989; Owen et al. 1992, 1993) and coupled with R-band CCD photometry (Ledlow & Owen 1995). A total of 188 galaxies in Abell clusters were used to derive the local RLF, i.e. redshift $z < 0.09$ and radio power in the range $\log P$ (W Hz^{-1}) from 22.4 to 25.6. Comparison between their RLF and the Auriemma et al. (1977) RLF shows no difference, either in shape or normalisation. Furthermore, no dependence is apparent on richness class, Bautz-Morgan or Rood-Sastry cluster class.

Thanks to the large number of galaxies and to the homogeneous optical information available for the whole sample, Ledlow & Owen (1996) carried out an accurate study of the bivariate RLF and confirmed that it depends only on the optical magnitude (Fig. 6.12). From their study it is confirmed that the RLF break P^* depends on the optical luminosity L , following the law $P^* \propto L^2$. This reflects a relevant result for elliptical galaxies, i.e. the power division between FRI and FRII radio galaxies is a function of the magnitude of the host galaxy (Owen & Ledlow 1994).

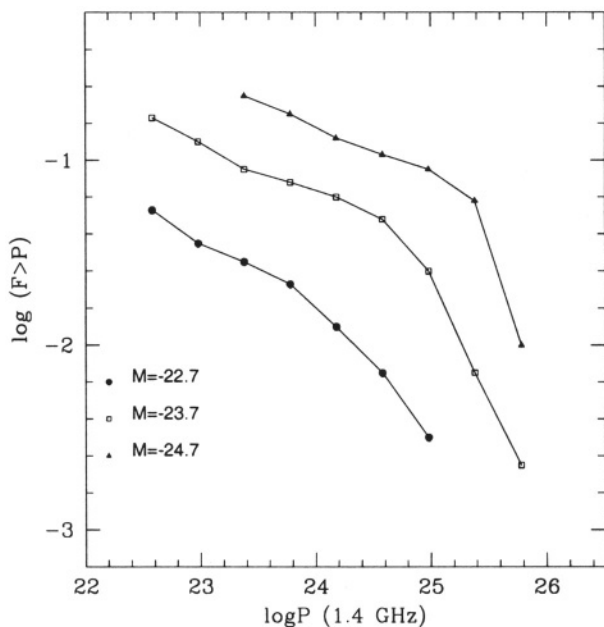


Figure 6.12. Integral bivariate luminosity function for elliptical galaxies given in Ledlow & Owen (1996), scaled for the cosmology adopted here. Absolute magnitudes are computed in R band, radio powers are in W Hz^{-1} .

The universality of the local RLF for early type galaxies can be generalised also to merging clusters. Apparently, the enhanced probability of galaxy interaction in merging clusters has no effect on the probability of galaxies to develop a radio active AGN in their centres. The central cluster complexes in the Shapley Concentration, the largest concentration of merging clusters in the local Universe (Bardelli et al. 1998, 2000; Schindler 1996), were observed at radio wavelengths, and the results show that even this exceptionally unrelaxed environment seems not to increase the probability for elliptical galaxies to develop a radio source. In two out of the three merging complexes studied thus far, the RLF is consistent with the other environments, and for the remaining one it is lower (Venturi et al. 2001).

It is interesting to note that no evolution of the RLF has been found out to redshift $z \sim 0.8$ for $\log P_{1.4GHz}$ ($W Hz^{-1}$) ~ 24 (Stocke et al. 1999). A deep radio survey of X-ray selected clusters with $z \leq 0.8$ shows that the global properties of radio galaxies in distant clusters, i.e. morphology, power range, core dominance, linear size and RLF, do not differ from those of rich nearby clusters.

4.3. RADIO EMISSION AND LARGE SCALE ENVIRONMENT

The galaxy density changes by orders of magnitude going from the innermost cluster regions to poor groups and to the field. Moreover the density and temperature distribution of the ambient medium change dramatically going from small groups, to clusters, to cluster merger regions. Both factors however seem not to affect the probability of early type galaxies to develop an AGN-type radio source.

One possible explanation, suggested by Owen et al. (1996), is that the outer environment is not so different as it may seem, and all radio galaxies live in a sort of “cluster-like” environment. ROSAT X-ray observations of elliptical galaxies show that they are often located in clumps of X-ray emitting gas, similar to the intracluster gas, regardless of the large scale environment hosting the galaxies. They propose that this “cluster-like” gas is all that matters in the development and evolution of a radio galaxy.

An alternative hypothesis is that the galaxy density is not a crucial factor in triggering nuclear radio emission in early type galaxies, and the local environment, i.e. the optical host, plays a much more important role.

5. RADIO POWER-SIZE CORRELATION

It is reasonable to expect that the higher density of the cluster medium and the presence of shocks, turbulence and bulk flows in the intracluster gas of merging clusters affects the propagation of the radio plasma, not only changing the radio source morphology but also preventing the radio galaxies from reaching large angular extents. This was investigated through the radio power-linear size relation for extended radio galaxies inside and outside clusters by Ledlow et al. (2001). They collected a large sample of cluster galaxies from the 1.4 GHz VLA survey of clusters of galaxies (Ledlow & Owen 1996 and references therein), and used the B2 and WP catalogues (Fanti et al. 1978 and Wall & Peacock 1985 respectively) to select the non-cluster sample.

It was found that there is a weak trend of increasing size with increasing radio power for the FRI sources, whereas essentially no dependence between power and size is present for the FRII's. The linear size is spread at low powers ($\log P_{1.4\text{GHz}} \lesssim 24.3$), with linear sizes ranging from sub-kpc sizes to hundred of kpc, and flattens at higher powers, with no difference between the cluster and non-cluster samples. The similarity between the sizes of radio sources living in different environments could be interpreted in the same way as the similarity of the RLF (see § 4.3).

Interestingly, Ledlow et al. (2001) found that the linear size of radio galaxies depends on the optical magnitude at fixed radio power, brighter galaxies being associated with smaller radio galaxies. It is not clear at present if this is an effect of the environment (the brighter galaxies being in higher density regions) or a consequence of different initial conditions (black hole and/or jet properties).

It is worth to note that the radio power-size relation at high luminosity and large size could be affected by evolutionary effects. Ishwara-Chandra & Saikia (1999) and Schoenmakers et al. (2001) find a deficit in the number of giant sources (> 1 Mpc) with high radio luminosity, which they interpret as an indication that the luminosity of radio sources decreases as they expand to very large dimensions.

6. ENVIRONMENT AND STARBURST RADIO EMISSION

The influence of the large scale environment, and in particular of cluster merging, on the starburst emission, is still a matter of debate. Numerical simulations carried out by Evrard (1991) lend support to the idea that the high fraction of starburst galaxies seen in high redshift clusters is due to a single burst of star formation, triggered by compression due to the increasing external pressure as the galaxy falls into the dense

intracluster medium. Different results are obtained by the modeling of Fujita et al. (1999), who argue that gas stripping during cluster collision is the dominant factor. This leads to a decrease in the star formation rate, hence weakening the starburst phenomenon during the merger. In the following we will briefly summarize the most recent observational results at optical and radio wavelengths.

6.1. RADIO SOURCES AND THE BUTCHER-OEMLER EFFECT

One of the most important examples of the impact of environment on the evolution of galaxies is the discovery made by Butcher & Oemler (1978) that a large fraction of galaxies in rich distant clusters ($z \geq 0.3$) have abnormally blue colours. This is the so called “Butcher-Oemler effect” (B-O). Subsequent studies, based on narrow band photometry and spectroscopy, provided the information that this population of blue objects includes both galaxies with emission line spectra typical of ongoing star formation, and galaxies with strong Balmer absorption lines but no emission, which is a signature of star formation only recently ceased (post-starburst, PSB, Dressler & Gunn 1983). Actually a large fraction of the photometrically red galaxies in distant clusters exhibit PSB spectra, indicating that they have also experienced episodes of recent star formation (Dressler & Gunn 1992). The B-O effect raises two key questions, in particular (1) why is the star formation we observe in galaxy clusters at $z \geq 0.3$ virtually absent in the present epoch; and (2) which mechanisms quench the star formation, leading to the presence of PSB galaxies.

Accurate spectroscopy and photometry carried out for a number of nearby rich Abell clusters by Caldwell & Rose (1997) shows that star formation is going on also at the present epoch, even though the starburst signature is much stronger in galaxies belonging to distant clusters. They also related the location of starburst (SB) and PSB galaxies with the cluster kinematics, and found a connection between the presence of SB/PSB and cluster substructure. This led them to propose that shocks in the intergalactic medium, produced by the infall of a subcluster or group into a main cluster condensation, could trigger the starburst mechanism, both in the local Universe and at earlier epochs. On the other hand, Balogh et al. (1997, 1998) reached different conclusions after comparing the emission line properties as a function of the environment in a very large sample of galaxies, i.e. over 2000 objects in the redshift range $0.2 < z < 0.55$. Their study shows that cluster

galaxies have suppressed star formation compared to the field, and they concluded that infalling actually truncates star formation.

Information on the connection between the SB and PSB phenomenon and cluster merger can also be obtained at radio wavelengths. At low radio power, i.e. $\log P_{1.4GHz} (W Hz^{-1}) \lesssim 22$, star formation becomes the dominant mechanism in the production of radio emission (Dwarakanath & Owen 1999; Burns 2001), therefore deep radio surveys of distant clusters and of dynamically unrelaxed clusters may shed light on the connection between cluster merger and the trigger of starburst activity. Only a few studies have been conducted thus far on the B-O effect at radio wavelengths, and the conclusions should be considered tentative.

Morrison (1999, 2000) reported on a radio B-O effect in a sample of 34 clusters in the redshift range $0.02 < z < 0.4$. He found evidence that distant clusters in the sample contain a significantly higher number of low power radio sources, i.e. $\log P_{1.4GHz} (W Hz^{-1})$ in the range 22.6 – 23.1, compared to the local clusters.

A detailed multifrequency study of the two clusters A2125 and A2645 was carried out by Owen et al. (1999). Both clusters have similar intermediate redshift ($z \sim 0.25$) and the same richness class ($R=4$), but they differ in the fraction of blue galaxies, i.e. only A2125 is a B-O cluster. The authors found a significantly higher number of radio galaxies with $\log P_{1.4GHz} (W Hz^{-1}) \lesssim 23.2$ in A2125 compared to A2645 (27 and 4 respectively). Actually, the radio sources in excess are not only SB, but also AGN, in similar number. The SB galaxies are mainly located in the outskirts of the cluster, far from the core and in regions with low X-ray emission. The X-ray emission of A2125 shows substructure, which is indication of cluster merger. On the other hand, the X-ray emission of A2645 shows that it is a much more relaxed cluster. On the basis of these results, Owen et al. (1999) suggested that the ongoing cluster merger in A2125 could be responsible for the excess radio source population, even though the details are unknown. The radio emission could be affected either by galaxy-galaxy or ICM-galaxy interaction, or both.

Different results were obtained from deep radio observations of the three merging clusters A3556, A3558 and A3562, which form the A3558 complex, in the central region of the Shapley Concentration, at redshift $\langle z \rangle \sim 0.05$. Bardelli et al. (1998) proposed that this complex is the result of a cluster-cluster collision, seen just after the first core-core encounter. This scenario is supported by the substructure seen between the cores of the two clusters A3558 and A3562, where an enhanced fraction of blue galaxies was also found. The large sky region occupied by the A3558 complex (more than 4 deg^2) was uniformly covered by radio observations to a power limit of $\log P_{1.4GHz} (W Hz^{-1}) \sim 22$ (Venturi et

al. 1997, 2000), and only three candidate starburst radio galaxies were detected, which is a very low number even allowing for the low percentage of galaxies with optical starburst signatures in this merging cluster complex (Baldi et al. 2001).

In conclusion, the information available so far does firmly establish whether or not cluster mergers have any influence in triggering the radio emission by the starburst mechanism, and if there is any relation with the cosmological epoch. Therefore it is important to pursue the investigation along this line on large samples, and down to lower power limits, both in the local Universe and at higher redshifts.

6.2. FIR/RADIO CORRELATION FOR SPIRALS IN CLUSTERS

The role of environment in the starburst mechanism is best studied for late type galaxies (normal) galaxies, where star formation is a common process. Among others, a powerful tool to this aim is to compare the far-infrared to the radio flux density ratio for normal galaxies in different environments.

The very tight correlation between the far-infrared emission (at $60\mu\text{m}$ and $100\mu\text{m}$) and the radio emission at 1.4 GHz in normal galaxies is a very well established result (see Condon 1992). It is believed that both far-infrared and radio emission arise from star-forming processes. In particular, the thermal far-infrared emission would originate in dusty HII regions heated by massive stars, and the non-thermal radio emission would be due to cosmic ray electrons, presumably produced by supernovae, i.e. the massive stars in their final evolutionary stage.

The ratio q is defined as:

$$q \equiv \log(FIR/3.75 \times 10^{12} W m^{-2}) - \log(S_{1.4GHz}/W Hz^{-1} m^{-2}) \quad (3)$$

The FIR emission is defined as $FIR(W m^{-2}) \equiv 1.26 \times 10^{-14} (2.58 S_{60\mu\text{m}} + S_{100\mu\text{m}})$ (Jy), where $S_{60\mu\text{m}}$ and $S_{100\mu\text{m}}$ are the flux densities at $60\mu\text{m}$ and $100\mu\text{m}$ respectively. The value of q is 2.3 for normal galaxies, with a low dispersion, i.e. 0.2, and holds over many orders of magnitude. Lower values of q indicate a radio excess. Assuming that the local environment affects the star formation history and evolution, this should reflect in the FIR/radio correlation.

Results obtained on the basis of optical (UVB and H_α photometry), infrared (IRAS) and radio (1.4 GHz) data for spiral galaxies in the Coma and Hercules superclusters and in the Cancer cluster show that the star formation rate (SFR) in clusters and in the field is the same. Similar conclusions were reached on the basis of ISO data for spiral/irregular galaxies in A1367 and Coma (Contursi et al. 2001). The radio emission

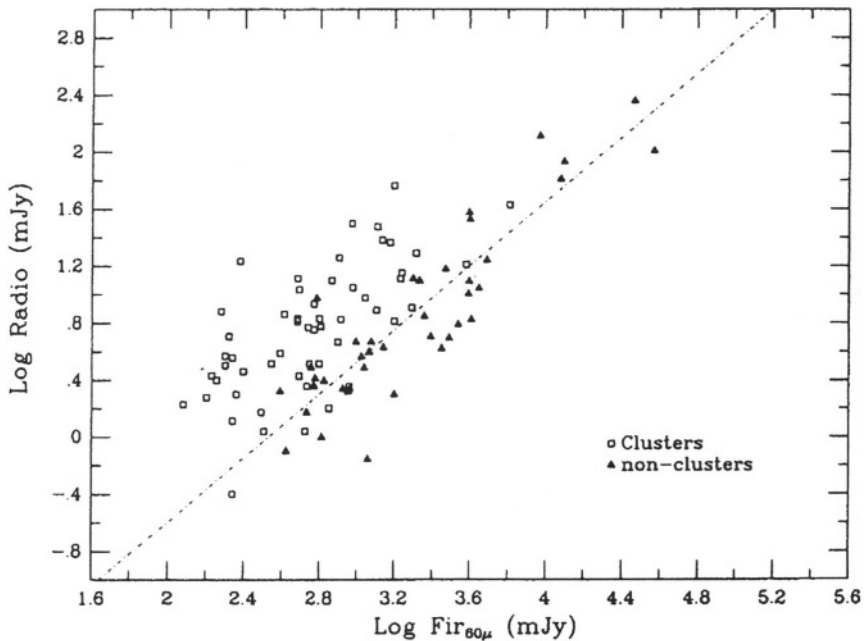


Figure 6.13. Relation between the $60\ \mu\text{m}$ FIR flux and 1.4 GHz radio flux for a sample of nearby cluster and non-cluster spirals. The broken line represents the linear best fit to the non cluster data (figure from Gavazzi et al. 1991).

and the far-infrared vs radio correlation, on the other hand, differ in the two cases, as it is clear from Fig. 6.13 (Gavazzi et al. 1991). In particular, for a given SFR, spirals in clusters are much more powerful in the radio band; moreover, the ratio q is lower in clusters. Given that the SFR does not depend on the environment, these results were interpreted in terms of magnetic field compression due to ram pressure, as the cluster spirals move through the intracluster gas.

The study of the FIR/radio correlation has been recently extended to a much larger number of clusters and cluster late type galaxies, and for regions extending up to few Mpc from the cluster centres, hence allowing to study the dependence of the ratio q on the large scale environment as well as on the local galaxy density (Miller & Owen 2001; Andersen & Owen 1995). Again it is found that the FIR/radio ratio is lower for spirals in rich clusters, while there seems to be no significant difference between galaxies in poor clusters and the field. It was also found that q is correlated with the distance from the cluster centre, in the sense that more centrally located spirals have lower ratios, while no correlation

was found with the galaxy dispersion velocity with respect to the cluster velocity. This last result suggests that the ram pressure model may not be enough to explain the significant radio excess in cluster galaxies, and other mechanisms need to be invoked.

7. GAS STRIPPING AND HI DEFICIENCY IN CLUSTER SPIRALS

It is well known that spiral galaxies in nearby clusters are HI deficient with respect to the parent field population (see van Gorkom 1996 for a review). Imaging of HI in various clusters, such as for example Virgo (van Gorkom et al. 1984; Cayatte et al. 1994), Coma (Gavazzi 1987, 1989) and A3128 (Chengalur et al. 2001), showed that the neutral gas component is strongly affected by the interaction with the intergalactic medium. The mechanism removing HI from cluster spirals has not been uniquely established yet, and both tidal interactions and interaction of the interstellar medium with the hot intracluster gas could play a relevant role.

The effect of such interaction is evident both in terms of a poor content of neutral hydrogen and in terms of extent of the HI emission. The lack of HI is more severe in spirals located in the vicinity of the cluster centres, where the HI extent is usually smaller than the optical disk. Distortions in the distribution of HI are also common for spirals located in regions where the intergalactic gas is known to be denser (Cayatte et al. 1990, 1994). An example is given in Fig. 6.14 for the spirals in the Coma cluster.

The existence of a possible correlation between HI deficiency and the cluster X-ray luminosity is still unclear. Early investigations of Giovanelli & Haynes (1985) were suggestive of a larger fraction of HI deficient galaxies in clusters with high X-ray luminosity. Accordingly, in Ursa Major, a cluster with low X-ray luminosity, spirals seem not to suffer from HI stripping even close to the cluster centre (Verheijen 1996). On the other hand, Solanes et al. (2001), studied the HI distribution in a very large sample of cluster galaxies, and found no correlation between the fraction of HI depleted galaxies and the cluster X-ray luminosity. The same authors report on the evidence that gas deficient galaxies move on radial orbits, a feature first noted by Dressler (1986) and confirmed also by Vollmer et al. (2001) for the Virgo cluster.

A recent work carried out for the bright spiral galaxies in the Coma cluster (Bravo-Alfaro et al. 2000, 2001) proved that the study of HI in clusters, in particular the distribution of deficient and non-deficient spirals within the cluster itself, is a powerful tool to investigate the dy-

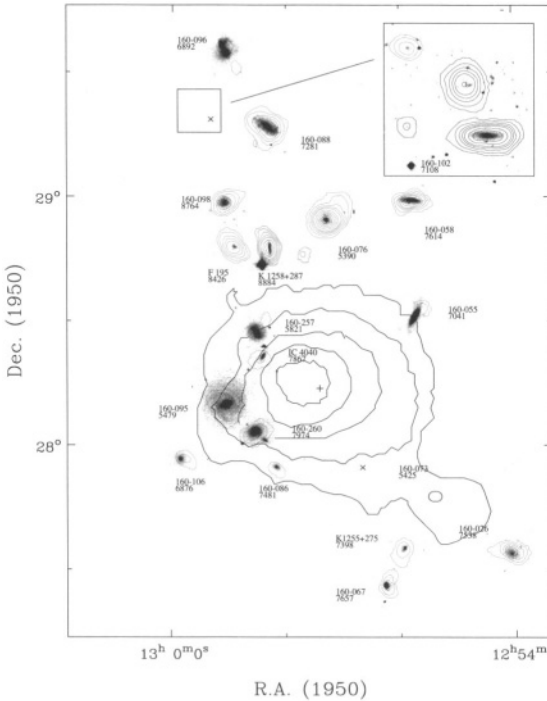


Figure 6.14. Composite plot of the HI emission of spiral galaxies in the Coma cluster. The large scale contours represent the X-ray emission (figure from Bravo-Alfaro et al. 2000).

namical state of the environment, and may significantly contribute to our understanding of cluster mergers. The Bravo-Alfaro et al. VLA survey of spirals in a region within 1.2 degrees from the cluster centre yielded relevant results. As expected, HI deficient spirals and non-detections are mainly located within 30 arcmin from the cluster centre, roughly the extent of the X-ray emission (Vikhlinin et al. 1997) where gas stripping due to interaction with the dense intergalactic medium is expected to be more severe. Moreover, Bravo-Alfaro et al. (2000) noted that the distribution of HI deficiency both inside and outside the central 30 arcmin is clumpy. Spiral rich galaxies are located mainly north of the centre, while the eastern and south-western cluster regions are HI poor. These results were interpreted in the light of cluster merging in the Coma region: the HI poor eastern group is probably undergoing infall and stripping at the current time while the northern gas rich group has still to fall into the cluster centre.

Similar studies are currently in progress for other clusters, such as for example the more distant A2670 (Poggianti & van Gorkom 2001), to confirm the connection between the HI content and the cluster dynamical history.

Acknowledgments

The authors acknowledge partial financial support from the Italian Space Agency ASI.

References

- Andersen, V. & Owen, F.N., 1995, *AJ*, 109, 1582
- Auriemma, C.G., Perola, G.C., Ekers, R.E., Fanti, R., Lari, C., Jaffe & W. Ulrich, M.H. 1977, *A&A*, 57, 41
- Baan, W.A. & McKee, M. R. 1985, *A&A*, 143, 136
- Baldi, A., Bardelli, S. & Zucca, E. 2001, *MNRAS*, 324, 509
- Balogh, M.L., Morris, S.L., Yee, H.K.C., Carlberg, R.G. & Ellingson, E. 1997, *ApJL*, 488, L75
- Balogh, M.L., Shade, D., Morris, S.L., Yee, H.K.C., Carlberg, R.G. & Ellingson, E. 1998, *ApJL*, 504, L75
- Bardelli, S., Pisani, A., Ramella, M., Zucca, E. & Zamorani, G. 1998, *MNRAS*, 300, 598
- Bardelli, S., Zucca, E., Zamorani, G., Moscardini, L. & Scaramella, R. 2000, *MNRAS*, 312, 540
- Baum, S.A. & O'Dea, C.P. 1991, *MNRAS*, 250, 737
- Begelman, M.C., Rees, M.J. & Blandford, R.D. 1979, *Nature*, 279, 770
- Bird C.M. 1994, *AJ*, 107, 1637
- Birkinshaw, M. & Worrall, D.M. 1996, in: *Energy Transport in Radio Galaxies and Quasars*, ASP Conference Series, eds. P.E. Hardee, A.H. Bridle & J.A. Zensus, 100, 335
- Bliton, M., Rizza, E., Burns, J.O., Owen, F.N. & Ledlow, M.J. 1998, *MNRAS*, 301, 609
- Böhringer, H., Voges, W., A.C., Fabian, A.C., Edge, A.C. & Neumann, D.M. 1993, *MNRAS*, 264, L25
- Bravo-Alfaro, H., Cayatte, V., van Gorkom, J.H. & Balkowski, C. 2000, *AJ*, 119, 580
- Bravo-Alfaro, H., Cayatte, V., van Gorkom, J.H. & Balkowski, C. 2001, *A&A*, in press, astro-ph/0109316
- Briel, U.G., Henry, J.P., Schwarz, R.A., Böhringer, H., Ebeling, H., Edge, A.C., Hartner, G.D., Schindler, S., Trümper, J. & Voges, W. 1991, *A&A*, 246, L10
- Burns, J.O. 1990, *AJ*, 99, 14

- Burns, J.O. 2001, in *Life Cycles of Radio Galaxies*, eds. J. Biretta et al., New Astronomy Reviews, in press
- Burns, J.O., Rhee, G., Owen, F.N. & Pinkney, J. 1994, ApJ, 423, 94
- Butcher, H. & Oemler, A. 1978, ApJ, 219, 18
- Caldwell, N. & Rose, J.A. 1997, AJ, 113, 492
- Calvani, M., Fasano, G. & Franceschini, A. 1989, AJ, 97, 1319
- Carilli, C.L., Perley, R.A. & Harris, D.E. 1994, MNRAS, 270, 173
- Cavaliere, A. & Fusco-Femiano, R. 1981, A&A, 100 194
- Cayatte, V., Kotanyi, C., Balkowski, C. & van Gorkom, J.H. 1994, AJ, 107, 1003
- Cayatte, V., van Gorkom, J.H., Balkowski, C. & Kotany, C. 1990, AJ, 100, 604
- Chengalur, J.N., Braun, R. & Wieringa, M. 2001, A&A, 372, 768
- Colberg, J.M., White, S.D.M., Jenkins, A. & Pearce, F.R. 1999, MNRAS, 308, 593
- Condon, J.J. 1992, ARA&A, 30, 575
- Contursi, A., Boselli, A., Gavazzi, G., Bertagna, E., Tuffs, R. & Lequeux, J. 2001, A&A, 365, 11
- David, L.P, Slyz, A., Jones, C., Forman, W. & Vrtilik, S.D. 1993, ApJ, 412, 479
- Dressler, A. 1986, ApJ, 301, 35
- Dressler, A. & Gunn, J.E. 1983, ApJ, 270, 7
- Dressler, A. & Gunn, J.E. 1992, ApJS, 78, 1
- Dwarakanath, K.S. & Owen, F.N. 1999, AJ, 118, 625
- Edge, A.C., Stewart, G.C. & Fabian, A.C. 1992, MNRAS, 258, 177
- Eilek, J.A., Burns, J.O., O'Dea, C.P. & Owen, F.N. 1984, ApJ, 278, 37
- Evrard, A.E. 1991, MNRAS, 248, 8
- Fabian, A.C. 1994, ARA&A, 32, 277
- Fabian, A.C. et al. 2001, MNRAS, 321, L33
- Fanaroff, B.L. & Riley, J.M. 1974, MNRAS, 167, 31P
- Fanti, R. 1984, in *Clusters and Groups of Galaxies*, eds. F. Mardirossian, G. Giuricin & M. Mezzetti, Publ. Reidel, Dordrecht, 185
- Fanti, R., Gioia, I., Lari, C. & Ulrich, M.H. 1978, A&AS, 34, 341
- Feretti, L., Böhringer, H., Giovannini, G. & Neumann, D. 1997, A&A, 317, 432
- Feretti, L., Dallacasa, D., Giovannini, G. & Venturi, T. 1990, A&A, 232, 337
- Feretti, L., Dallacasa, D., Govoni, F., Giovannini, G., Taylor, G.B. & Klein, U. 1999, A&A, 344, 472
- Feretti, L., Fanti, R., Parma, P., Massaglia, S., Trussoni, E. & Brinkmann, W. 1995, A&A, 298, 699

- Feretti, L., Giovannini, G., Klein, U., Mack, K.-H., Sijbring, L.G. & Zech, G. 1998, *A&A*, 331, 475
- Feretti, L., Perola, G.C. & Fanti, R. 1992, *A&A*, 265, 9
- Forman, W. & Jones, C. 1982, *ARA&A*, 20, 547
- Fujita, Y., Takizawa, M., Nagashima, M. & Enoki, M. 1999, *PASJ*, 51, 1
- Gavazzi, G. 1987, *ApJ*, 320, 96
- Gavazzi, G. 1989, *ApJ*, 346, 59
- Gavazzi, G., Boselli, A. & Kennicutt, R. 1991, *AJ*, 101, 1207
- Giovannelli, R. & Haynes, M.P. 1985, *ApJ*, 292, 404
- Gómez, P.L., Pinkney, J., Burns, J.O., Wang, Q., Owen, F.N. & Voges, W. 1997, *ApJ*, 474, 580
- Hardcastle, M.J. & Worrall, D.M. 2000, *MNRAS*, 319, 562
- Hardcastle, M.J., Worrall, D.M. & Birkinshaw, M. 1998, *MNRAS*, 296, 1098
- Ishwara-Chandra, C.H. & Saikia, D.J. 1999, *MNRAS*, 309, 100
- Jones, C. & Forman, W. 1999, *ApJ*, 511, 65
- Killeen, N.E.B., Bicknell, G.V. & Ekers, R.D. 1988, *ApJ*, 325, 180
- Leahy, J.P. 1984, *MNRAS*, 208, 323
- Leahy, J.P. & Gizani, N.A.B. 2001, in *Life Cycles of Radio Galaxies*, eds. J. Biretta et al., *New Astronomy Reviews*, in press, astro-ph/9909121
- Ledlow, M.J. & Owen, F.N. 1995, *AJ*, 110, 1959
- Ledlow, M.J. & Owen, F.N. 1996, *AJ*, 112, 9
- Ledlow, M.J., Owen, F.N. & Eilek, J.A. 2001, in *Life Cycles of Radio Galaxies*, eds. J. Biretta et al., *New Astronomy Reviews*, in press, astro-ph/9908336
- Liang, H., Pierre, M., Unewisse, A. & Hunstead, R.W. 1997, *A&A*, 321, 64
- Loken, C., Burns, J.O., Norman, M.L. & Clarke, D.A. 1993, *ApJ*, 417, 515
- Loken, C., Roettiger, K., Burns, J.O. & Norman, M. 1995, *ApJ*, 445, 80
- Longair, M.S. 1966, *MNRAS*, 133, 421
- McNamara, B.R. et al. 2000, *ApJ*, 534, 135
- Meier, D.L., Ulrich, M.-H., Fanti, R., Gioia, I. & Lari, C. 1979, *ApJ*, 229, 25
- Miley, G.K., Perola, G.C., van der Kruit, P.C. & van der Laan, H. 1972, *Nature*, 237, 269
- Miller, N.A. & Owen, F.N. 2001, *AJ*, 121, 1903
- Miller, N.A., Owen, F.N., Burns, J.O., Ledlow, M.J. & Voges, W. 1999, *AJ*, 118, 1988
- Mohr, J.J., Fabricant, D.G. & Geller, M.J. 1993, *ApJ*, 413, 492

- Morganti, R., Fanti, R., Gioia, I.M., Harris, D.E., Parma, P. & de Ruiter H. 1988, A&A, 189, 11
- Morrison, G.E. 1999, Ph.D. Thesis, University of New Mexico
- Morrison, G.E. 2000, AAS, 197, 5704
- Mulchaey, J.S., Davis, D.S., Mushotzky, R.F. & Burstein, D. 1993, ApJL, 404, L9
- Novikov, D.I., Melott, A.L., Wilhite, B.C., Kaufman, M., Burns, J.O., Miller, C.J. & Batuski, D.J. 1999, MNRAS, 304, L5
- O'Dea, C.P. & Owen, F.N. 1985, AJ, 90, 927
- O'Dea, C.P., Sarazin, C.L. & Owen, F.N. 1987, ApJ, 316, 113
- O'Donoghue, A.Q., Eilek, J.A. & Owen, F.N. 1990, ApJS, 72, 75
- O'Donoghue, A.Q., Eilek, J.A. & Owen, F.N. 1993, ApJ, 408, 428
- Owen, F.N. & Ledlow, M.J. 1994, in *The First Stromlo Symposium: The Physics of Active Galaxies*, eds. G.V. Bicknell, M.A. Dopita & P.J. Quinn, ASP Conference Series, 54, 319
- Owen, F.N., Dwarakanath, K.S., Smith, C.C., Ledlow, M.J., Keel, W.C., Morrison, G.E., Voges, W. & Burns, J.O. 1996, in *Energy Transport in Radio Galaxies and Quasars*, eds. P.E. Hardee, A.H. Bridle & J.A. Zensus, ASP Conference Series, 100, 353
- Owen, F.N., Ledlow, M.J., Keel, W.C. & Morrison, G.E. 1999, AJ, 118, 633
- Owen, F.N., O'Dea, C.P. & Keel, W.C. 1990, ApJ, 352, 44
- Owen, F.N. & Rudnick, L. 1976, ApJL, 205, L1
- Owen, F.N., White, R.A. & Burns, J.O. 1992, ApJS, 80, 501
- Owen, F.N., White, R.A. & Ge, J.-P. 1993, ApJS, 87, 135
- Pinkney, J., Burns, J.O., Ledlow, M.J., Gómez, P.L. & Hill, J.M. 2000, AJ, 120, 2269
- Pinkney, J., Rhee, G., Burns, J.O., Hill, J. M., Oegerle, W., Batuski, D. & Hintzen, P. 1993, ApJ, 416, 36
- Poggianti, B.M. & van Gorkom, J.H. 2001, in *Gas and Galaxy Evolution*, eds. J. E. Hibbard, M. P. Rupen & J. H. van Gorkom, ASP Conference Series, p. 599
- Prestage, R.M. & Peacock, J.A. 1988, MNRAS, 230, 131
- Quintana, H. & Lawrie, D.G. 1982, AJ, 87, 1
- Roettiger, K., Burns, J.O. & Loken, C. 1993, ApJL, 407, L53
- Roettiger, K., Burns, J.O. & Loken, C. 1996, ApJ, 473, 651
- Roland, J., Hanisch, R.J., Véron, P. & Fomalont E. 1985, A&A, 148, 323
- Röttgering, H., Snellen, I., Miley, G., de Jong, J.P., Hanisch, B. & Perley, R. 1994, ApJ, 436, 654
- Rudnick, L. & Owen, F.N. 1976, ApJL, 203, L107
- Sadler, E.M., Jenkins, C.R. & Kotanyi, C.G. 1989, MNRAS, 240, 591

- Sakelliou, I. & Merrifield, M.R. 1999, MNRAS, 305, 417
- Sakelliou, I. & Merrifield, M.R. 2000, MNRAS, 311, 649
- Sarazin, C.L. 1986, Rev. Mod. Phys., 58, 1
- Sarazin, C.L. 1997, in *Galactic and Cluster Cooling Flows*, ed. N. Soker, ASP Conference Series, 115, 172
- Sarazin, C.L., Baum, S.A. & O’Dea, C.P. 1995, ApJ, 451, 125
- Schindler, S. 1996, MNRAS, 280, 309
- Schoenmakers, A.P., de Bruyn, A.G., Röttgering, H.J.A. & van der Laan, H. 2001, A&A, 374, 861
- Solanes, J.M., Manrique, A., Gonzales-Casado, G., Giovannelli, R. & Haynes, M.P. 2001, ApJ, 548, 97
- Soker, N. & Sarazin, C.L. 1988, ApJ, 327, 66
- Stocke, J.T., Perlman, E.S., Gioia, I.M. & Harvanek, M. 1999, ApJ, 117, 1967
- Taylor, G.B., Barton, E.J. & Ge, J.P. 1994, AJ, 107, 1942
- Vallée, J.P., Bridle, A.H. & Wilson, A.S. 1981, ApJ, 250, 66
- van Gorkom, J.V. 1996, in *The Minnesota Lectures on Extragalactic Neutral Hydrogen*, ed. E.D. Skillman, ASP Conference Series, 106, 293
- van Gorkom, J.H., Balkowski, C. & Kotanyi, C. 1984, in *Clusters and Groups of Galaxies*, eds. F. Mardirossian, G. Giuricin & M. Mezzetti, Publ. Reidel, Dordrecht, 261
- Venturi, T., Bardelli, S., Morganti, R. & Hunstead, R.W. 1997, MNRAS, 285, 898
- Venturi, T., Bardelli, S., Morganti, R. & Hunstead, R.W. 2000, MNRAS, 314, 594
- Venturi, T., Bardelli, S., Zambelli, G., Morganti, R. & Hunstead, R.W. 2001, MNRAS, 324, 1131
- Venturi, T., Feretti, L. & Giovannini, G. 1989, A&A, 213, 49
- Verheijen, M.A.W. 1996, in *Cold Gas at High Redshifts*, eds. M.N. Bremer, P.P. van der Werf, H.J.A. Röttgering & C.L. Carilli, Kluwer Academic Publishers, 165
- Vikhlinin, A., Forman, W. & Jones, C. 1997, ApJL, 474, L7
- Vollmer, B., Cayatte, V., Balkowski, C. & Duschl, W.J. 2001, ApJ, in press, astro-ph/0107237
- Wan, L. & Daly, R.A. 1996, ApJ, 467, 145
- Wall, J. & Peacock, J.A. 1985, MNRAS, 216, 173
- Wellington, K.J., Miley, G.K. & van der Laan, H. 1973, Nature, 244, 502
- White, S.D.M., Briel, U.G. & Henry, J.P. 1993, MNRAS, 261, L8
- Worrall, D.M. & Birkinshaw, M. 2000, ApJ, 530, 719
- Worrall, D.M., Birkinshaw, M. & Cameron, R.A. 1995, ApJ, 449, 93
- Zhao, J.-H., Burns, J.O. & Owen, F.N. 1989, AJ, 98, 64

This page intentionally left blank

Chapter 7

DIFFUSE RADIO SOURCES AND CLUSTER MERGERS

Radio Halos and Relics

Gabriele Giovannini*

Dipartimento di Fisica, Universita' di Bologna

Viale Bertini Pichat, 6/2

I-40127 Bologna, Italy

ggiovann@ira.bo.cnr.it

Luigina Feretti

Istituto di Radioastronomia, CNR

Via Gobetti, 101

I-40129 Bologna, Italy

lferetti@ira.bo.cnr.it

Abstract The historical course in the search of extended halo and relic sources in clusters of galaxies is summarized, and it is shown that only in recent years has a significant improvement in the knowledge of the properties of these sources been reached. The study of diffuse sources is very important in understanding the role of large scale magnetic fields and relativistic particles in the intracluster medium and for testing the physical conditions in clusters of galaxies. The properties of halos and relics are presented, and the connection between radio emission and cluster X-ray emission is emphasized. The evidence is presented that the formation of extended diffuse sources is related to the cluster mass and to the existence of strong merger events. Moreover, current models on the formation of the magnetic fields and of the population of relativistic electrons which give rise to the halo and relic radio emission are briefly illustrated.

*also Istituto di Radioastronomia, CNR, Bologna

Introduction

In 1959, Large et al. mapped for the first time the Coma cluster at radio wavelengths with the 250-ft. radio telescope at Jodrell Bank with a Dicke-type radiometer, and detected at the center of the Coma cluster a radio source (Coma C) noticeably extended even with a resolution of 40' (Fig. 7.1). Further observations showed that Coma C has an extremely steep spectrum ($\alpha = 1.6^1$; Bozyan 1968), but were not able to individuate its nature and identification.

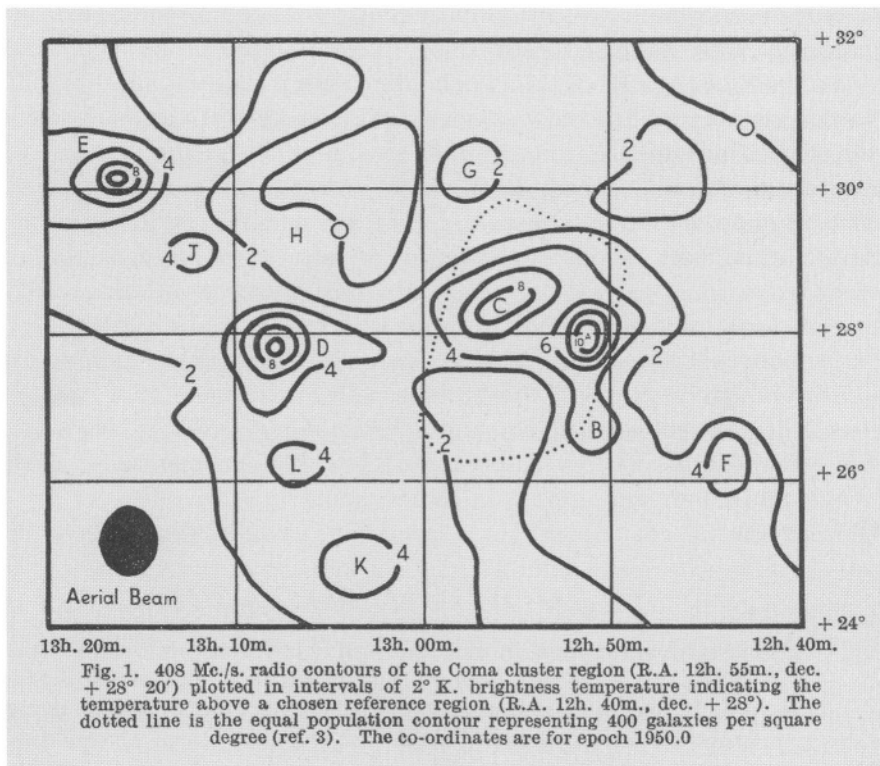


Figure 7.1. The radio image of the Coma cluster region obtained by Large et al. (1959). The Coma Cluster emission coincides with the extended C source while Coma A is the strong 3C 277.3 radio galaxy.

Willson (1970) confirmed the existence of this extended radio source associated with the Coma cluster by comparing his interferometric radio data, obtained with the Cambridge One-Mile telescope, with single dish observations of Large et al. (1959). Willson also determined that the

$$^1S(\nu) \propto \nu^{-\alpha}$$

observed *halo* consists of diffuse emission and not of discrete sources possibly associated with cluster galaxies.

A **radio halo** was defined as a large diffuse non-thermal radio source not associated with any single active galaxy but rather with the cluster as a whole.

This new class of radio sources became a target for many scientific projects. Observations carried out mostly with the Westerbork Synthesis Radio Telescope (WSRT) and with single dish radio telescopes (Arecibo, Green Bank 300-ft, Effelsberg and others) found about 10 other clusters with a diffuse halo-type radio emission (Hanisch 1982a). In the Perseus cluster a high dynamic range observation (Noordam & de Bruyn 1982) showed a localized halo surrounding NGC 1275 (3C 84). In other clusters as A1367 (Gavazzi 1978; Ballarati et al. 1981) and A3667 (Goss et al. 1982: the 2006-56 region) a diffuse source was detected, but it was not located at the cluster center.

Jaffe & Rudnick (1979), in their search for radio halos, found an extended emission region in the Coma cluster near the strong radio source Coma A (3C 277.3). Ballarati et al. (1981), thanks to observations at 408 MHz with the Northern Cross Radio Telescope at better angular resolution, ruled out the possible association of this extended source to Coma A. These authors suggested that the extended feature is a halo type radio source related to the Coma cluster. Further Effelsberg, WSRT, and Very Large Array (VLA) observations tried to identify this source as a relic radio galaxy, but due to the impossibility of finding a reasonable candidate, to its radio morphology, and to its spectral properties, it was clear that this source and the few others found at the periphery of A1367 and A3667, were a different class of extended sources, similar to radio halos but located at the cluster periphery (Giovannini et al. 1991). These sources are usually named **relic radio sources**.

The discovery of cluster diffuse radio sources, produced by synchrotron emission from the intracluster gas (ICM), represents an important step in the understanding of the physical processes within clusters of galaxies. The existence of halos and relics provides a significant test for several theories concerning the origin of relativistic particles in the intracluster gas and particle propagation in astrophysical plasmas. In addition, these sources reveal the existence of large scale magnetic fields in clusters. In this paper we present the observational properties of these sources, and of their parent clusters, and briefly summarize the models for their formation and evolution.

A Hubble constant $H_0 = 50 \text{ km s}^{-1} \text{ Mpc}^{-1}$, and $q_0=0.5$ are adopted.

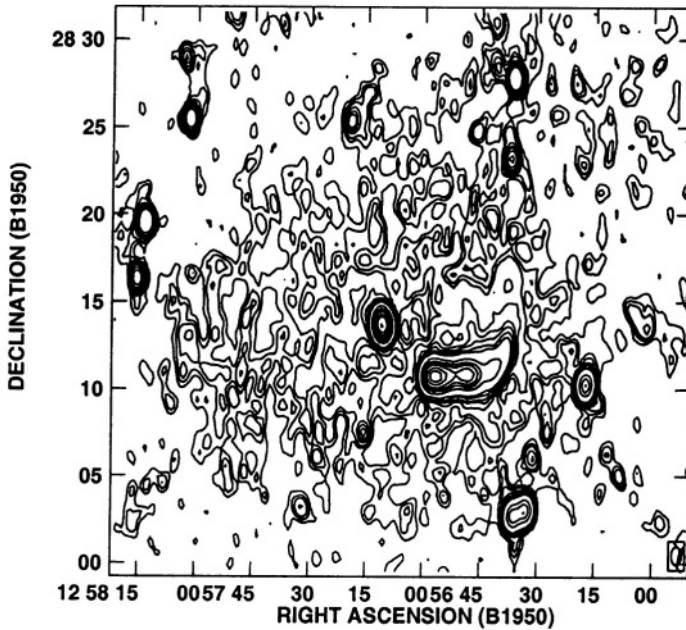


Figure 7.2. WSRT radio image of the Coma C radio halo at 50 cm, with angular resolution of $35'' \times 63''$ (RA \times DEC). Contour levels are at 1, 1.5, 2, 3, 4, 5, 7, 10, 30, 50, 70, 100, 150, 200, 300, 400 mJy/beam.

1. A WORKING DEFINITION

Feretti & Giovannini (1996), using definitions given in the literature, classified diffuse cluster radio sources in three classes: cluster-wide halos, relics and mini-halos.

- Cluster-wide halos are extended diffuse radio sources with low surface brightness. They permeate the cluster center and are not associated with any cluster galaxy. Their prototype is Coma C (Fig. 7.2). Halo sources have a steep radio spectrum, are characterized by a regular shape, and show low or negligible polarized emission. They have a typical size of the order of ~ 1 Mpc or more, but also diffuse sources smaller than 500 kpc have been detected.
- Relic sources are similar to halos with low surface brightness, large size and steep spectrum, but they are located in cluster peripheral regions. Relic sources show, in most cases, an elongated structure

and are highly polarized. Originally they were suggested to be relics of currently non active galaxies, however no evidence is found in support of this identification. The prototype of this class is 1253+275, in the Coma cluster (see § 2.2). A spectacular example of sources of this class can be found in A3667 (Fig. 7.3).

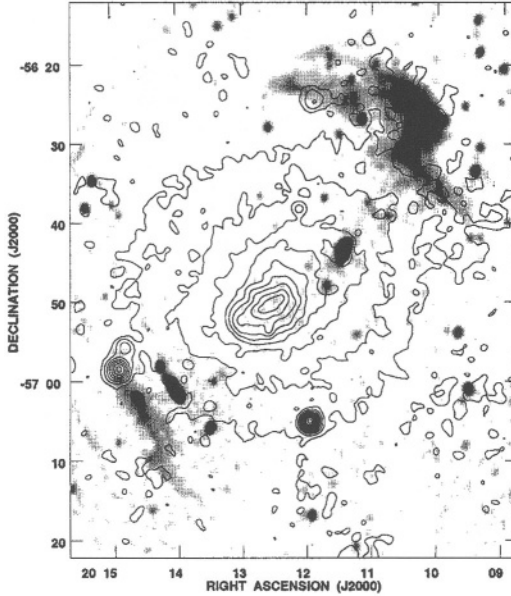


Figure 7.3. A contour representation of the X-ray image of the cluster A3667, overlaid on a grey-scale radio image at 843 MHz (from Röttgering et al. 1997). The powerful giant relic source is at the NW with respect to the cluster center and it shows a peculiar inverted S-shaped morphology. In a symmetric position at SE, with respect to the cluster center, an additional weaker inverted S-shaped relic source is present.

- Mini-halos are diffuse extended radio sources surrounding a dominant powerful radio galaxy at the cluster center. Examples of this class are detected in the Perseus (Fig. 7.4) and Virgo clusters. The radio emission in this case is not due to extended radio lobes fed by an Active Galactic Nucleus (AGN), as in classical radio galaxies, but it reflects the presence of diffuse relativistic particles and a magnetic field in the ICM at the cluster center. In this respect, mini-halos are similar to halos. However, in mini-halos the active galaxy is the most obvious origin of relativistic particles. Moreover, it has been found that these sources are not connected to cluster merger activity. Therefore, we will not consider here this class of sources.

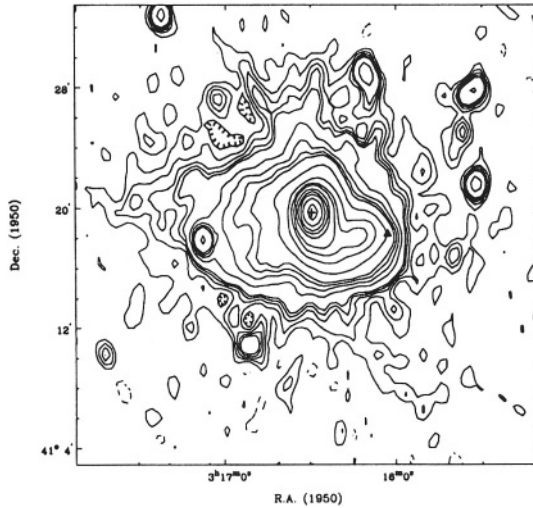


Figure 7.4. 3C84 image at 92 cm, obtained with the WSRT at a resolution of $51'' \times 77''$ (RA \times DEC). The contour levels are: -4, 4, 8, 12, 16, 20, 40, 60, 80, 100, 200, 400, 600, 800, 1500, 2500, 4000, 8000, 16000 mJy/beam. The cross indicates the position of NGC1275, the triangle marks the position of NGC1272. The mini-halo size in this image is $\sim 25'$. This image is from the Sijbring PhD Thesis (1993).

2. OBSERVATIONS AND RESULTS

Diffuse extended radio sources are difficult to detect because of their low surface brightness and large size. In observations performed with interferometers, the lack of short spacings prevents the detection of large scale structures. Observations with filled aperture telescopes, on the other hand, do not have high enough resolution to distinguish a real diffuse emission from a blend of point sources. Despite of these observational difficulties, several surveys were undertaken to detect radio halos and determine how common they are (see for example: Jaffe & Rudnick 1979; Cane et al. 1981; Hanisch 1982b), but the general conclusion was that such sources are extremely rare. In the review paper by Feretti & Giovannini (1996), the reported number of known halo and relic sources was still very low; only a dozen of them were at that time unambiguously detected. The number of known diffuse sources has increased recently to about 40 objects, thanks to the improved sensitivity of radio telescopes and the existence of deep surveys.

In the following we report the observational results, in approximate chronological order.

2.1. THE RADIO HALO COMA C

An image of the radio emission in the Coma cluster is given in Fig. 7.5. Coma C is the prototype and best studied example of cluster radio halos. The halo is located at the cluster center, it shows a rather regular shape and a low surface brightness ($\sim \mu\text{Jy}/\text{arcsec}^2$ at 1.4 GHz). The integrated radio spectrum is steep ($\alpha=1.34$). A possible steepening at frequencies higher than 1.4 GHz could be due to a flux density underestimate because of the small area covered (Deiss et al. 1997). The radio halo scale size is a monotonically decreasing function of the frequency. This supports the suggestion by Giovannini et al. (1993) of a spectrum steepening in the peripheral regions.

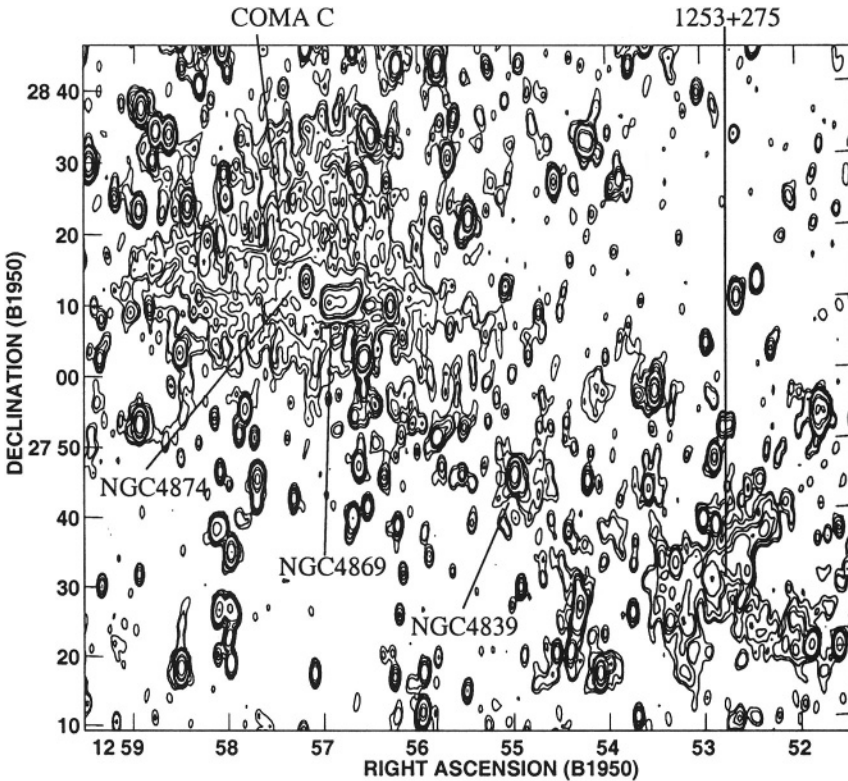


Figure 7.5. WSRT radio image of the Coma cluster region at 90 cm, with angular resolution of $55'' \times 125''$ (HPBW, RA \times DEC). Labels refer to the halo source Coma C and the relic source 1253+275 as well as to some bright Coma cluster radio galaxies. Contour levels are at 2, 3, 5, 7, 10, 30, 50, 100, 300, 500 mJy/beam. The bridge of radio emission connecting Coma C to 1253+275 is resolved at this angular resolution and is visible only as a region with an apparent higher positive noise.

The Coma C halo is the only radio halo for which a high resolution map of the spectral index has been obtained so far. The spectral index distribution between 327 and 1400 MHz shows a central plateau with $\alpha \sim 0.8$, and an outer region with a steeper spectrum, up to $\alpha = 1.8$. This behaviour provides evidence that the source of energy is more efficient at the cluster/halo center, in a region approximately coincident with the optical core radius. The radiative lifetime of the relativistic electrons estimated from the spectrum is $\sim 10^8$ yr. Deiss et al. (1997) obtained a map at 1.4 GHz of the halo, after subtraction of all discrete sources. They pointed out the close similarity between the X-ray and radio images. Both emissions are extended in the E-W direction and towards the NGC 4839 group. This similarity indicates a close link between the physical conditions of the radio source and those of the thermal component.

The equipartition magnetic field is $0.4 h_{50}^{2/7} \mu\text{G}$ and the minimum energy density is $1.6 \times 10^{-14} \text{ erg cm}^{-3}$, as estimated by Giovannini et al. (1993). No polarized flux is detected down to a level of $\sim 10\%$ at 1.4 GHz.

2.2. DIFFUSE EMISSION IN THE COMA CLUSTER PERIPHERY

Besides the existence of the central Coma C halo, the Coma cluster is characterized by the presence of another diffuse extended source, named 1253+275 (Fig. 7.5), located at ~ 2.7 Mpc from the cluster center, in the direction of the cluster A1367.

The radio source morphology and the trend of the spectral index suggest that this source is an extended radio source not strictly related to the activity of a single galaxy, but to the cluster.

Its large size, brightness and spectrum are similar to those of Coma C. Unlike Coma C it shows an elongated shape, and is 30% polarized at 1.4 GHz. The high polarization degree in this source is naturally explained by a tangled magnetic field associated with the cluster intergalactic medium. In this case, a larger number of magnetic field cells along the line of sight is present at the cluster center compared to the outer regions.

Additional diffuse emission is present in the Coma cluster: a bridge of radio emission is detected in the region connecting Coma C to 1253+275 (Kim et al. 1989; Giovannini et al. 1990). The surface brightness of this diffuse emission is very low and it is only enhanced at low frequency and low resolution, so it is not easily visible in Fig. 7.5. In the recent

map presented by Deiss et al. (1997), the bridge is visible only as an asymmetric extension of the central halo Coma C.

2.3. CLUSTERS WITH WELL KNOWN DIFFUSE SOURCES

The best known examples of clusters with diffuse sources are A2256, A2255 and A2319. A2256 (Fig. 7.6) was studied in detail with the WSRT (Bridle & Fomalont 1976; Bridle et al. 1979). These authors found a faint central diffuse emission (halo) extended ~ 0.9 Mpc with a relatively steep spectrum, and a more peripheral emission with a size of 1×0.3 Mpc and a remarkably uniform spectrum ($\alpha \sim 0.8$) between 610 and 1415 MHz. The peripheral source is strongly polarized (20% at 1415 MHz) and it is likely to be a relic emission. Further VLA observations (Röttgering et al. 1994; Clarke & Enßlin 2001) allowed a detailed study of the radio emission in this cluster. From a comparison with the X-ray emission, it was concluded that the radio properties of A2256 could be explained by a merging process of the main cluster with a subgroup.

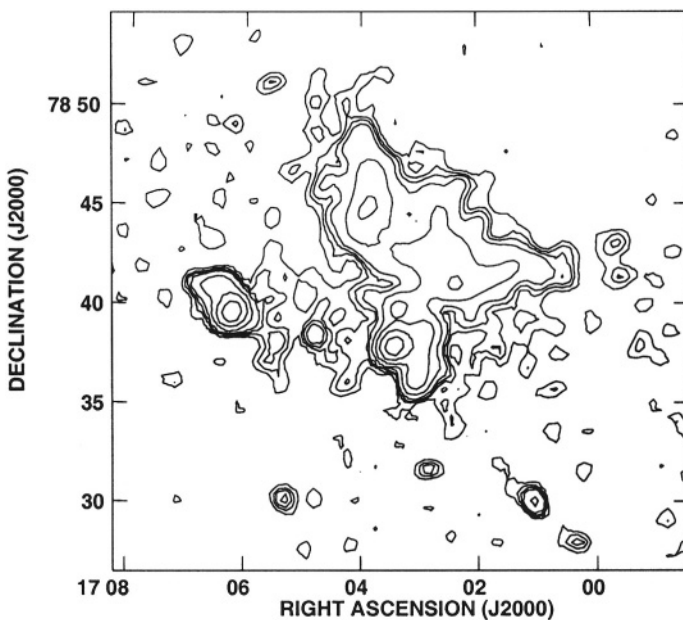


Figure 7.6. The radio image of A2256, retrieved from the WENSS at 327 MHz.

For the clusters A2255 (Jaffe & Rudnick 1979, Harris et al. 1980) and A2319 (Harris & Miley 1978), a sensitive radio and X-ray study was performed by Feretti et al. (1997a, 1997b, see Fig. 7.7 and Fig. 7.8), who concluded that the radio halo morphology is correlated with

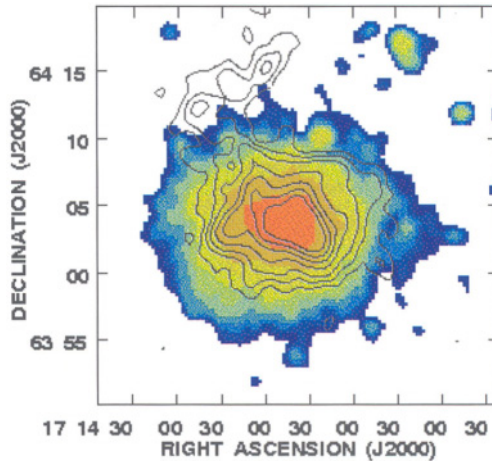


Figure 7.7. Contours of the halo image in A2255 after subtraction of discrete sources, superimposed on the X-ray PSPC image (colour). Contour levels are at -4, 4, 7, 10, 15, 30 mJy/beam. The extended elongated feature just outside the X-ray emission, at \sim R.A.: 17 13 30; Dec.: 64 15; is a peripheral relic source.

the X-ray structure and pointed out the existence of merger processes in the two clusters, possibly related to the halo formation. In A2255, a peripheral elongated relic is also present at ~ 1.2 Mpc projected distance from the cluster center.

Despite the low number of known halo sources, the comparison between radio and X-ray images suggested a strong connection between the presence of an extended source and the X-ray emission. In particular it was proposed that recent cluster mergers may provide the energy to these extended sources, playing an important role in the reacceleration of the radio emitting relativistic particles and in the amplification of the magnetic field.

2.4. NEW HALO AND RELIC SOURCES

Information on a larger sample of halos and relics is crucial for investigating their formation and evolution, and their relation to other cluster properties. With this aim Giovannini et al. (1999) undertook a search for new halo and relic candidates using the NRAO VLA Sky Survey (NVSS, Condon et al. 1998). As a cluster sample they used the X-ray-brightest Abell-type clusters (XBACs) presented by Ebeling et al. (1996). The cross correlation between the XBACs and the radio survey NVSS provided a list of 29 candidates. Out of them 11 clusters were already known from the literature to contain a diffuse cluster-wide

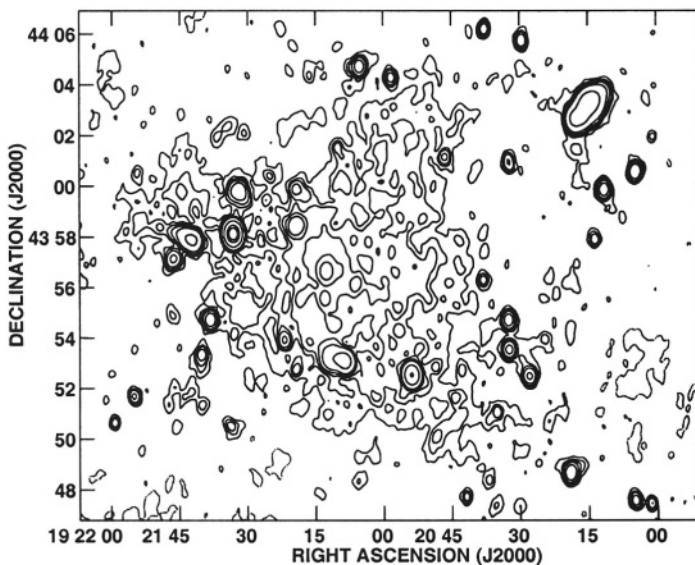


Figure 7.8. WSRT radio image at 1.4 GHz of the central region of A2319. The angular resolution is $20.4'' \times 29''$ (HPBW, RA \times DEC). The σ noise level is 0.035 mJy/beam. Contour levels are -0.1, 0.1, 0.2, 0.3, 0.5, 1, 5, 25, 50 mJy/beam.

source. In the remaining 18 clusters the existence of this type of source was indicated for the first time.

Kempner & Sarazin (2001) made a search for radio halos and relics in all the Abell clusters present in the Westerbork Northern Sky Survey (WENSS, Rengelink et al. 1997) at 327 MHz. They found 18 candidates (7 new). All the 18 clusters show evidence of a recent or ongoing merger. A search for new halo and relic sources is also in progress with the data from the Sidney University Molonglo Sky Survey (Hunstead et al. 1999).

Recently, detailed studies of halos and relics have been performed, providing more information on these sources. High radio luminosity halos have been studied in distant clusters, as A665 ($z = 0.1818$; Fig. 7.9; Giovannini & Feretti 2000), A2163 ($z = 0.203$; Fig. 7.10; Feretti et al. 2001), A2744 ($z = 0.308$; Govoni et al. 2001b), and Cl 0016+16 ($z = 0.5545$; Giovannini & Feretti 2000). A powerful radio halo was found in the hottest known cluster of galaxies (1E 0657–56, $kT = 15.6$ keV; $z = 0.296$) by Liang et al. (2000). From low frequency VLA observations, the existence of a halo and a possible relic has been confirmed in A754

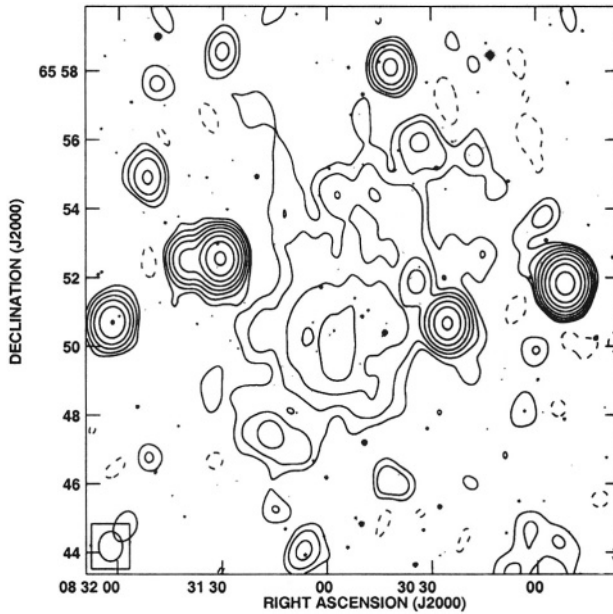


Figure 7.9. Contour map at 20 cm of the central region of A665, superimposed onto the optical image from the Digitized Palomar Sky Survey. The HPBW is $52'' \times 42''$ (PA = 0°); the noise level is 0.065 mJy/beam. Contour levels are: -0.2, 0.2, 0.4, 0.8, 1.5, 3, 6, 12, 25 mJy/beam.

(Kassim et al. 2001), where the presence of diffuse emission was debated in the literature.

Remarkably, in some clusters both a radio halo and a relic have been detected, e.g. in Coma, A2255, A2256, A1300 (Reid et al. 1999), A2744. In A3667 (Röttgering et al. 1994, Fig. 7.3) two giant relics are seen, at opposite positions with respect to the cluster center, separated by about 5 Mpc from each other.

3. STATISTICAL PROPERTIES OF RADIO HALOS AND RELICS

The increase in number of known halo and relic sources allows us to derive some statistical considerations on the properties of these sources and on their hosting clusters, and to make further progress in our understanding of the formation of extended sources in clusters of galaxies.

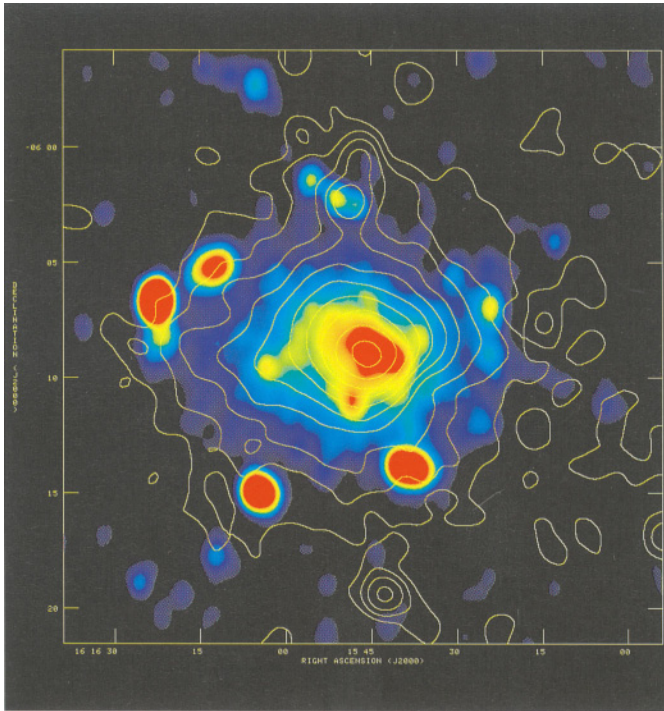


Figure 7.10. Color scale image of the halo source in A2163 at 20 cm, superimposed on contours of the X-ray ROSAT PSPC image.

The properties of radio halos and relics are summarized in the following sub-sections (see also Feretti 2001).

3.1. RADIO PROPERTIES

The size of halos is typically larger than 1 Mpc. Peripheral relics are elongated in shape with the distribution of their largest sizes not statistically different from that of halos.

The distribution of projected distances of halo and relic sources from the cluster center is strongly peaked around zero, indicating that halos are likely to be really located at the cluster center and not simply projected onto it.

Typical radio powers for halo sources are of the order of $10^{24} - 10^{25} \text{ W Hz}^{-1}$ at 1.4 GHz. Halos with a higher radio power are more extended, but no strong correlation is present between the radio size and the radio power.

Equipartition magnetic fields are of the order of $\sim 0.1 - 1 \mu\text{G}$. Minimum energy densities in diffuse sources are between $\sim 5 \cdot 10^{-14}$ and $2 \cdot 10^{-13} \text{ erg cm}^{-3}$. Therefore the energy content in the non-thermal component of the intracluster medium is about 2–3 order of magnitude lower than that of the thermal gas.

3.2. OCCURRENCE

Giovannini et al. (1999), using only data relative to a complete cluster sample, found that 5% of clusters have a radio halo source and 6% a peripheral relic source. The detection rate of diffuse radio sources increases with the cluster X-ray luminosity as shown in Table 7.1 (Giovannini & Feretti 2001), reaching $\sim 33\%$ in clusters with X-ray luminosity larger than 10^{45} erg/s . The clusters hosting a diffuse radio source have a significantly higher X-ray luminosity than clusters without a diffuse source ($> 99.9\%$ confidence level with a KS test).

Table 7.1 . Halo and Relic sources detection rate

$L_x(0.1-2.4 \text{ keV})$ $10^{44} \text{ erg s}^{-1}$	Relics %	Halos %	Total %
0-3	1.3(1)	–	1.3
3-5	3.0(1)	3.0(1)	6.0
5-7	4.5(1)	4.5(1)	9.0
7-10	16.1(5)	9.7(3)	25.8
>10	8.3(1)	25.0(3)	33.3

Note: in parentheses the number of detected sources is given

The presently available data (Giovannini et al. 2001) show no correlation between the number of clusters with diffuse radio sources and the cluster redshift, suggesting that no redshift evolution is present.

3.3. CORRELATIONS WITH CLUSTER PROPERTIES

The radio halo structures show a close similarity to the X-ray structures, suggesting a causal connection (Deiss et al. 1997; Feretti 1999; Liang et al. 2000). The similarity was quantitatively confirmed by Govoni et al. (2001a) who compared the point-to-point brightness surface of the radio and X-ray emission in four clusters and found a nearly linear relationship in two cases (A2255, A2744) and a power-law relation with index < 1 in the other two (Coma, A2319; see Fig. 7.11). A power-law

correlation with index = 0.64 is also obtained for A2163 (Feretti et al. 2001).

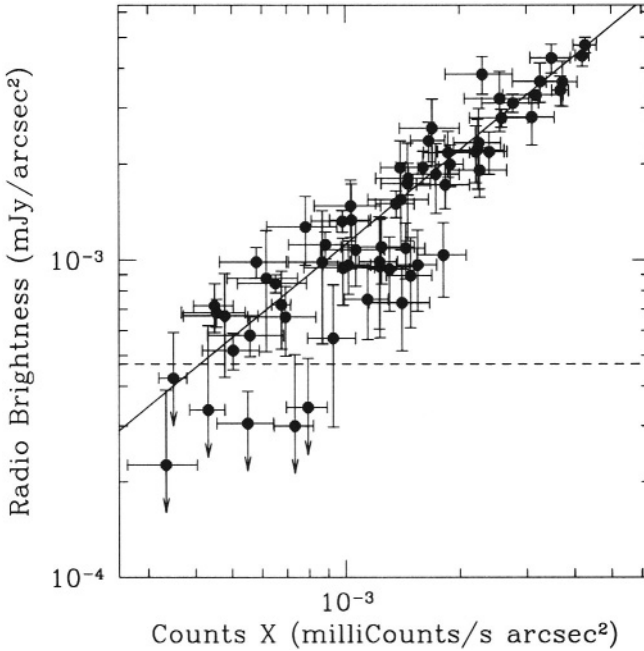


Figure 7.11. Radio surface brightness of the halo F_{radio} versus the cluster X-ray brightness F_X for A2255. Each point is the brightness mean in a cell $90''$ in size, while error bars indicate the r.m.s. of the brightness distribution. The horizontal dashed line indicates the 3 sigma noise level of the radio map. The best fit, indicated by the solid line, indicates a nearly linear relation: $F_{radio} \propto F_X^{0.98}$ (from Govoni et al. 2001a)

A correlation seems to exist between the largest radio size of diffuse sources and the cluster X-ray luminosity, with more X-ray luminous clusters hosting larger radio diffuse sources. The correlation is more evident for radio halos than for relics (Feretti 2001).

Feretti (2001) found that the monochromatic radio power at 1.4 GHz ($P_{1.4GHz}$) of halos increases with the bolometric X-ray luminosity of the parent cluster, implying a correlation between radio power and cluster temperature, as shown by Colafrancesco (1999), Liang (1999) and Liang et al. (2001), and also a direct connection between the radio and X-ray plasmas. Since the cluster X-ray luminosity and mass are correlated, as well as the temperature and the mass (Neumann & Arnaud 1999; Neumann & Arnaud 2001), it follows that radio halo power correlates with the cluster mass. Govoni et al. (2001b) analyzed 6 halo clusters with a

homogeneously estimated gravitational mass and found that $P_{1.4\text{GHz}} \propto M^{2.2}$ (Fig. 7.12). All analyzed clusters containing a radio halo or a relic source have a gravitational mass larger than 10^{15} solar masses within 3 Mpc.

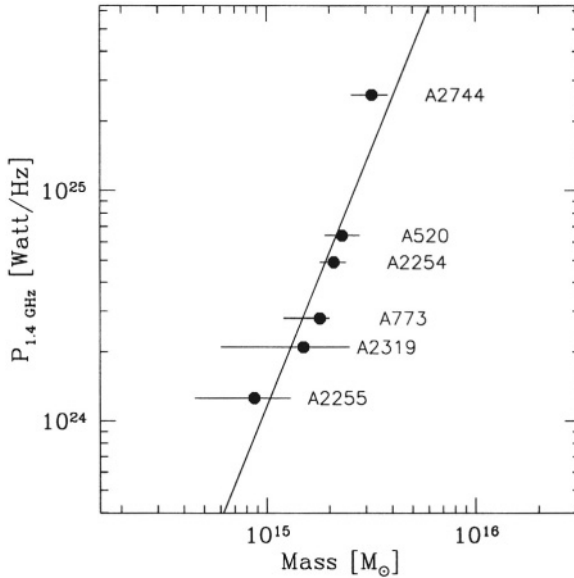


Figure 7.12. Relation between the halo radio power at 1.4 GHz and the gravitational mass for six clusters (see Govoni et al. 2001b). The continuous line is the best fit: $P_{1.4} \propto M^{2.2}$.

The cluster mass is a logical candidate for a fundamental parameter since the energy available to accelerate relativistic particles in a merger scales as $\sim M^2$ as discussed by Buote (2001). The serendipitous detection of halos in massive clusters observed in Sunyaev-Zeldovich detection experiments is a confirmation that massive clusters have the highest probability to possess a halo.

4. RELEVANCE OF CLUSTER MERGER EVENTS

In the first studies of clusters of galaxies containing a halo source (see § 2.3), it was noted that these clusters are characterized by the presence of a merger process. This is indicated by the existence of substructures and distortions in the brightness distribution, and by temperature gradients, which can be interpreted as the result of sub-clump interaction.

In the sample presented by Giovannini et al. (1999) merger evidence has been reported in 10 clusters with a central halo (see Feretti 1999). For other clusters with radio halos, no detailed study exists to confirm or reject a merger event. The 18 candidates found by Kempner & Sarazin (2001) in the WENSS show evidence of a recent or ongoing merger event. *At present we are not aware of any radio halo source in a cluster where the presence of a merger was clearly excluded.* As for relic sources, merger evidence has been found in 9 clusters containing a relic source. For other relic source clusters no data are available to confirm or reject the merger scenario.

Further indications can be obtained with statistical arguments. Significant substructure is detected in halo/relic clusters (Böhringer & Schuecker, this volume). Feretti (2001) derived that: i) the X-ray core radii of clusters with halos/relics are significantly larger (>99% level using a KS test) than those of clusters classified as single/primary by Jones & Forman (1999). According to the last authors, the large core radius clusters are multiple systems in the process of merging and tend to have larger core radii; ii) in halo/relic clusters the values of spectroscopic β are on average larger than 1, indicating the presence of substructure (Edge & Stewart 1991); iii) clusters with halos and relics have larger distances to their next neighbours compared to ordinary clusters with similar X-ray luminosity, i.e. similar cluster mass (Schuecker & Böhringer 1999). The fact that they appear more isolated supports the idea that recent merger events lead to a depletion of the nearest neighbours.

Moreover, clusters with halos do not have a strong cooling flow, in agreement with the fact that a strong merger process is expected to disrupt the cooling flow (Peres et al. 1998; Roettiger et al. 1996). As a consequence, no halo source has been found in cooling flow clusters with the exception of the small size radio halo in A2142 (Giovannini & Feretti 2000). A2142 is peculiar since the central cooling flow has been disturbed but not destroyed by a merger (Markevitch et al. 2000; Ettori & Fabian 2000).

By using radio power vs magnitude of the dipole power ratio to relate gravitational potential fluctuations to substructure in X-ray images, Buote (2001) provided the first quantitative comparison of the dynamical states of clusters with halo or relic sources. A correlation between the 1.4 GHz radio power of the radio halo or relic and the magnitude of the dipole power ratio (P_1/P_0 , Buote & Tsai 1996) was found such that approximately $P_{1.4} \propto P_1/P_0$: the strongest radio halos are found in those clusters currently experiencing the largest departure from a virialized status (Buote 2001, Fig. 7.13). Radio halos form only when

a sufficiently large dynamical disturbance has proceeded fully into the core of a cluster (see also Buote, this volume).

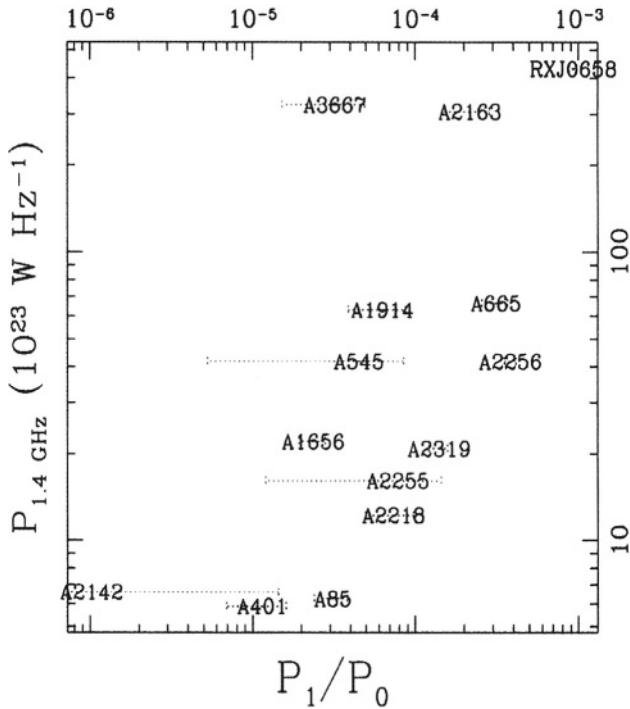


Figure 7.13. Radio power at 1.4 GHz of halos and relics versus the cluster dipole power ratio P_1/P_0 . The figure is from Buote (2001)

Taking into account this result and the arguments presented above, we conclude, in agreement with Buote (2001), that the occurrence of radio halos can be understood when both the dynamical state and the mass of the cluster are taken in account. The need for a high mass (high L_x and high T) can explain the rarity of radio halos in low luminous X-ray clusters. However, cluster mass on its own cannot account for the frequency of radio halos, the presence of a violent, core-disrupting, merger is also necessary. For example no halo source has been found in the massive cluster A2029 which is apparently a nearly relaxed system (Buote 2001).

Most of the peripheral relics have been found in clusters with properties similar to clusters with a halo source, and relic sources correlate with cluster properties as the halo sources do (see e.g. Buote 2001). However a few relic sources are present in the peripheral regions of cooling flow

clusters (e.g. A85), suggesting that peripheral sources are less affected, or not affected at all, by the central physical conditions. This point needs further investigation in light of relic source formation models.

5. MODELS

As discussed in the previous sections, the emission from halos and relics, produced by synchrotron radiation, demonstrates that the cluster ICM is characterized not only by the thermal hot gas, but also of non-thermal components, i.e. magnetic field and relativistic particles, detected with radio observations. We summarize in the following the models related to the production of these two components (see also Enßlin 2001 and the review on magnetic fields by Carilli & Taylor 2002).

5.1. MAGNETIC FIELD

5.1.1 Observational results. The large scale magnetic field in a cluster of galaxies can be estimated using different observational approaches.

i) Clusters with radio halos and relics. From high quality radio images it is possible to estimate the cluster magnetic field under the assumption of energy *equipartition*, i.e. in the case that the non-thermal energy density within the extended radio source is minimum and the contributions of relativistic particles and magnetic fields are approximately equal. Values of the order of $0.1 - 1 \mu\text{G}$ have been derived assuming that homogeneous magnetic fields fill the whole radio source volume.

Another estimate of the magnetic field can be derived from the emission in a different band. The high energy relativistic electrons, with $\gamma \sim 10^4$, responsible for the radio emission in the ICM, scatter off the cosmic microwave background (CMB), boosting photons from this radiation field to the X-ray and γ -ray regions and producing inverse-Compton emission. Measurements of this radiation, combined with results from radio observations, enables the direct determination of the electron density and mean magnetic field, without the need to invoke equipartition. The recent detections of non-thermal hard X-ray emission from the Coma cluster and A2256 (Fusco-Femiano et al. 1999, 2000; Rephaeli et al. 1999) can be explained in the framework of the inverse-Compton model. The values of the volume-averaged intracluster magnetic field obtained in this way are of $\sim 0.16 \mu\text{G}$ in the Coma cluster, $\sim 0.5 \mu\text{G}$ and $\sim 0.05 \mu\text{G}$ in A2256 (center and peripheral northern region, respectively). These values are consistent with the equipartition estimates.

ii) Faraday Rotation of background or cluster sources. Using high resolution images of radio sources in or behind clusters of galaxies one

can derive an average of the magnetic field along the line of sight. The first study of background rotation measures (RMs) for a single cluster was obtained by Kim et al. (1990) with deep VLA observations of 18 sources in the Coma cluster region. They obtained an estimate of $\sim 2 \mu\text{G}$ for the Coma cluster field, while Feretti et al. (1995) studying the extended tailed radio galaxy NGC4869, located at the Coma cluster center, found a strongly tangled magnetic field component (cellsize ~ 1 kpc) of intensity $\sim 6 \mu\text{G}$ and a weaker magnetic field component ($0.1 - 0.2 \mu\text{G}$), ordered on a scale of about a cluster core radius. In the clusters A119 and A514 cluster magnetic fields in the range $4 - 10 \mu\text{G}$, tangled on a scale of few kpc have been found by Feretti et al. (1999), and Govoni et al. (2001c), respectively.

From statistical studies Kim et al. (1991) obtained a significant positive detection of a RM excess associated with clusters of galaxies. When combined with available X-ray data, the RM data indicates that the field strength is of the order of $1 \mu\text{G}$ if the field is tangled on scales similar to the galaxy sizes. They found also that the field strength decreases with radius more slowly than Jaffe's (1980) suggestion or that the tangling field scale increases with radius. Recently Clarke et al. (2001) analyzed the RM of radio sources in a sample of 16 Abell clusters. They found that the ICM is permeated by magnetic fields with a high filling factor at levels of $4 - 8 \mu\text{G}$ and a correlation length of ~ 15 kpc, up to ~ 0.75 Mpc from the cluster center.

Strong magnetic fields, up to the value of tens of μG have been found in the central regions of cooling flow clusters where it has been suggested that the cooling flow process may play a relevant role in the magnetic field amplification (Taylor et al. 1999, 2001 and references therein), but these are not relevant to the present discussion.

5.1.2 Interpretation. The magnetic field strengths obtained from RM arguments are higher than the equipartition values derived from the radio data, and from those estimated via inverse-Compton X-ray emission. We note, however, that values deduced from radio synchrotron emission and from inverse-Compton refer to averages on large volumes. On the contrary, RM estimates give a weighted average of the field along the line of sight, and could be sensitive to the presence of filamentary structure in the cluster and/or to the existence of local turbulence around the radio galaxies, and could therefore be higher than the average cluster value (see also Goldshmidt & Rephaeli 1993).

From the observational evidence, we can generally conclude that clusters of galaxies are pervaded by magnetic fields at least of the order of $\sim 1 \mu\text{G}$ even if no halo or relic source is present. According to these

findings, the energy associated with the magnetic field is comparable to the turbulent and thermal energy, i.e. the fields are strong enough to be dynamically important in a cluster.

The ICM magnetic field could be primordial (Olinto 1998) or injected from galactic winds, or active galaxies (Kronberg et al. 1999; Völk & Atoyan 1999), or produced in shock waves of large scale structure formation (Kang et al. 1997). The seed fields, whose strength has been calculated to be up to 10^{-9} G (see Kronberg 1994; Blasi et al. 1999), need to be amplified to give the fields that we observe at present. Amplification by hydrodynamic turbulence excited by galactic motions has been suggested as a likely possibility (Jaffe 1980; Ruzmaikin et al. 1989). However, it has been shown that this process is unlikely to give mean field values higher than a few $0.1 \mu\text{G}$ over large cluster regions (De Young 1992; Goldshmidt & Rephaeli 1993), mainly because of the small turbulent velocities driven by galactic wakes, and because turbulent energy cascades to the dissipation scale more rapidly than the dynamo process could amplify the field (see also Schindler, this volume).

The most likely possibility is that the magnetic field is amplified by turbulence following a cluster merger (Tribble 1993; Roettiger et al. 1999a; Dolag et al. 1999). The simulations of Roettiger et al. (1999a) show that the magnetic field energy increases by greater than a factor of 10–20 in localized regions. It is likely that massive clusters undergo several major mergers during their lifetime and that each successive merger will further amplify the field.

The observations are often interpreted in terms of the simplest possible model, i.e. in this case a constant field through the cluster. However, Jaffe (1980) suggested that the magnetic field distribution depends on the thermal gas density and on the distribution of massive galaxies and therefore would decline with the cluster radius, as also derived by Brunetti et al. (2001a) in Coma. Moreover, the magnetic field in a magnetized plasma is more likely to be bunched into elongated high-field regions, i.e. to show structures of filaments or flux-ropes (Eilek 1999).

5.2. RELATIVISTIC PARTICLES IN HALOS

The difficulty in explaining radio halos arises from the combination of their large size, more than 1 Mpc, and the short synchrotron lifetime of relativistic electrons. The expected diffusion velocity of the electron population is of the order of the Alfvén speed ($\sim 100 \text{ km s}^{-1}$) making it difficult for the electrons to diffuse over a megaparsec-scale region within their radiative lifetime.

5.2.1 Primary electron models. Jaffe (1977) and Rephaeli (1977) suggested that the radio halo results from synchrotron emission of relativistic electrons diffusing away from one or more active radio galaxies in the cluster. This diffusion model was favoured by Valtaoja (1984) who used it to explain the spatial radio intensity distribution at 430 MHz of the Coma cluster. Rephaeli (1979) extended his primary electron model by including ionization and bremsstrahlung losses. However, as mentioned above, if the electrons are constrained by the canonical streaming limit of the Alfvén speed, there is no way they can reach the large distances implied by the extent of the radio halo without having already radiated away most of their energy. Holman et al. (1979) showed that relativistic electrons streaming through a hot background plasma will not be constrained to the Alfvén speed, but rather will stream at speeds of about the ion sound speed. This is larger than the Alfvén speed but still lower than the speed required by the observed sizes of radio halos.

5.2.2 Primary electron reacceleration models. To solve the Alfvén speed limit Jaffe (1977) proposed continuous in-situ reacceleration of the radiating electrons, operating in the ICM. Roland (1981) and Roland et al. (1981) suggested that the necessary turbulent magnetic fields are due to the wakes of galaxies moving through the cluster medium. Schlickeiser et al. (1987), from a quantitative comparison between the observational results of Coma and the predictions from halo models, concluded that the observations are consistent with the in-situ reacceleration.

Harris et al. (1980) first suggested that radio halos are formed in cluster mergers where the merging process creates the shocks and turbulence necessary for the magnetic field amplification and high-energy particle acceleration. Later, Tribble (1993) showed that the energetics involved in a merger are more than enough to power a radio halo. He also suggested that the halos thus produced are expected to be transient since the relativistic electrons lose energy on time scales of $\sim 10^8$ yr and the time interval between mergers is of the order of $\sim 10^9$ yr. This argument was used to explain why radio halos are rare.

The hypothesis that the cluster merger is the most likely process acting in the reacceleration of relativistic particles has been worked on in recent years (Brunetti et al. 2001a; Blasi 2001; Petrosian 2001; see also Sarazin, this volume). In major mergers, hydrodynamical shocks dissipate energies of $\sim 3 \cdot 10^{63}$, which is partly converted into the acceleration of relativistic electrons. Simulations are presented by Takizawa & Naito (2000). Petrosian (2001) showed that the most likely scenario appears

indeed to be an episodic injection-acceleration model, whereby one obtains a time dependent spectrum that for certain phases of its evolution satisfies all the requirements.

5.2.3 Origin of the primary relativistic electrons. In the past it was suggested that the radio emitting particles could have been produced by radio galaxies (Jaffe 1977; Rephaeli 1977, 1979; Valtaoja 1984; Giovannini et al. 1993). This implies that they have to escape out of the radio plasma, which is difficult since the necessary diffusion across the magnetic field is an extremely slow process. Enßlin (1999) showed that turbulence in the ICM can strongly increase the diffusion coefficient and especially shortly after major merger events there is a time window when particles might be able to escape. However, Giovannini & Feretti (2000) derived that the halo source phenomenon does not appear to be correlated with the presence of cluster radio galaxies (in particular head tail radio sources). Moreover Brunetti et al. (2001b) estimated that the fresh-injected population supplied in the Coma cluster by the tailed radio source present at the cluster center (NGC4869) does not significantly contribute to the ≥ 300 MHz spectrum of the radio halo but it could significantly contribute to the emission at lower radio frequencies and extreme ultraviolet. The energy of this population is indicated by a solid line in Fig. 7.14.

Alternatively, Liang et al. (2000) proposed that the relativistic particles could be accelerated out of the thermal pool. Petrosian (2001) pointed out that this possibility suffers from two serious difficulties: 1) the conditions required for the acceleration are different from those in the ICM, 2) the acceleration process must overcome the heavy losses the electrons will suffer as they are pulled from their low energy. This would imply a high level of turbulence and would lead to a high amount of energy in the ICM, which would heat up the ICM plasma to above 10^8 K in less than 10^8 yr.

According to a recent model proposed by Brunetti et al. (2001a), the relativistic particles are injected into the cluster volume by strong shocks from earlier mergers, and by starburst and/or AGN activity, and their presence is therefore connected to the dynamical history of the clusters (see § 5.2.5).

5.2.4 Secondary electron model. To avoid the energy loss problems of the radiating electrons during their diffusion through the cluster, Dennison (1980) suggested that the radio emission in the halos results from a population of secondary electrons produced by energetic protons leaking from the cluster galaxies. The secondary electrons re-

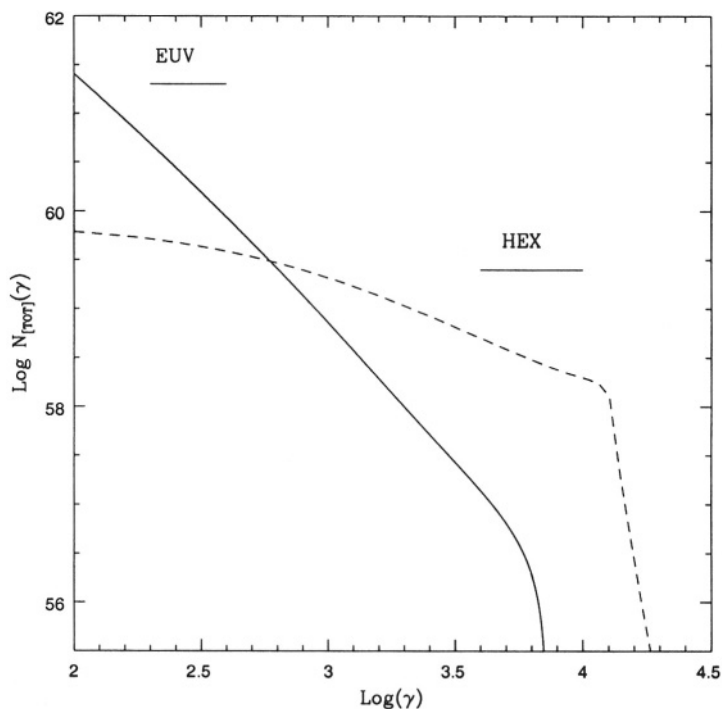


Figure 7.14. Plot of the energy distribution of the relativistic electron populations in the Coma cluster. The dashed line represents the main electron population, integrated over the cluster volume, injected during the first phase and reaccelerated during the second phase. The solid line refers to the additional electron population injected by the radio galaxy NGC 4869. The typical energies of the electrons emitting via IC in the hard X-ray band (HEX) and in the EUV band are also indicated (from Brunetti et al. 2001b).

sult from inelastic nuclear collisions between the relativistic protons and the thermal ions of the ambient intracluster medium (Sarazin, this volume). The protons diffuse on large scales because their energy losses are negligible and they can produce in situ electrons distributed through the cluster volume. This model has been recently analyzed by Blasi & Colafrancesco (1999) and by Dolag & Enßlin (2000). The first authors calculate the fluxes of radio, hard X-rays and gamma-ray emission and apply the calculations to the Coma cluster. They find that very small values of the magnetic field ($\sim 0.1 \mu\text{G}$) are required, whereas the gamma-ray fluxes can easily exceed the EGRET limit at 100 Mev. Dolag & Enßlin (2000) performed cosmological magneto-hydrodynamic simu-

lations to derive the gas and magnetic field distribution, reproducing several observational results.

The model can explain the radio power-temperature relation. A major argument against the secondary electron model is that protons have long lifetimes against radiative losses, therefore any cluster that has been the site of a moderate amount of radio activity might be expected to contain a radio halo. Moreover, the observed association between mergers and radio halos is not explained by this model as well as the spectral index distribution found in Coma C (see § 2.1).

5.2.5 The Two Phase model. In principle, current models invoking a continuous injection of relativistic electrons may explain the total synchrotron spectrum of halo sources and of Coma C in particular, but they fail to reproduce the spectral steepening with radius observed in Coma C. Since the diffusion velocity of the relativistic particles is low in relation to their radiative lifetimes, the spectral steepening cannot be due to the diffusion of rapidly ageing electrons from the central regions into the cluster volume (Berezinsky et al. 1997; Sarazin 1999). It could be related to the intrinsic evolution of the local electron spectrum and to the radial profile of the cluster magnetic strength.

In view of the above arguments, a two phase scenario was suggested by Brunetti et al. (2001a) for Coma C. Their model includes a *first phase* of particle injection, followed by a *second phase* during which the aged electrons are reaccelerated by recent merging processes. In the framework of this model, two general results are obtained:

- The formation of luminous radio halos may not be a common phenomenon. Indeed the injected relativistic electrons suffer efficient radiation and Coulomb losses and rapidly cool. This prevents the formation of a radio halo if the time gap between the *first* and *second phase* Δt is larger than $\sim 2 - 3$ Gyr. Furthermore, in order to allow the formation of a radio halo during the reacceleration *phase*, the number of relativistic electrons injected during the *first phase* should be large enough, increasing with increasing Δt . In this framework one could claim that the radio halo formation is favoured in the case of massive clusters which probably derive from a stronger merger activity in the past and where the injection of larger quantities of cosmic rays is more efficient.

- Central radio halos triggered during the *second phase* by diffuse reacceleration processes are expected to show a steepening in the synchrotron spectrum with increasing distance from the center of the cluster. Indeed, the magnetic field strength is expected to be a decreasing function of the radius and so probably also the reacceleration efficiency.

The model has been applied in detail to the well studied radio halo Coma C (Brunetti et al. 2001a). The radial steepening of the radio spectrum observed in Coma C (Giovannini et al. 1993; Deiss et al. 1997) has been used to constrain the physical conditions in the cluster, obtaining reacceleration efficiencies of the order of 10^{-8}yr^{-1} and average magnetic field strengths ranging from $1\text{--}3\ \mu\text{G}$ in the central regions to $0.05\text{--}0.1\ \mu\text{G}$ in the external parts of the cluster (at $\sim 2\text{--}3\ \text{Mpc}$). The model satisfactorily reproduces the total radio spectrum of Coma C and the size of the halo. The expected hard X-ray inverse-Compton emission, mainly produced at relatively large distances from the cluster center ($\geq 1.5\ \text{Mpc}$), is consistent with the flux detected by BeppoSAX (Fusco-Femiano et al. 1999). In Fig. 7.14 the energy of electron populations present in the Coma cluster is shown.

5.3. RELATIVISTIC PARTICLES IN RELICS

The relics were originally considered as remnants of galaxies active in the past, and therefore of different and established origin with respect to radio halos. There are several difficulties, however, with this interpretation: the identification of a parent galaxy, the discovery of large relics and the problem, already mentioned for the halos, that the age of the electron population is too short to allow the diffusion of relativistic electrons over very large distances. In recent years, there is increasing evidence that the relics are related to ongoing merger events, and are tracers of shock waves, as first proposed by Enßlin et al. (1998). Enßlin (1999) proposed that active radio galaxies fill large volumes in the ICM with radio plasma, which becomes rapidly invisible to radio telescopes because of radiation losses of the relativistic electrons. These patches of fossil radio plasma, called “radio ghosts”, are revived by adiabatic compression in a shock wave produced in the ICM by the flows of cosmological large-scale structure formation (Enßlin & Gopal-Krishna 2001). If the fossil radio plasma were not too old, the upper cutoff of the electron energy spectrum might be adiabatically shifted to radio observable energies. Radio plasma younger than $\sim 0.1\ \text{Gyr}$ close to the centers of galaxy clusters, and $\sim 1\ \text{Gyr}$ at peripheral regions can be revived to radio emission in typical shock waves. This helps to explain the observed rarity of relics with respect to the high frequency of merging clusters. Recently Enßlin & Brüggen (2001) presented 3-D MHD simulations of a hot, magnetised bubble that traverses a shock wave in a much colder environment. The derived simulated maps reproduce very well the filamentary structure and polarization seen in a few relic sources with high resolution radio observations (Slee et al. 2001). Enßlin &

Brüggen (2001) conclude that there is a strong evidence that cluster radio relics indeed consist of fossil radio plasma that has been compressed adiabatically by a shock wave as proposed by Enßlin & Gopal-Krishna (2001). Further confirmation in support of this model is provided by the simulations for A3667 (Roettiger et al. 1999b) and by the recent images of A754 (Kassim et al. 2001).

6. SUMMARY

The presence of diffuse halos and relics in clusters of galaxies is now well established. After the discovery of the Coma halo, new sources of this class were found. Presently, we know about 40 clusters hosting diffuse sources, many of which have been found in recent years.

Halos and relics are related to the ICM, and therefore they demonstrate that important non-thermal components (magnetic fields and relativistic particles) are present in galaxy clusters.

Until recently these sources were considered to be rare. This is no longer true. The much improved sensitivity of radio telescopes and the existence of deep radio surveys have shown that halos and relics are relatively common in high X-ray luminosity clusters, i.e. hot and massive clusters. In addition both halos and relics seem to be associated with clusters which have undergone recent merging processes. The properties (radio power, size, brightness) of halos and relics are strictly connected to the properties of their parent clusters (X-ray luminosity, temperature, mass), indicating the existence of a causal connection between the thermal and relativistic plasma in clusters of galaxies.

The formation of halos and relics seems to be strongly affected by the dynamical behaviour of the clusters. The origin of relativistic particles and magnetic fields is related to the past cluster formation history, whereas the energy for the maintenance of diffuse sources, i.e. the re-acceleration of radio emitting particles and the amplification of magnetic fields, is crucially supplied by recent cluster/subcluster mergers.

Acknowledgments

We acknowledge partial financial support from the Italian Space Agency ASI.

References

- Ballarati, B., Feretti, L., Ficarra, A., Giovannini, G., Nanni, M., Olori, C. & Gavazzi, G. 1981, *A&A*, 100, 323
Berezinsky, V.S., Blasi, P. & Ptuskin, V.S. 1997, *ApJ*, 487, 529

- Blasi, P. 2001, *Astroph. Phys.*, 15, 223
- Blasi, P., Burles, S. & Olinto, A.V. 1999, *ApJL*, 514, L79
- Blasi, P. & Colafrancesco, S. 1999, *Astroph. Phys.*, 12, 169
- Bozayan, E.P. 1968, *ApJL*, 152, L155
- Bridle, A.H. & Fomalont, E.B. 1976, *A&A*, 52, 107
- Bridle, A.H., Fomalont, E.B., Miley, G.K. & Valentijn, E.A. 1979, *A&A*, 80, 201
- Brunetti, G., Setti G., Feretti, L. & Giovannini, G. 2001a, *MNRAS*, 320, 365
- Brunetti, G., Setti G., Feretti, L. & Giovannini, G. 2001b, *New Astron.*, 6, 1
- Buote, D.A. 2001, *ApJL*, 553, L15
- Buote, D.A. & Tsai, J.C. 1996, *ApJ*, 458, 27
- Cane, H.V., Erickson, W.C., Hanisch, R.J. & Turner, P.J. 1981, *MNRAS*, 196, 409
- Carilli, C.L. & Taylor, G.B. 2002, *ARA&A*, 40, in press, astro-ph/0110655
- Clarke, T.E. & Enßlin, T.A. 2001, in *Galaxy Clusters and the High Redshift Universe Observed in X-rays*, XXI Moriond Astrophysics Meeting (March 2001), eds. D. Neumann, F. Durret, & J. Tran Thanh Van, in press, astro-ph/0106137
- Clarke, T.E., Kronberg, P.P. & Böhringer, H. 2001, *ApJL*, 547, L111
- Colafrancesco, S. 1999, in *Diffuse thermal and relativistic plasma in galaxy clusters*, eds. H. Böhringer, L. Feretti & P. Schuecker, MPE Report 271, 269
- Condon, J.J., Cotton, W.D., Greisen, E.W., Yin, Q.F., Perley, R.A., Taylor, G.B. & Broderick, J.J. 1998, *AJ*, 115, 1693
- Deiss, B.M., Reich, W., Lesch, H. & Wielebinski, R. 1997, *A&A*, 321, 55
- Dennison, B. 1980, *ApJL*, 239, L93
- De Young, D.S. 1992, *ApJ*, 386, 464
- Dolag, K., Bartelmann, M. & Lesch, H. 1999, *A&A*, 348, 351
- Dolag, K. & Enßlin, T.A. 2000, *A&A*, 362, 151
- Ebeling, H., Voges, W., Böhringer, H., Edge, A.C., Huchra, J.P. & Briel, U.G. 1996, *MNRAS*, 281, 799
- Edge, A.C. & Stewart, G.C. 1991, *ApJ*, 252, 428
- Eilek, J. 1999, in *Diffuse thermal and relativistic plasma in galaxy clusters*, eds. H. Böhringer, L. Feretti & P. Schuecker, MPE Report 271, 71
- Enßlin, T.A. 1999, in *Diffuse thermal and relativistic plasma in galaxy clusters*, eds. H. Böhringer, L. Feretti & P. Schuecker, MPE Report 271, 275
- Enßlin, T.A. 2001, in *The Universe at Low Frequencies*, Pune 1999, ASP Conference Series, in press, astro-ph/0001433

- Enßlin, T.A. & Brüggem, M. 2001, MNRAS submitted, astro-ph/0104233
- Enßlin, T.A. & Gopal-Krishna 2001, A&A, 366, 26
- Enßlin, T.A., Biermann, P.L., Klein, U. & Kohle, S. 1998, A&A, 332, 395
- Ettori, S. & Fabian, A.C. 2000, MNRAS, 317, L57
- Feretti, L. 1999, in *Diffuse thermal and relativistic plasma in galaxy clusters*, eds. H. Böhringer, L. Feretti & P. Schuecker, MPE Report 271, 3
- Feretti, L. 2001, in *The Universe at Low Frequencies*, Pune 1999, ASP Conference Series, in press, astro-ph/0006379
- Feretti, L. & Giovannini, G. 1996, in *Extragalactic radio sources*, eds. R. Ekers, C. Fanti & L. Padrielli, Kluwer Academic Publishers, 333
- Feretti, L., Böhringer, H., Giovannini, G. & Neumann, D. 1997b, A&A, 317, 432
- Feretti, L., Dallacasa, D., Giovannini, G. & Tagliani, A. 1995, A&A, 302, 680
- Feretti, L., Dallacasa, D., Govoni, F., Giovannini, G., Taylor, G.B. & Klein, U. 1999, A&A, 344, 472
- Feretti, L., Fusco-Femiano, R., Giovannini, G. & Govoni, F. 2001, A&A, 373, 106
- Feretti, L., Giovannini, G. & Böhringer, H. 1997a, New. Astron., 2, 501
- Fusco-Femiano, R., dal Fiume, D., Feretti, L., Giovannini, G., Grandi, P., Matt, G., Molendi, S. & Santangelo, A. 1999, ApJL, 513, L21
- Fusco-Femiano, R., Dal Fiume, D., De Grandi, S., Feretti, L., Giovannini, G., Grandi, P., Malizia, A., Matt, G. & Molendi, S. 2000, ApJL, 534, L7
- Gavazzi, G. 1978, A&A, 69, 355
- Giovannini, G. & Feretti, L. 2000, New Astron., 5, 335
- Giovannini, G. & Feretti, L. 2001, in *Cluster Mergers and their Connection to Radio Sources*, 24th meeting of the IAU, JD 10, Manchester, Highlights of Astronomy, Vol 12, in press
- Giovannini, G., Feretti, L. & Govoni, F. 2001, in *The Universe at Low Frequencies*, Pune 1999, ASP Conference Series, in press, astro-ph/0006380
- Giovannini, G., Feretti, L. & Stanghellini, C. 1991, A&A, 252, 528
- Giovannini, G., Feretti, L., Venturi, T., Kim, K.-T. & Kronberg, P.P. 1993, ApJ, 406, 399
- Giovannini, G., Kim, K.-T., Kronberg, P.P. & Venturi, T. 1990, IAU Symposium n. 140, eds. R. Beck, P.P. Kronberg & R. Wielebinski, 492
- Giovannini, G., Tordi, M. & Feretti, L. 1999, New Astron., 4, 141
- Goldshmidt, O. & Rephaeli, Y. 1993, ApJ, 411, 518

- Goss, W.M., Ekers, R.D., Skellern, D.J. & Smith, R.M. 1982, MNRAS, 198, 259
- Govoni, F., Enßlin, T.A., Feretti, L. & Giovannini, G. 2001a, A&A, 369, 441
- Govoni, F., Feretti, L., Giovannini, G., Böhringer, H., Reiprich, T.H. & Murgia, M. 2001b, A&A, 376, 803
- Govoni, F., Taylor, G.B., Dallacasa, D., Feretti, L. & Giovannini, G. 2001c, A&A, in press, astro-ph/0110178
- Hanisch, R.J. 1982a, A&A, 116, 137
- Hanisch, R.J. 1982b, A&A, 111, 97
- Harris, D.E. & Miley, G.K. 1978, A&AS, 34, 117
- Harris, D.E., Kapahi, V.K. & Ekers, R.D. 1980, A&AS, 39, 215
- Holman, G.D., Ionson, J.A. & Scott, J.S. 1979, ApJ, 228, 576
- Hunstead, R.W. et al. 1999, in *Diffuse thermal and relativistic plasma in galaxy clusters*, eds. H. Böhringer, L. Feretti & P. Schuecker, MPE Report 271, 19
- Jaffe, W.J. 1977, ApJ, 212, 1
- Jaffe, W.J. 1980, ApJ, 241, 925
- Jaffe, W.J. & Rudnick, L. 1979, ApJ, 233, 453
- Jones, C. & Forman, W. 1999, ApJ, 511, 65
- Kang, H., Rachen, J.P. & Biermann, P. 1997, MNRAS, 286, 257
- Kassim, N.E., Clarke, T.E., Enßlin, T.A., Cohen, A.S. & Neumann, D.M. 2001, ApJ, 559, 785
- Kempner, J.C. & Sarazin, C.L. 2001, ApJ, 548, 639
- Kim, K.-T., Kronberg, P.P., Dewdney, P.E. & Landecker, T. L. 1990, ApJ, 355, 29
- Kim, K.-T., Kronberg, P.P., Giovannini, G. & Venturi, T. 1989, Nature, 341, 720
- Kim, K.-T., Kronberg, P.P. & Tribble, P.C. 1991, ApJ, 379, 80
- Kronberg, P.P. 1994, Rep. Prog. Phys., 325, 382
- Kronberg, P.P., Lesch, H. & Lepp, U. 1999, ApJ, 511, 56
- Large, M.I., Mathewson, D.S. & Haslam, C.G.T. 1959, Nature, 183, 1663
- Liang, H. 1999, in *Diffuse thermal and relativistic plasma in galaxy clusters*, eds. H. Böhringer, L. Feretti & P. Schuecker, MPE Report 271, 33
- Liang, H. 2001, in *Cluster Mergers and their Connection to Radio Sources*, 24th meeting of the IAU, JD 10, Manchester, in press, astro-ph/0012166
- Liang, H., Hunstead, R.W., Birkinshaw, M. & Andreani, P. 2000, ApJ, 544, 686
- Markevitch, M. et al. 2000, ApJ, 541, 542
- Noordam, J.E. & de Bruyn, A.G. 1982, Nature, 299, 597
- Neumann, D.M. & Arnaud, M. 1999, A&A, 348, 711

- Neumann, D.M. & Arnaud, M. 2001, *A&A*, 373, L33
- Olinto, A. 1998, in *Particle Cosmology*, eds. K. Sato, T. Yanagida & T. Shiromizu, Univ. Academy Press, Inc., 151
- Peres, C.B., Fabian, A.C., Edge, A.C., Allen, S.W., Johnstone, R.M. & White, D.A. 1998, *MNRAS*, 298, 416
- Petrosian, V. 2001, *ApJ*, 557, 560
- Reid, A.D., Hunstead, R.W., Lemonon, L. & Pierre, M.M. 1999, *MNRAS*, 302, 571
- Rengelink, R.B., Tang, Y., de Bruyn, A.G., Miley, G.K., Bremer, M.N., Röttgering, H.J.A. & Bremer, M.A.R. 1997, *A&AS*, 124, 259
- Rephaeli, Y. 1977, *ApJ*, 212, 608
- Rephaeli, Y. 1979, *ApJ*, 227, 364
- Rephaeli, Y., Gruber, D. & Blanco, P. 1999, *ApJL*, 511, L21
- Roland, J. 1981, *A&A*, 93, 407
- Roland, J., Sol, H., Pauliny-Toth, I. & Witzel, A. 1981, *A&A*, 100, 7
- Roettiger, K., Burns, J.O. & Loken, C. 1996, *ApJ*, 473, 651
- Roettiger, K., Burns, J.O. & Stone, J.M. 1999b, *ApJ*, 518, 603
- Roettiger, K., Stone, J.M. & Burns, J.O. 1999a, *ApJ*, 518, 594,
- Röttgering, H.J.A., Snellen, I., Miley, G., de Jong, J.P., Hanisch, R.J. & Perley, R. 1994, *ApJ*, 436, 654
- Röttgering, H.J.A., Wieringa, M.H., Hunstead, R.W. & Ekers, R.D. 1997, *MNRAS*, 290, 577
- Ruzmaikin, A., Sokoloff, D. & Shukurov, A. 1989, *MNRAS*, 241, 1
- Sarazin, C.L. 1999, *ApJ*, 520, 529
- Schlickeiser, R., Sievers, A. & Thiemann, H. 1987, *A&A*, 182, 21
- Schuecker, P. & Böhringer, H. 1999, *Diffuse thermal and relativistic plasma in galaxy clusters*, eds. H. Böhringer, L. Feretti & P. Schuecker, MPE Report 271, 43
- Sijbring, L.G. 1993, PhD Thesis Groningen University
- Slee, O.B., Roy, A.L., Murgia, M., Andernach, H. & Ehle, M. 2001, *AJ*, 122, 1172
- Takizawa, M. & Naito, T. 2000, *ApJ*, 535, 586
- Taylor, G.B., Allen, S.W. & Fabian, A.C. 1999, in *Diffuse thermal and relativistic plasma in galaxy clusters*, eds. H. Böhringer, L. Feretti & P. Schuecker, MPE Report 271, 77
- Taylor, G.B., Govoni, F., Allen, S.A. & Fabian, A.C. 2001, *MNRAS*, 326, 2
- Tribble P.C. 1993, *MNRAS*, 263, 31
- Valtaoja E. 1984, *A&A*, 135, 141
- Völk H.J. & Atoyan A.M. 1999, *Astroph. Phys.*, 1, 73
- Willson, M.A.G. 1970, *MNRAS*, 151, 1

This page intentionally left blank

Chapter 8

MERGERS OF GALAXY CLUSTERS IN NUMERICAL SIMULATIONS

Sabine Schindler

Astrophysics Research Institute

Liverpool John Moores University,

Twelve Quays House

Birkenhead CH41 1LD, UK

sas@astro.livjm.ac.uk

Abstract Simulations of clusters of galaxies reveal how clusters form and evolve. Models of cluster mergers show many characteristics of these very energetic events: shock structure and strength, temperature variations and gas distribution. Also detailed observational signatures of the dynamical state can be derived from the models. The simulations show that mergers have effects on the magnetic field, on the X-ray luminosity, on mass determination, on metal enrichment processes and other physical processes in clusters of galaxies.

Introduction

The time scales of the evolution of large astrophysical objects like clusters of galaxies are of the order or little less than the age of the universe. Hence with observations one can never follow the evolution of clusters, but observations provide only snapshots of the different evolutionary stages. Numerical simulations provide therefore a unique way to follow the evolution and the dynamics of galaxy clusters and their components.

Such numerical models do not only help to understand how the clusters form and evolve, but cluster models can also be compared directly with observations. This comparison is useful for many different purposes. One application is the correct interpretation of observations: from the models observational quantities can be derived. With these “simulated

observations” one can for example distinguish which observable feature corresponds to which dynamical state. Moreover, observational methods can be tested with the simulated data. The results can be compared to the input parameters of the calculations and, in an iterative procedure, the methods can be refined. In this way not only can physical processes in clusters and on larger scales be understood, but there is also an opportunity to constrain cosmological models.

Merging of subclusters is a particularly interesting phenomenon to study with simulations. Irregular cluster morphologies in cluster X-ray images as well as indications from optical observations suggest that many clusters are not relaxed. Hence major mergers and the infall of smaller structures are quite common in clusters of galaxies. Such mergers of subclusters are very energetic events, which affect clusters strongly, e.g. shocks emerge. These shocks are important for the conditions in clusters because they are the major heating source for the intra-cluster gas. Moreover particles can be (re-)accelerated in these shock waves. Numerical models are ideal to reveal where shocks emerge, where they move to and how strong they are.

This article is structured as follows. In § 1 the simulation methods are explained briefly. After some general features of the models (§ 2) the effects of mergers are discussed in § 3. § 4 lists additional physical processes: cooling, star formation and magnetic fields. In § 5 the connection between mergers and the metallicity of the intra-cluster gas is reviewed. The mass determination in merging clusters is discussed in § 6. A summary is given in § 7.

1. SIMULATION METHODS

As many recent X-ray and optical observations have shown, most clusters of galaxies are not spherically symmetric systems. Therefore three-dimensional calculations are required to perform realistic simulations. Furthermore, the different cluster components must be taken into account. It is necessary to follow the evolution of the dark matter, and the galaxies as well as the intra-cluster medium (ICM). Dark matter and galaxies can be regarded as collisionless particles and can therefore be modeled by N-body simulations. In this kind of simulations only the gravitational interaction between the particles is taken into account. Each particle is moved in the force field of all the other particles. For current particle numbers of 128^3 or 256^3 it would take a lot of computing time to calculate the force by simply summing over all the other particles contributions. To accelerate the calculations different techniques have been developed, e.g. the particles are sorted onto a grid or into a tree

structure. In this way several particles are combined and treated simultaneously without losing much accuracy but gaining a lot of computing time. Many simulations have been performed which simulate only the dark matter component and apply therefore only N-body calculations. Such simulations are very useful for many purposes because the dark matter makes up 75% - 85% of the gravitational mass. In this article, however, I will concentrate only on models which include the effect of the ICM.

For the simulation of the ICM the pressure must also be taken into account, i.e. the full hydrodynamic equations must be solved. Although the mean free path of the ions and electrons in the gas is sometimes larger than the typical size of the grid cells, the hydrodynamic treatment can be justified by the magnetic fields present in clusters. Although the fields are weak (of the order of $1 \mu\text{G}$, see e.g. Kim et al. 1991) they are large enough to couple the particles on scales of a few kpc.

Two different methods have mainly been developed for the hydrodynamic treatment: (1) Smoothed Particle Hydrodynamics (SPH; Lucy 1977; Monaghan 1985). This is a Lagrangian approach, i.e. the calculation follows the fluid. The gas is treated as particles in this approach. Examples of this type of simulations are: Evrard (1990), Dolag et al. (1999), Takizawa (1999), and Takizawa & Naito (2000). (2) Grid-based codes. This is an Eulerian approach, i.e. the simulation volume is divided into cells and the fluid is moving in these cells which are fixed in space. Examples of simulations using grid codes can be found in Schindler & Müller (1993), Bryan et al. (1994), Roettiger et al. (1997), Ricker (1998), and Quilis et al. (1998).

Fortunately, the choice of simulation technique is not critical. Calculations with both methods yield very similar results. This was tested in a large project, the Santa Barbara Cluster Comparison Project (Frenk et al. 1999), in which the formation of a galaxy cluster was simulated using 12 different techniques developed by 12 different groups. Both methods, SPH and grid codes, were applied. Each simulation started with exactly the same initial conditions. The comparison showed very good agreement in the properties of the dark matter. Also, relatively good agreement was found in the gas temperature, the gas mass fraction and the gas profiles of the final cluster. The largest discrepancies were found in the X-ray luminosity which differed by up to a factor of 2. This discrepancy is probably not only an effect of different methods but also of different spatial resolutions.

2. CLUSTER MODELS

Combined N-body/hydrodynamic simulations produce in general very realistic cluster models. The simulations can in general reproduce cluster morphologies and other parameters known from observations quite well. The temperatures of the X-ray emitting intra-cluster gas are typically very well simulated. Also the spatial distributions are realistic. For the dark matter component the so-called NFW profile (Navarro et al. 1995) is usually found, while the gas profile is well fit by the so-called β -profile (Cavaliere & Fusco-Femiano 1976).

The models can discriminate between cosmological parameters. Simulations on large scales show distinctly different distributions of matter for a mean matter density value of $\Omega_m = 1$ and for $\Omega_m = 0.3$ (Ostriker & Cen 1996; Thomas et al. 1998; Jenkins et al. 1998). While in the $\Omega_m = 0.3$ models the distribution changes only slightly between a redshift $z=1$ and now, in the $\Omega_m = 1$ model significant differences are visible in the same time interval. Many smaller structures merge to form larger structures, so that the distribution looks much less smooth at $z=0$ than at $z=1$. A distinction between $\Lambda = 0$ models and $\Lambda \neq 0$ models is more difficult, because there are only small differences between these models.

By plotting cuts through the models at particular interesting planes like for example a plane containing the collision axis, or by plotting projections of the models onto different planes, one can follow every detail of the evolution. Interesting quantities are for instance cuts in the ICM density, the velocities (see Fig. 8.1) projections like the X-ray emission, the X-ray emission-weighted temperature and/or the particle positions are useful (see Fig. 8.2).

3. EFFECTS OF MERGERS

It is particularly interesting to study cluster mergers with simulations since one can clearly distinguish the different stages of a cluster merger (see Figs. 8.1 and 8.2). In the pre-merger phase the subclusters, which are approaching each other, are still well separated units (Figs. 8.1a,b, and 8.2a,b). The collision, i.e. the moment when the cores pass through each other, is characterized by high central density and high temperature (Figs. 8.1d and 8.2d). In the subsequent post-merger stage shock waves emerge – mainly in the direction of the original collision axis – and propagate outwards (Figs. 8.1e and 8.2e). In the next paragraphs we will discuss in detail the shocks and their observational appearance since they are very important for the dynamics of the ICM and for the conversion of kinetic energy into thermal energy.

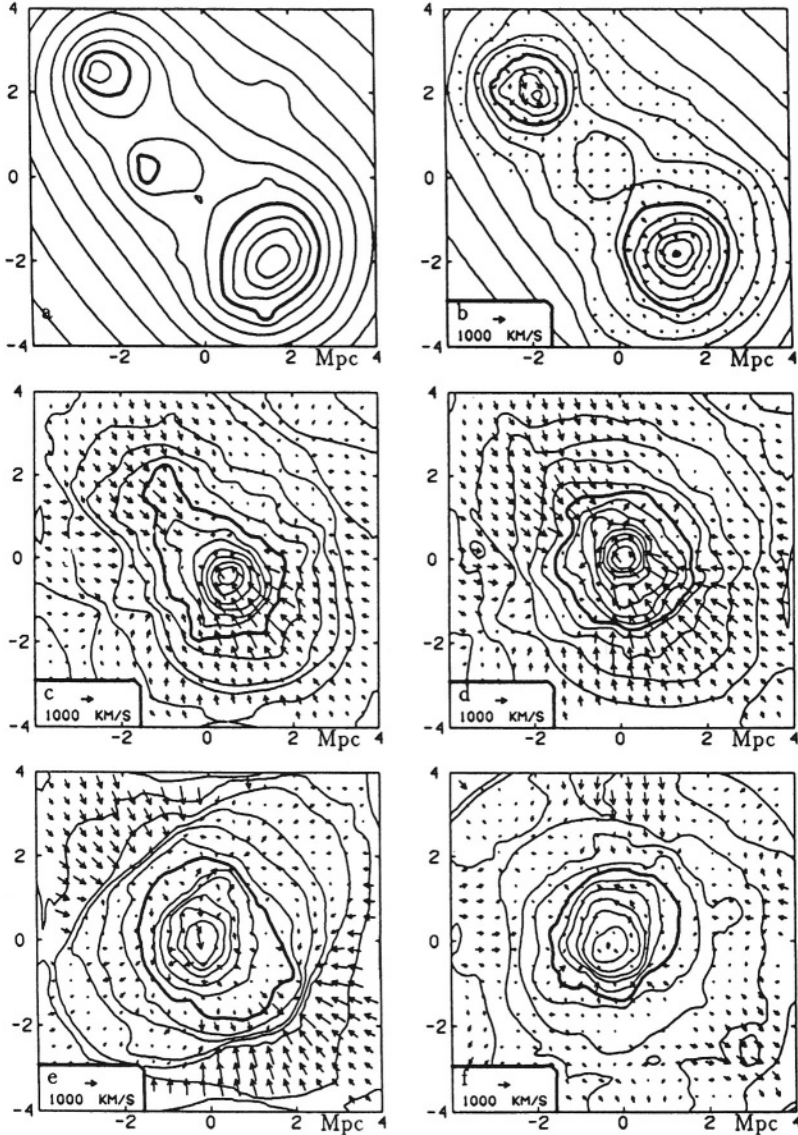


Figure 8.1. Evolution of a model cluster. Each snapshot shows ICM density contours together with the flow pattern. The contours are logarithmically spaced with $\Delta \log \rho = 0.2$, the bold line corresponding to a density of 10^{-28} g/cm^3 . The six snapshots are taken at b) $t = 0.95 \text{ Gyr}$, c) $t = 2.7 \text{ Gyr}$, d) $t = 3.2 \text{ Gyr}$, e) $t = 4.4 \text{ Gyr}$, f) $t = 6.1 \text{ Gyr}$ after the configuration shown in a) (from Schindler & Müller 1993).

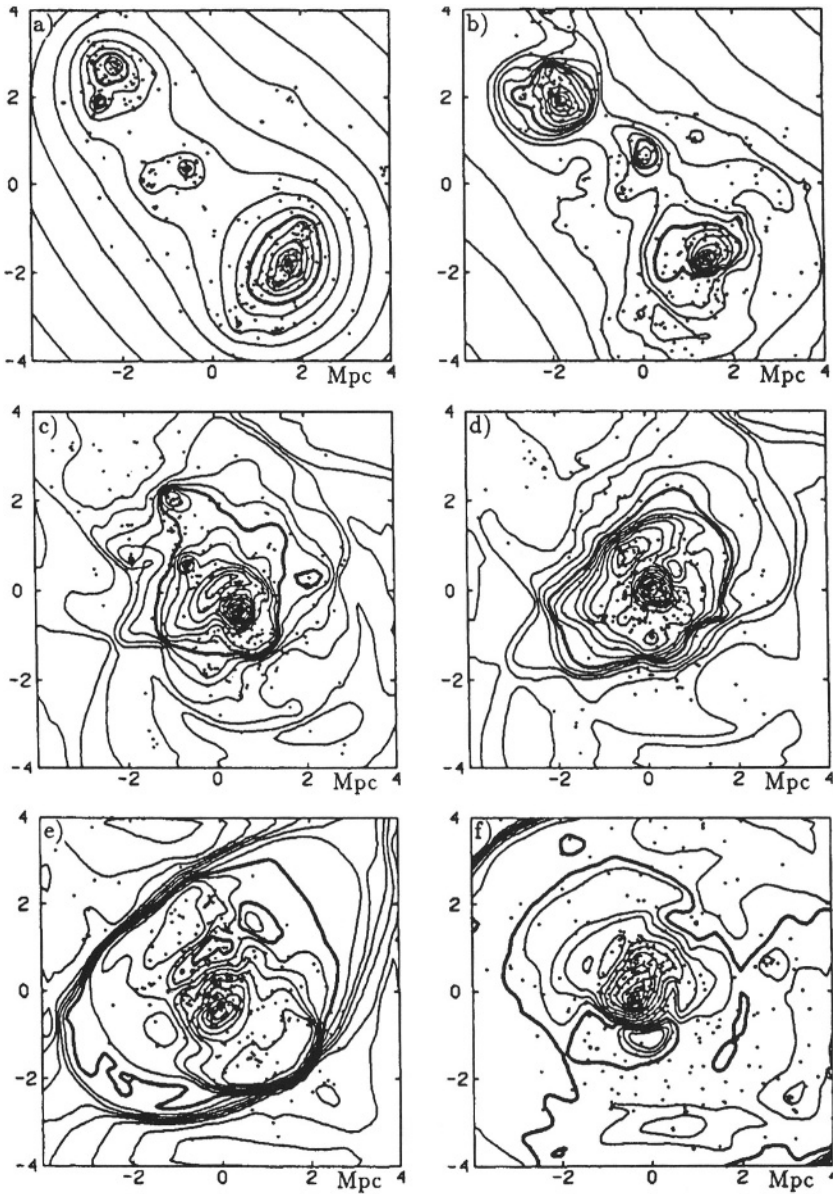


Figure 8.2. Evolution of the X-ray temperature of the same model as shown in Fig. 8.1. The temperature contours are logarithmically scaled with $\Delta \log T = 0.05$, the bold contour line corresponding to a temperature of 10^8 K. The six snapshots are taken at the same times as in Fig. 8.1 (from Schindler & Müller 1993).

3.1. SHOCKS

Shock waves in the ICM are the most prominent features emerging from mergers. Due to relative velocities of the colliding subclusters of up to ≈ 3000 km/s, shocks of Mach numbers up to about 3 are produced. These are relatively mild shocks.

When a dense subcluster falls into a cluster a shock is observed before the core passage, and it manifests itself as a bow shock visible in front of the infalling subcluster (Roettiger et al. 1997). The strongest shock waves are produced after the collision of subclusters, and they propagate outwards along the original collision axis (Schindler & Müller 1993; Roettiger et al. 1999a; see Figs. 8.1e and 8.2e). The shocks are visible as steep gradients in the gas density and in the gas temperature. In general, the shock structure is found to be more filamentary at early epochs and quasi-spherical at low redshifts (Fig. 8.3; Quilis et al. 1998).

Observationally, the shocks are best visible in X-ray temperature maps, because they show up as steps in these maps (Schindler & Müller 1993, see Fig 8.2e). They are visible also in X-ray surface brightness images, even if less prominently, because other effects like for example the presence of substructure, can cause irregularities in the images. Therefore it is ideal to measure and compare both, either the X-ray surface brightness image and the temperature map.

For the temperature maps, spatially resolved X-ray spectroscopy is necessary which can be performed now with high accuracy thanks to the new X-ray observatories XMM and CHANDRA. A number of clusters shocks and complicated temperature distributions in the intra-cluster gas have already been found; see for instance the Coma cluster (Arnaud et al. 2001), A665 and A2163 (Markevitch & Vikhlinin 2001), and A2142 (Markevitch et al. 2000).

These shocks are not only the major source of heating for the intra-cluster gas, but they are also particularly important for particle (re-) acceleration models. Relativistic particles, which were originally emitted by active galaxies, age quickly below the detection threshold of radio telescopes. Later these particles could be (re-)accelerated to relativistic energies in the shocks.

These relativistic particles are probably responsible for the non-thermal emission. Their interaction with the cluster magnetic field shows up as synchrotron emission of diffuse radio sources like radio halos and/or relics (see review by Giovannini & Feretti in this book).

The shocks heat primarily the thermal ions. This has been shown in simulations which treat ions and electrons separately (see Fig. 8.4;

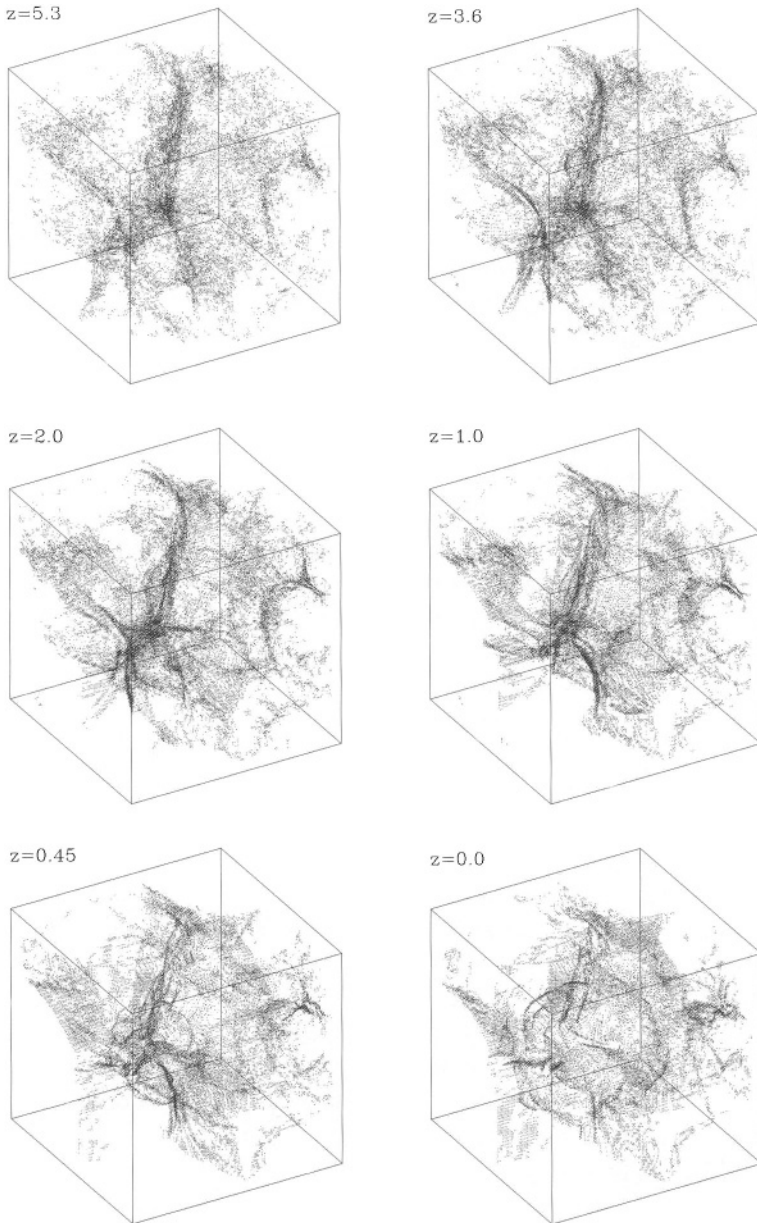


Figure 8.3. Shocked cells in cubes of 20 Mpc (comoving) at different redshifts. At first the shock structure is more filamentary, later it is quasi-spherical (from Quilis et al. 1998).

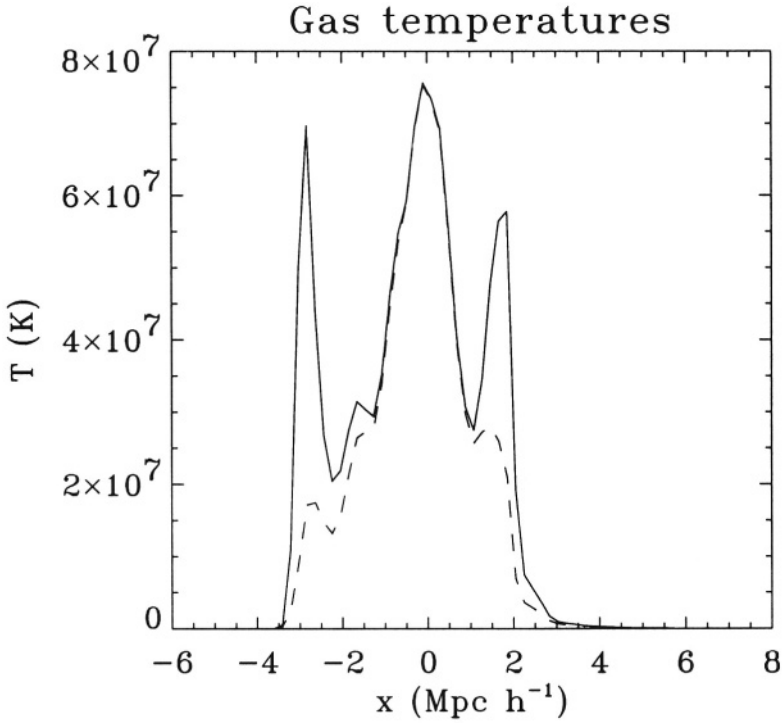


Figure 8.4. Temperature of the ions (solid line) and of the electron (dashed line) versus distance from the cluster centre. At the positions of the shocks (left: 3 Mpc, right: 2 Mpc from the cluster centre) the ions have higher temperatures than the electrons (from Chièze et al. 1998).

Chièze et al. 1998; Takizawa 1999). Only later is the energy transferred also to the thermal electrons.

3.2. OBSERVABLE EFFECTS OF MERGERS

Apart from shocks, mergers have many other observable effects. For example, the X-ray luminosity increases during the collision of two subclusters (Schindler & Müller 1993). The reason is that, when gas is compressed, its gas density increases. Since the X-ray emission is proportional to the square of the density one sees enhanced X-ray emission during the core passage of two subclusters.

Shortly before the collision the gas between the subclusters is heated due to compression. An elongated region of hot gas can be seen in the temperature maps of simulated models (Fig. 8.2c). Such hot regions

between two sub-clusters have been observed also in X-rays, see for instance A3528 (Schindler 1996b) or A401 (Markevitch et al. 1998).

During the core passage and at each rebound an increase in the magnetic field is visible in the models (peaks in Fig. 8.5; Dolag et al. 1999; Roettiger et al. 1999b). Afterwards the magnetic field decreases again, but the values stay always higher than before the collision (Fig. 8.5).

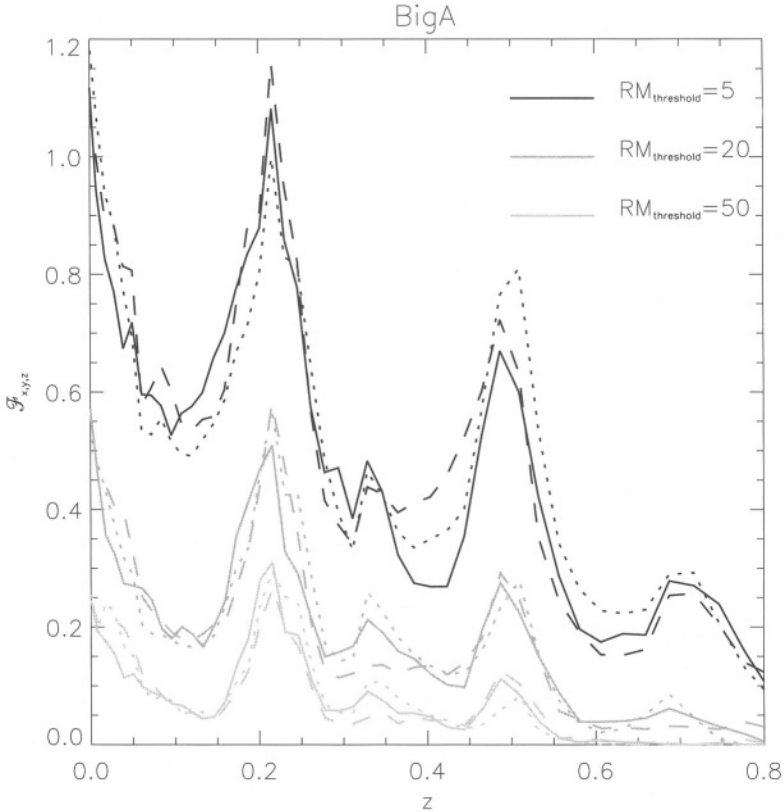


Figure 8.5. Area exceeding a certain threshold of Faraday rotation measure versus redshift. The rotation measure is the rotation of the polarization vectors of radio sources due to the presence of the cluster magnetic field along the line of sight. Different shades of grey correspond to the different thresholds given in the figure in units of rad m^{-2} . The area is normalized to the area emitting 95% of the cluster X-ray luminosity. During the core passage of two subclusters (visible at $z \sim 0.5$ and $z \sim 2$) and the subsequent rebounds (visible at $z \sim 0.3$, $z \sim 0$, and $z \sim 0.7$ from an older core passage) there is always an increase in the rotation measure, i.e. in the magnetic field (from Dolag 2001). Different projection directions are shown as different line types.

Mergers also cause a lot of turbulence and motion in the intra-cluster gas. This motion can move the gas around very efficiently, which can result in changed metallicity distributions (see § 5). Moreover the gas motion and the increased density during a merger increase the amount of gas stripped from galaxies due to ram pressure (see § 5). Ram pressure is proportional to $\rho_{ICM} \times v_{rel}^2$ with v_{rel} being the relative velocity of the cluster gas with respect to the galaxy and ρ_{ICM} being the density of the ICM.

Off-centre collisions produce in addition angular momentum and spiral-shaped shocks (Ricker 1998; Roettiger et al. 1998).

Observationally mergers can be identified not only by multiple X-ray maxima, but also by isophote twisting with centroid shift and elongations. In central collisions the dark matter component is always elongated along the collision axis, before and after the core passage. The gas is first elongated along the collision axis. During the core passage it is pushed out perpendicular to the collision axis, so that later an elongation perpendicular to the collision axis can be seen (Schindler & Müller 1993; see Fig. 8.1). Offsets between the collisionless component and the gas are also found (Roettiger et al. 1997). If more than one merger occurs in a relatively short time interval the temperature structure can become very complex.

4. PHYSICAL PROCESSES

So far only the gravitational interaction and the gas dynamic effects have been discussed, but there are additional physical processes taking place in clusters of galaxies.

4.1. SIMULATIONS OF MERGERS WITH MAGNETIC FIELDS

Faraday rotation measurements indicate that clusters are permeated by magnetic fields of the order of $1\mu\text{G}$ (e.g. Kim et al. 1991). Also radio halos require the existence of magnetic fields in clusters on scales of a few Mpc (e.g. Giovannini et al. 1991, 1993). Therefore magnetohydrodynamic calculations have been performed (Dolag et al. 1999; Roettiger et al. 1999b) to investigate the origin, distribution, strength and evolution of the magnetic fields (see Fig. 8.6). The results of these simulations show that the initial field distribution at the beginning of the simulations at high redshift is irrelevant for the final structure of the magnetic field. The final structure is dominated only by the cluster collapse. Faraday rotation measurements can be reproduced by the simulations for magnetic fields of the order of $1\mu\text{G}$, in very good agreement

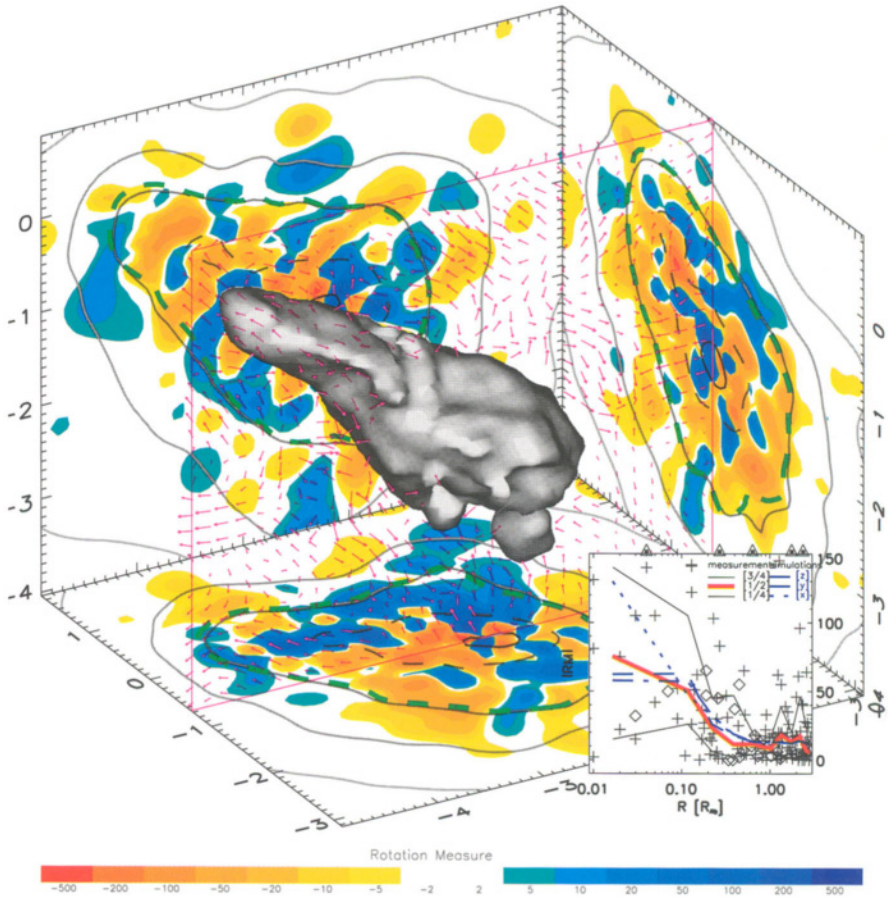


Figure 8.6. Isodensity surface of a cluster model with a central magnetic field of $1.1\mu\text{G}$ at redshift $z=0$. The three projections show the rotation measure (colour) and the gas density (contours). The purple arrows indicate the orientation and the strength of the magnetic field in a plane containing the cluster centre. The inset shows the rotation measure versus distance from the cluster centre plotted using various simulations (lines) and observations in several clusters (symbols) (from Dolag 2001).

with the value inferred from observations. The models reproduce very well also the radial decline of the magnetic field found in the observations (Clarke et al. 2001, Dolag et al. 2001).

Shear flows are extremely important for the amplification of the magnetic field, while the compression of the gas is of minor importance. Mergers change the local magnetic field strength drastically. But also

the structure of the cluster-wide field is influenced. At early stages of the merger the filamentary structures prevail. This structure breaks down later ($\sim 2\text{--}3$ Gyr) and leaves a stochastically ordered magnetic field.

4.2. COOLING AND STAR FORMATION

The star formation rate in galaxies can be affected by cluster mergers in two ways. The interstellar medium in a galaxy can be compressed during a merger because of the higher pressure. This would lead to an increased star formation rate. This effect was predicted in simulations by Evrard (1991). Also in a number of observations a connection between mergers and enhanced star formation rate has been found, e.g. in the Coma cluster (Caldwell et al. 1993), in A2111 (Wang et al. 1997), in A2125 (Owen et al. 1999), in several other clusters (Moss & Whittle 2000).

In contrast to these results Fujita et al. (1999) found through simulations that the interstellar medium in the galaxies is stripped off due to the increased ram pressure during the merger, which causes the galaxies to lose their gas. Therefore less gas is left to fuel the star formation process and hence the star formation activity decreases. Fujita et al. (1999) found an increase of post-starburst galaxies at the moment of the subcluster collision, which indicates that a rapid drop in star formation must have occurred.

In simulations without radiative cooling and star formation, it is found that the gas is less concentrated than the dark matter. Also the X-ray luminosity – temperature relation, inferred from simulations, is in disagreement with observations (Eke et al. 1998; Bryan & Norman 1998; Yoshikawa et al. 2000). The question arises whether this is a numerical artifact due to neglecting physical processes or due to the difficulty in determining the X-ray luminosity of numerical models correctly. It may also be connected with the observational findings of different profiles of baryonic and dark matter (Schindler 1999) and deviation of the X-ray luminosity – temperature relation from a pure power law (Ponman et al. 1999). Both findings could be explained by non-gravitational heating processes.

In order to answer this question several groups have performed simulations which include cooling and star formation. These groups came up with quite different conclusions. Lewis et al. (2000) found that models with cooling and star formation have a 20% higher X-ray luminosity and a 30% higher temperature in the cluster centre. Also Sugimotohara & Ostriker (1998) found that radiative cooling increases the X-ray luminosity. In contrast to these results Pearce et al. (2000) and Muanwong et al.

(2001) found that radiative cooling decreases the total X-ray luminosity. In terms of temperature they obtained the same result as the other authors.

In order to test whether the gas is less concentrated than the dark matter because of preheating (= early non-gravitational heating) Bialek et al. (2001) performed simulations with an initially elevated adiabat. They find that keV cm^2 , i.e. preheating could be a possible explanation for the effect, they can reproduce the observations with an initial entropy of 55 - 150

Mathiesen & Evrard (2001) took a different approach and tested with their models how good the observational temperature determination is. They simulated CHANDRA spectra and found that the temperature can be underestimated by up to 20% by the standard temperature determination method. The reason is that cold material falls into the cluster from any side, including along the line of sight. This results in a cold contribution to the cluster spectrum and hence to a lower temperature determination. So far no final conclusion has been reached on the question of the gas distribution.

Bryan & Norman (1998) showed that in the simulations the mass - temperature relation is much more robust than the X-ray luminosity - temperature relation and hence suggested to use the former relation to draw conclusions on the cluster formation process.

Radiative cooling can result in a cooling flow which can be severely affected by a merger. Gómez et al. (2001) found in 2D simulations that cluster mergers can destroy cooling flows if the ram pressure of the gas of the infalling subcluster is sufficiently high. The ram pressure is able to displace the high-density gas in the cooling core as well as to heat it through compression, shocks and turbulence. The time scale on which a new cooling flow re-establishes itself depends on the initial cooling time of the cluster and on the severity of the merger. The cooling flow is not disrupted immediately. Gómez et al. found a lag of at least 1 - 2 Gyr between the core passage and the point at which the central cooling time exceeds the Hubble time. Also rotation of the ICM as a consequence of a merger can have effects on the cooling flow (Garasi et al. 1998).

5. METALLICITY-MERGER CONNECTION

The ICM has a metallicity of ≈ 0.3 in solar units. That means the ICM cannot be purely of primordial origin, but it must have been processed at least partially in the cluster galaxies, and later it must have been expelled from the galaxy potential into the cluster potential and hence into the ICM. As mentioned already in § 4.2, the star formation activity,

i.e. the metal production rate, and its connection to mergers, is still controversial. The gas ejection processes and their time scales are also still under discussion. Several gas ejection processes have been suggested in the seventies: ram-pressure stripping (Gunn & Gott 1972), supernova-driven galactic winds (De Young 1978), galaxy-galaxy interaction and jets emerging from active galaxies.

In order to decide which process is dominating at what time, observations and simulations were performed and compared, in particular with respect to the metallicity distribution within clusters and to the metallicity evolution with redshift. So far the best measured metal abundance distributions based on a large sample of clusters is the one derived using BeppoSAX data (De Grandi & Molendi 2001; Irwin & Bregman 2001). The metallicity is found to be relatively homogeneous, except for cooling flow clusters, where a decrease of metallicity with radius is observed. New XMM measurements confirm this result (Arnaud 2001; Mushotzky 2001). The new measurements also show that the ratio of elements is not solar everywhere in the clusters, but an underabundance on Oxygen is found e.g. in the centre of the cluster Sersic 159/03 (Kaastra et al. 2001). XMM and CHANDRA observations will provide measurements of the evolution of the metallicity with redshift out to redshifts of unity and beyond, which were hardly possible with previous instruments (Schindler 1999).

As many different scales are involved in the metal enrichment process, the existing numerical models must span a large range of scales. Simulations on cosmological scales taking into account the effects of galactic winds were performed by Cen & Ostriker (1999). They found that the average metallicity increases from 0.01 solar at $z=3$ to 0.2 solar at present. The metallicity distribution is not constant but denser regions have generally higher metal abundances. Gnedin (1998) took into account not only galactic winds but also galaxy-galaxy interactions and concluded that most metals are ejected by galaxy mergers. In contrast to this result Aguirre et al. (2001) found that galaxy-galaxy interactions and ram-pressure stripping are of minor importance while galactic winds dominate the metal enrichment of the ICM. A problem with this kind of simulations is that they must cover large scales as well as galaxy scales. Therefore the resolution is not very good at small scales and hence the results have large uncertainties, which is probably the reason for the discordant results.

Also the effects of supernova-driven winds have been investigated with models on cluster scales. David et al. (1991) calculated the first models and found that the results depend sensitively on the input parameters: the stellar initial mass function, the adopted supernova rate and the

primordial fraction of intra-cluster gas. In the first 3D models which took into account the full gas dynamics and the effects of galactic winds on cluster scales, Metzler & Evrard (1994, 1997) showed that winds can account for the observed metal abundances. Very strong metallicity gradients were found (almost a factor of ten between cluster centre and virial radius) which are not in agreement with the observations. The authors found that these metallicity gradients are hardly affected by cluster mergers. From simulations on galaxy scale Murakami & Babul (1999) concluded that galactic winds are not very efficient for the metal enrichment process.

Another process which is probably important for metal enrichment is ram-pressure stripping. As a galaxy approaches the cluster centre it experiences an increasing pressure and at some point the galaxy potential is not strong enough to retain the galaxy gas. The gas is stripped off starting from the outer regions of the galaxies and the metals are released into the intra-cluster medium. Two spectacular examples where the stripping process can be observed are two galaxies in the Virgo cluster, NGC4501 and NGC4548 (Cayatte et al. 1990).

Simulations of ram-pressure stripping are relatively difficult to carry out because not only the conditions of the gas inside the galaxy and the potential of the galaxy must be taken into account, but also the conditions of the surrounding medium. In early models the effect was calculated with relatively simple means (Takeda et al. 1984; Gaetz et al. 1987; Portnoy et al. 1993; Balsara et al. 1994).

Recently, high resolution simulations were carried out to study the stripping process in different types of galaxies. Abadi et al. (1999) and Quilis et al. (2000) performed simulations of spiral galaxies. They found that the interstellar medium can be removed if it is not homogeneous. For dwarf galaxies Mori & Burkert (2000) found in their simulations that the gas can be easily stripped off when these galaxies move through the intra-cluster medium. Simulations of elliptical galaxies (Fig. 8.7; Toniazzo & Schindler 2001) showed that the gas cannot only be stripped off as the galaxy approaches the cluster centre, but the galaxy can again accumulate some gas when it is in the apocentre of its orbit. Also the X-ray morphologies of simulated and observed galaxies can be compared (see Fig. 8.8).

All these simulations show that ram-pressure stripping can be an important metal enrichment process for the ICM. Merging activity increases the effect even more because the ram pressure is proportional to the square of the relative velocity of intra-cluster gas and galaxies. During mergers, not only is the gas density increased but also the rel-

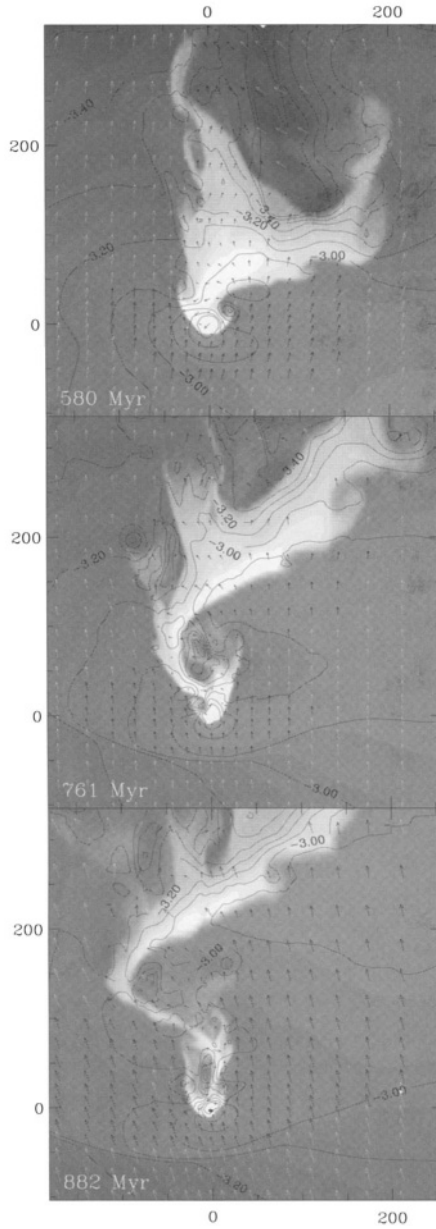


Figure 8.7. Gas density (grey scale) and pressure (contours) of a galaxy moving downwards towards the cluster centre. The arrows show the Mach vectors (white when $M > 1$, black otherwise). The gas of the galaxy is stripped due to ram pressure (from Toniazzo & Schindler 2001).

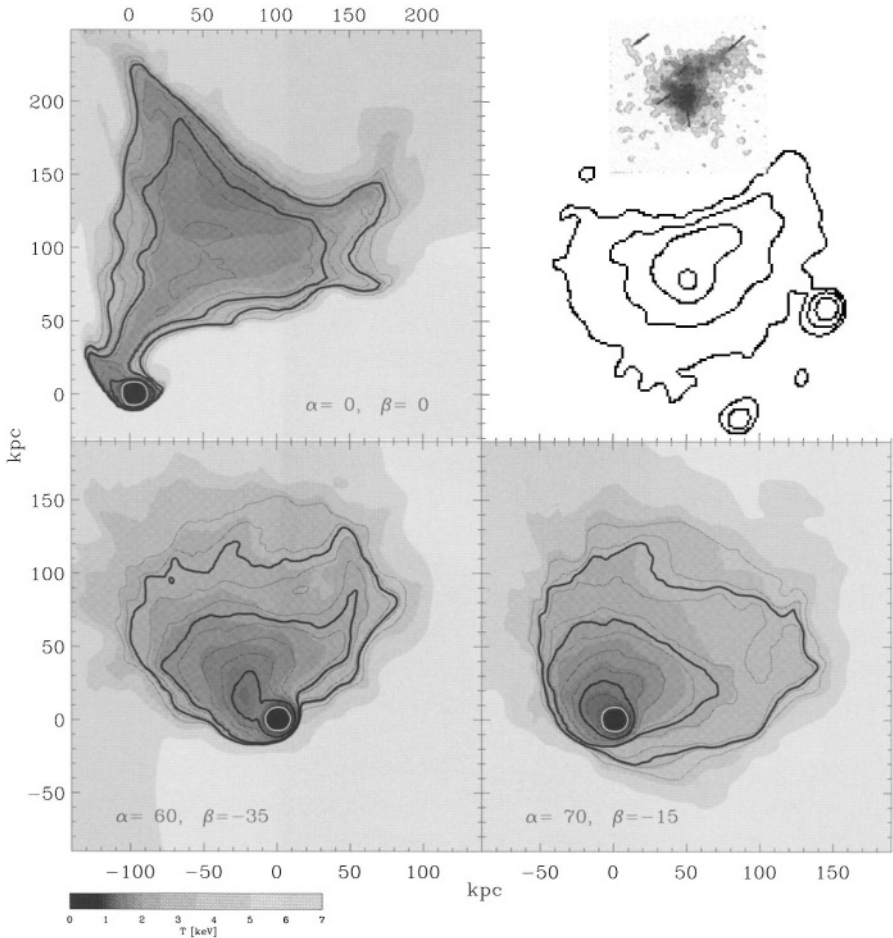


Figure 8.8. Simulated X-ray images (contours) and temperatures (grey scale) of a galaxy affected by ram-pressure stripping in three different projections. For comparison the ROSAT image of M86 (from Rangarajan et al. 1995) is shown in the upper right panel (from Toniazzo & Schindler 2001).

ative velocities are higher than in a relaxed cluster. Therefore a large influence of merging processes on the stripping rate is expected.

6. MASS DETERMINATION IN MERGING CLUSTERS

Simulations are ideal tools to test observational methods. An example is the mass determination from X-ray observations. In this method

the X-ray emitting gas is used as a tracer for the potential. With the assumption of hydrostatic equilibrium and spherical symmetry the total cluster mass depends only on two observable quantities which can be inferred from X-ray observations: the gas temperature T_{ICM} and the gas density ρ_{ICM} . The integral total cluster mass is

$$M(r) \propto -T_{ICM}r \left(\frac{d \ln \rho_{ICM}}{d \ln r} + \frac{d \ln T_{ICM}}{d \ln r} \right), \quad (1)$$

with r being the distance from the cluster centre. The advantage of the numerical simulations is that all quantities are known at each position of the cluster and at each time step. Therefore the true total mass of a model is known exactly at each time step and within any radius. On the other hand the X-ray emission of the model cluster can be simulated and the standard X-ray mass determination method can be applied to these simulated X-ray data. A comparison of the true mass and the X-ray mass yields the accuracy of the method.

While the X-ray mass determination method proved to be quite reliable in relaxed clusters it can be affected strongly during mergers (Evrard et al. 1996; Roettiger et al. 1996; Schindler 1996a). The reason is that cluster merging can cause quite strong deviations from the two assumptions necessary for the mass determination – hydrostatic equilibrium and spherical symmetry. For example, at the positions of shocks the gas is not in hydrostatic equilibrium. Shocks cause gradients – both in temperature and in density – and can cause therefore an overestimation of the mass at the radius of the shock (see equation 1). Locally, this can lead to a mass estimate up to twice the true mass. Substructure on the other hand tends to flatten the azimuthally averaged profile and hence leads to an underestimation of the mass (see equation 1), in extreme cases to deviations up to 50% of the true mass.

In some cases these deviations can be corrected, for instance in clusters in which substructures are well distinguishable. In these cases the disturbed part of the cluster can be excluded from the mass analysis and a good mass estimate can be obtained for the rest of the cluster. In general, though, mass determinations in non-relaxed clusters should be done very cautiously.

The effect of magnetic fields on the mass determination has also been investigated. A considerable magnetic pressure compared to the thermal pressure would lead to an underestimation of the mass. Magneto-hydrodynamic simulations by Dolag et al. (1999) were used to perform the same comparison as described above. Dolag & Schindler (2000) found that in relaxed clusters the mass is underestimated due to magnetic fields by a few percent, at most, and only in the cluster centre.

In mergers, however, the mass can be considerably underestimated due to magnetic pressure. The reason is that during the merger the gas is compressed and, with it, the magnetic field lines as well. Hence the magnetic field is stronger and affects the mass determination.

7. SUMMARY AND PROSPECTS

Simulations provide a unique way to follow the dynamics of galaxy clusters. In particular merger processes can be studied in detail. The most prominent features of mergers are shocks, which can be seen in X-ray images and X-ray temperature maps. Each stage of the merger (pre-merger, collision, post-merger) is characterised by different observational signatures in the temperature and gas distribution. Therefore simulations do not only help to distinguish merger clusters from relaxed clusters in the observations but they also help in determine the exact dynamical state through a detailed comparison of models with observations. Hence numerical models are helpful tools for the interpretation of the observational data.

In addition, numerical models can be used to test observational methods like for instance the mass determination or the temperature determination. The models define the limits of these methods and help improving them.

Mergers have also effects on other physical processes. They can affect the star formation activity in cluster galaxies. Metal enrichment processes and the subsequent distribution of metals in the ICM can be influenced. Moreover the strength and the structure of magnetic fields are changed due to mergers.

Increasing computing power promises good prospects for the future. For more realistic simulations two aspects are essential: the increase of resolution (as larger scales are involved higher resolution is necessary to resolve also the small scales); and the inclusion of physical effects (e.g. radiative cooling, star formation, magnetic fields and others) which is crucial to understand various aspects. In particular the combination of new, more detailed, simulations with the X-ray observations coming from the new generation of X-ray satellites, XMM and CHANDRA, will result in a big leap forward in our understanding of cluster physics and dynamics and hence will make clusters excellent diagnostic tools for cosmology.

References

Abadi, M.G., Moore, B. & Bower, R.G. 1999, MNRAS, 308, 947

- Aguirre, A., Hernquist, L., Schaye, J., Weinberg, D.H., Katz, N. & Gardner, J. 2001, ApJ, 560, 599
- Arnaud, M. 2001, in *Galaxy Clusters and the High Redshift Universe Observed in X-rays*, XXI Moriond Astrophysics Meeting (March 2001), eds. D. Neumann, F. Durret, & J. Tran Thanh Van, in press
- Arnaud, M. et al. 2001, A&A, 365, L67
- Balsara, D., Livio, M. & O'Dea, C.P. 1994, ApJ, 437, 83
- Bialek, J.J., Evrard, A.E. & Mohr, J.J. 2001, ApJ, 555, 597
- Bryan, G.L. & Norman, M.L. 1998, ApJ, 495, 80
- Bryan, G.L. Klypin, A., Loken, C., Norman, M.L. & Burns, J.O. 1994, ApJL, 437, L5
- Caldwell, N., Rose, J.A., Sharples, R.M., Ellis, R.S. & Bower, R.G. 1993, AJ, 106, 473
- Cavaliere A. & Fusco-Femiano R. 1976, A&A 49, 137
- Cayatte, V., Balkowski, C., van Gorkom, J.H. & Kotanyi, C. 1990, AJ, 100, 604
- Cen, R. & Ostriker, J.P. 1999, ApJL, 519, L109
- Chièze, J.-P., Alimi J.-M. & Teyssier, R. 1998, ApJ, 495, 630
- Clarke, T.E., Kronberg, P.P. & Böhringer, H., 2001, ApJL, 547, L111
- David, L.P., Forman, W. & Jones, C. 1991, ApJ, 380, 39
- De Grandi, S. & Molendi, S. 2001, ApJ, 551, 153
- De Young, D.S. 1978, ApJ, 223, 47
- Dolag, K. 2001, in *Galaxy Clusters and the High Redshift Universe Observed in X-rays*, XXI Moriond Astrophysics Meeting (March 2001), eds. D. Neumann, F. Durret, & J. Tran Thanh Van, in press
- Dolag, K., Schindler, S., Govoni, F. & Feretti, L. 2001, A&A, 378, 777
- Dolag, K. & Schindler, S. 2000, A&A, 364, 491
- Dolag, K., Bartelmann, M. & Lesch, H. 1999, A&A, 348, 351
- Eke, V.R., Navarro, J.F. & Frenk, C.S. 1998, ApJ, 503, 569
- Evrard, A.E. 1990, ApJ, 363, 349
- Evrard, A.E. 1991, MNRAS, 248, L8
- Evrard, A.E., Metzler, C.A. & Navarro, J.N. 1996, ApJ, 469, 494
- Frenk, C.S. et al., 1999, ApJ, 525, 554
- Fujita, Y., Takizawa, M., Nagashima, M. & Enoki, M. 1999, PASJ, 51, L1
- Gaetz, T.J., Salpeter, E.E. & Shaviv, G. 1987, ApJ, 316, 530
- Garasi, C., Loken, C., Burns, J.O. & Roettiger, K. 1998, MNRAS, 298, 697
- Giovannini, G., Feretti, L. & Stanghellini, C. 1991, A&A, 252, 528
- Giovaninni, G., Feretti, L., Venturi, T., Kim, K.T. & Kronberg, P.P. 1993, ApJ, 406, 399
- Gnedin, N.Y. 1998, MNRAS, 294, 407

- Gómez, P.L., Loken, C., Roettiger, K. & Burns, J.O. 2001, ApJ, in press, astro-ph/0009465
- Gunn, J.E. & Gott, J.R. 1972, ApJ, 176, 1
- Irwin, J.A. & Bregman, J.N. 2001, ApJ, 546, 150
- Jenkins, A. et al. 1998, ApJ, 499, 20
- Kaastra, J.S., Ferrigno, C., Tamura, T., Paerels, F.B.S., Peterson, J.R. & Mittaz, J.P.D. 2001, A&A, 365, L99
- Kim, K.T., Tribble, P.C. & Kronberg, P.P. 1991, ApJ, 379, 80
- Lewis G.F., Babul, A., Katz, N., Quinn, T., Hernquist, L. & Weinberg, D.H. 2000, ApJ, 536, 623
- Lucy, L. 1977, AJ, 82, 1013
- Markevitch, M. & Vikhlinin, A. 2001, ApJ, in press, astro-ph/0105093
- Markevitch, M., Forman, W.R., Sarazin, C.L. & Vikhlinin, A. 1998, ApJ, 503, 77
- Markevitch, M. et al. 2000, ApJ, 541, 542
- Mathiesen, B.F. & Evrard A.E. 2001, ApJ, 546, 100
- Metzler, C.A. & Evrard, A.E. 1994, ApJ, 437, 564
- Metzler, C.A. & Evrard, A.E. 1997, ApJ submitted, astro-ph/9710324
- Monaghan, J.J. 1985, Comp. Phys. Rept., 3, 71
- Mori, M. & Burkert, A. 2000, ApJ, 538, 559
- Moss, C. & Whittle, M. 2000, MNRAS, 317, 667
- Muanwong, O., Thomas, P.A., Kay, S.T., Pearce, F.R. & Couchman, H.M.P. 2001, ApJL, 552, L27
- Murakami, I. & Babul, A. 1999, MNRAS, 309, 161
- Mushotzky, R.F. 2001, in *Galaxy Clusters and the High Redshift Universe Observed in X-rays*, XXI Moriond Astrophysics Meeting (March 2001), eds. D. Neumann, F. Durret, & J. Tran Thanh Van, in press
- Navarro, J.F., Frenk, C.S. & White, S.D.M. 1995, MNRAS 275, 720
- Ostriker, J. & Cen, R. 1996, ApJ, 464, 27
- Owen, F.N., Ledlow, M.J., Keel, W.C. & Morrison, G.E. 1999, AJ, 118, 633
- Pearce, F.R., Thomas, P.A., Couchman, H.M.P. & Edge, A.C. 2000, MNRAS, 317, 1029
- Ponman, T.J., Cannon, D.B. & Navarro, J.F. 1999, Nature 397, 135
- Portnoy, D., Pistinner, S. & Shaviv, G. 1993, ApJS, 86, 95
- Quilis, V., Ibáñez, J.M. & Sáez, D. 1998, ApJ, 502, 518
- Quilis, V., Moore, B. & Bower, R. 2000, Science, 288, 1617
- Rangarajan, F.V.N., White, D.A., Ebeling, H. & Fabian, A.C. 1995, MNRAS, 277, 10
- Ricker, P.M. 1998, ApJ, 496, 670
- Roettiger, K., Burns, J.O. & Loken, C. 1996, ApJ, 473, 651
- Roettiger, K., Burns, J.O. & Stone J.M. 1999a, ApJ, 518, 603

- Roettiger, K., Loken, C. & Burns, J.O. 1997, *ApJS*, 109, 307
Roettiger, K., Stone J.M. & Burns, J.O. 1999b, *ApJ*, 518, 594
Roettiger, K., Stone J.M. & Mushotzky, R.F. 1998, *ApJ*, 493, 62
Schindler, S. 1996a, *A&A*, 305, 756
Schindler, S. 1996b, *MNRAS*, 280, 309
Schindler, S. 1999, *A&A*, 349, 435
Schindler, S. & Müller, E. 1993, *A&A*, 272, 137
Suginohara, T. & Ostriker, J.P. 1998, *ApJ*, 507, 16
Takeda, H., Nulsen, P.E.J. & Fabian, A.C. 1984, *MNRAS*, 208, 261
Takizawa, M. 1999, *ApJ*, 529, 514
Takizawa, M. & Naito, T., 2000, *ApJ*, 535, 586
Toniazzo, T. & Schindler, S. 2001, *MNRAS* 325, 509
Thomas, P.A., Colberg, J.M., Couchman, H.M.P., Efstathiou, G. & Frenk, C.S. 1998, *MNRAS*, 296, 1061
Yoshikawa, K., Jing, Y.P. & Suto, Y. 2000, *ApJ*, 535, 593
Wang, Q.D., Ulmer, M.P. & Lavery, R.J. 1997, *MNRAS*, 288, 702

This page intentionally left blank

Chapter 9

CLUSTERS, COSMOLOGY AND MERGERS

August E. Evrard

Physics and Astronomy Departments

University of Michigan

Ann Arbor, MI 48109-1120 USA

evrard@umich.edu

Isabella M. Gioia

Istituto di Radioastronomia del CNR

Via Gobetti 101

I-40129, Bologna, ITALY

gioia@ira.bo.cnr.it

Abstract The character of the galaxy cluster population holds clues to the identity of the particular world model that best describes our universe. Although clusters are complex in their fine detail, their dark matter and intracluster medium (ICM) content appear to be well described by relatively simple processes driven by gravitationally induced mergers. After reviewing theoretical frameworks of spherical collapse and hierarchical clustering, we separate the problem of extracting cosmological parameters from observations into two parts: describing the space density of clusters as a function of total mass and calibrating relations that connect total mass to observable quantities.

Guided by computational modeling of cluster formation, we examine the effects of cluster mergers on their hydrostatic boundaries, on their internal density structure, and on the variance exhibited about the mean virial relation connecting mass to temperature. We summarize constraints on the clustered matter density Ω_m and power spectrum normalization σ_8 derived from X-ray observations of the ICM, including new estimates of systematic uncertainties in these measures derived from Hubble Volume simulations. The mean baryon fraction of clusters presents the most precise constraint favoring a low density universe, $\Omega_m (h/0.7)^{2/3} = 0.30 \pm (0.02)_{\text{stat}} \pm (0.06)_{\text{sys}}$, with uncertainty in the mass-temperature relation being the leading source of systematic error.

Introduction

Gravitational instability in a spatially expanding world model is the process by which the tiny perturbations observed in the microwave background radiation (Wright et al. 1992; De Bernardis et al. 2000) were transformed into the large-scale structure exhibited in nearby galaxy surveys (De Lapparent 1986; Tully 1987; Geller & Huchra 1989; Da Costa 1988). The broad theoretical framework describing this process is now well developed in a number of textbooks (Peebles 1980; 1993; Padmanabhan 1993; Coles and Lucchin 1995; Peacock 1999). The specific set of model parameters representing our universe remains to be derived from observations, and clusters of galaxies play a number of important roles in this enterprise.

The enormous gravitational potentials of clusters trap the cosmic mix of clustered matter components. By providing the tools to ‘weigh’ cluster component masses, X-ray and optical studies of clusters offer the means to constrain the ratio Ω_b/Ω_m of universal baryonic (Ω_b) and total clustered matter (Ω_m) densities. The local space density of clusters as a function of their gravitational potential, measured by X-ray temperature T and galaxy velocity dispersion σ_{gal} , is a sensitive indicator of the present amplitude of the power spectrum of density fluctuations on $\sim 10 h^{-1}$ Mpc scales. The evolution of the cluster space density with redshift reflects the growth rate of large-scale, linear perturbations. Since this rate is mostly sensitive to the matter density, comparison of local and distant cluster counts provides constraints on Ω_m . Finally, clusters obey scaling relations between distance-dependent (*e.g.*, isophotal size) and distance-independent (*e.g.*, temperature) measures that enable use of the population as standard cosmological markers. Constraints on the geometry of the universe, analogous to those provided by type-Ia supernovae (Perlmutter et al. 1998; Riess et al. 1998), can be derived from the redshift evolution of apparent cluster sizes.

Whereas the precision of constraints on cosmological parameters is determined by statistical factors (number of objects per sample, photons per object, etc.), the *accuracy* of such constraints is limited largely by systematics, particularly in our ability to model the non-linear dynamical evolution of clusters with sufficient fidelity to trust detailed observational predictions. Given that large-scale structure formed hierarchically via gravity, cluster mergers become an essential ingredient of the modeling process. Numerical simulations, reviewed by Schindler in this volume, are required to understand the detailed aspects of merg-

ers, from ‘micro-physical’ features of individual mergers to the impact of random collections of such events on the population as a whole.

In this chapter, we present a brief review of selected cosmological constraints arising from galaxy clusters. Accurate constraints require a sound physical description of the cluster population, so we devote the first two-thirds of this report to theoretical and phenomenological issues involved in describing clusters.

We begin in § 1 by discussing the non-linear action of gravity and some characteristics of the structure formed by it. This section contains background material that the suitably prepared reader may skip, although we recommend § 1.3 to all readers since it introduces computational examples that are expanded and referenced by later sections. In § 2, we consider the problem of describing the observable properties of the cluster population within a given cosmology. We treat the problem in two parts. First, we show how the space density of clusters as a function of mass and redshift is described by a single functional form that is now calibrated at the 10 percent level by N-body simulations. We then discuss efforts to calibrate total mass estimates through the virial theorem, and present evidence that a combined variable, the product $H(z) M_{\Delta}$ of Hubble parameter and mass at fixed critical density threshold, is a natural measure of the virial mass of a cluster. Relevant observable properties of clusters are touched on.

In § 3, we move from theory to the practice of deriving constraints on cosmological parameters from current observations. We review two independent lines of evidence that strongly support a low matter density universe with $\Omega_m \sim 0.3$, and we present world values for the power spectrum amplitude σ_8 , a parameter tightly constrained by the local space density of clusters. We discuss recent calibration of sample (or *cosmic*) variance in σ_8 derived from Hubble Volume simulations, and we discuss the impact of an enlarged error budget in this parameter on determinations of Ω_m from distant cluster counts.

A number of relevant and important subjects are not considered here due to lack of space. These include peculiar velocities of clusters (Gramann 1998; Bahcall & Oh 1996; Feldmann & Watkins 1994), power spectra and clustering of clusters (Schuecker et al. 2001; Colberg et al. 2000; Dalton et al. 1994; Bahcall & Soniera 1983), the optical content of clusters (Girardi et al. 1997; Giuricin et al. 2001), measurements of H_0 from combined X-ray and Sunyaev-Zel’dovich observations (Mason & Myers 2000; Jones et al. 2001), the frequency of strong gravitational lensing (Bartlemann et al. 1998) and the evolution of X-ray isophotal sizes with redshift (Mohr et al. 2000). Bertschinger (1998) gives an introduction to techniques and issues in computational cosmology. For

a detailed comparison of twelve codes simulating a single galaxy cluster, see Frenk et al. (1999). White (1997) reviews phenomenology of large-scale structure.

1. GRAVITATIONAL INSTABILITY: THEORY AND COMPUTATION

After briefly reviewing some basic elements of late-time cosmology, we move on to contrast a highly idealized picture of clusters as isolated, spherical objects with the more complex and realistic picture of clusters forming from a process of hierarchical merging.

1.1. THE LATE UNIVERSE

In a perfectly homogeneous and isotropic universe, the structure of space-time is described by the Robertson-Walker line element

$$ds^2 = c^2 dt^2 - a^2(t) \left[\frac{dr^2}{1 - kr^2} + r^2 d(\cos\theta) d\phi \right] \quad (1)$$

with $a(t)$ the scale factor, c the speed of light and k a curvature constant that takes on negative, zero and positive values for hyperbolic, flat and closed geometries, respectively. Recent landmark observations of the first acoustic peak in the microwave background radiation (Padin et al. 2001; Netterfield et al. 2001; Pryke et al. 2001) strongly favor a flat metric, so hereafter we will assume the case $k=0$. Einstein's equations of general relativity applied to this metric reduce to the Friedmann–Lemaître equations that govern the evolution of the scale factor $a(t)$. We consider here world models dominated by non-relativistic matter $\rho_m(a) \propto a^{-3}$ and a non-zero vacuum energy density (or cosmological constant) $\rho_\Lambda = \text{const}$, for which the scale factor obeys

$$H^2(a) = \left(\frac{\dot{a}}{a} \right)^2 = H_0^2 [\Omega_m a^{-3} + \Omega_\Lambda] \equiv \frac{8\pi G \rho_c(a)}{3} \quad (2)$$

where $\Omega_X = \rho_X/\rho_c$ is the present density of component X expressed in units of the present critical density $\rho_c \equiv 3H_0^2/8\pi G$. By definition, the Hubble parameter $H(a)$ defines the critical density $\rho_c(a)$ at any epoch. A spatially flat universe satisfies $\Omega_m + \Omega_\Lambda = 1$, with the extremes of this condition being the Einstein–de Sitter model with $\Omega_m = 1$, $a \propto t^{2/3}$ and the inflating de Sitter model with $\Omega_\Lambda = 1$, $a \propto e^{Ht}$

Since a *perfectly* homogeneous and isotropic universe is not terribly anthropomorphic, spatial fluctuations are introduced into the matter density

$$\delta(\mathbf{x}, a) \equiv \rho_m(\mathbf{x}, a)/\rho_m(a) - 1 \quad (3)$$

as a function of comoving position \mathbf{x} to seed the formation of galaxies, planets, DNA, the internet and so on. The gravitational potential $\phi(\mathbf{x}, a)$ associated with these fluctuations satisfies Poisson's equation in a comoving frame

$$\nabla^2 \phi = 4\pi G \rho_m(a) a^2 \delta. \quad (4)$$

A test particle at some location experiences a gravitational acceleration from the potential gradient and obeys an equation of motion

$$\frac{d^2 \mathbf{x}}{dt^2} = -H(a) \frac{d\mathbf{x}}{dt} - \frac{1}{a} \nabla \phi. \quad (5)$$

The first term on the right hand side, the 'Hubble drag', implies that momentum of an isolated particle is not conserved in an expanding universe. In a non-zero vacuum energy universe, $H(a)$ tends to a constant while the potential gradient term declines as a becomes very large. Ultimately, the drag term comes to dominate the large-scale dynamics, shutting down the growth of structure. Current data support the notion that our metric is on the verge of entering just such a phase. We are observing a special time in the history of our universe.

1.2. ISOLATED, SPHERICAL CLUSTERS

A starting point for understanding cluster formation is to consider a single point-like perturbation in an otherwise homogeneous, Einstein-de Sitter universe. In this case, the enclosed excess density within a sphere of radius r centered on the perturbation scales as r^{-3} , and all spherical mass layers (or 'shells') have negative total energy. Each shell expands to a maximum radius, then contracts and relaxes to hydrostatic and virial equilibrium, either through shock heating, for a collisional gas (the ICM in the case of clusters), or through caustic formation and phase wrapping for a collisionless fluid (dark matter and/or galaxies). The imposed radial density gradient forces an 'inside-out' or 'bottom-up' process; inner shells collapse earlier than their outer counterparts (Gunn & Gott 1972).

Since neither gravity nor the Einstein-de Sitter background introduce a characteristic scale into the problem, Gunn (1977) suggested the existence of a similarity solution in a variable $\lambda \propto r/t^\eta$. Similarity solutions for this problem were subsequently developed by Fillmore & Goldreich (1984) and Bertschinger (1985). Bertschinger derived $\eta = 8/9$ for the Einstein-de Sitter case and numerically solved the full internal structure for cases of pure gas, pure collisionless fluid, and a mixed case in the limit of negligible gas mass fraction.

The mean radial velocity (V) and density (D) profiles of the solution for a classical ($\gamma = 5/3$) collisional gas is shown in Figure 9.1. A number

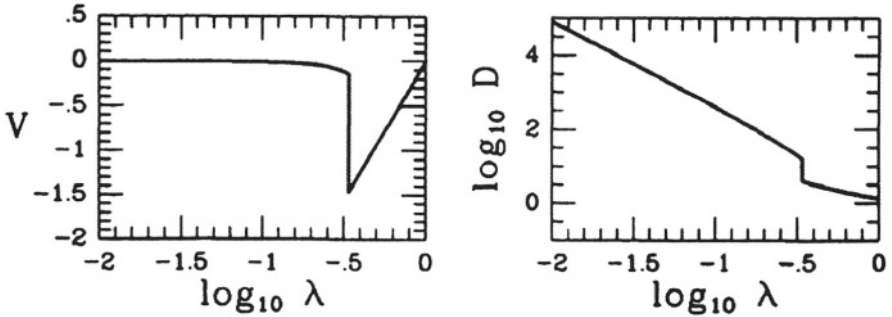


Figure 9.1. Collisional gas velocity (left) and density (right) structure from the self-similar infall solution of Bertschinger (1985).

of features characterize the structure. The radial coordinate is scaled to the zero-velocity surface, or turn-around radius $r_{ta}(t) \propto t^{8/9}$, so the mean radial velocity is zero at $\lambda = r/r_{ta}(t) = 1$. Interior to this radius, an infall regime, where gas is contracting, extends to $\lambda \sim 0.3$. At this point, infalling material is halted by outward propagating shock front. Under the assumption of cold, infalling gas satisfying the Rankine-Hugoniot jump conditions (see Sarazin's contribution), a jump in density of a factor four occurs at the shock. The mean mass density interior to the shock is a fixed multiple (factor ~ 100) of the critical density. Note that the gas is not exactly hydrostatic directly behind the shock; the radial velocity is small and negative as the gas settles adiabatically into hydrostatic equilibrium. The density interior to the shock is a power-law $\rho(r) \propto r^{-9/4}$.

Despite the absence of a shock, the collisionless solution is remarkably similar to the collisional case. In place of a shock, the collisionless solution displays a series of caustic surfaces, each located at a zero-crossing of the dark matter radial velocity. From the radial phase space structure shown in Figure 9.2, we see that the outermost caustic surface lies at the same radial location as the shock front in the $\gamma = 5/3$ gas case. Interior to this radius, the density solution of the dark matter (not shown) is, excepting the caustics, well described by the same $r^{-9/4}$ power-law profile displayed by the gas.

From this idealized case of pure accretion, a number of characteristic aspects of clusters emerge.

- o Clusters have a well-defined boundary, located at $\sim 1/3$ of their current turn-around radii and characterized by a mean interior density $\sim 100\rho_c$, that separates static from infalling regions. Within this region, hydrostatic and virial equilibrium are quickly established.

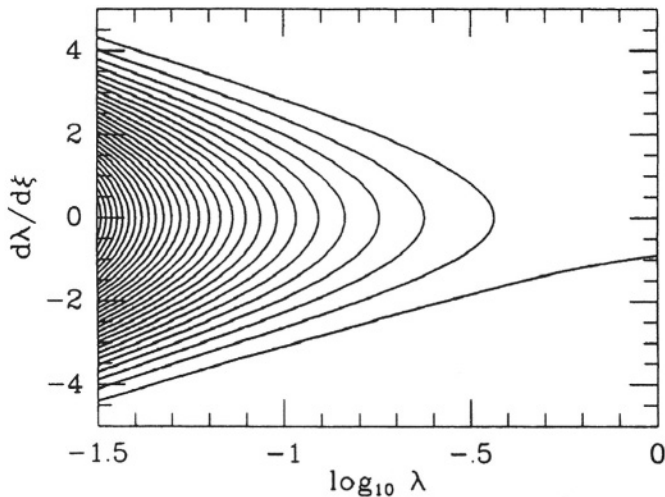


Figure 9.2. Collisionless (dark matter or galaxy) radial velocity structure of the self-similar infall solution of Bertschinger (1985). The variable ξ is a scaled unit of time.

- The radial profiles of the collisionless dark matter and collisional gas are similar; no strong radial segregation occurs between the two components.

As we will shortly see, the lessons derived from this simple example require some degree of modification when carried over to the more realistic case of formation by hierarchical mergers.

1.3. 3-D HIERARCHICAL CLUSTERING

Clusters in the sky are neither isolated nor exactly spherical, so the degree of symmetry in the above example is artificial. Observations of the large-scale galaxy distribution support the postulate that such structure originated as a low-amplitude Gaussian random noise field, thought to have been generated by quantum fluctuations in the dominant field (or fields) that drove a very early epoch of rapid expansion known as inflation. In this case, the initial density field is described as a superposition of plane waves $\delta_{\mathbf{k}}$. Isotropy demands that statistics of $\delta_{\mathbf{k}}$ not depend on direction, so the character of the field is summarized by a function of scalar wavenumber k , the matter power spectrum $P(k) = |\delta_{\mathbf{k}}|^2$ at the epoch of recombination. For a particular world model, $P(k)$ requires assumption of a very early, or ‘primordial’, spectrum $P_{\text{prim}}(k)$ and assumptions regarding the nature and amounts of the dark matter/energy

components. Calculation of the transfer function $T(\mathbf{k}) \equiv P(\mathbf{k})/P_{\text{prim}}(\mathbf{k})$ is accomplished by solving the coupled Boltzmann equations governing the radiation and matter components (Efstathiou 1990). For cosmologies dominated by cold dark matter (CDM), such calculations are now effectively standardized by codes such as CMBFAST (Seljak and Zaldarriaga 1996).

The Fourier description of independent modes $\delta_{\mathbf{k}}$ is natural for linear evolution. But clusters are non-linear structures characterized by total mass M . Directly linking linear and non-linear scales is a complex problem (Bond & Myers 1996), but a convenient approximate link is established by convolving the linear fluctuations $\delta(\mathbf{x}, a)$ with a spherical filter of comoving scale $R = (3M/4\pi\rho_m)^{1/3}$. A typical choice of filter is a Heaviside, or ‘top-hat’, function $W(r) = 1$ for $r \leq R$ and $W(r) = 0$ for $r > R$. Power in the density field associated with structures smaller than M is removed by the filter; what remains is the variance associated with mass scale M

$$\sigma^2(M) = \int d^3k P(k) \hat{W}(kR) \quad (6)$$

where $\hat{W}(y) = 3(\sin y - y \cos y)/y^3$ is the Fourier transform of the spherical top-hat filter.

It is conventional to express the power spectrum normalization in terms of the *rms* level of fluctuations on a comoving scale $R = 8 h^{-1}$ Mpc. For the purpose of addressing Hubble Volume simulations discussed below, we introduce two flat-metric CDM variants listed in Table 9.1; a matter dominated τ CDM and vacuum dominated Λ CDM. Assuming a featureless primordial power spectrum $P_{\text{prim}}(k) \propto k$, the postrecombination spectra of these models are progressively damped at higher k and have oscillatory features on sub-horizon scales whose amplitude depends on the ratio of baryonic to total clustered matter Ω_b/Ω_m . For $\Omega_b/\Omega_m \lesssim 0.1$, the oscillation amplitude is small, and the local shape of the present filtered power spectrum is well described by a low order quadratic in logarithmic variables

$$\ln \sigma(M) = \ln \sigma_{15} - a \ln M - b (\ln M)^2 \quad (7)$$

where M is mass in units of $10^{15} h^{-1} M_{\odot}$. Explicit use of subtractive terms ensures that the coefficients a and b are positive and signals that both models are ‘bottom-up’ in their evolution: small scale structure develops before large.

In Fig. 9.3, we show filtered density fluctuations $\sigma(M)$ for the models listed in Table 9.1. The Λ CDM values are computed using CMBFAST (Seljak & Zaldarriaga 1996) assuming $h = 0.7$ and baryon density

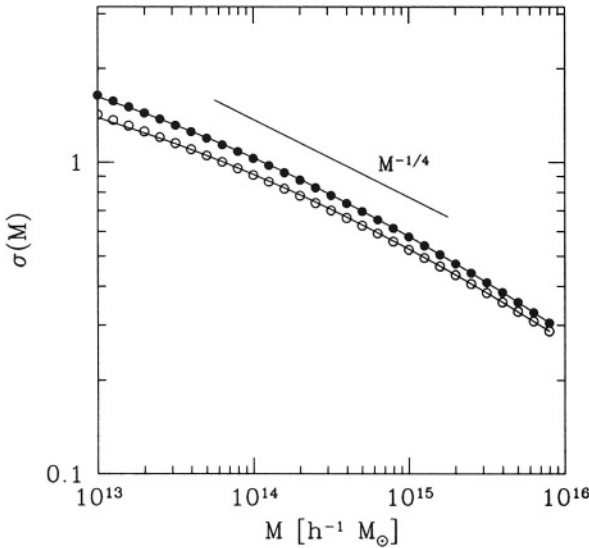


Figure 9.3. Filtered power spectra for the Λ CDM (filled circles) and τ CDM (open) models along with fits (solid lines) to the approximate form of equation (7). The solid line shows a power law form $\sigma \propto M^{-1/4}$.

Table 9.1. CDM Models and Fit Parameters for $\ln \sigma(M)$.[†]

Model	Ω_m	Ω_Λ	σ_8	σ_{15}	a	b
Λ CDM	0.3	0.7	0.9	0.578	0.281	0.0123
τ CDM	1.0	0	0.6	0.527	0.267	0.0122

[†]equation (7).

$\Omega_b h^2 = 0.0196$ (Burles and Tytler 1998) while the τ CDM values are derived from the functional fit to the transfer function calculations of Bond & Efstathiou (1984) and does not include a baryon contribution. Parameters of the fits to equation (7) are also given in the table. The *rms* fluctuation amplitude σ_{15} at $10^{15} h^{-1} M_\odot$ is directly proportional to the fiducial power spectrum normalization σ_8 within each model. Although the values of σ_8 differ by 50% between the models, the larger spatial scale required to gather $10^{15} h^{-1} M_\odot$ in the Λ CDM model leads to values of σ_{15} that differ by only 10%. This similarity reflects the constraint that τ CDM and Λ CDM models produce similar space densities of clusters at the present epoch.

Formation of structure in these models occurs in a hierarchical fashion. At a given time, the density field exhibits a web-like topology in which expanding, underdense voids are surrounded by contracting walls and filaments of moderate (\lesssim factor 10) density contrast relative to the mean. Fig. 9.4 illustrates the appearance of the cosmic web on gigaparsec scales. Clusters emerge as knots in the web that are interspersed within the network in a complex manner. The most massive clusters form at the intersection of large filaments and are much more strongly clustered than the overall mass. Smaller clusters tend to populate walls and voids and are less strongly clustered. Analytic descriptions of this ‘biased’ spatial clustering have been developed, and their predictions are confirmed by N-body simulations (Kaiser 1984; Mo & White 1996; Jing 1998).

The behavior of clusters in this more realistic, fully three-dimensional setting is, not surprisingly, more complex than the spherical case discussed previously. To illustrate the differences, we show results from the simulation of a particular cluster that forms the basis for comparison of a number of cosmological gas dynamic codes. Termed the ‘Santa Barbara’ (SB) cluster (because the project originated at a workshop sponsored by the Institute for Theoretical Physics at UC, Santa Barbara), we show a particular solution modeled by the P3MSPH code of Evrard (1988). The model cluster is evolved in a standard CDM cosmology with $\Omega_m = 1$ and $\Omega_b = 0.1$. Details of the initial conditions and run parameters can be found in Frenk et al. (1999).

Fig. 9.5 shows the evolution over time of the dark matter mass of this cluster determined from a percolation algorithm. The so-called friends-of-friends algorithm clusters sets of dark matter particles that are interlinked by separations less than 0.15 times the mean interparticle spacing at all epochs (Lacey & Cole 1994).

The growth history of this cluster is complex. Periods of relatively gentle accretion are punctuated by mergers, such as that near $z \sim 0.7$, that signal rapid growth. Note that, contrary to the spherical model behavior, the mass in the case of hierarchical clustering does not always increase in time. Short periods during which the mass declines by $\lesssim 5\%$ are not uncommon.

The phase space structure of this cluster highlights other departures from spherical model expectations. Fig. 9.6 shows the spatial and radial velocity structure of the ‘Santa Barbara’ (SB) cluster at redshifts $z = 0.9, 0.6, 0.3$ and 0. As a radial scale, we employ r_{200} , the physical radius within which the mean enclosed mass density is 200 times the critical value. Letting M_{200} be the enclosed mass within that radius, a natural velocity unit is $v_{200}^2 = GM_{200}/r_{200}$. The growth of the physical size and

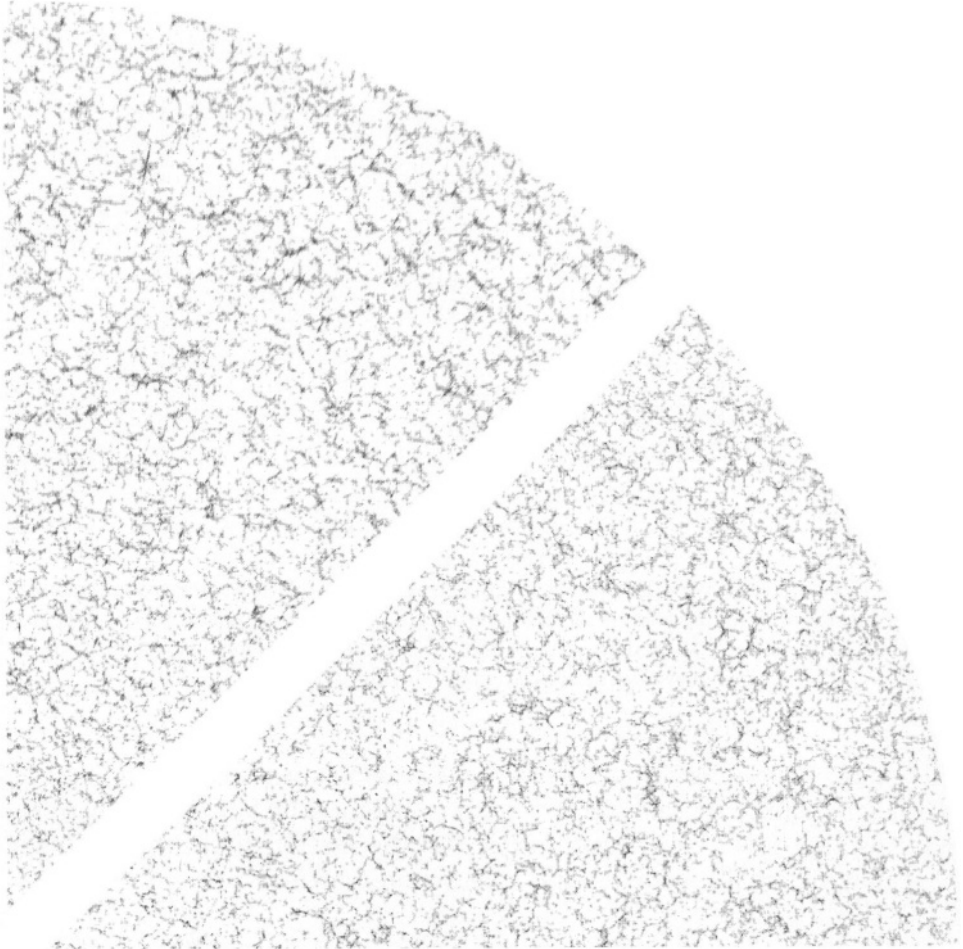


Figure 9.4. Maps of the dark matter density in slices through a deep artificial sky survey of a Λ CDM Hubble Volume simulation. The survey origin is located at the vertex and the grey scale represents the matter density of overdense material ($\delta > 0$) relative to the mean, using Lagrangian smoothing on a mass scale $2 \times 10^{13} h^{-1} M_{\odot}$. Two representations of a single region are shown, reflected about the diagonal. Horizontal images display structure in the comoving metric on an overall scale of $2.6 h^{-1}$ Gpc while the vertical images display structure in redshift space to $z = 1.25$. In the latter, positions of clusters at the intersection of filaments are evident through the radial distortions arising from their internal velocity dispersions (so-called ‘fingers of God’). Note the very hot cluster, visible as a long finger in the velocity direction, at $z = 1.04$ in the upper left.

mass of the largest cluster progenitor conspires keep the potential well depth v_{200}^2 nearly constant in time.

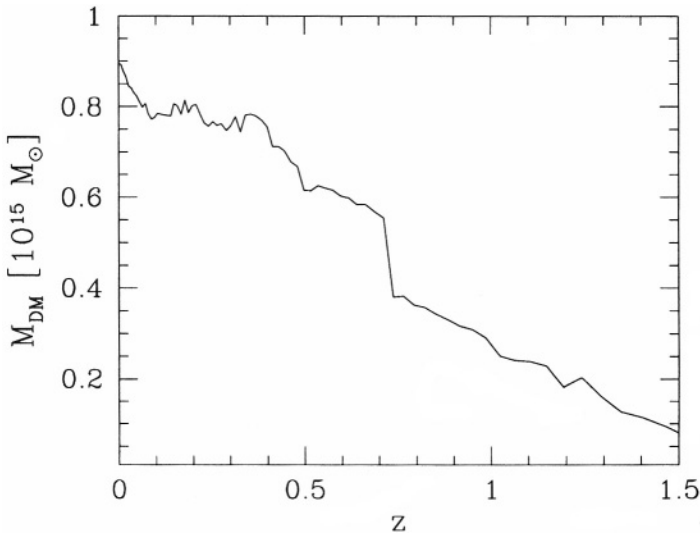


Figure 9.5. Formation history of a typical cluster in a CDM universe derived from the P3MSPH contribution to the Santa Barbara cluster comparison project (Frenk *et al.* 1999). The mass in dark matter M_{DM} derived from a percolation algorithm is shown at roughly eighty epochs spaced equally in proper time.

The particle positions reflect a large-scale filament oriented along the diagonal of the image. Mergers occur preferentially, but not exclusively, along this axis. Large-scale torques on the matter distribution in this region are small, so the cluster orientation remembers this direction at all times.

The radial phase-space structure resembles the perfectly spherical case of Fig. 9.2 in some ways. Material interior to r_{200} is close to hydrostatic; the mean radial velocity is small compared to the dispersion. Important differences are also apparent. The infalling stream contains collapsed structures and therefore shows dispersion in velocity at radii beyond r_{200} . This is most apparent for the clump at $z = 0.9$ visible in the projected image at a distance of ~ 3 Mpc (upper right corner of the lower panel).

Perhaps the biggest difference with respect to the spherical expectation is the existence of orbits, shown in red in Fig. 9.6, that indicate material is expelled to locations well outside r_{200} after passing through the cluster center. The fraction of mass involved in this ‘spray’ is considerable, growing from 4 to 17% of M_{200} over the four frames plotted. The spatial distribution of this spray is aligned with the merger axis at early times, but at late times is more isotropically distributed. The existence of galaxies on such orbits is potentially observable if star formation

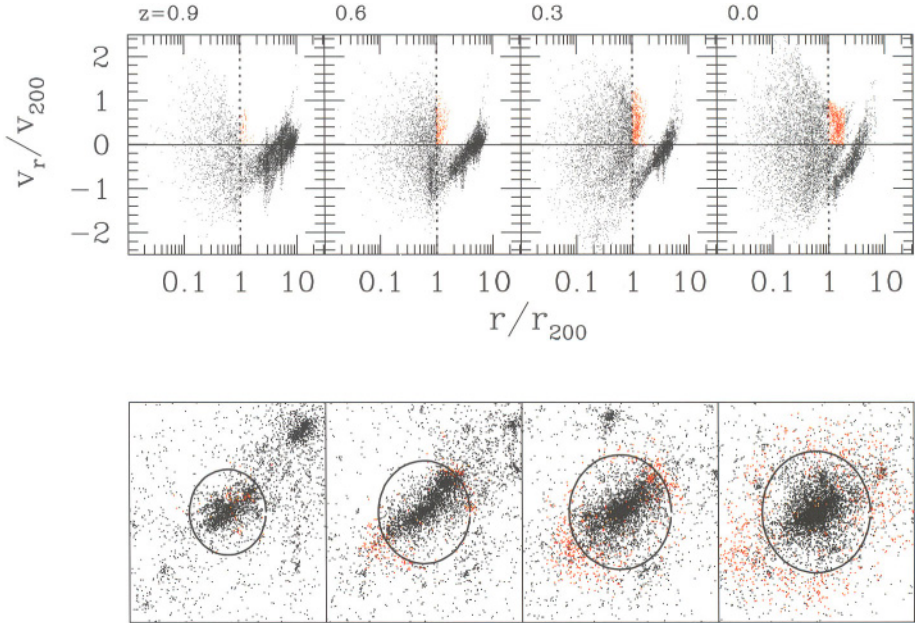


Figure 9.6. Radial velocity (top) and spatial (bottom) structure of dark matter in the SB cluster simulation at the redshifts indicated. Only one in four randomly selected particles are shown. Specific values at the redshifts shown are: $r_{200} = 1.02, 1.46, 2.00$ and $2.76 h^{-1} \text{ Mpc}$; $M_{200} = 0.39, 0.67, 0.93$ and $1.10 \times 10^{15} h^{-1} M_{\odot}$; $v_{200} = 1272, 1403, 1409$ and 1310 km s^{-1} . The lower panels are 10 Mpc (comoving) in scale and the circle indicates r_{200} . Red particles lying between r_{200} and $2r_{200}$ with $v_r > 0$ represent material heading toward its first apocentric passage after infall.

ceases or is otherwise strongly altered on the initial infall (Larson et al. 1980; Dressler & Gunn 1983; Couch & Sharples 1988). One would expect clustered populations of reddened and possibly k+A-type galaxies on the outskirts of clusters (Balogh et al. 2000).

The SB cluster solutions for the gas assume that gravitationally-induced shocking is the only physical mechanism that changes its entropy. Although certainly an idealization, the fact that such shocks are the only viable mechanism capable of generating the large thermal energy content of a massive cluster's ICM ($\sim 10^{64} \text{ erg}$) means that this simple approximation is remarkably accurate (see Sarazin's and Schindler's contributions to this book).

Simulations of head-on collisions between two-component (dark matter + gas), self-gravitating spheres show that a small amount of energy is transferred from the dark matter to the gas core during pericentric passage (Pearce et al. 1994), resulting in a final gas distribution that

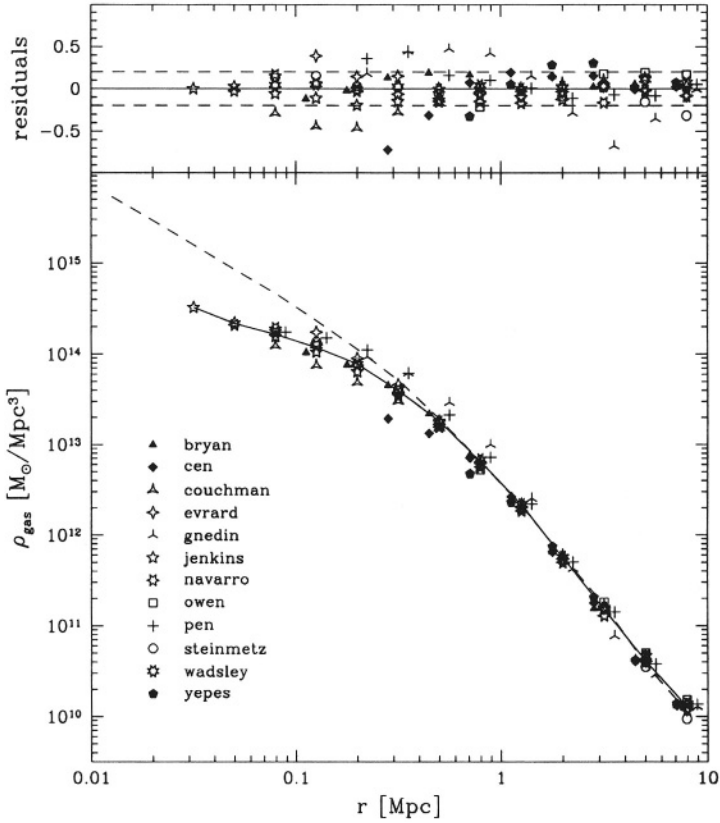


Figure 9.7. Gas density profiles from the SB cluster simulation project (from Frenk *et al.* 1999). Symbol types denote different classes of numerical schemes: open, Lagrangian; filled, Eulerian; skeletal, hybrid. The solid line shows the average gas profile while the dashed line gives the mean dark matter profile, scaled by a factor $\Omega_b/(\Omega_m - \Omega_b)$.

is less centrally concentrated than the dark matter. The radial profiles of the SB cluster study confirm this finding in the case of fully three-dimensional clustering. Fig. 9.7 shows the final density distributions of the gas derived from the twelve pseudo-independent cosmological codes, along with the scaled, average profile of the dark matter. The gas is less concentrated than the dark matter within $\sim 0.2 r_{200}$, but seems to trace the dark matter faithfully beyond this scale. Within r_{200} , the mean interior gas fraction differs from the global value by an amount

$$\Upsilon_{200} = \frac{M_{\text{gas}}(< r_{200})}{M_{\text{tot}}(< r_{200})} \frac{\Omega_m}{\Omega_b} = 0.92 \pm 0.06 \quad (8)$$

where the mean and scatter are derived from the twelve different code solutions.

Observations support the existence of a more extended gas distribution. In massive clusters, X-ray imaging indicates core radii of about $200 h^{-1}$ kpc while strong lensing reconstruction of the total mass distribution requires a more cusped central density profile (Wu & Hammer 1993; Wu 2000).

From this brief treatment of the fully three-dimensional case, we can modify the lessons from the spherical model in the following manner.

- The radius r_{200} serves as a useful approximate marker of the boundary between static and infalling regions of clusters formed in a fully three dimensional environment, but the amount of matter exterior to r_{200} that has passed through the central regions of the cluster can be significant ($\sim M_{200}/6$). Still, M_{200} remains a viable measure to use for ordering the cluster population.
- In the absence of radiative cooling, the radial structure of the gas is slightly more extended than that of the dark matter, resulting in a modest ($\lesssim 10\%$) depletion of baryons within r_{200} .

2. THE DISCRETE CLUSTER POPULATION

The preceding section emphasized clusters as part of the continuous density field of large-structure. A more practical perspective is to consider the cluster population as a set of discrete objects, each described by a list of internal properties (mass, temperature, luminosity, etc.) that can be used to construct cluster catalogs. From the same underlying population of clusters, catalogs with varying degrees of overlap can be constructed using different selection criteria (*e.g.*, limiting X-ray flux, optical richness, total or ICM mass content).

From intercomparison of large and homogeneous cluster catalogs defined at multiple wavelengths, and from efforts to reconstruct such catalogs computationally via direct simulation and semi-analytic modeling, we stand to gain a much firmer understanding of both the cosmology underlying our local universe and the astrophysical processes that govern the content of the clusters within it. In this section, we outline an approach to describing the cluster population that serves to decouple the cosmological and astrophysical information contained in survey data.

2.1. FROM CLUSTER SURVEYS TO COSMOLOGY

Deciphering the cosmological and astrophysical information in the coming era of large survey data sets requires the ability to accurately compute expectations for observables. Given some survey observations

\mathcal{R} , a likelihood analysis requires the probability $p(\mathcal{R}|\mathcal{C}, \mathcal{A})$ that such data would arise within a model described by particular sets of cosmological $\mathcal{C} \equiv \{C_i\}$ and astrophysical $\mathcal{A} \equiv \{A_j\}$ parameters. This probability is central to likelihood constraints on cosmological parameters through Bayes' theorem

$$p(\mathcal{C}|\mathcal{R}, \mathcal{A}) = \frac{p(\mathcal{C})p(\mathcal{R}|\mathcal{C}, \mathcal{A})}{p(\mathcal{R})} \quad (9)$$

where $p(\mathcal{C})$ is an independent prior and $p(\mathcal{R})$ is a normalization obtained by a weighted integration $p(\mathcal{R}|\mathcal{C}, \mathcal{A})$ over the range of interesting cosmological and astrophysical parameters.

With cluster redshift surveys in mind, we can think of the observations as a set $\mathcal{R} \equiv \{R_k, z_k\}$ of individual measurements R_k (e.g., of X-ray luminosity, galaxy velocity dispersion or Sunyaev-Zel'dovich decrement) at corresponding redshifts z_k . Considering total mass as the natural variable to use in ordering the discrete population, we can consider the likelihood of a specific measurement $p(R, z|\mathcal{C}, \mathcal{A})$ as a product

$$p(R, z|\mathcal{C}, \mathcal{A}) = p(M, z|\mathcal{C}) p(R|M, z, \mathcal{A}) \quad (10)$$

of the likelihood $p(M, z|\mathcal{C})$ that a cluster of mass M exists in the survey of interest at redshift z in cosmology \mathcal{C} and the likelihood $p(R|M, z, \mathcal{A})$ that the specific observable R is associated with such a cluster given the astrophysical model \mathcal{A} .

The $p(M, z|\mathcal{C})$ term has been the subject of exhaustive investigation and, as argued in the next section, can now be considered essentially solved for the case of Gaussian random initial conditions. Its explicit lack of dependence on astrophysical parameters \mathcal{A} reflects the assumption that weakly interacting dark matter dominates the total cluster mass M (see § 3.2).

The second term, $p(R|M, z, \mathcal{A})$, is dependent, often critically, on the astrophysical model, as it generally expresses the answer to the question "how do dark matter potential wells light up?" The question of how group and cluster potentials light up is complex, and detailed answers remain elusive.

2.2. THE MASS FUNCTION

A starting point for cosmological investigations using clusters is the probability of finding, in a comoving volume element dV , a cluster at redshift z with total mass M or larger

$$p(>M, z|\mathcal{C}) \propto n(>M, z|\mathcal{C}) dV \quad (11)$$

where $n(>M, z|\mathcal{C})$ is the cumulative comoving number density of clusters at redshift z . Although we omit explicit astrophysical dependence

in the space density here, it is important to bear in mind that this assumption may be in error at the few percent level in smaller systems such as poor groups where baryon losses may occur.

In deriving the differential version of the number density $n(M, z)d \ln M$ (known as the *mass function*) from either simulations and observations, several complications arise. One is simply semantic. As we have seen, clusters do not possess sharp physical boundaries. So what mass do we assign to a particular cluster? A number of conventions have developed in the literature, discussed by Lacey & Cole (1994) and White (2001). We employ here the spherical density threshold mass M_{200} , defined relative to the critical density $\rho_c(z)$ at the epoch of interest z .

A second and more profound complication is that it is not possible to directly observe the theoretically defined mass M . Instead, a surrogate estimator \mathcal{M} is employed that will be, in general, a biased and noisy representation of M . For example, mass estimates derived from weak gravitational lensing distortions measure the mass within a projected cylinder weighted broadly as a function of depth. Attempts at calibrating estimated versus true masses with N-body simulations suggest that the latter are overestimated by typically $\sim 30\%$, with a dispersion of similar magnitude (Metzler et al. 2001). It is not clear to what degree such projection biases can be removed for individual observations, nor is it known to what extent the biases are sensitive to sample selection rules.

Beginning with the 1000-particle experiments of Press & Schechter (1974; PS), the form of the mass function has been subject to investigation by N-body simulations of increasing size and scope. Recent billion particle computations by the Virgo Consortium (Jenkins et al. 2001) and GC³ (Bode et al. 2001) are the latest and, at least presently, largest such investigations. The Hubble Volume (HV) simulations of the Virgo Consortium model the dark matter in random cubes of side length $3 h^{-1}$ Gpc for Λ CDM and $2 h^{-1}$ Gpc for τ CDM. The simulations are unique in their creation of mock sky survey data sets that record structure along the past light-cone of hypothetical observers in the computational volume (Evrard 1998; Evrard et al. 2001), an approach pioneered for pencil-beam surveys by Park & Gott (1991).

Jenkins et al. (2001, hereafter J01) use output of the Hubble Volume (HV) set as well as ten smaller Virgo simulations to calibrate the mass function over four orders of magnitude in mass for three CDM variant cosmologies. They show that the space density of clusters, defined by either friends-of-friends or spherical overdensity (SO) algorithms, in all models is well described by a single functional form when expressed in terms of $\ln \sigma^{-1}(M)$, where $\sigma^2(M)$ is the variance of the filtered linear

density field, equation (6). Defining the mass fraction $f(\sigma^{-1}(M))$ by

$$f(\sigma^{-1}(M)) \equiv \frac{M}{\bar{\rho}(z)} \frac{dn(>M, z)}{d \ln \sigma(M)} \quad (12)$$

with $\bar{\rho}(z)$ the background matter density at the epoch of interest, the general form found by J01 for the mass function is

$$f(\sigma^{-1}(M)) = A \exp[-|\ln \sigma^{-1}(M) + B|^\epsilon]. \quad (13)$$

The fit parameters A , B and ϵ depend on the particular cluster finding scheme implemented, but J01 show that algorithms which define mass relative to the mean background density yield to fits that are independent of epoch and/or cosmological model, at least within the set of 22 outputs studied. The amplitude A sets the overall mass fraction in collapsed objects, e^B plays the role of a linearly evolved collapse perturbation threshold, (similar to the parameter δ_c in the standard PS model), and ϵ is a stretch parameter that provides the correct shape to the mass function at the very dilute limit.

Using equation (7), and defining the effective logarithmic slope

$$\alpha_{\text{eff}}(M) \equiv d \ln \sigma^{-1} / d \ln M = a + 2b \ln M \quad (14)$$

which, for both Λ CDM and τ CDM, varies slowly between 0.2 – 0.3 over the interval 10^{13} to $10^{15.5} h^{-1} M_\odot$ (Fig. 9.3), we can express the Jenkins mass function (JMF) in the more familiar terms of mass and redshift

$$n_{\text{JMF}}(M, z) = \frac{A \bar{\rho}(z)}{M} \alpha_{\text{eff}}(M) \exp[-|\ln \sigma^{-1}(M) + B|^\epsilon]. \quad (15)$$

Mass functions from the HV simulations, derived for the spherical density threshold mass M_{200} at $z=0$ from samples of 1.39 million (Λ CDM) and 1.48 million (τ CDM) clusters above $5 \times 10^{13} h^{-1} M_\odot$, are shown in Figure 9.8. Fits to equation (15) are shown as dotted lines, with fit parameters listed in Table 9.2. The upper panels of Figure 9.8 show the fractional deviations in space density between the binned simulation data and the fits. For bins with 100 or more clusters ($M_{200} \lesssim 2 \times 10^{15} h^{-1} M_\odot$), the *rms* deviations between the fit and experimental data are $\lesssim 3\%$. The overall accuracy of this calibration is more difficult to estimate, but Evrard et al. (2001) use various arguments to suggest that systematic biases are at the $\sim 10\%$ level.

The impressive statistics provided by billion particle simulations will only improve as future experiments of even larger size are realized. We can anticipate sub-percent level accuracy in calibration of the mass function within the next few years. Compared to the thornier issues related

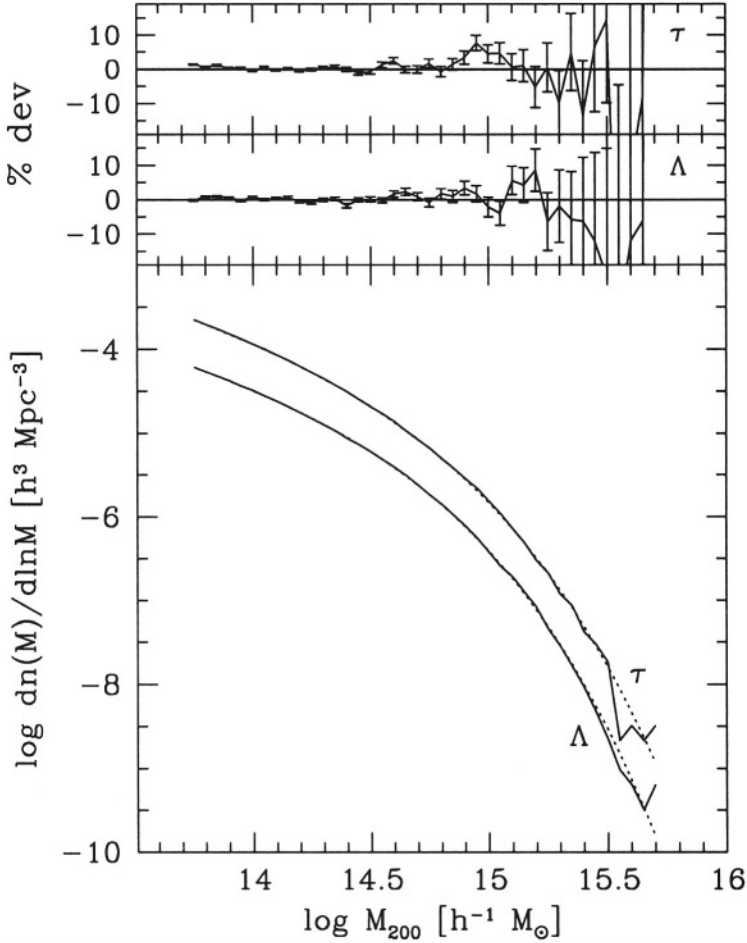


Figure 9.8. Mass functions at $z=0$ derived from HV simulations (solid lines) are shown in the lower panel, along with fits to equation (15) using parameters listed in Table 9.2 (dotted lines). Upper panels show the percent deviation in number between the HV data and the fits, with error bars based on Poisson statistics in each mass bin. From Evrard *et al.* (2001).

Table 9.2. SO(200) mass function parameters.[†]

Model	A	B	ϵ
Λ CDM	0.22	0.73	3.86
τ CDM	0.27	0.65	3.77

[†]equation (15).

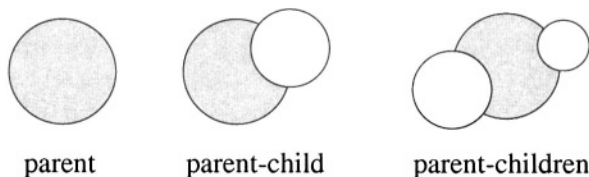


Figure 9.9. Schematic illustrating the classes of clusters that can result from application of the SO algorithm discussed in the text: an isolated cluster (parent), a cluster with a single overlapping satellite (parent–child) and multiple overlapping satellites (parent–children). The mass limit imposed on the parent and child populations will control the fractions of clusters in each classification.

to how clusters light up, the $p(M, z | \mathcal{C})$ question is essentially solved for the class of popular CDM–dominated cosmologies.

2.2.1 Frequency of Mergers. A question of interest to this volume is the fraction of clusters undergoing mergers. The conditional Press–Schechter formulae (Bower 1991; Lacey & Cole 1993) provide a means to compute statistics of merging probabilities. We provide here a related statistic based on so-called ‘child’ clusters defined in the HV cluster surveys.

The algorithm employed to define the cluster sample is a simple type of spherical overdensity filter. It starts by generating a density estimate for each particle using the distance to its eighth nearest neighbor, equivalent to filtering on a Lagrangian scale of $2 \times 10^{13} h^{-1} M_{\odot}$. Sorting density values in decreasing order provides a list of potential sites for cluster centers. Beginning with the first member of the sorted list, a sphere of radius r_{200} enclosing mass M_{200} is defined about that particle, enclosing density $\rho(< r_{200}) \equiv 200 \rho_c(z)$. Particles lying within this sphere are recorded as members of this group and are removed from the list of potential cluster centers. The process is repeated sequentially, centering the next cluster on the next available particle in the ordered list, until the list is exhausted.

The algorithm allows particles to belong to more than one cluster, but the center of a given cluster cannot be contained within the spherical boundary of any other. This leads naturally to a classification system outlined in Fig. ???. A *parent* cluster is either isolated or the most massive member of an overlapping set. Smaller members of an overlapping pair are termed *child* clusters. In § ??, we show that the virial relation of the child population is slightly hotter than that of the parents, a fact which we interpret to indicate that many ‘child’ clusters are the product of advanced states of mergers.

The child population identified by the SO algorithm is significant in number, representing about 10 percent of the overall population more

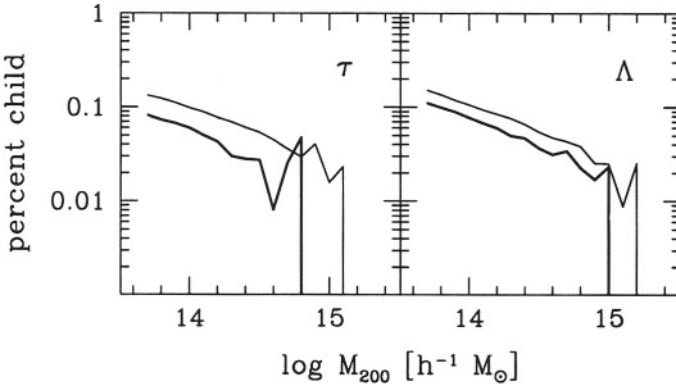


Figure 9.10. Fraction of child clusters (Fig. 9.9) identified in HV sky survey catalogs of τ CDM (left) and Λ CDM (right) cosmologies. Light lines are clusters lying at $z < 0.5$, bold are at $z > 0.5$.

massive than $10^{14} h^{-1}M_{\odot}$. Fig. 9.10 shows the differential fractions of children as a function of mass for samples of low ($z < 0.5$) and high ($z > 0.5$) redshift clusters. Although, as one might expect, there is a trend toward decreasing child fraction at higher masses, it is interesting that even systems as massive as Coma ($10^{15} h^{-1}M_{\odot}$) have a one percent chance of being the minor member of an overlapping cluster pair. At $10^{14} h^{-1}M_{\odot}$, one in ten clusters is a minor member of such a pair or group. The redshift dependence is milder in the Λ CDM model, as expected from the weaker evolution with redshift of $\sigma(M)$ in the mass function, equation (13).

Such multiply overlapping clusters are signatures of ongoing mergers. Observationally, such child clusters would be manifested in the form of off-center peaks in X-ray or smoothed galaxy images. Such situations are commonly observed, and Fig. 9.11 shows the well studied case of MS 1054.4–0321 at $z = 0.83$ (Gioia & Luppino 1994). Other examples are RX J1716+6708 at $z = 0.81$ (Henry et al. 1997; Gioia et al. 1999) and RX J0152.7–1357 at $z = 0.83$ (Delia Ceca et al. 2000; Ebeling et al. 2000). These three clusters, all at high redshift, show a high degree of optical and X-ray substructure and are consistent with the scenario of cluster formation by mass infall along large-scale filaments (Bond et al. 1996). Their dynamical state may be in large part dominated by infall and merging, and the majority of them are actually composed of two or more distinct components. They have high velocity dispersions ($\geq 1300 \text{ km s}^{-1}$) and high temperature ($kT \geq 6 \text{ keV}$). The velocity dispersion could be inflated by the presence of a larger than average fraction of

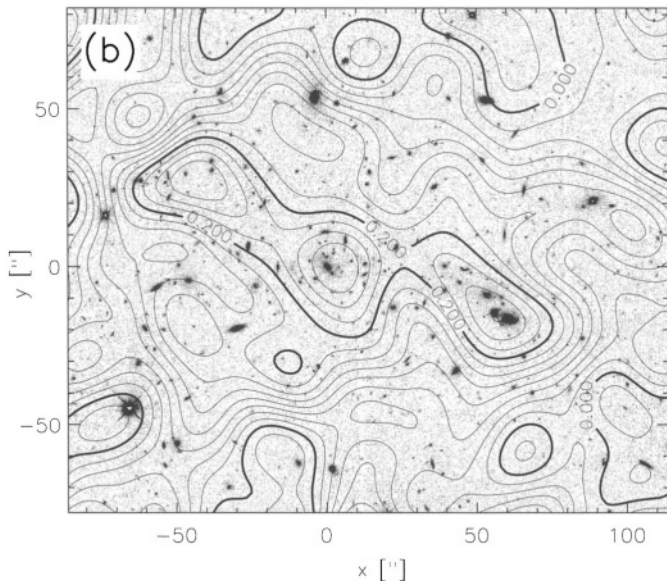


Figure 9.11. HST optical image of the cluster MS 1054.4–0321 at $z = 0.83$ with superposed contours of the clustered matter distribution determined by weak gravitational lensing (from Hoekstra *et al.* 2000). Multiple peaks in both components reflect an ongoing merger between at least two, and possibly three, sub-systems.

recently accreted galaxies moving along radial orbits. Thus, the few distant clusters available to us today suggest that highly unrelaxed systems may indeed be common at high redshift. The appearance that the known high- z clusters are still in the process of formation through merging implies that their X-ray luminosity may be temporarily biased high, as shown by numerical simulations (Ricker & Sarazin 2001). Unfortunately, a detailed statistical analysis of this effect has not yet been done. The next generation of deep, homogeneous samples of observed clusters will provide strong motivation for careful study.

2.3. CLUSTER INTERNAL STRUCTURE

As clusters grow through mergers, their internal structure evolves. Simulations suggest that this evolution is sufficiently well ordered that the cluster population remains rather close to a one-parameter family. In this section, we briefly review the form of the radial dark matter density profile and the virial theorem, emphasizing the role of mergers in each.

2.3.1 Dark matter density profiles. Analysis of the radial density profiles of dark matter clusters in N-body experiments by

Navarro, Frenk & White (NFW) (1996; 1997) revealed a degree of regularity that was anticipated by, but not recognized in, previous experiments addressing the issue. Defining the scaled radius $x = r/r_{200}$, the spherically averaged density profile of dark matter halos derived from their experiments takes the form

$$\rho_{\text{NFW}}(x) = \frac{200 c^3 \rho_c}{3[\ln(1+c) - c/(1+c)]} \frac{1}{cx(1+cx)^2}. \quad (16)$$

The concentration parameter c , the single free parameter of the fit given M_{200} , correlates with mass in the sense that lower mass clusters are more centrally condensed than their high mass counterparts.

NFW97 develop an analytic model for this mass dependent shape based on the different merger histories anticipated for clusters of different mass. The rarest, most massive systems are very likely to have undergone a major merger recently whereas more abundant objects of lower mass are likely to have been assembled through mergers at earlier epochs. Linking the contrast $\delta_c \simeq c^3$ in density near the characteristic radius $x = 1/c$ to the critical density $\rho_c(z_{\text{merg}})$ at the epoch of the last major merger reproduces qualitatively the trend exhibited by the simulations. Although the specific approach of NFW97, as well as recent updates by Bullock et al. (2001) and Eke et al. (2001), do not explicitly make reference to merger epochs, the essence of their calculations is the same. Merger history controls cluster shape.

The experiments of NFW97 display very narrow ($\sim 10\%$) scatter in concentrations c at fixed mass. Linking c to z_{merg} , this result seems to imply that objects of a given mass must be built from very similar merging histories. However, NFW analyzed a simulated cluster sample that was biased against objects involved in ongoing or recent mergers. For cluster mass halos, the fraction of objects eliminated by this selection could be substantial. Observers wishing to compare to NFW predictions using a single cluster or small sample (*e.g.*, Fischer & Tyson 1999), cannot easily address the question of whether the objects under consideration would have passed the selection criteria applied by NFW.

Jing (2000) recently extended the work of NFW to a complete set of co-eval clusters. His sample is derived from an impressive ensemble of twenty-one 256^3 particle simulations of seven different cosmologies. For each cosmology, he extracts roughly 400 halos resolved by 10,000 or more particles (comparable to the degree of resolution of NFW) at the final epoch. After fitting the radial density profile within r_{200} , he classifies each by the maximum fractional deviation dvi_{max} between the fit and the binned profile. Jing uses this quantification to measure the fraction of clusters that fall into three categories: good ($dvi_{\text{max}} < 0.15$);

intermediate ($0.15 < \text{dvi}_{\text{max}} < 0.30$); and poor ($\text{dvi}_{\text{max}} > 0.30$). For clusters above $10^{14} h^{-1} M_{\odot}$ in the Λ CDM model, for example, roughly 40% of clusters have good fits and 20% are poor. The ‘good’ clusters confirm the NFW expectations and display a narrow dispersion (17%) in concentration. The ‘poor’ clusters have values of c lower by a factor 2.5, on average, than the good fits (and the NFW models), and they display a wider (33%) dispersion.

Jing shows that dvi_{max} correlates with two measures of recent merging — the redshift at which half the final mass of a cluster is assembled into its largest progenitor, and the mass fraction $M(z=0.5)/M(z=0)$ of the largest progenitor at $z=0.5$. These correlations provide direct evidence that poor fits to the NFW profile are linked to recent mergers.

By creating transient departures from the NFW form, cluster mergers broaden the distribution of c expected within a co-eval population. A practical consequence of this is that observational programs should be designed in expectation of the full distribution of c . Although morphological signatures of mergers in optical and X-ray images could be used to select against systems undergoing mergers, this approach is not likely to be completely effective. Projections onto the sky closely aligned with the merger axis will be difficult to recognize from morphology alone.

2.3.2 The dark matter virial theorem. The gravitational potential well depth GM/r of clusters offers a convenient route to estimate cluster masses through the virial theorem. This is the path that led Zwicky (1933) to infer the existence of dark matter in the Coma cluster. Assuming that both the dark matter (or galaxies) and ICM gas are thermalized in a common potential well of mass M and size r , we expect the dark matter (DM) velocity dispersion σ_{DM} and ICM temperature T to scale as $\sigma_{\text{DM}}^2 \sim T \sim GM/r$ (Cavaliere & Fusco-Femiano 1976). Evaluating the last term within a radius encompassing a fixed multiple Δ of the critical density (meaning $M \equiv M_{\Delta} = 4\pi\Delta\rho_c(z)r_{\Delta}^3/3$), and recalling that $\rho_c(z) = \rho_c(0)(H(z)/H_0)^2$, we derive the following compact expression

$$\sigma_{\text{DM}}^2 \propto T \propto [h(z)M_{\Delta}]^{2/3} \quad (17)$$

where $h(z) = H(z)/100 \text{ km s}^{-1} \text{ Mpc}^{-1}$.

The HV simulated cluster data sets allow calibration of this relation with unprecedented precision. Fig. 9.12 shows that clusters in both models obey a common scaling of the median dark matter velocity dispersion with mass. The Λ CDM and τ CDM sky survey samples extend in redshift to $z=1.45$ and 1.25, respectively, where the Hubble parameter takes on values $h(z) = 2.3$ and 3.4. The role of the Hubble factor is significant. To produce a cluster of a given velocity dispersion at $z=1$,

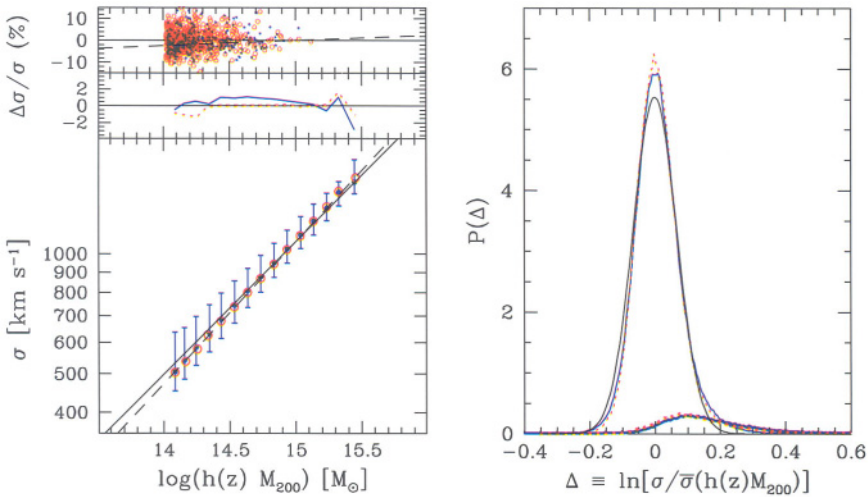


Figure 9.12. Dark matter virial relations derived from Hubble Volume sky survey samples of 400,000 (Λ CDM) and 200,000 (Λ CDM) clusters above $10^{14} h^{-1} M_{\odot}$ (Evrard & Horikawa, in preparation). Left panel, lower: the median velocity dispersion for parent clusters in Λ CDM (filled points) and τ CDM (open), with error bars showing the 5 – 95 percentile range of σ for both parents and children in each mass bin. Solid line gives the slope-constrained fit, equation (18); dashed line with slope 0.36 is the best fit to the parent median values. Left, middle: percent deviation between the medians and best fit for Λ CDM (solid) and τ CDM (dotted). Left, upper: deviations about equation (18) from higher resolution Virgo models, dashed line is deviation of the best fit relation from slope 1/3 power law. Right panel: the probability distribution function of velocity dispersion residuals about the best fit power law for parent (light) and child (bold) clusters in the Λ CDM (solid) and τ CDM (dotted) models. Also shown is a log-normal approximation to the parent distribution with 7% standard deviation.

the τ CDM model requires a factor 1.6 smaller mass than that required in Λ CDM. As we shall see in more detail below, the Hubble factor plays a critical role in tightening the virial relation. Because of this role, the product $h(z)M_{200}$ rightfully deserves to be known as the ‘virial mass’ of a cluster.

The dashed line in Fig. 9.12 shows that the best fit relation to parent clusters $\sigma_{\text{DM}} = 1075 [h(z)M_{200}/10^{15} M_{\odot}]^{0.36} \text{ km s}^{-1}$ has a slope biased slightly high compared to the expected value of 1/3. Although this steeper slope could signal a gradual trend with mass in the internal structure of clusters, a more likely explanation is that the finite force resolution ($100 h^{-1} \text{ kpc}$) of the simulations is slightly suppressing the velocity dispersion at low masses. Analysis of smaller volume Virgo runs (Jenkins et al. 1998) with roughly ten times better mass and spatial resolution confirms a modest bias in slope (upper left panel). Fixing the

slope to the original expectation, the best estimate calibration for parent clusters is

$$\sigma_{\text{DM}} = 1075 [h(z)M_{200}/10^{15}M_{\odot}]^{1/3} \text{ km s}^{-1}. \quad (18)$$

Because of the percent level agreement between the pair of cosmologies studied, it is reasonable to expect that this relation applies to clusters formed in the broad class of CDM-like models.

Inspection of the percentile ranges shown in Fig. 9.12 reveals an asymmetry in the velocity distribution, skewed toward higher values of σ . The right panel of Fig. 9.12 shows the full probability distribution function (pdf) of the velocity dispersion residuals about the best fit, separated into parent and child cluster distributions. Evidently, it is the child population that is largely responsible for skewing the overall distribution. The center of the child velocity distribution is displaced 10% higher in σ and is broadened relative to the parent population. A picture that emerges from this analysis is that the child population contains a significant fraction of clusters that are merger remnants lying outside r_{200} of their corresponding parent. We have seen in Fig. 9.6 that such a situation is not only possible, but should be expected to involve $\sim 10\%$ of the parent cluster mass. This fraction is consistent with the measured child fraction given in Fig. 9.10. Such clusters are tidally heated on their first passage through the parent, but remain spatially coherent at apocenter so that the SO algorithm identifies them as distinct clusters. Ultimately, they will be assimilated into the parent system.

2.3.3 The ICM virial relation. Gas dynamic simulations show that the ICM gas follows a similar virial relation (Evrard 1990; Evrard et al. 1996; Bryan & Norman 1998; Yoshikawa et al. 2000; Thomas et al. 2000; Mathiesen & Evrard 2001). In Fig. 9.13, we show results from a set of 48 P3MSPH cluster simulations described in Mohr & Evrard (1997). The solid line reflects a least squares logarithmic fit to the 192 samples of mass and mass-weighted temperature (each cluster is sampled at four widely spaced redshifts)

$$h(z)M_{200} = (2.32 \pm 0.06) \times 10^{15}M_{\odot} (kT/10 \text{ keV})^{1.53 \pm 0.02}. \quad (19)$$

The scatter about this relation is remarkably small, only 14% in $h(z)M_{200}$ at fixed T . This small variation is, at first glance, difficult to reconcile with the fact that a substantial fraction of the population is undergoing a merger at the measurement epoch. The scatter is also small compared to the $h(z)$ factor, which ranges by a factor 4 over the redshift range and flavors of CDM models shown.

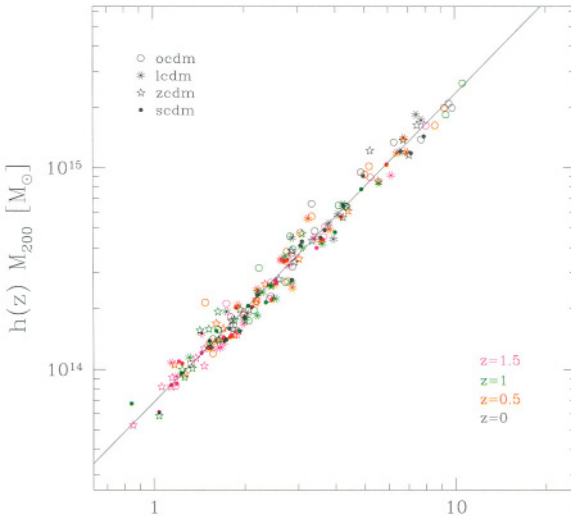


Figure 9.13. Virial mass–temperature relation derived from 192 P3MSPH simulation outputs (Mohr & Evrard 1997), consisting of twelve clusters in four cosmological models evaluated at the four redshifts indicated. The line is a fit given in equation (19).

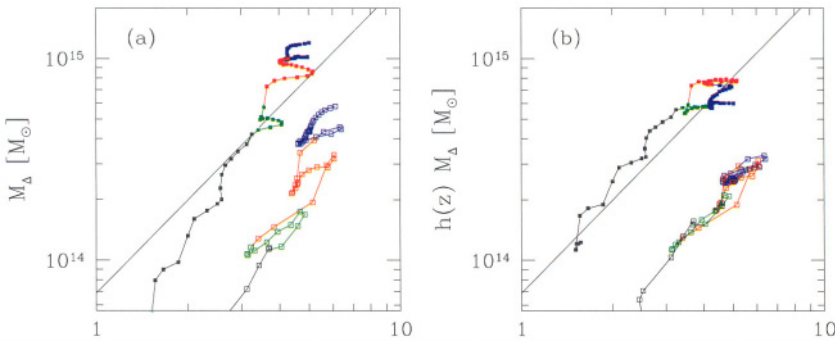


Figure 9.14. Time evolution of masses and temperatures of SB cluster evaluated within density contrasts $\Delta = 200$ (filled symbols) and $\Delta = 2000$ (open symbols): (a) measured masses; (b) virial mass $h(z)M_{\Delta}$. Note $h(z=0) = 0.5$. Colors denote redshift ranges: $z > 0.9$ (black); $0.9 > z > 0.6$ (green); $0.6 > z > 0.3$ (red); $z < 0.3$ (blue). Images of the dark matter and gas at redshifts dividing these ranges are shown in Fig. 9.6 and Fig. 9.15, respectively. Solid line is the fit shown in Fig. 9.13.

How can such a tight relation survive the existence of major mergers? Fig. 9.14 returns to the SB cluster in search of an answer. The mass

and mass-weighted temperatures within density contrasts $\Delta = 200$ and 2000 of the most massive progenitor are shown at the same set of epochs shown in the growth history of Fig. 9.5. Panel (a) shows the measured mass M_Δ while panel (b) displays the virial mass $h(z)M_\Delta$.

The situation near the core of the cluster, at $\Delta = 2000$, exhibits some subtle differences relative to $\Delta = 200$. The first is that the mass-weighted temperature is consistently higher by 10—20% than the value at $\Delta = 200$, signaling a radial temperature gradient. Another is that the excursions during mergers are broader in the T direction and tend to track the virial relation more directly, displaying less of the ‘up-and-over’ character seen at $\Delta = 200$. Presumably, the shorter relaxation time of the core plays a role in the latter.

At both values of the density contrast, the virial mass $h(z)M_\Delta$ displays a marked tighter relation with temperature than does the mass M_Δ alone. Under the reasonable assumption of ergodicity, the lessons learned from the time evolution of this single cluster apply to the general population shown in Fig. 9.13, and help explain the small scatter displayed in that figure.

It is important to remember that these simulations assume only gravitational heating of the gas. Other physics — magnetic fields, non-equilibrium thermodynamics, galactic winds, and radiative cooling to name a few — are certainly operating within the ICM. The impact of magnetic fields (Dolag et al. 2000; Dolag & Schindler 2000) and electron temperature differences (Teyssier et al. 1998; Takahara 1999) have been shown to affect the thermal temperature within r_{200} at the level of a few percent. Galactic winds (including AGN heating) and radiative cooling are likely to have a more substantial effect, but these are complex processes. Approximate models of winds suggest that the effect on T is $\lesssim 10\%$ for high mass clusters (Evrard et al. 1996; Wu et al. 2000; Bialek et al. 2001).

The effect of radiative cooling is more complicated and controversial. Several authors (Muanwong et al. 2001; Pearce et al. 2000; Bryan 2000) argue that, by eliminating low entropy gas, cooling allows higher entropy material to collapse further within the cluster potential, leading to increases in X-ray temperatures by up to 50% in groups of $T \sim 2 - 5$ keV and by smaller amounts in hotter systems. The existence of metals in the ICM, now seen at a level of 1/3 solar at $z = 0.8$ (Jeltema et al. 2001), is difficult to explain if cooling is not accompanied by outflows and, hence, some degree of heating (Renzini 1998). We await self-consistent modeling of the full galaxy formation problem within clusters, coupled to constraints imposed by multi-wavelength observations, to ultimately settle this issue.

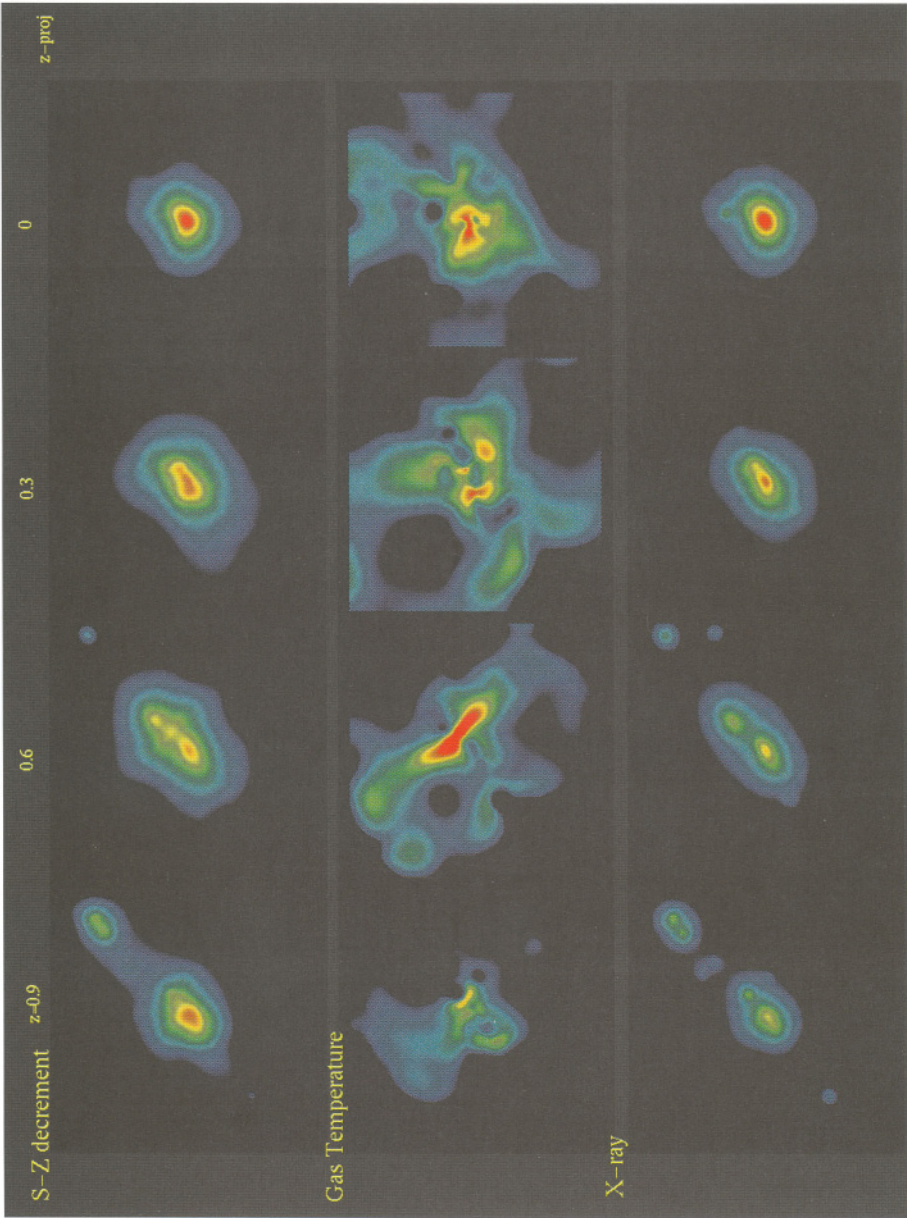


Figure 9.15. Views of ICM evolution derived from the P3MSPH solution of the SB cluster. Epochs chosen and the comoving 10 Mpc window used in each panel are the same as in Fig. 9.6. Rows show evolution of the thermal Sunyaev-Zel’dovich effect (upper), pseudo-emission weighted temperature (middle) and pseudo-bolometric, intrinsic X-ray surface brightness (lower) using logarithmic color scales that span two decades, a factor 4 and four decades, respectively.

2.4. CLUSTER OBSERVABLES

We round out this section by using the SB cluster simulation to sample some observable features associated with cluster mergers. Since this topic is also discussed by others in this volume (Schindler and Sarazin, in particular), we offer here only a brief treatment intended to complement the results already presented from this simulation.

Fig. 9.15 displays projected images of ICM properties of the P3MSPH SB cluster. The perspective is the same as that of Fig. 9.6, largely perpendicular to the merger axis. The X-ray emission is approximated by a measure of $\rho^2 T^{1/2}$, and the temperature map is a mass-weighted value. Both are integrated along a 64 Mpc line of sight (see Frenk et al. 1999 for details).

At $z = 0.9$, the projected X-ray emission reveals a linear chain of clusters oriented along the large-scale filament. The bodies of both the main and largest satellite clusters display significant substructure oriented along the same direction. The temperature map shows spatial variation of a factor ~ 2 with peaks in the X-ray image tending to be cooler than their surroundings. A strong shock generates a hot plume of gas that extends to well beyond r_{200} in a direction perpendicular to the merger axis. Since the mass of gas involved in this plume is small, its visibility in either X-ray emission or Sunyaev-Zel'dovich (SZ) signal is poor.

The $z = 0.6$ column shows classic signatures of a major merger in progress. A zone of strongly compressed and mildly shocked gas lies between the peaks of the X-ray surface brightness map. The temperature gradient along the merger axis is large: the X-ray surface brightness peaks define local T minima that are cooler by a factor 4 than the intervening maximum. Note the existence of an unusual feature in the SZ map. Since the thermal SZ measures a line integral of the gas pressure, the non-equilibrium nature of the merger can produce a peak in pressure located between the cores of the merger progenitors. So rather than two peaks, as in the X-ray map, the SZ image shows three, with the third located along the merger axis at the location of the local temperature maximum. An observational counterpart with this particular set of features awaits discovery in future SZ and X-ray surveys.

By $z = 0.3$, the major merger has been largely played out, but traces remain in the twisting and shifting of the X-ray and SZ isophotes (Mohr et al. 1995). The temperature map continues to show factor 2 spatial variation on several 100 kpc scales, but the map is less well ordered than at $z = 0.6$.

At $z=0$, a minor merger is in progress. Being a ρ^2 measure, the X-ray emission enhances the contrast of this substructure compared to the ρ -weighted SZ map. The infalling satellite shows up as a cool spot on the projected temperature map. Mathiesen & Evrard (2001) show that cool emission from such subclusters can bias broad-beam temperature estimates derived from 10,000 photon X-ray spectra to values $\lesssim 20\%$ below the corresponding mass-weighted values.

Despite the relative simplicity of the X-ray and SZ images, the temperature map exhibits complex spatial variations beyond that of the infalling satellite. Azimuthal averaging smooths these features considerably — the radial temperature profile shows a nearly isothermal core extending to $\sim r_{200}/3$ and a mild negative gradient thereafter. Observations support the idea of spatially complex temperature structure with an overall negative radial gradient (Markevitch et al. 1999).

Chandra Observatory images of MS 1054.4–0321 (Jeltema et al. 2001) exhibit a complex morphology similar to the high redshift images of the SB cluster. Fig. 9.16 shows the X-ray emission superposed on the lensing map of Hoekstra et al. (2000). Two of the three peaks in the lensing map have corresponding features in the X-ray. The lack of an X-ray counterpart to the northwest image has several possible explanations. One is that the lensing is caused by a projected filament that has no dense core to generate X-ray emission. Another is that the northwest clump in dark matter is the core of a merger remnant whose associated gas has been stripped. In any case, the morphology is strongly suggestive of an ongoing merger. We will return to this cluster below in discussion of constraints on Ω_m from the high redshift cluster space density.

3. CONSTRAINTS ON COSMOLOGICAL PARAMETERS

We now discuss the status of selected cosmological parameter determinations from observations of clusters. After noting the status and importance of cluster surveys, we discuss how the clustered matter density Ω_m can be derived by combining primordial nucleosynthesis limits on Ω_b with the population mean baryon fraction. We then present constraints on the power spectrum amplitude σ_8 and Ω_m derived from the local and distant space density of clusters, respectively. For these topics, we return to the Hubble Volume simulations to present recent work on estimates of systematic errors in these parameters.

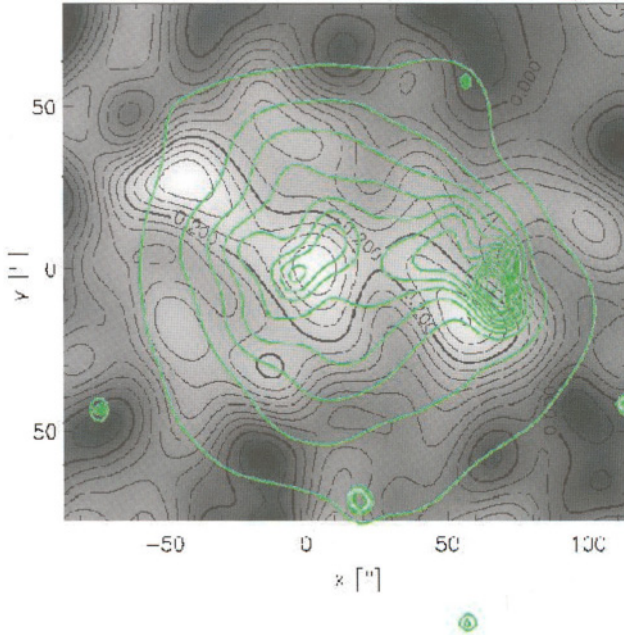


Figure 9.16. Chandra X-ray surface brightness image (white) of MS 1054.4–0321 at $z=0.83$ (Jeltema *et al.* 2001) superposed on a weak lensing mass map derived from HST mosaic imaging by Hoekstra *et al.* (2000). For a Λ CDM cosmology, a physical scale of $320 h^{-1}$ kpc subtends one arcmin at $z=0.83$

3.1. CLUSTER SURVEYS

Searches for clusters have greatly benefitted from new technologies and observational capabilities, such as faint spectroscopy with Keck and VLT, deep optical and near-infrared imaging in space (HST), X-ray observations of the ICM with ROSAT, ASCA, now enhanced with the spectroscopic imaging capabilities of Chandra and XMM-Newton, and Sunyaev–Zel’dovich observations with telescope arrays (Carlstrom *et al.* 1996; Mason & Myers 2000) or sensitive bolometers (DASI, Pryke *et al.* 2001; CBI, Padin *et al.* 2001).

Gioia (2000) provides a review of several dozen cluster surveys, most of which have appeared in the literature in the past decade. In the optical, the wide-field 2dF (De Propris *et al.* 2000) and SDSS (Kepner *et al.* 1999; Nichol *et al.* 2001; Annis *et al.* 2001) surveys will map the galaxy and cluster distributions over large fractions of the sky to moderate ($z \sim 0.3$) depth. Deeper surveys are probing of order tens of degrees of sky to $z \sim 1$ (Postman *et al.* 1996; Dalton *et al.* 1997; Zaritsky *et al.* 1997; Ostrander *et al.* 1998; Scodreggio *et al.* 1999; Gal

et al. 2000; Gladders & Yee 2000; Willick et al. 2001; Gonzalez et al. 2001). In the X-ray, serendipitous surveys from Einstein (such as the original Einstein Medium Sensitivity Survey, EMSS, Gioia et al. 1990a), compilations from archival images (Jones & Forman 1999) and archival surveys from pointed ROSAT images (Scharf et al. 1997; Rosati et al. 1998; Ebeling et al. 1998; Vikhlinin et al. 1998a) or from the ROSAT All-Sky Survey (De Grandi et al. 1999; Böhringer et al. 2001; Ebeling et al. 2001a and 2001b; Henry et al. 2001; Gioia et al. 2001) have generated samples of several hundred clusters. Similar surveys from the developing Chandra and XMM archives (*e.g.*, Romer et al. 2001) will lead to order of magnitude improvements in sample size and limiting sensitivity. Finally, the detection of clusters via their spectral imprint on the microwave background (Sunyaev and Zel'dovich 1972; Birkinshaw 1999) offers a new mode of efficiently surveying for very distant ($z > 1$) clusters with hot, intracluster plasma (Barbosa et al. 1996; Holder et al. 2001; Kneissl et al. 2001).

In the cosmological tests we discuss here, the first — Ω_m from the cluster baryon fraction and nucleosynthesis — can be performed with clusters at any redshift and is fairly immune to survey selection, as it requires a simple assumption that the internal content of galaxy clusters reflects that of the universe at large. The second — σ_8 from the local temperature function — requires a complete census of the deepest nearby potential wells. In practice, this is achieved using spectroscopic follow-up of relatively bright X-ray flux-limited catalogs. The third topic — Ω_m from distant cluster counts — requires a similar census at high redshift. Since X-ray surveys are pushed to the faintest flux limits to identify massive, distant clusters, and since the observational evidence suggests ongoing mergers in most of the systems found so far, the constraints on Ω_m from this method are most likely to be susceptible to selection biases.

We saw in the previous section that excursions in T and X-ray luminosity of factor few are to be expected during mergers. Qualitatively, the brightest sources close to the survey flux limit are likely to be massive objects whose luminosity is being temporarily boosted by a merger. Quantitatively, this topic has not yet received detailed treatment, but Ricker & Sarazin (2001) have begun analysis of merger simulations with this endpoint in mind.

3.2. Ω_M FROM THE CLUSTER BARYON FRACTION

The great depth of cluster gravitational potentials makes it hard for baryons to escape them. As discussed in § 1.3, the gas does seem to gain a small excess of energy from the dark matter during mergers and a mild depletion of baryons within r_{200} results $\Upsilon = 0.92 \pm 0.06$. Although the simulations that determined this depletion do not incorporate galaxy formation or feedback from galactic winds, the large mass of ICM gas compared to that in galaxies — White et al. (1993a) derive a ratio of 9.4 ± 2.6 within an Abell radius in Coma — is used to argue that this value of Υ is appropriate for massive clusters.

The exercise to estimate Ω_m from this method is straightforward. Estimating the mean ICM gas mass fraction in hot clusters, adding the contribution of baryons in galaxies, and correcting for the modest loss of baryons discussed above results in a measure of the ratio Ω_m/Ω_b . Multiplying by the best estimate of Ω_b derived from primordial nucleosynthesis results in the desired constraint on the matter density.

White & Fabian (1995) used a deprojection technique to measure the ICM and total masses of 19 clusters observed with the *Einstein* Observatory. For a refined sample of 13, they constrained the ICM mass fraction to lie in the range $6-13 (h/0.7)^{-3/2}$ per cent. David et al. (1995) examined ROSAT data for systems ranging from elliptical galaxies to clusters and derived a somewhat higher gas fraction of $\sim 18 (h/0.7)^{-3/2}$ per cent within r_{200} . Working with these data, Evrard (1997) showed that the mild (2.4σ) discrepancy in median gas fractions of these two samples could be resolved by applying a common virial estimator for the total mass $M \propto T^{3/2}$. Using the calibration of mass estimates within r_{500} derived from a set of 58 cluster simulations by Evrard et al. (1996), the resultant mean ICM mass fraction of the combined samples within $\Delta = 500$ was found to be $\langle f_{\text{ICM}}(r_{500}) \rangle = 0.102 \pm 0.005 (h/0.7)^{-3/2}$. Applying corrections for the mass contribution of galaxies (using Coma as typical of the ensemble average) and for the loss of baryons during mergers, results in an estimate of the universal ratio of mass densities

$$\frac{\Omega_m}{\Omega_b} = 7.8 \pm 0.4 (h/0.7)^{4/3}. \quad (20)$$

The quoted 68% confidence error is purely statistical. Combined with the current estimate on baryon density $\Omega_b (h/0.7)^2 = 0.039 \pm 0.002$ (Burles & Tytler 1998), this yields a constraint on the clustered matter density

$$\Omega_m = 0.30 \pm (0.02)_{\text{stat}} \pm (0.06)_{\text{sys}} (h/0.7)^{-2/3}. \quad (21)$$

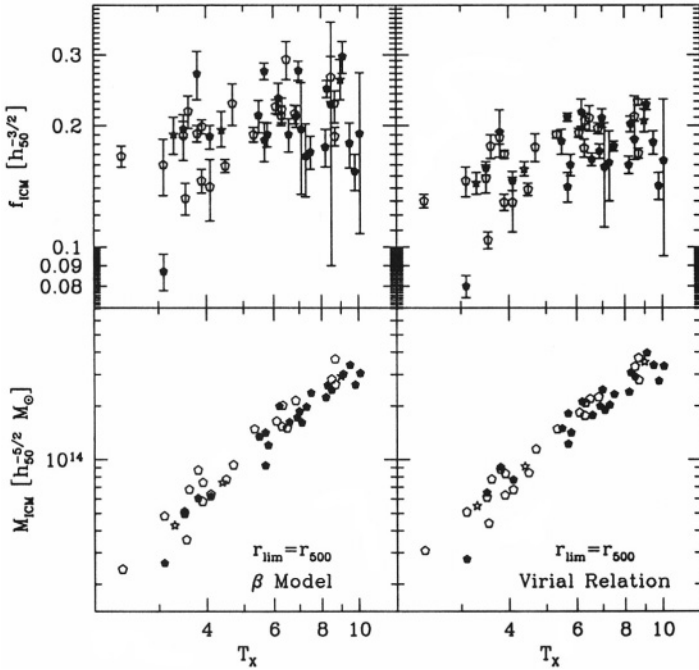


Figure 9.17. Temperature dependence of the intracluster gas mass (lower panels) and inferred gas mass fraction (upper) for the Edge sample of 45 clusters. Total masses are estimated either by the isothermal- β model (left) or the virial theorem (right). Open symbols are cooling flow clusters. (From Mohr et al. 1999.)

The quoted systematic error reflects an estimated 20% uncertainty in the calibration of the total mass–temperature relation.

With the exception of recent analysis by Sadat & Blanchard (2001), results to date are all consistent with equation (21). The mean gas fraction was derived for larger samples of clusters, based on Ginga (Arnaud & Evrard 1999) and ROSAT (Mohr et al. 1999; Viklinin et al. 1999; Ettori & Fabian 1999). In contrast to Ettori & Fabian (1999), who point out possibly significant deviations in gas fraction among clusters, the other works emphasize the regularity of the population, with scatter in f_{ICM} limited to $\lesssim 20\%$ for clusters hotter than about 3 keV.

Fig. 9.17 shows the ICM mass–temperature relation within characteristic radius r_{500} for 45 clusters in the X–ray flux–limited Edge sample derived from archival ROSAT imaging analysis (Mohr et al. 1999; original sample of 55 clusters published by Edge et al. 1990). The *rms* variation in M_{ICM} at fixed T_X is only 14%, regardless of the presence or absence of a cooling flow. The correspondence between the observed intracluster mass behavior and the simulation expectations for the total

mass shown in Fig. 9.13 is striking. The results support a nearly constant gas fraction, at least within r_{500} and for clusters with $kT \gtrsim 4$ keV. Most important, perhaps, is the fact that the variance in M_{ICM} at fixed T already equals that expected from simulations with minimal physics (gravity and shocks). This result puts strong limits on the possible variation of galaxy formation efficiency within clusters, and suggests that no substantial piece of physics is missing from the current modeling.

A possibly important source of systematic uncertainty, clumping of the gas, has been essentially eliminated by recent measurement of ICM masses based on the Sunyaev-Zel'dovich effect (Grego et al. 2001; Mason & Myers 2000; Jones et al. 2001). Grego et al. (2001) observed a sample of 18 clusters with arrays at OVRO and BIMA and determined a mean gas fraction $\langle f_{\text{ICM}}(r_{500}) \rangle = 0.116_{-0.016}^{+0.013} (h/0.7)^{-1}$, consistent with X-ray determinations. Mason & Myers (2001) drive Hubble constant $H_0 = 66_{-11}^{+14} \pm 15(\text{sys}) \text{ km s}^{-1} \text{ Mpc}^{-1}$ from seven clusters assuming no clumping. Consistency with the HST Key Project value of $H_0 = 72 \pm 8 \text{ km s}^{-1} \text{ Mpc}^{-1}$ (Freedman et al. 2001) validates the assumption of no clumping. Combining the implied ICM mass fraction with the nucleosynthesis baryon density, Mason & Myers quote $\Omega_m = 0.32 \pm 0.05$, again consistent with X-ray studies that assume no clumping.

This is not to imply that the ICM at a give radius has no variation in density. Local variations in density exist due to weak shocks and sonic disturbances driven by mergers. Mathiesen et al. (1999) show that this clumping does have a small effect on ICM mass estimates. Comparing ICM masses based on standard reduction of mock X-ray images of cluster simulations to their true values, a 14% bias toward overestimating M_{ICM} is found. Validating this effect with observations awaits sensitive X-ray and SZ observations of a moderate sample of nearby clusters.

3.3. σ_8 FROM THE LOCAL TEMPERATURE FUNCTION

Since the number density of massive clusters is exponentially sensitive to the power spectrum amplitude σ_8 (see equations (15) and (7)), even small samples of clusters should allow sensitive constraints of this parameter. Since the theoretically preferred mass M_Δ is not directly measurable, the X-ray temperature is used as a surrogate. This introduces a functional degree of freedom — the virial relation — into the analysis. Calibrations derived from simulations, such as that presented in Fig. 9.13 above, are currently used to connect temperature to mass.

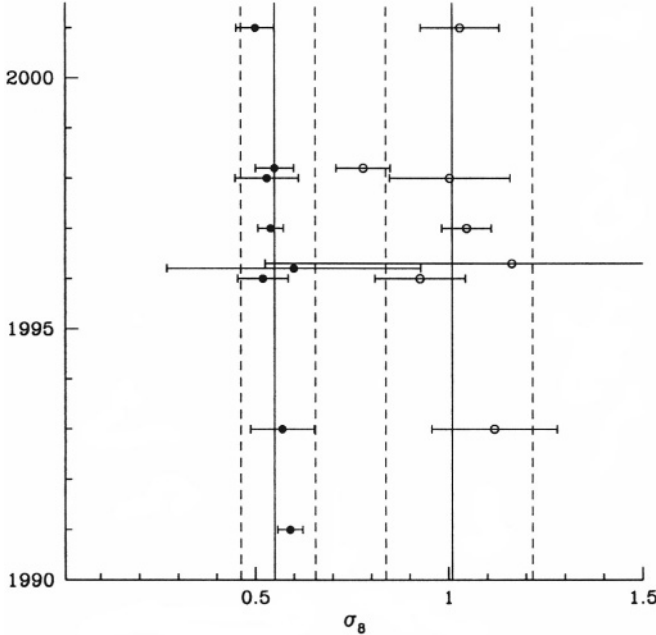


Figure 9.18. Published 90 percent confidence constraints on σ_8 derived from the local temperature function for $\Omega_m = 1$ (filled symbols) and $\Omega_m = 0.3$ (open). Solid and dashed lines give the historical mean and 90 percent confidence region, including cosmic variance and virial calibration uncertainties.

We await sensitive weak lensing observations to provide an improved, empirical calibration.

Fig. 9.18 gives a world history of σ_8 measures for $\Omega_m = 1$ and 0.3. Henry and Arnaud (1991) derived $\sigma_8 = 0.59 \pm 0.02$ from temperatures of 25 clusters in a bright, X-ray flux limited sample, assuming $\Omega_m = 1$. Subsequent analysis of this sample (White et al. 1993b; Eke et al. 1996; Viana and Liddle 1996; Fan et al. 1997; Kitayama & Suto 1997; Pen 1998) and revised samples (Markevitch 1998; Blanchard et al. 2000) generated largely consistent results and extended constraints to arbitrary Ω_m . Most recently, Pierpaoli et al. (2001), reanalyzed the Markevitch sample using revised temperatures of White (2000) and find

$$\sigma_8 = 0.495^{+0.034}_{-0.037} \Omega_m^{-0.60}. \tag{22}$$

The 7% fractional error is typical of the uncertainties quoted by previous studies.

A source of uncertainty that has not been considered in previous studies is sample, or *cosmic*, variance. Large-scale density fluctuations modify the development of smaller, non-linear structures (Kaiser 1984), with slightly overdense regions exhibiting more advanced structure while un-

derdense regions are retarded with respect to the global mean evolution. On the scale of the survey volume limit of the sample used by Pierpaoli et al. and previous authors, $5 \times 10^7 h^{-1}$ Mpc, fluctuations in mass density of 1 – 2% about the mean are expected for viable CDM models. At first glance, this seems too small to be interesting, but careful analysis suggests otherwise.

Using the full $z=0$ volumes of the Hubble Volume simulations, Evrard et al. (2001) calibrate the cosmic variance uncertainty error in σ_8 . The distributions of maximum likelihood values derived from this analysis, shown in Figure 9.19, are nearly log-normal with standard deviations 0.064 and 0.050 in $\ln(\sigma_8)$ (Λ CDM and τ CDM, respectively). Adding this uncertainty in quadrature with the other sources of error noted in previous studies, particularly a 20 percent calibration uncertainty in the zero-point of the mass-temperature relation, Evrard et al. estimate that the 90% confidence limit uncertainty in σ_8 is at least 16 per cent. The dashed lines in Fig. 9.18 show the range about the historical averages anticipated by this level of error. The range is larger than the spread of the central values, as expected since common observations were used in many analyses, and also larger than the quoted uncertainties on many of the individual measurements. The global average values and 90% total errors are $\sigma_8 = 0.55 \exp(\pm 0.16)$ and $\sigma_8 = 1.01 \exp(\pm 0.18)$ for $\Omega_m = 1$ and $\Omega_m = 0.3$, respectively.

This level of uncertainty has important consequences for predictions of the space density of high redshift clusters, a subject to which we now turn.

3.4. Ω_M FROM DISTANT CLUSTER COUNTS

Estimates of the space density of high redshift clusters require sensitive, well calibrated surveys. Serendipitous searches in archival X-ray images offers a means to survey tens or even hundreds of square degrees to varying flux limits. Despite advances in multi-fiber and multi-slit spectroscopy, however, measuring redshifts for cluster member galaxies remains a painstaking task that often takes many years for surveys of significant size. Examples of recently published X-ray selected samples with complete or nearly complete redshift information are the RDCS (Rosati et al. 1998; Borgani et al. 1999, 2001), bright SHARC (Romer et al. 2000), WARPS (Scharf et al. 1997; Jones et al. 1998; Fairley et al. 2000; Ebeling et al. 2000), NEP (Henry et al. 2001; Gioia et al. 2001; Mullis et al. 2001; Voges et al. 2001), MACS (Ebeling et al. 2001b) and REFLEX (Böhringer et al. 2001).

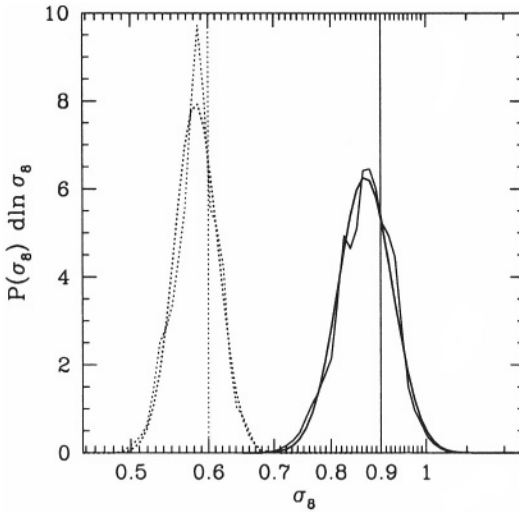


Figure 9.19. Frequency distributions of the maximum likelihood value of σ_8 derived from fitting local mass functions within 1000 (τ CDM, dotted) and 4096 (Λ CDM, solid) sub-volumes of the $z=0$ outputs to mass limits chosen to generate an average sample size of ~ 30 clusters within the sub-volumes. Cosmic variance leads to variation in derived σ_8 values that are well described by log-normal distributions (smooth curves) with standard deviations 0.050 (τ CDM) and 0.064 (Λ CDM).

The original survey of this type, the EMSS (Gioia et al. 1990a), is a collection of 835 X-ray sources identified serendipitously in archival exposures of the *Einstein* satellite. Correlation with optical images identified most objects as individual galaxies or quasars, but 93 of the 835 sources were identified with emission from hot ICM of clusters. Subsequent optical and X-ray spectroscopy (Stocke et al. 1991; Maccacaro et al. 1994; Donahue et al. 1998, 1999; Tran et al. (1999); van Dokkum et al. (2000); Jeltama et al. 2001) led to the finding that 3 of the 93 are both very hot ($kT \gtrsim 8$ keV) and distant ($z \gtrsim 0.5$). Given the effective sky search area of these sources (Henry 2000), one derives a sky density of 35 sterad^{-1} (0.011 per sq deg) for clusters lying at $z > 0.5$ with $kT > 8$ keV.

Despite small number statistics, multiple analyses of this sample have generally excluded the possibility that $\Omega_m = 1$ (Luppino & Kaiser 1997; Bahcall et al. 1997; Donahue et al. 1998; Eke et al. 1998; Bahcall & Fan 1998). Some recent papers have voiced disagreement (Sadat et al. 1998; Blanchard & Bartlett 1998; Viana & Liddle 1999), citing possible incompleteness of local surveys against which the high redshift data are compared. Increasing the local space density would add room for more

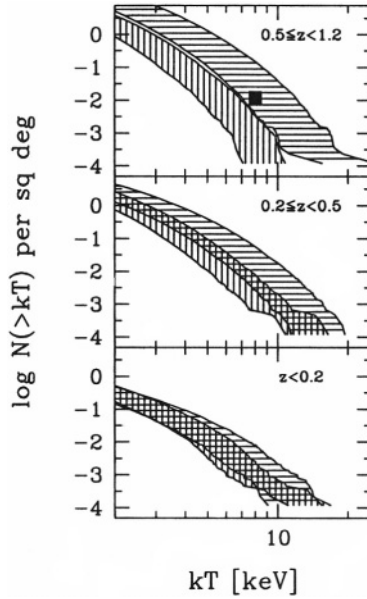


Figure 9.20. Allowed ranges of the cumulative sky surface density of clusters as a function of temperature for Λ CDM (horizontal hatched) and τ CDM (vertical) cosmologies. Within each redshift band, allowed ranges are defined by varying the power spectrum normalization σ_8 within its overall 5 to 95% confidence interval. The solid square is the EMSS result for clusters hotter than 8 keV at $z > 0.5$.

evolution in the mass function, and stronger evolution favors a higher value of Ω_m . Uncertainty in σ_8 is a way to parameterize this ambiguity, as recently illustrated by Borgani et al. (1999a). In an analysis of 16 EMSS clusters at redshifts $0.17 \leq z \leq 0.55$ observed by the CNOC group, Carlberg et al. (1997) find the estimated value of Ω_m to shift by a factor 3, from 0.35 to 1.05, as σ_8 is varied by only 20%, from 0.5 to 0.6.

The HV simulations provide another illustration of this sensitivity. Figure 9.20 shows the range of cumulative counts of clusters as a function of temperature within three broad redshift intervals, and derived from discrete sky survey samples of π sterad. Expectations for the ICM are derived from the dark matter solution by assuming a constant specific energy in each component $T \propto \sigma_{\text{DM}}^2$. Since the models are constrained to match the local observations, there is nearly completely overlap in the temperature functions of the two cosmologies at $z < 0.2$. However, effectively varying σ_8 within its 90% confidence range leads to roughly an order of magnitude range in expected number at a given temperature.

The models begin to separate at intermediate redshifts, but significant overlap remains. In the high redshift interval, the 90% confidence regions for the counts in each model become disjoint. The observational value from the EMSS survey, shown as the square in the upper panel of Figure 9.20, is consistent with Λ CDM expectations and rules out τ CDM at 95% confidence. This result, which hinges on only three clusters, needs to be confirmed by the larger statistical samples now being assembled.

3.4.1 SZ survey yields. Counts of mass-limited samples, as promised by planned SZ cluster searches, are similarly sensitive to σ_8 variation. As pointed out by Oukbir & Blanchard (1992) and others since, knowledge of the redshift distribution adds crucial information capable of breaking the degeneracy between σ_8 and Ω_m that affects sky counts. Using HV sky survey data, Fig. 9.21 provides a demonstration of the relative behavior of counts and the median redshift z_{med} expected in a random 10 sq deg survey. Statistics shown are the counts at all redshifts $z < 1.25$, counts at high redshift $0.8 < z < 1.25$, and the median redshift in 3000 randomly oriented 10 sq deg patches selected from deep surveys covering a total of π sterad in each model. To define the cluster population at values of σ_8 different from the default, transformations in mass and number are developed, described in Evrard et al. (2001). In order to drive the counts in both models toward each other, σ_8 is effectively increased in τ CDM and decreased in Λ CDM.

The behavior of the counts within the limiting survey redshift of $z = 1.25$ is quite dramatic. At the default values of σ_8 (lower left), the distributions, with means of 117 and 45 for Λ CDM and τ CDM, respectively, are such that unambiguous discrimination between the two models could be made solely from the counts within a single 10 sq deg field. However, biasing σ_8 by only 10% in the chosen directions produces essentially identical expectations for the overall counts (lower middle), with both models expecting 72 ± 12 clusters per field. For a 16% bias (lower right), the sense of the overall counts are reversed from the default, with the τ CDM model producing 60% more clusters, on average, than Λ CDM.

The situation at redshifts $0.8 < z < 1.25$ is similar, if less dramatic. For the default values of σ_8 , the Λ CDM model predicts roughly 40 clusters per field while τ CDM expects only 3. A shift of 10% in σ_8 causes the distributions of counts to overlap, and the blending increases as the bias in σ_8 is increased. The numbers in each panel of Fig. 9.21 are a frequentist's measure of the power of Λ CDM observations to correctly rule out the τ CDM model. For cases where the Λ CDM median exceeds that of τ CDM, the value quoted is the fraction of the Λ CDM pdf that

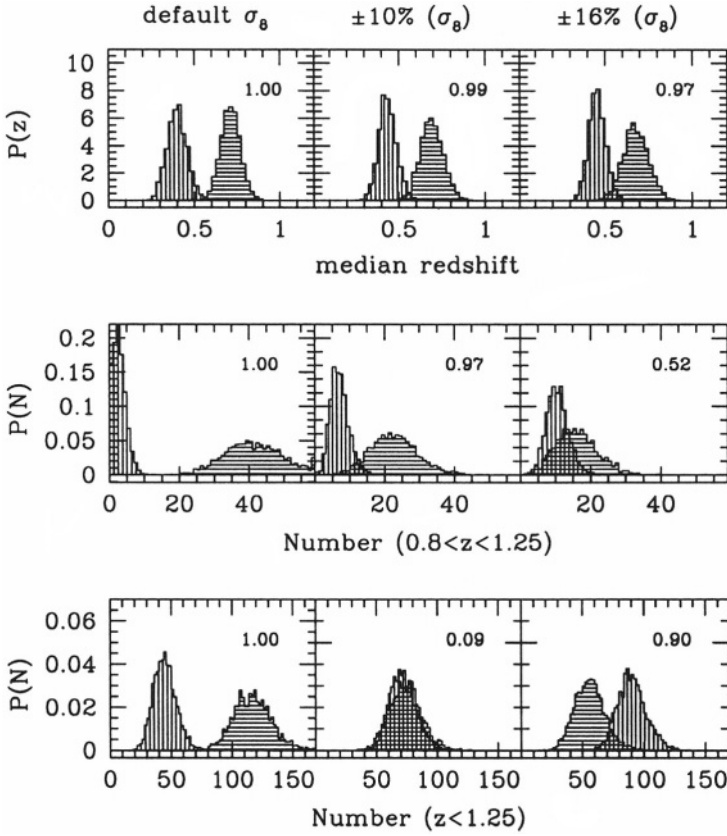


Figure 9.21. Distribution functions of expected counts and median redshifts for clusters with $M_{200} > 10^{14} h^{-1} M_{\odot}$ in random 10 sq deg fields derived from Λ CDM (horizontal hatched) and τ CDM (vertical) Hubble Volume sky survey catalogs. In each model, 3000 random sky survey patches are sampled at the default σ_8 values (left column), (+/-)10% (middle) and (+/-)16% (right) variation (τ CDM/ Λ CDM, respectively). Rows show the counts at all redshifts $z < 1.25$ (bottom), counts in the high redshift interval $0.8 < z < 1.25$ (middle) and the median cluster redshift (top). Numbers in each panel quote the power of a single Λ CDM field to rule out τ CDM at the 95% confidence level. As σ_8 is varied, the power of counts diminishes while that of the median redshift remains high.

lies above the the 95-th percentile value of the τ CDM distribution. Essentially, this measure conveys the likelihood that a single 10 sq deg field observation of the Λ CDM sky will correctly rule out τ CDM at 95 per cent confidence. Although the power of high redshift counts is high at the default σ_8 values, it drops to roughly 50% when σ_8 is pushed to its allowed limits.

In contrast to the behavior of the counts, the distributions of median redshift z_{med} in 10 sq deg fields are far more stable to σ_8 variation. At 0, 10 and 16 percent biased values of σ_8 , the 95-th percentile value of z_{med} for τ CDM hardly shifts, moving from 0.498 to 0.528 to 0.538. The probability that z_{med} in a single Λ CDM field lies below these values are 0.0003, 0.01 and 0.03, respectively. The comparative robustness of this statistic is due to the fact that, as σ_8 is varied, the space density of massive clusters changes by roughly the same fractional amount at all redshifts. The net effect on the counts can be large while the distribution in redshift is hardly affected.

3.4.2 X-ray flux limited samples from ROSAT. The EMSS sample has had the advantage of a full decade of observational follow-up. Surveys based on archival ROSAT observations are developing their cadre of supporting observations. For instance, the recently completed ROSAT NEP (North Ecliptic Pole) survey (Gioia et al. 2001; Henry et al. 2001; Voges et al. 2001; Mullis et al. 2001) which is based on data from the deepest region of the ROSAT All Sky Survey, has sixty-four sources, out of 445 overall sources detected at $> 4\sigma$, which are identified with clusters. Follow-up observations of the cluster sample are in progress.

Evidence for a lower space density of the most X-ray luminous clusters at high redshift is found in the NEP data. The first evidence of such ‘negative’ evolution came from the EMSS (Gioia et al. 1990b; Henry et al. 1992). Comparing the number of the observed clusters in the NEP survey with the number of expected clusters assuming no-evolution in the X-ray luminosity function, there is a deficit of clusters with respect to the local universe that is significant at $> 4.7\sigma$ Gioia et al. (2001). This finding is supported by six out of seven surveys published to date. The original EMSS (Gioia et al. 1990b; Henry et al. 1992), 160 deg² (Vikhlinin et al. 1998b), SHARC (Nichol et al. 1999), RDCS (Rosati et al. 2000), MACS (Henry 2001) and NEP (Gioia et al. 2001) surveys are reporting negative evolution at varying levels of significance from $\sim 1\sigma$ to greater than 5σ .

Unfortunately, converting evolution in the luminosity function into constraints on cosmological parameters can only be accomplished in a model-dependent fashion. Without additional constraints, one simply has the freedom to arrange for potential wells existing in any cosmology to ‘light-up’ in a fashion that matches the observations. In an analysis of the most recent RDCS data, Borgani et al. (2001) parameterize this degree of freedom by introducing redshift dependence into the zero-point of the X-ray luminosity–temperature relation $L_{\text{bol}} \propto T^\alpha (1+z)^A$. They

argue that current data on cluster temperatures suggest no evolution, $A \sim 0$. From the redshift distribution of 107 cluster sources identified over roughly 50 sq deg and extending to the same limiting flux as the NEP, Borgani et al. derive a limit on the clustered matter density

$$\Omega_m = 0.35_{-0.10}^{+0.13} \quad (23)$$

assuming $A = 0$.

The agreement between this result and the determination based on the baryon fraction argument, equation (21), is reassuring. Under economical assumptions, two independent methods point to a universe with low matter content.

4. SUMMARY

Clusters of galaxies are the highest peaks in a cosmic terrain driven by gravitational clustering. Their internal mix of components, as well as the space density of the most massive clusters, can be used to determine fundamental cosmological parameters. Accurate constraints on parameters require a detailed physical understanding of cluster evolution, and steadily improving computational models are aimed at supplying this information. Mergers are a necessary ingredient of the hierarchical formation picture, and their transient effects, particularly on faint X-ray selected samples, need to be more carefully studied.

Current constraints on the clustered mass density point to a low density universe, with the baryon fraction test providing the most stringent constraint $\Omega_m = 0.30 \pm (0.02)_{\text{stat}} \pm (0.06)_{\text{sys}}$. Recent estimates of Ω_m and Ω_b based on analysis of acoustic peaks in the cosmic microwave background are consistent with this value. From the DASI experiment assuming $h = 0.7$, Pryke et al. (2001) conclude $\Omega_{\text{tot}} = 1.00 \pm 0.04$ with $\Omega_m = 0.40 \pm 0.15$ and $\Omega_b = 0.045 \pm 0.008$. Similar constraints are derived from the BOOMERANG experiment (Netterfield et al. 2001). The flat metric with sub-critical mass density requires either a vacuum energy density $\Omega_\Lambda = 0.60 \pm 0.15$ or a similar level of a possibly different form of dark energy.

The space density of nearby clusters is controlled by the amplitude of the fluctuation spectrum σ_8 . Current samples of a few dozen clusters with accurate temperatures are insufficient to constrain this parameter to better than 10%. Roughly half of the current variance comes from spatial variation in the number of massive clusters within volumes probed by current surveys ($\sim 10^7 h^{-3} \text{ Mpc}^3$). Constraints on σ_8 will surely become more precise as SDSS and other large surveys explore larger volumes. At that point, uncertainties will be limited by systematic effects, most important being the calibration of total mass-temperature relation.

To achieve percent level constraints on cosmological parameters, understanding of the detailed form of the likelihood $p(M \setminus T)$ must be achieved. Simulations point to a power-law relation between virial mass $h(z)M_\Delta$ and mass- or emission-weighted temperature, with ~ 15 percent Gaussian scatter in $\log(M)$ at fixed T . When gravitationally-induced shocks dominate the heating of the ICM, the action of mergers appears to preserve the form of the virial relation. The exact values of the slope, intercept and degree of scatter remain subjects of active investigation, from both the first-principles approach of simulations and from an empirical direction using weak gravitational lensing and X-ray observations.

Acknowledgments

AEE acknowledges support from NSF (AST-9803199) and NASA (NAG5-7108) and the Scientific Visitor Program at Carnegie Observatories in Pasadena. He also thanks collaborators John Bialek, Ben Mathiesen, Joe Mohr, and members of the Virgo Consortium for generously allowing presentation of joint work in this chapter. IMG acknowledges partial support from NSF (AST 91-19216 and AST 95-00515), NASA (NAG5-9994) and from the Italian Space Agency ASI. She is very grateful to her NEP collaborators P. Henry, C. Mullis, H. Böhringer, U. Briel, W. Voges and J. Huchra, without whose support the work described here would not have been possible. We wish to thank Tesla Jeltema and Henk Hoekstra for providing images of MS 1054.4-0321.

References

- Annis, J., Garzoglio, G., Kent, S., Kim, R., Goto, T. and the SDSS Collaboraion 2001, BAAS, 198, 2601
 Arnaud, M. & Evrard, A.E. 1999, MNRAS, 305, 631
 Bahcall, N.A. & Fan, X. 1998, ApJ, 504, 1
 Bahcall, N.A. & Oh, S.P. 1996, ApJL, 462, L49
 Bahcall, N.A. & Soneira, R.M. 1983, ApJ, 270, 20
 Bahcall, N.A., Fan, X. & Cen, R. 1997, ApJL, 485, L53
 Balogh, M.L., Navarro, J.F. & Morris, S.L. 2000, ApJ, 540, 113
 Barbosa, D., Bartlett, J., Blanchard, A. & Oukbir, J. 1996, A&A, 314, 13
 Bartelmann, M., Huss, A., Colberg, J.M., Jenkins, A. & Pearce, F.R. 1998, A&A, 330, 1
 Bertschinger, E. 1985, ApJS, 58, 39
 Bertschinger, E. 1998, ARA&A, 36, 559
 Bialek, J.J., Evrard, A.E. & Mohr, J.J. 2001, ApJ, 555, 597

- Birkinshaw, M. 1999, *3K cosmology*, eds. L. Maiani, F. Melchiorri & N. Vittorio, American Institute of Physics, Woodbury, NY, 476, 298
- Blanchard A. & Bartlett, J.G. 1998, *A&A*, 332, L49
- Blanchard, A., Sadat, R., Bartlett, J.G. & Le Dour, M. 2000, *A&A*, 362, 809
- Bode, P., Bahacall, N.A., Ford, E.B. & Ostriker, J.P. 2001, *ApJ*, 551,15
- Böhringer, H. et al. 2001, *A&A*, 369, 826
- Bond, J.R. & Efstathiou, G. 1984, *ApJL*, 285, L45
- Bond, J.R. & Myers, S.T. 1996, *ApJS*, 103, 63
- Bond, J.R., Kofman, L. & Pogosyan, D. 1996, *Nature*, 380, 603
- Borgani, S., Girardi, M., Carlberg, R.G., Yee, H.K.C., Ellingson, E. 1999, *ApJ*, 527, 561
- Borgani, S., Rosati, P., Tozzi, P. & Norman, C. 1999b, *ApJ*, 517, 40
- Borgani, S. et al. 2001, *ApJ*, in press, astro-ph/0106428
- Bower, R.G. 1991, *MNRAS*, 24, 332
- Bryan, G.L. 2000, *ApJL*, 544, L1
- Bryan, G.L. & Norman, M.L. 1998, *ApJ*, 495, 80
- Bullock, J.S., Kolat, T.S., Sigad, Y., Somerville, R.S., Kravstov, A.V., Klypin, A.A., Primack, J.R. & Dekel, A. 2001, *MNRAS*, 321, 559
- Burles, S. & Tytler, D. 1998, *ApJ*, 507, 732
- Carlberg, R.G., Yee, H.K.C., Ellingson, E. 1997, *ApJ*, 478, 462
- Carlstrom, J.E., Joy, M. & Grego, L. 1996, *ApJ*, 456, 45
- Cavaliere, A. & Fusco-Femiano, R. 1976, *A&A*, 49, 137
- Colberg, J.M. et al. 2000, *MNRAS*, 319, 209
- Coles, P. & Lucchin, F. 1995, *Cosmology: the origin and Evolution of Cosmic Structure*, John Wiley & Sons, Chirchester
- Couch, W.J. & Sharpies, R.M. 1988, *MNRAS*, 229, 423
- da Costa, L. et al. 1988, *ApJ*, 327, 544
- Dalton, G.B., Croft, R.A.C., Efstathiou, G., Sutherland, W.J., Maddox, S.J. & Davis, M. 1994, *MNRAS*, 271, 47
- Dalton, G.B., Maddox, S.J., Sutherland, W.J. & Efstathiou, G. 1997, *MNRAS*, 289, 263
- David, L., Jones, C. & Forman, W. 1995, *ApJ*, 445, 578
- De Bernardis, P. et al. 2000, *Nature*, 404, 955
- De Grandi, S. et al. 1999, *ApJL*, 513, L17
- De Lapparent, V., Geller, M.J., Huchra, J.P. 1986, *ApJL*, 302, L1
- Delia Ceca, R., Scaramella, R., Gioia, I.M., Rosati, P., Fiore, F. & Squires, G. 2000, *A&A*, 353, 498
- De Propris, R., Couch, W.J. & the 2dFGRS Team, in *Mining The Sky*, Springer-Verlag series "ESO Astrophysics Symposia", in press, astro-ph/0010498
- Dolag, K., Evrard, A. & Bartelmann, M. 2001, *A&A*, 369, 36

- Dolag, K. & Schindler, S. 2000, *A&A* 364, 491
- Dolag, K., Evrard, A.E. & Bartelmann, M. 2001, *A&A* 369, 36
- Donahue, M., Voit, G.M., Gioia, I.M., Luppino, G., Hughes, J.P. & Stocke, J.T. 1998, *ApJ*, 502, 550
- Donahue, M., Voit, G.M., Scharf, C.A., Gioia, I.M., Mullis, C.R., Hughes, J.P. & Stocke, J.T. 1999, *ApJ*, 513, 51
- Dressler, A. & Gunn, J.E. 1983, *ApJ*, 270, 7
- Ebeling, H., Edge, A.C., Böhringer, H., Allen, S.W., Crawford, C.S., Fabian, A.C., Voges, W. & Huchra, J. P., 1998, *MNRAS*, 301, 881
- Ebeling, H., Jones, L.R., Perlman, E., Scharf, C., Homer, D., Wegner, G., Malkan, M., Fairley, B.W. & Mullis, C.R. 2000, *ApJ*, 534, 133
- Ebeling, H., Edge, A.C. & Henry, J.P. 2001b, *ApJ*, 553, 668
- Ebeling, H., Jones, L.R., Fairley, B.W., Perlman, E., Scharf, C. & Horner, D. 2001a, *ApJL*, 548, L23
- Edge, A.C., Stewart, G.C., Fabian, A.C. & Arnaud, K.A. 1990, *MNRAS*, 245, 559
- Efstathiou, G. 1990, in *Physics of the Early Universe* 36th Scottish Universities Summer School, eds. J. Peacock et al., Hilger, 361.
- Eke, V.R., Cole, S. & Frenk, C.S. 1996, *MNRAS*, 282, 263
- Eke, V.R., Cole, S., Frenk, C.S. & Henry, J.P. 1998, *MNRAS*, 298, 1145
- Eke, V.R., Navarro, J.F. & Steinmetz, M. 2001, *ApJ*, 554, 114
- Ettori, S. & Fabian, A.C. 1999, *MNRAS*, 305, 834
- Evrard, A.E. 1988, *MNRAS*, 235, 911
- Evrard, A.E. 1990, *ApJ*, 363, 349
- Evrard, A.E. 1997, *MNRAS*, 292, 289
- Evrard, A.E. 1998, in *A New Vision of an Old Cluster: Untangling Coma Berenices*, eds. A. Mazure, F. Casoli, F. Durret & D. Gerbal, World Scientific Publishing, 136
- Evrard, A.E., Metzler, C. & Navarro, J.F. 1996, *ApJ*, 469, 494
- Evrard, A.E. et al. 2001, *ApJ* submitted, astro-ph/01110246
- Fairley, B.W., Jones, L.R., Scharf, C., Ebeling, H., Perlman, E., Horner, D., Wegner, G. & Malkan, M. 2000, *MNRAS*, 315, 669
- Fan, X., Bahcall, N.A. & Cen, R. 1997, *ApJ*, 490, 123
- Feldmann, H.A. & Watkins, R. 1994, *ApJL*, 430, L17
- Fillmore, J.A. & Goldreich, P. 1984, *ApJ*, 281, 1
- Fischer, P. 1999, *AJ*, 117, 2024
- Freedman, W.L. et al. 2001, *ApJ*, 553, 47
- Frenk, C.S. et al. 1999, *ApJ*, 525, 554
- Gal, R.R., de Carvalho, R.R., Odewahn, S.C., Djorgovski, S.G. & Mag-oniner, V.E. 2000, *AJ*, 119, 12
- Geller, M.J. & Huchra, J.P. 1989, *Science*, 246, 897

- Gioia, I.M. 2000, in *Constructing the Universe with Clusters of Galaxies* eds. F. Durret & D. Gerbal, available on CD-Rom and at <http://www.iap.fr/Conferences/Colloque/coll2000/>, Reference: 3.1.
- Gioia, I.M. & Luppino, G.A. 1994, *ApJS*, 94, 583
- Gioia, I.M., Henry, J.P., Maccacaro, T., Morris, S.L., Stocke, J.T. & Wolter, A. 1990b, *ApJL*, 356, L35
- Gioia, I.M., Maccacaro, T., Morris, S.L., Schild, R.E., Stocke, J.T, Wolter, A. & Henry, J.P. 1990a, *ApJS*, 72, 567
- Gioia, I.M., Henry, J.P., Mullis, C.R., Ebeling, H. & Wolter, A. 1999, *AJ*, 117, 2608
- Gioia, I.M., Henry, J.P., Mullis, C.R., Voges, W., Briel, U.G., Böhringer, H. & Huchra, J.P. 2001, *ApJL*, 553, L105
- Girardi, M., Escalera, E., Fadda, D., Giuricin, G., Mardirossian, F. & Mezzetti, M. 1997, *ApJ*, 482, 41
- Giuricin, G., Srdjan, S., Girardi, M., Mezzetti, M. & Marinoni, C. 2001, *ApJ*, 554, 872
- Gladders, M.D. & Yee, H.K.C. 2000, *AJ*, 120, 2148
- Gonzales, A.H., Zaritsky, D., Dalcanton, J.J. & Nelson, A. 2001, *ApJS*, in press, astro-ph/0106055
- Gramann, M. 1998, *ApJ*, 493, 28
- Grego, L., Carlstrom, J.E., Reese, E.D., Holder, G.P., Holzappel, W.L., Joy, M.K., Mohr, J.J. & Patel, S. 2001, *ApJ*, 552, 2
- Gunn, J.E. 1977, *ApJ*, 218, 592
- Gunn, J.E. & Gott, J.R. 1972, *ApJ*, 176, 1
- Henry, J.P. 2000, *ApJ*, 534, 580
- Henry, J.P. 2001, to appear in *New Century of X-ray Astronomy*, Yokohama, Japan, in press, astro-ph/0108128
- Henry, J.P. & Arnaud, K. A. 1991, *ApJ*, 372, 410
- Henry, J.P., Gioia, I.M., Maccacaro, T., Morris, S.L., Stocke, J.T. & Wolter, A. 1992, *ApJ*, 386, 408
- Henry, J.P., Gioia, I.M., Mullis, C.R., Clowe, D.I., Luppino, G.A., Böhringer, H., Briel, U., Voges, W. & Huchra, J.P. 1997, *AJ*, 114, 1293
- Henry, J.P., Gioia, I.M., Mullis, C.R., Voges, W., Briel, U.G., Böhringer, H. & Huchra, J.P. 2001, *ApJL*, 553, L109
- Hoekstra, H., Franx, M. & Kuijken, K. 2000, *ApJ*, 532, 88
- Holder, G.P., Haiman, Z. & Mohr, J.J. 2001, *ApJ*, 560, L111
- Jeltema, T.E., Canizares, C.R., Bautz, M.W., Malm, M.R., Marshall, H.L., Bryan, G.L., Donahue, M. & Garmire, J.P. 2001, *ApJ*, in press, astro-ph/0107314
- Jenkins, A. et al. 1998, *ApJ*, 499, 20
- Jenkins, A. et al. 2001, *MNRAS*, 321, 372 (J01)
- Jing, Y.P., 1998, *ApJL*, 503, L9

- Jing, Y.P., 2000, *ApJ*, 535, 30
- Jones, L.R., Scharf, C., Ebeling, H., Perlman, E., Wegner, G., Malkan, M., Horner, D. 1998, *ApJ*, 495, 100
- Jones, C. & Forman, W. 1999, *ApJ*, 511, 65
- Jones, M.E. et al. 2001, *MNRAS* submitted, astro-ph/0103046
- Kaiser, N. 1984, *ApJL*, 284, L9
- Kepner, J., Fan, X., Bahcall, N., Gunn, J.E., Lupton, R. & Xu, G. 1999, *ApJ*, 517, 78
- Kitayama, T. & Suto, Y. 1997, *ApJ*, 490, 557
- Kneissl, R., Jones, M.E., Saunders, R., Eke, V.R., Lasenby, A.N., Grainge, K. & Cotter, G. 2001, *MNRAS* submitted, astro-ph/0103042
- Lacey, C. & Cole, S. 1993, *MNRAS*, 262, 627
- Lacey, C. & Cole, S. 1994, *MNRAS*, 271, 676
- Larson, R.B., Tinsley, B.M. & Caldwell, C.N. 1980, *ApJL*, 237, L692
- Luppino, G.A. & Kaiser, N. 1997, *ApJL*, 475, L20
- Maccacaro, T., Wolter, A., McLean, B., Gioia, I.M., Stocke, J.T., Della Ceca, R., Burg, R. & Faccini, R., 1994, *Astrophysical Letters and Communications*, 29, 1
- Markevitch, M. 1998, *ApJ*, 504, 27
- Markevitch, M., Sarazin, C.L. & Vikhlinin, A. 1999, *APJ*, 521, 526
- Mason, B.S. & Myers, S.T. 2000, *ApJ*, 540, 614
- Mathiesen, B., Evrard, A.E. & Mohr, J.J. 1999, *ApJL*, 520, L21
- Mathiesen, B.F. & Evrard, A.E. 2001, *ApJ*, 546, 100
- Metzler, C.A., White, M. & Loken, C. 2001, *ApJ*, 547, 560
- Mo, H.J. & White, S.D.M. 1996, *MNRAS*, 282, 34
- Mohr, J., Evrard, A.E., Fabricant, D. & Geller, M.J. 1995, *ApJ*, 447, 8
- Mohr, J. & Evrard, A.E. 1997, *ApJ*, 491, 38
- Mohr, J.J., Mathiesen, B. & Evrard, A.E. 1999, *ApJ*, 517, 627
- Mohr, J.J., Reese, E.D., Ellingson, E., Lewis, A.D. & Evrard, A.E. 2000, *ApJ*, 544, 109
- Muanwong, O., Thomas, P.A., Kay, S.T., Pearce, F.R. & Couchman, H.M.P. 2001, *ApJL*, 552, L27
- Mullis, C.R., Henry, J.P., Gioia, I.M., Böhringer, H., Briel, U.G., Voges, W. & Huchra, J.P. 2001, *ApJL*, 553, L115
- Navarro, J.F., Frenk, C.S. & White, S.D.M. 1996, *ApJ*, 462, 563
- Navarro, J.F., Frenk, C.S. & White, S.D.M. 1997, *ApJ*, 490, 493
- Netterfield, C.B. et al. 2001, *ApJ* submitted, astro-ph/0104460
- Nevalainen, J., Markevitch, M. & Forman, W. 2000, *ApJ*, 532, 694
- Nichol, R.C., Romer, A.K., Holden, B.P., Ulmer, M.P., Pildis, R.A., Adami, C., Merrelli, A.J., Burke, D.J. & Collins, C.A. 1999, *ApJL*, 521, L21

- Nichol, R. et al. 2001, in *Mining The Sky conference*, Springer-Verlag series "ESO Astrophysics Symposia", in press, astro-ph/0011557
- Ostrander, E.J., Nichol, R.C., Ratnatunga, K.U. & Griffiths, R.E. 1998, AJ, 116, 2644
- Oukbir, J. & Blanchard, A. 1992, A&A, 262, 21
- Padin, S. et al. 2001, ApJL, 549, L1
- Padmanabhan, T. 1993, *Structure Formation in the Universe*, Cambridge University Press, Cambridge, UK
- Park, C. & Gott, J.R. 1991, ApJ, 378, 457
- Pearce, F.R., Thomas, P.A. & Couchman, H.M.P. 1994, MNRAS, 268, 953
- Pearce, F.R., Thomas, P.A., Couchman, H.M.P. & Edge, A.C. 2000, MNRAS, 317, 1029
- Peacock, J.A. 1999, *Cosmological Physics*, Cambridge University Press, Cambridge, UK
- Peebles, P.J.E. 1980 *The Large Scale Structure of the Universe*, Princeton University Press, Princeton, NJ
- Peebles, P.J.E. 1993, *Principles of Physical Cosmology*, Princeton University Press, Princeton, NJ
- Pen, U.-L. 1998, ApJ, 498, 60
- Perlmutter, S. 1998 Nature, 391, 51
- Pierpaoli, E., Scott, D. & White, M. 2001, MNRAS, 325, 77
- Postman, M., Lubin, L.M., Gunn, J.E., Oke, J.B., Hoessel, J.G., Schneider, D.P., Christensen, J.A. 1996, AJ, 111, 615
- Press, W.H. & Schechter, P. 1974, ApJ, 187, 425
- Pryke, C., Halverson, N.W., Leitch, E.M., Kovac, J., Carlstrom, J.E., Holzzapfel, W.L. & Dragovan, M. 2001, ApJ submitted, astro-ph/0104490
- Renzini, A. 1998, in *The Young Universe: Galaxy Formation and Evolution at Intermediate and High Redshift*, eds. S. D'Odorico, A. Fontana & E. Giallongo, ASP Conference Series, 146, 298
- Ricker, P.M. & Sarazin, C.L., ApJ, in press, astro-ph/0107210
- Riess, A.G. et al. 1998, AJ, 116, 1009
- Romer, A.K. et al. 2000, ApJS, 126, 209
- Romer, A.K., Viana, P.T.P., Liddle, A.R. & Mann, R.G. 2001, ApJ, 547, 594
- Rosati, P., Della Ceca, R., Norman, C. & Giacconi, R., 1998, ApJL, 492, L21
- Rosati, P., Borgani, S., Della Ceca, R., Stanford, A., Eisenhardt, P. & Lidman, C. 2000, in *Large Scale Structure in the X-ray Universe*, eds. Plionis, M. & Georgantopoulos, I., Atlantisciences, Paris, 13
- Sadat, R. & Blanchard, A. 2001, A&A, 371, 19
- Sadat, R., Blanchard A. & Oukbir, J. 1998, A&A, 329, 21

- Scharf, C.A., Jones, L.R., Ebeling, H., Perlman, E., Malkan, M. & Wegner, G. 1997, *ApJ*, 477, 79
- Schuecker, P. et al. 2001, *A&A*, 368, 86.
- Scodreggio, M. et al. 1999, *A&A*, 137, 83
- Seljak, U. & Zaldarriaga, M. 1996, *ApJ*, 469, 437
- Stocke, J.T., Morris, S.L., Gioia, I.M., Maccacaro, T., Schild, R.E., Wolter, A., Fleming T.A. & Henry, J.P. 1991, *ApJS*, 76, 813
- Sunyaev, R. & Zel'dovich, Y.B. 1972, *Comments Astrophys. Space Phys.*, 4, 173
- Takahara, F. 1999, *Astronom. Nachrichten*, 320, 167
- Teyssier, R., Chiéze, J.-P. & Alimi, J.-M. 1998, *ApJ*, 509, 62
- Thomas, P.A., Muanwong, O., Pearce, F.R., Couchman, H.M.P., Edge, A.C., Jenkins, A. & Onuora, L. 2001, *MNRAS* submitted, *astro-ph/0007348*
- Tran, K.-V.H., Kelson, D.D., van Dokkum, P.G., Franx, M., Illingworth, G.D. & Magee, D. 1999, *ApJ*, 522, 39
- Tully, R.B. 1987, *ApJ*, 323, 1
- van Dokkum, P.G., Franx, M., Fabricant, D., Illingworth, G.D. & Kelson, D.D. 2000, *ApJ*, 541, 95
- Viana, P.T.P. & Liddle, A.R. 1996, *MNRAS*, 281, 323
- Viana, P.T.P. & Liddle, A.R. 1999, *MNRAS*, 303, 535
- Voges, W., Henry, J.P., Briel, U.G., Böhringer, H., Mullis, C.R., Gioia, I.M. & Huchra, J.P. 2001, *ApJL*, 553, L119
- Vikhlinin, A., Forman, W. & Jones, C. 1999, *ApJ*, 525, 47
- Vikhlinin, A., McNamara, B.R., Forman, W., Jones, C., Quintana, H. & Hornstrup, A. 1998a, *ApJ*, 502, 558
- Vikhlinin, A., McNamara, B.R., Forman, W., Jones, C., Quintana, H. & Hornstrup, A. 1998b, *ApJL*, 498, L21
- White, S.D.M. 1997, in *it Cosmology and Large-Scale Structure*, 60th Les Houches School, eds. R. Schaeffer et al., Elsevier, 349
- White, D.A. 2000, *MNRAS*, 312, 663
- White, M. 2001, *A&A*, 367 27
- White, D.A. & Fabian, A.C. 1995, *MNRAS*, 273, 72
- White, S.D.M., Efsthathiou, G. & Frenk, C.S. 1993b, *MNRAS*, 262, 1023
- White, S.D.M., Navarro, J.F., Evrard, A.E. & Frenk, C.S. 1993a, *Nature*, 366, 429
- Willick, J.A., Thompson, K.L., Mathiesen, B.F., Perlmutter, S., Knop, R.A. & Hill, G.J. 2001, *PASP*, 113, 658
- Wright, E.L. et al. 1992, *ApJL*, 396, L13
- Wu, K.K., Fabian, A.C. & Nulsen, P.E.J. 2000, *MNRAS*, 318, 889
- Wu, X.-P. & Hammer, F. 1993, *MNRAS*, 262, 187
- Wu, X.-P. 2000, *MNRAS*, 316, 299

- Yoshikawa, K., Jing, Y.P. & Suto, Y. 2000, *ApJ*, 535, 593
Zaritsky, D., Nelson, A.E., Dal Canton, J.J. 1997, *ApJ*, 480, 91
Zwicky, F. 1933, *Helv. Phys. Acta*, 6, 110

Topic Index

- Active galactic nuclei (AGN), 22, 25, 27, 103, 110, 123–128, 165, 181, 183, 186, 201, 217–219, 222, 235, 243, 280
- Active galaxies, see Active galactic nuclei
- Adaptive kernel method, 45, 54
- Angular momentum, 6–9, 55, 239
- Angular separation test, 43
- Brightest cluster member (BCM), 64–66, 124
- Butcher-Oemler (BO) effect, 185–186
- β statistics, 43, 150–152, 156–157, 159
- β model, 82, 137, 232, 287
 - See also Hydrostatic isothermal model
- β_{spec} , 47, 57, 62, 213
- cD galaxies, 15, 44–45, 58, 65–66, 102, 145, 172, 175–176
- Center-shift method, 86, 97
- Cluster surveys, 110, 152, 254, 267–269, 272, 283–285, 290–296
- Cluster mass, 54–57, 212–214, 246–247, 268, 276, 278, 286–288
- Cold dark matter models (CDM), 3, 94–95, 155, 260–264, 269–273, 276–278, 290–295
- Cold fronts, 16, 18–21, 112–120, 139
- Collision impact parameter, 5–10, 141
- Cooling flows (cores), 15–18, 90–92, 96, 102–103, 129, 134, 139, 142, 145–147, 150–152, 157–159, 167–168, 172, 174–177, 179, 213–214, 216, 242–243, 287
- Cooling
 - radiative, 8, 128, 241–242, 248, 267, 280
 - rate, 15–16
 - time, 15–17, 102, 167, 242
- Cosmic Microwave Background (CMB), 23, 29, 126, 215, 254, 256, 285, 296
- Cosmic rays, 14, 22–23, 25, 27–28, 31, 33–34, 187, 221
- Dark matter, 8, 40, 56, 62, 79, 95–96, 120, 230–232, 239, 241–242, 257–259, 262–269, 274–279, 283, 286, 292
- Dedica method, 45, 47–49, 60–61
- Density contrast test, 43
- Density gradients, 17, 56, 235, 247
- Distant clusters, see High redshift clusters
- Dynamical equilibrium, 56, 134, 149
- Δ statistics, 46, 48–49, 62
- Einstein–de Sitter model, 4, 92, 148, 256–257
- Entropy, 2, 11, 18, 134, 242, 265, 280
- Equipartition values, 124, 177–178, 204, 210, 215–216
- Extreme ultraviolet emission (EUV), 2, 29–30, 33, 219–220
- PEL statistics, 150–153, 156–157
- Fermi acceleration, 26–27
- Filaments, 10, 54, 56, 58–59, 62–63, 65–66, 84, 111–112, 124–125, 156, 216–217, 222, 235–236, 241, 262–264, 273, 282–283
- Friedmann–Lemaître equation, 92, 256
- Friedmann–Robertson–Walker universe, 92, 256
- Friends-of-friends algorithm, 262, 269
- Gamma ray emission, 2, 33, 215, 220
- Gas stripping, 55, 67, 185, 189–190, 243–244, 246
- Grid-based codes, 231
- Hard X-ray emission, 2, 29, 31–33, 215, 220, 222
- Hierarchical clustering, 3, 39, 48, 50, 57, 62, 92, 133–134, 148, 154, 164, 254, 256, 259–267
- High redshift clusters, 62–63, 69, 91–92, 118, 183–186, 207, 239, 254–255, 273–274, 283, 285, 290–295
- h–method, 48
- Hydrostatic equilibrium, 10, 15, 17, 56, 82, 118, 134, 141, 167, 247, 257–258, 264
- Hydrostatic isothermal model, 166
- Infrared emission, 187–188, 284

- Intra Cluster Medium (ICM), 1–2, 10–11, 15–16, 22–23, 25–27, 30, 34, 40, 55, 84, 101, 110, 112–113, 115–116, 118, 122–123, 134–135, 137–138, 145, 164, 167–170, 172–174, 177–179, 183–186, 188–189, 199, 201, 210, 215–220, 222, 230–233, 235, 239, 242–244, 247, 257–259, 265, 267, 276, 278–282, 284–288, 291–292
- Kelvin-Helmholtz instabilities, 21, 117
- King model see Hydrostatic isothermal model
- KMM algorithm, 44–46, 48, 50, 60
- LEE method, 43, 46–47, 49–50, 150–152, 156–157
- Lorentz factor, 24–26
- Magnetic field, 14, 21–24, 31, 117–118, 122, 124, 169, 172, 177, 188, 199, 201, 204, 206, 210, 215–222, 230–231, 235, 238–241, 247–248, 280
- Mass deposition, 90–91, 103, 118, 142, 157
- Mass function, 154, 243, 268–273, 291–292
- Maximum likelihood, 43, 45, 290–291
- Merger
 - consequences, 52–57, 145–147, 170–174, 212–215, 232–241
 - energy sources, 25–27, 96–98, 218–221
 - kinematics, 5–14, 52, 58
 - rates and substructure occurrence rate (SOR), 2–5, 90, 148–154, 272–274
 - shocks, 10–15, 25–29, 121–122, 235–237
 - Virgo cluster, 142–145
- Metal distribution (metallicity), 145–147, 230, 239, 242–246, 280
- Mini halos, 200–201
- NAT, see Tailed radio galaxies
- Neutrino emission, 33
- NFW profile, 18, 232, 275–276
- Non-thermal pressure, 177–178, 215
- Numerical simulations, 14, 16–17, 28, 41, 43, 46–53, 55, 54, 56–58, 61, 65, 68, 83, 95–96, 111, 120, 127–129, 139, 141–142, 148, 150, 155, 167, 174, 184, 217–218, 220, 222–223, 229–248, 253–296
- Ω , 4–6, 61–62, 92–96, 134, 148, 150, 155, 232, 254–256, 260–262, 266, 283, 285–286, 288–296
- Plasma bubbles, 110, 123–129
- Power ratio, 86–90, 93–95, 97, 102–103, 213–214
- Preheating, 242
- Pressure equilibrium, 114, 127, 139, 177–179
- Press & Schechter theory (PS or EPS), 2–6, 148–150, 154–155, 269–270, 272
- Primary electrons, 28–29, 218–219
- Radio halos, 27, 29, 31, 96–98, 110, 112, 121–122, 134, 147–148, 152, 157–159, 197–223, 235, 239
- Radio luminosity function, 179–183
- Radio ghosts, 222
- Radio power–linear size relation, 184
- Ram–pressure stripping, see Gas stripping
- Rankine-Hugoniot jump conditions, 11–13, 258
- Relativistic particles, 2, 22–34, 98, 122, 126, 177–178, 199, 201, 204, 206, 212, 215, 217–223, 235
- Relics, 27, 29, 31–32, 97–98, 141, 148, 157–158, 197–223, 235
- Robertson-Walker line element, 256
- Secondary electrons, 27, 33, 219–221
- Smoothed Particle Hydrodynamics (SPH), 67, 231
- Star bursts (post-), 8, 25, 27, 41, 67–70, 164–165, 184–187, 219, 230, 241–242, 264
- Star formation, see Star bursts
- S–tree technique, 48
- Subclump, see Substructure
- Subcluster, see Substructure
- Substructure
 - detection, 41–44, 82–89, 151–154
 - frequency, 50–52, 149–154
 - general, 5–11, 40, 79–85, 135–142, 167
 - nature, 50–52
 - spatial, 45–48
 - survival time, 52, 62
 - velocity, 44–48, 52–55
- Sunyaev-Zel'dovich (SZ), 212, 255, 268, 281–283, 288, 293–295
- Superclusters, 46, 51, 58–59, 61–62, 156, 174, 187
- σ_8 , 4, 255, 261, 283, 285, 288–296
- Tailed radio galaxies, 168–175, 178, 216, 219
- Temperature
 - function, 285, 289, 292
 - gradients, 102, 145, 164, 212, 235, 247
 - maps, 10–11, 13–14, 42, 98–101, 112–113, 116, 121–122, 128, 136–145, 148, 234–235, 237, 282–283
 - morphology, 101–103
- Thermal pressure, 118, 168, 177–178, 247
- Two phase model, 221–222
- Two point correlation function, 44
- Virial mass, 48, 53–54, 255, 277–280
- WAT, see tailed radio galaxies
- Wavelet analysis, 43–45, 47–49, 83–86

X-ray

- ellipticity, 86–87, 142
- holes, 123–124, 128, 176
- luminosity, 98, 143, 179, 210–211, 231, 237, 241–242, 268, 274, 285

luminosity function, 295

morphology, 10, 82, 85–89, 129, 140, 144, 148–151

surveys, 151–152, 284–285, 290–296

This page intentionally left blank

Object Index

- A70, 58
A85, 13, 16, 21, 32, 54, 58–59, 81, 88–89,
111, 215
A87, 58–59
A89, 58–59
A91, 58
A119, 170–171, 216
A426, 55, 123–124, 128, 169, 176, 199, 201
A496, 65, 175
A514, 81, 88–89, 216
A517, 58, 60
A518, 58, 60
A521, 50, 58, 60, 65–66, 84–85
A528, 58, 60
A548, 42, 48
A562, 175
A665, 13, 120–122, 207–208, 235
A697, 66
A754, 56–57, 65, 136, 139–141, 208, 223
A1060, 57
A1300, 208
A1367, 46, 59, 83–84, 187, 199, 204
A1656, 27, 29, 32–34, 41, 46, 50, 55, 57, 59,
65–69, 80, 83, 99, 110, 135–139,
145–146, 150, 167, 170, 187, 189–190,
198–199, 201, 203–204, 208, 211,
215–220, 222, 235, 241, 273, 276, 286
A1689, 54, 58
A1750, 81, 88–89
A1795, 29, 137, 142, 175
A2029, 81, 88–89, 175, 214
A2065, 13, 16, 18
A2111, 241
A2125, 186, 241
A2142, 18, 112–115, 120, 213, 235
A2163, 121, 207, 209, 211, 235
A2199, 29, 32
A2255, 178, 205–206, 208, 210–211
A2256, 32, 80, 83, 136, 138–140, 167, 205,
208, 215
A2319, 205, 207, 211
A2390, 70
A2634, 65, 173
A2645, 186
A2670, 49, 65, 191
A2744, 207–208, 210
A3128, 189
A3266, 49, 66, 69
A3395, 10
A3526, 42, 47, 54
A3530, 66
A3532, 66
A3556, 59, 186
A3558, 59, 61, 69, 186
A3562, 59, 69, 186
A3667, 11, 13, 21, 100, 115–117, 199, 201,
208, 223
A4038, 29
A4059, 29
Cancer Cluster, 46, 187
Centaurus Cluster, see A3526
CL 0016+16 (also 0016+1609), 207
CL J0023+0423, 62
CL 0024+17 (also ZwCl 0024.0+1652),
91–92
Coma cluster, see A1656
Coma A, see 3C277.3
Coma C, 198, 200, 203–205, 221–222
Coma supercluster, 46, 187
Cygnus A, 10–11, 13–14, 16, 100, 175–176,
178
DC 0326–53, 69
DC 0329–52, 69
Fornax, 69
HCG 062, 123
Hercules supercluster, 61, 187
Hydra A, 123–124, 128, 177
MKW 03s, 123
MS 1054.4–0321, 62, 69, 273–274, 283–284
M49, 143
M84, 124–125, 128
M86, 144, 246
M87, 122, 125–127, 129, 143, 145–146
NGC326, 175

- NGC1265, 169
 NGC1272, 202
 NGC1275, 122–124, 176, 199, 202
 NCG4374, see M84
 NGC4501, 244
 NGC4548, 244
 NGC4839, 46, 57, 67–68, 99, 136–137, 204
 NGC4869, 170, 216, 219–220
 NGC4874, 67, 83
 NGC4889, 67, 83
 NGC4911, 67
 Perseus cluster, see A426
 Perseus-Pisces supercluster, 58
 PKS 0745-191 (also PKS 0745-19), 176–177
 RX J0152.7-1357, 273
 RX J1347.5-1145, 91–92
 RX J1716.6+6708, 62–63, 273
 RX J1720.1+2638, 21, 118, 120
 Sérsic 159/03, 243
 Shapley Concentration, 59–60, 66, 183, 186
 Virgo cluster, 29, 41–42, 52, 59, 66, 124,
 142–146, 189, 201, 244, 269, 277
 ZW3146, 118–119
 1E 0657-56 (also 1ES 0657-558), 56, 207
 104420.8+055739, 63–64
 1253+275, 201, 203–204
 2A 0335+096, 176–177
 2006-56, 199
 3C75, 173
 3C84, see NGC 1275
 3C109, 166
 3C272.1, see M84
 3C277.3, 198–199
 3C295, 175
 3C317, 176
 3C449, 165
 3C465, 172–173, 175

Copyright Credits

Review by Girardi & Biviano:

The galaxy environment of a quasar at $z = 1.226$: a possible cluster merger, Haines et al., 2001, MNRAS, 323, 688, Fig. 6, Copyright 2001 Blackwell Science Ltd.

A substructure analysis of the A3558 cluster complex, Bardelli et al., 1998, MNRAS, 300, 589, Fig. 5, Copyright 1998 Blackwell Science Ltd.

The rich cluster of galaxies ABCG 85. III. Analyzing the ABCG 85/87/89 complex, Durret et al., 1998, A&A, 335, 41, Fig. 15, Copyright 1998 Springer

A521: A cluster forming at the crossing of two filaments?, Arnaud et al., 2000, A&A, 355, 461, Fig. 9, Copyright 2000 Springer

RX J1716.6+6708: A Young Cluster at $Z=0.81$, Gioia et al., 1999, AJ, 117, 2608, Fig. 1, Copyright 1999 The American Astronomical Society

Star formation in early-type galaxies in the Coma cluster, Caldwell et al., 1993, AJ, 106, 473, Fig. 17, Copyright 1993 The American Astronomical Society

Evidence for substructure in rich clusters of galaxies from radial-velocity measurements, Dressler & Schectman, 1988, AJ, 95, 985, Fig. 1 (part of), Copyright 1988 The American Astronomical Society

Evaluation of Statistical Tests for Substructure in Clusters of Galaxies, Pinkney et al., 1996, ApJS, 104, 1, Fig. 29, Copyright 1996 The American Astronomical Society

Structure and Dynamics of the Coma Cluster, Colless & Dunn, 1999, ApJ, 458, 435, Fig 9a, Copyright 1999 The American Astronomical Society

Structures in Galaxy Clusters, Escalera et al., 1994, ApJ, 423, 539, Fig. 11 (a, b), Copyright 1994 The American Astronomical Society

Substructure within clusters of galaxies, Geller & Beers, 1982, PASP, 94, 421, Fig. 3 (part of), Copyright 1982 The Astronomical Society of the Pacific

Review by Buote:

The X-ray morphology of the relaxed cluster of galaxies A2256. I - Evidence for a merger event, Briel et al., 1991, A&A, 246, L10, Fig. 1, Copyright 1991 Springer

An X-ray Temperature Map of Coma, Briel & Henry, 1998, in "A New Vision of an Old Cluster: Untangling Coma Berenices", eds. F. Durret et al., World Scientific, 170, Fig. 1, Fig. 2 Copyright 1998 World Scientific Publishing Co. Ltd.

A wavelet analysis search for substructures in eleven X-ray clusters of galaxies, Slezak et al., 1994, AJ, 108, 1996, Fig. 4, Copyright 1996 The American Astronomical Society

Unveiling Hidden Structures in the Coma Cluster, Biviano et al., 1996, A&A, 311, 95, Fig. 9, Copyright 1996 Springer

Wavelet Transform Analysis of the Small-Scale X-Ray Structure of the Cluster A1367, Grebenev et al., 1995, ApJ, 445, 607, Fig. 3, Copyright 1995 The American Astronomical Society

A Cluster Forming at the Crossing of Two Filaments, Arnaud et al., 2000, A&A, 355, 461, Fig. 1, Fig. 3, Copyright 2000 Springer

ROSAT/HRI and ASCA Observations of the Most Luminous X-ray Cluster RXJ 1347.5-1145, Schindler et al., 1997, A&A, 317, 646, Fig. 1, Copyright 1997 Springer

Morphology of the Lensing Galaxy Cluster CL0024+17, Böhringer et al., 2000, A&A, 353, 124, Fig. 1, Copyright 2000 Springer

A Lower Limit on the Cosmic Mean Density From the Ages of Clusters of Galaxies, Richstone et al., 1992, ApJ, 393, 477, Fig. 3, Copyright 1992 The American Astronomical Society

Physics of Merging Clusters Cygnus-A, A3667, and A2065, Markevitch et al., 1999, ApJ, 521, 526, Fig. 1, Copyright 1999 The American Astronomical Society

Review by Forman et al.:

Chandra Observation of Abell 2142: Survival of Dense Subcluster Cores in a Merger, M. Markevitch et al., 2000, ApJ, 541, 542, Fig. 2a, Fig. 4 (b, c), Fig. 5, Copyright 2000 The American Astronomical Society

A Moving Cold Front in the Intergalactic Medium of A3667, A. Vikhlinin et al., 2001, ApJ, 551, 160, Fig. 3a, Fig. 4, Fig. 5, Copyright 2001 The American Astronomical Society

Merger shocks in galaxy clusters A665 and A2163 and their relation to radio halos, Markevitch & Vikhlinin, 2001, ApJ, in press, Fig. 9, Copyright 2001 The American Astronomical Society

Chandra Observation of M84, a Radio Lobe Elliptical Galaxy in the Virgo Cluster, Finoguenov & Jones, 2001, ApJL, 547, L107, Fig. 1, Copyright 2001 The American Astronomical Society

Evolution of Buoyant Bubbles in M87 by Churazov et al., 2001, ApJ, 554, 261, Fig. 1 (a, b, c), Fig. 4, Fig. 6, Copyright 2001 The American Astronomical Society

Review by Böhringer & Schuecker:

XMM-Newton observation of the Coma Galaxy cluster. The temperature structure in the central region, Arnaud et al., 2001, A&A, 365, L67, Fig. 6, Fig. 8, Copyright 2001 EDP Sciences

The NGC 4839 group falling into the Coma cluster observed by XMM-Newton, Neumann et al., 2001, A&A, 365, L74, Fig. 1, Copyright 2001 EDP Sciences

The morphology and metal abundance of M86 from ROSAT PSPC and HRI observations: dust destruction in supersonic ram-pressure stripping, Rangarajan et al., 1995, MNRAS, 277, 1047, Fig. 2, Copyright 1995 Blackwell Science Ltd.

Temperature Map of the Virgo Cluster of Galaxies Observed with ASCA, Shibata et al., 2001, ApJ, 549, 228, Fig. 3, Copyright 2001 The American Astronomical Society

Metallicity Gradients in X-Ray Clusters of Galaxies, De Grandi & Molendi, 2001, ApJ, 551, 153, Fig. 2, Fig. 3, Copyright 2001 The American Astronomical Society

A Collision of Subclusters in Abell 754, Zabludoff & Zaritsky, 1995, ApJ, 467, L21, Plate 1, Copyright 1995 The American Astronomical Society

Chandra observation of A2256 - a cluster at the early stage of merging, Sun et al., 2001, ApJ, in press, Fig. 1, Fig. 3, Copyright 2001 The American Astronomical Society

Review by Feretti & Venturi:

Unusual Radio Structures in the Cooling flow cluster 2A 0335+096, Sarazin et al., 1995, ApJ, 451, 125, Fig 2c, Copyright 1995 The American Astronomical Society

VLA HI imaging of the brightest spiral galaxies in Coma, Bravo-Alfaro et al., 2000, ApJ, 119, 580, Fig. 2, Copyright 2000 The American Astronomical Society

Multifrequency windows on spiral galaxies. I. UVB and Halfa aperture photometry, Gavazzi et al., 1991, AJ, 101, 1207, Fig. 6, Copyright 1991 The American Astronomical Society

ROSAT X-ray observations of Abell Clusters with wide angle tailed radio sources, Gómez et al., 1997, ApJ, 474, 580, Fig. 4, Copyright 1997 The American Astronomical Society

High resolution map of NGC1265, Wellington et al., 1973, Nature, 244, 502, Fig. 1, Copyright 1973 Macmillan Magazines Limited

The X-ray morphology of the relaxed cluster of galaxies. I. Evidence for a merger event, Briel et al., 1991, A&A, 246, L10, Fig. 2, Copyright 1991 Springer

Review by Giovannini & Feretti:

A radio continuum and HI Line study of the Perseus cluster, Sijbring L.G., 1993, PhD Thesis Groningen University, Fig. 2

On the origin of radio halos in galaxy clusters, Buote D.A., 2001, ApJ, 553, L15, Fig. 6, Copyright 2001 The American Astronomical Society

A comparison of radio and X-ray morphology of four clusters of galaxies containing radio halos, Govoni et al., 2001, A&A, 369, 441, Fig. 3, Copyright 2001 EDP Sciences

A high-resolution survey of the Coma cluster of galaxies at 408 Mc/s, Large et al., 1959, Nature, 133, 1663, Fig. 1, Copyright 1959 Macmillan Magazines Limited

The extended radio emission in the luminous X-ray cluster A3667, Rotgering et al., 1997, MNRAS, 290, 577, Fig. 6, Copyright 1997 Blackwell Science Ltd.

Review by Schindler:

Simulations of the evolution of galaxy clusters. II. Dynamics of the intra-cluster gas, Schindler & Müller, 1993, A&A, 272, 137, Fig. 2, Fig. 3, Copyright 1993 Springer

On the Role of Shock Waves in Galaxy Cluster Evolution, Quilis et al., 1998, ApJ, 502, 518, Fig. 1, Copyright 1998 The American Astronomical Society

Are Large X-Ray Clusters at Thermal Equilibrium?, Chièze et al., 1998, ApJ, 495, 630, Fig. 1 (part of), Copyright 1998 The American Astronomical Society

Gas dynamic stripping and X-ray emission of cluster elliptical galaxies, Toniazzo & Schindler, 2001, MNRAS 325, 509, Fig. 3 (part of), Fig. 13, Copyright 2001 Blackwell Science Ltd.

Simulating magnetic fields in galaxy clusters, a tool to learn more about this obscure ingredient of clusters, Dolag K., 2001, in "Galaxy Clusters and the High Redshift Universe Observed in X-rays", XXI Moriond Astrophysics Meeting (March 2001), eds. D. Neumann, F. Durret, & J. Tran Thanh Van, in press, Fig. 5

Review by Evrard & Gioia:

Self-similar secondary infall and accretion in an Einstein-de Sitter universe, Bertschinger, 1985, ApJS, 58, 39, Fig. 2, Fig. 6, Copyright 1985 The American Astronomical Society

The Santa Barbara Cluster Comparison Project: A Comparison of Cosmological Hydrodynamics Solutions, Frenk et al., 1999, ApJ, 525, 554, Fig. 10, Copyright 1999 The American Astronomical Society

Hubble Space Telescope Weak-Lensing Study of the $z=0.83$ Cluster MS 1054-03, Hoekstra et al., 2000, ApJ, 532, 88, Fig. 18b, Copyright 2000 The American Astronomical Society

Properties of the Intracluster Medium in an Ensemble of Nearby Galaxy Clusters, Mohr et al., 1999, ApJ, 517, 627, Fig. 14, Copyright 1999 The American Astronomical Society

Chandra X-Ray Observatory Observation of the High-Redshift Cluster MS 1054-0321, Jeltema et al., 2001, ApJ, in press, Fig. 9, Copyright 2001 The American Astronomical Society

Previously published in Astrophysics and Space Science Library book series:

- **Volume 269: Mechanics of Turbulence of Multicomponent Gases**
Authors: Mikhail Ya. Marov, Aleksander V. Kolesnichenko
Hardbound, ISBN 1-4020-0103-7, December 2001
- **Volume 268: Multielement System Design in Astronomy and Radio Science**
Authors: Lazarus E. Kopilovich, Leonid G. Sodin
Hardbound, ISBN 1-4020-0069-3, November 2001
- **Volume 267: The Nature of Unidentified Galactic High-Energy Gamma-Ray Sources**
Editors: Alberto Carramiñana, Olaf Reimer, David J. Thompson
Hardbound, ISBN 1-4020-0010-3, October 2001
- **Volume 266: Organizations and Strategies in Astronomy II**
Editor: André Heck
Hardbound, ISBN 0-7923-7172-0, October 2001
- **Volume 265: Post-AGB Objects as a Phase of Stellar Evolution**
Editors: R. Szczerba, S.K. Górný
Hardbound, ISBN 0-7923-7145-3, July 2001
- **Volume 264: The Influence of Binaries on Stellar Population Studies**
Editor: Dany Vanbeveren
Hardbound, ISBN 0-7923-7104-6, July 2001
- **Volume 262: Whistler Phenomena Short Impulse Propagation**
Authors: Csaba Ferencz, Orsolya E. Ferencz, Dániel Hamar, János Lichtenberger
Hardbound, ISBN 0-7923-6995-5, June 2001
- **Volume 261: Collisional Processes in the Solar System**
Editors: Mikhail Ya. Marov, Hans Rickman
Hardbound, ISBN 0-7923-6946-7, May 2001
- **Volume 260: Solar Cosmic Rays**
Author: Leonty I. Miroshnichenko
Hardbound, ISBN 0-7923-6928-9, May 2001
- **Volume 259: The Dynamic Sun**
Editors: Arnold Hanslmeier, Mauro Messerotti, Astrid Veronig
Hardbound, ISBN 0-7923-6915-7, May 2001
- **Volume 258: Electrohydrodynamics in Dusty and Dirty Plasmas Gravito-Electrodynamics and EHD**
Author: Hiroshi Kikuchi
Hardbound, ISBN 0-7923-6822-3, June 2001
- **Volume 257: Stellar Pulsation - Nonlinear Studies**
Editors: Mine Takeuti, Dimitar D. Sasselov
Hardbound, ISBN 0-7923-6818-5, March 2001
- **Volume 256: Organizations and Strategies in Astronomy**
Editor: André Heck
Hardbound, ISBN 0-7923-6671-9, November 2000
- **Volume 255: The Evolution of the Milky Way Stars versus Clusters**
Editors: Francesca Matteucci, Franco Giovannelli
Hardbound, ISBN 0-7923-6679-4, January 2001

- **Volume 254: Stellar Astrophysics**
 Editors: K.S. Cheng, Hoi Fung Chau, Kwing Lam Chan, Kam Ching Leung
 Hardbound, ISBN 0-7923-6659-X, November 2000
- **Volume 253: The Chemical Evolution of the Galaxy**
 Author: Francesca Matteucci
 Hardbound, ISBN 0-7923-6552-6, May 2001
- **Volume 252: Optical Detectors for Astronomy II**
State-of-the-art at the Turn of the Millennium
 Editors: Paola Amico, James W. Beletic
 Hardbound, ISBN 0-7923-6536-4, December 2000
- **Volume 251: Cosmic Plasma Physics**
 Author: Boris V. Somov
 Hardbound, ISBN 0-7923-6512-7, September 2000
- **Volume 250: Information Handling in Astronomy**
 Editor: André Heck
 Hardbound, ISBN 0-7923-6494-5, October 2000
- **Volume 249: The Neutral Upper Atmosphere**
 Author: S.N. Ghosh
 Hardbound, ISBN 0-7923-6434-1, (in production)
- **Volume 247: Large Scale Structure Formation**
 Editors: Reza Mansouri, Robert Brandenberger
 Hardbound, ISBN 0-7923-6411-2, August 2000
- **Volume 246: The Legacy of J.C. Kapteyn**
Studies on Kapteyn and the Development of Modern Astronomy
 Editors: Piet C. van der Kruit, Klaas van Berkel
 Hardbound, ISBN 0-7923-6393-0, August 2000
- **Volume 245: Waves in Dusty Space Plasmas**
 Author: Frank Verheest
 Hardbound, ISBN 0-7923-6232-2, April 2000
- **Volume 244: The Universe**
Visions and Perspectives
 Editors: Naresh Dadhich, Ajit Kembhavi
 Hardbound, ISBN 0-7923-6210-1, August 2000
- **Volume 243: Solar Polarization**
 Editors: K.N. Nagendra, Jan Olof Stenflo
 Hardbound, ISBN 0-7923-5814-7, July 1999
- **Volume 242: Cosmic Perspectives in Space Physics**
 Author: Sukumar Biswas
 Hardbound, ISBN 0-7923-5813-9, June 2000
- **Volume 241: Millimeter-Wave Astronomy: Molecular Chemistry & Physics in Space**
 Editors: W.F. Wall, Alberto Carramiñana, Luis Carrasco, P.F. Goldsmith
 Hardbound, ISBN 0-7923-5581-4, May 1999
- **Volume 240: Numerical Astrophysics**
 Editors: Shoken M. Miyama, Kohji Tomisaka, Tomoyuki Hanawa
 Hardbound, ISBN 0-7923-5566-0, March 1999
- **Volume 239: Motions in the Solar Atmosphere**
 Editors: Arnold Hanslmeier, Mauro Messerotti
 Hardbound, ISBN 0-7923-5507-5, February 1999

- **Volume 238: Substorms-4**
 Editors: S. Kokubun, Y. Kamide
 Hardbound, ISBN 0-7923-5465-6, March 1999
- **Volume 237: Post-Hipparcos Cosmic Candles**
 Editors: André Heck, Filippina Caputo
 Hardbound, ISBN 0-7923-5348-X, December 1998
- **Volume 236: Laboratory Astrophysics and Space Research**
 Editors: P. Ehrenfreund, C. Krafft, H. Kochan, V. Pirronello
 Hardbound, ISBN 0-7923-5338-2, December 1998
- **Volume 235: Astrophysical Plasmas and Fluids**
 Author: Vinod Krishan
 Hardbound, ISBN 0-7923-5312-9, January 1999
 Paperback, ISBN 0-7923-5490-7, January 1999
- **Volume 234: Observational Evidence for Black Holes in the Universe**
 Editor: Sandip K. Chakrabarti
 Hardbound, ISBN 0-7923-5298-X, November 1998
- **Volume 233: B[e] Stars**
 Editors: Anne Marie Hubert, Carlos Jaschek
 Hardbound, ISBN 0-7923-5208-4, September 1998
- **Volume 232: The Brightest Binaries**
 Authors: Dany Vanbeveren, W. van Rensbergen, C.W.H. de Loore
 Hardbound, ISBN 0-7923-5155-X, July 1998
- **Volume 231: The Evolving Universe**
Selected Topics on Large-Scale Structure and on the Properties of Galaxies
 Editor: Donald Hamilton
 Hardbound, ISBN 0-7923-5074-X, July 1998
- **Volume 230: The Impact of Near-Infrared Sky Surveys on Galactic and Extragalactic Astronomy**
 Editor: N. Epchtein
 Hardbound, ISBN 0-7923-5025-1, June 1998
- **Volume 229: Observational Plasma Astrophysics: Five Years of Yohkoh and Beyond**
 Editors: Tetsuya Watanabe, Takeo Kosugi, Alphonse C. Sterling
 Hardbound, ISBN 0-7923-4985-7, March 1998
- **Volume 228: Optical Detectors for Astronomy**
 Editors: James W. Beletic, Paola Amico
 Hardbound, ISBN 0-7923-4925-3, April 1998
- **Volume 227: Solar System Ices**
 Editors: B. Schmitt, C. de Bergh, M. Festou
 Hardbound, ISBN 0-7923-4902-4, January 1998
- **Volume 226: Observational Cosmology with the New Radio Surveys**
 Editors: M.N. Bremer, N. Jackson, I. Pérez-Fournon
 Hardbound, ISBN 0-7923-4885-0, February 1998
- **Volume 225: SCORE'96: Solar Convection and Oscillations and their Relationship**
 Editors: F.P. Pijpers, Jørgen Christensen-Dalsgaard, C.S. Rosenthal
 Hardbound, ISBN 0-7923-4852-4, January 1998

- **Volume 224: Electronic Publishing for Physics and Astronomy**
 Editor: André Heck
 Hardbound, ISBN 0-7923-4820-6, September 1997
- **Volume 223: Visual Double Stars: Formation, Dynamics and Evolutionary Tracks**
 Editors: J.A. Docobo, A. Elipe, H. McAlister
 Hardbound, ISBN 0-7923-4793-5, November 1997
- **Volume 222: Remembering Edith Alice Müller**
 Editors: Immo Appenzeller, Yves Chmielewski, Jean-Claude Pecker, Ramiro de la Reza, Gustav Tammann, Patrick A. Wayman
 Hardbound, ISBN 0-7923-4789-7, February 1998
- **Volume 220: The Three Galileos: The Man, The Spacraft, The Telescope**
 Editors: Cesare Barbieri, Jürgen H. Rahe†, Torrence V. Johnson, Anita M. Sohus
 Hardbound, ISBN 0-7923-4861-3, December 1997
- **Volume 219: The Interstellar Medium in Galaxies**
 Editor: J.M. van der Hulst
 Hardbound, ISBN 0-7923-4676-9, October 1997
- **Volume 218: Astronomical Time Series**
 Editors: Dan Maoz, Amiel Sternberg, Elia M. Leibowitz
 Hardbound, ISBN 0-7923-4706-4, August 1997
- **Volume 217: Nonequilibrium Processes in the Planetary and Cometary Atmospheres: Theory and Applications**
 Authors: Mikhail Ya. Marov, Valery I. Shematovich, Dmitry V. Bisikalo, Jean-Claude Gérard
 Hardbound, ISBN 0-7923-4686-6, September 1997
- **Volume 216: Magnetohydrodynamics in Binary Stars**
 Author: C.G. Campbell
 Hardbound, ISBN 0-7923-4606-8, August 1997
- **Volume 215: Infrared Space Interferometry: Astrophysics & the Study of Earth-like Planets**
 Editors: C. Eiroa, A. Alberdi, Harley A. Thronson Jr., T. de Graauw, C.J. Schalinski
 Hardbound, ISBN 0-7923-4598-3, July 1997
- **Volume 214: White Dwarfs**
 Editors: J. Isern, M. Hernanz, E. García-Berro
 Hardbound, ISBN 0-7923-4585-1, May 1997
- **Volume 213: The Letters and Papers of Jan Hendrik Oort as archived in the University Library, Leiden**
 Author: J.K. Katgert-Merkelijn
 Hardbound, ISBN 0-7923-4542-8, May 1997

Missing volume numbers have not been published yet.

For further information about this book series we refer you to the following web site: www.wkap.nl/series.htm/ASSL

To contact the Publishing Editor for new book proposals:

Dr. Harry (J.J.) Blom: harry.blom@wkap.nl